Session 10

FILTRATION, FILTER TESTING, AND AEROSOLS

TUESDAY: October 21, 1980
CHAIRMAN: H. Gilbert, Consultant
R. Dorman, AERE, Harwell

SURVEY OF LOADING PERFORMANCE OF CURRENTLY AVAILABLE TYPES OF HEPA FILTERS UNDER IN-SERVICE CONDITIONS
C.A. Gunn , J.B. McDonough

PERFORMANCE OF 1,000 AND 1,800 CFM HEPA FILTERS ON LONG EXPOSURE TO LOW ATMOSPHERIC DUST LOADINGS, II
M.W. First, S.N. Rudnick

A PRELIMINARY ASSESSMENT OF THE DUST LOADING VERSUS PRESSURE DROP CHARACTERISTIC OF HIGH CAPACITY HEPA FILTERS
R.P. Pratt

CLEANABLE SINTERED METAL FILTERS IN HOT OFF-GAS SYSTEMS
G.A. Schurr

HIGH EFFICIENCY PARTICULATE REMOVAL WITH SINTERED METAL FILTERS
B.E. Kirstein, W. J. Paplawsky, D.T. Pence , T.G. Hedahl

PERFORMANCE OF SAND FILTERS FOR THE SEPARATIONS AREAS AT THE SAVANNAH RIVER PLANT
D.A. Orth, G.H. Sykes, J.M. McKibben

SODIUM FIRE AEROSOL LOADING CAPACITY OF SEVERAL SAND AND GRAVEL FILTERS
J.R. Barreca, J.D. McCormack

INFLUENCE OF THERMOPHORESIS ON PARTICLE REMOVAL IN A MOVING GRANULAR BED FILTER AND HEAT EXCHANGER
S.N. Rudnick, M.W. First, J.M. Price

DEVELOPMENT OF ACID-RESISTENT HEPA FILTER COMPONENTS
K. Terada, R.W. Woodard, O.I. Buttedahl

ELECTROFIBROUS PREFILTERS FOR USE IN NUCLEAR VENTILATION SYSTEMS
W. Bergman

SURVEY OF LOADING PERFORMANCE OF CURRENTLY AVAILABLE TYPES HEPA FILTERS UNDER IN-SERVICE CONDITIONS

C. A. Gunn and J. B. McDonough
Mine Safety Appliances Company
Evans City, Pennsylvania 16033

Abstract

Atmospheric dust loading tests were conducted on various industrial grade High Efficiency Particulate Air Filters. The filters tested were the European Style, "Super-Flow", Standard U.S. Design, and a Super-Pak. Filters were installed on the roof of a 3-story building.

Test flows were set at a media velocity of 5 FPM (1.52 meters per min.) and results show that filter life varies from 8.8 to 12.7 months.

In addition, tests were conducted on the European Style filter at media velocities of 5.6 and 2.6 FPM. On the filter tested at 5.6 FPM an abrupt change in life was observed at 4 months. After more than 1 year operation at a lower velocity of 2.6 FPM the pressure rise with time is still very slow.

I. Introduction

There has been considerable effort in the HEPA filter industry to maximize the filter media area per unit volume of the filter cartridge. The principal objective of these designs is to have favorable pressure drop characteristics at higher volume flow rates. Unfortunately, with these new designs we have no way to theoretically compare or to predict their performance with respect to filter life. We can conduct accelerated dust loading life tests in accordance with acceptable standards (NBS or ASHRAE); however, we know from experience that these test results are not indicative of actual field service.[1] The reason is that these are coarse dust loading tests and the HEPA filter is not a heavy dust loading device. Therefore, the only true test for HEPA filters is with atmospheric air which is a time consuming test. Even the results of these tests are only good for the environmental conditions and types of dust encountered during the test period.

High flow design versions of HEPA filters are available on the U.S. market. Basically, all these filters incorporate more filter media than conventional type U.S. filters. However, it is questionable how effective the filter designs are when they are exposed to atmospheric air for long periods at rated flows of 5 FPM (1.52 meters per min.) through the filter media.

Long term exposure tests were conducted to compare filter performance. The results of original DOP tests and atmospheric dust loading are reported.

II. Atmospheric Air Test Arrangement

The test system as shown in Figure 1 is designed to compare atmospheric dust loading service life on HEPA filters at flow rates up to 2200 CFM (3740 m^3 per hr.). Each unit is composed of an inlet louvered grill to protect the filter from snow or rain, a side access filter plenum to house a 24 x 24 x 11½ (610 mm x 610 mm x 292 mm) filter and a flow measuring device (orifice plate). The blower is located on the downstream side of the filter. Air flow is controlled by a damper.

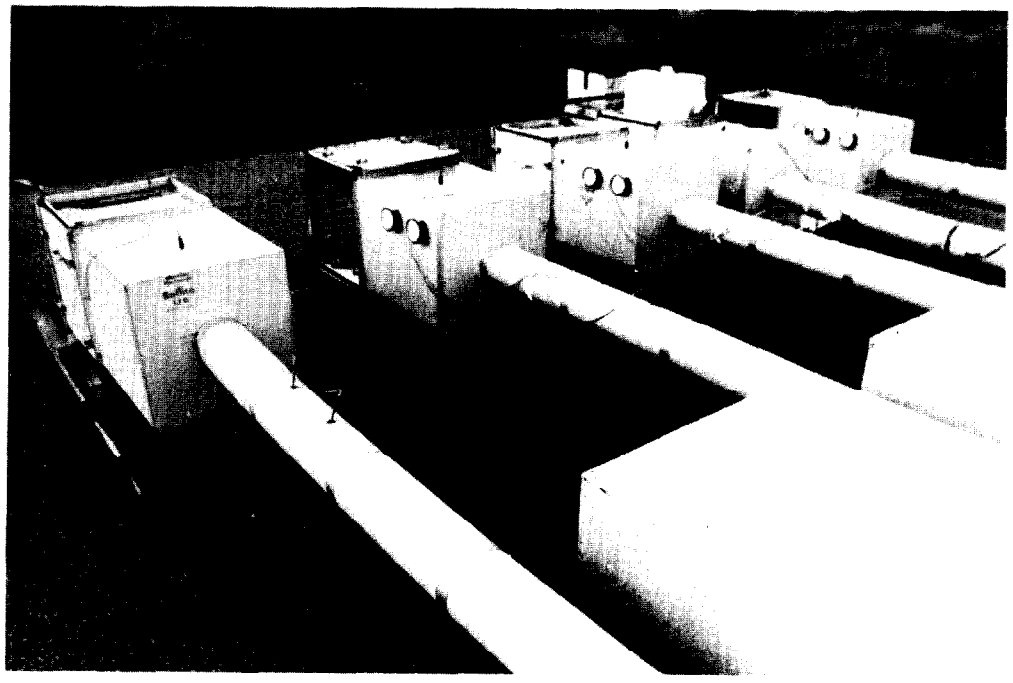

Figure 1 Test system.

A high volume dust sampler is employed to measure daily dust loads. The sampler is a compact unit with motor blower set at a predetermined flow. Dust is collected on 152 mm diameter HEPA filter media discs. The daily results are plotted as total cumulative dust loads as shown in Figure 2.

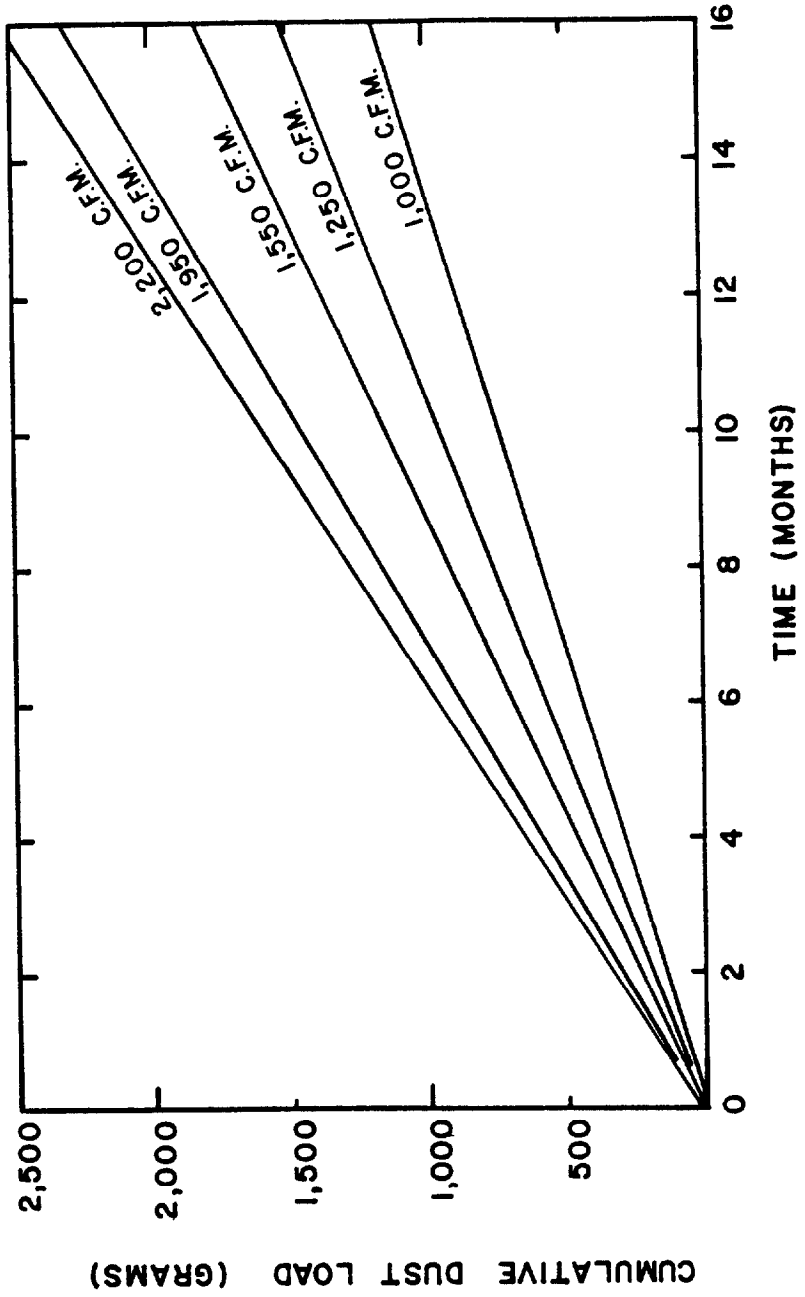

FIGURE 2 CUMULATIVE DUST LOAD (GRAMS).

III. Filter Description

The downstream sides of the spent filters tested are shown in Figure 3 and filter descriptions are as follows:

1) Standard U.S. Design fabricated in accordance with MIL F-51068E.[2] The filter size is 610 mm x 610 mm x 292 mm. Frame material is wood and the filter separators are aluminum.

2) Super-Pak (sometimes referred to as mini pleat) fabricated in accordance with MIL F-51068E. The filter is 610 mm x 610 mm x 292 mm. Frame material is wood and the separators are aluminum. This filter contains significantly more media than the standard U.S. Design. Shallower pitch in the aluminum separators results in increased folds in the filter media and/or a higher density filter pack. The standard filter pack contains about 20.1 square meters media vs. about 28.8 square meters for the Super-Pak.

3) "Super-Flow" filter is a separatorless filter. The filter slug is constructed by pleating a continuous corrugated HEPA media. The corrugated web paper is folded in such a manner that the filter pack is supported by adjacent folds. This style filter contains approximately 22.8 square meters filter area. The filter size is 610 mm x 610 mm x 292 mm and frame material is metal.

4) European Style filter (hereafter referred to as a Cassette filter) uses shallow pleated, closely spaced filter media. The media folds are separated by strips. The filter slug is mounted into a cartridge. The cartridges are then stacked and sealed to form the filter element. The filter size is 610 mm x 610 mm x 292 mm and it contains approximately 37.2 square meters of filter media. Frame material is wood.

IV. Results and Discussion

Each filter was initially tested on the Q107 thermal DOP test system.[3] All filters were well below the .03% penetration for the 0.3 micron particles. The recorded values for this test are listed in Table I. In addition cold DOP tests were conducted on the installed filters to insure a good filter to frame seal.

Filter resistance readings were taken daily. If necessary, flow adjustments were made. In addition the high volume sampler paper is changed daily and dust deposit rate is determined by weighing sampler paper. All filter tests were run on clean filters.

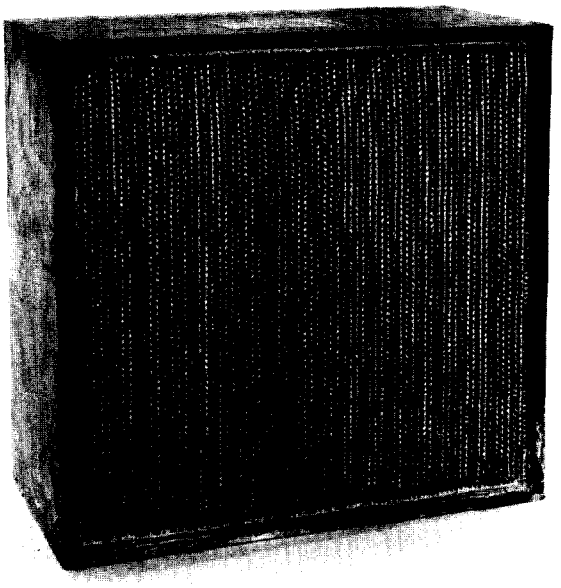

Figure 3A Spent filter - downstream and/or clean side (Standard U.S. Design).

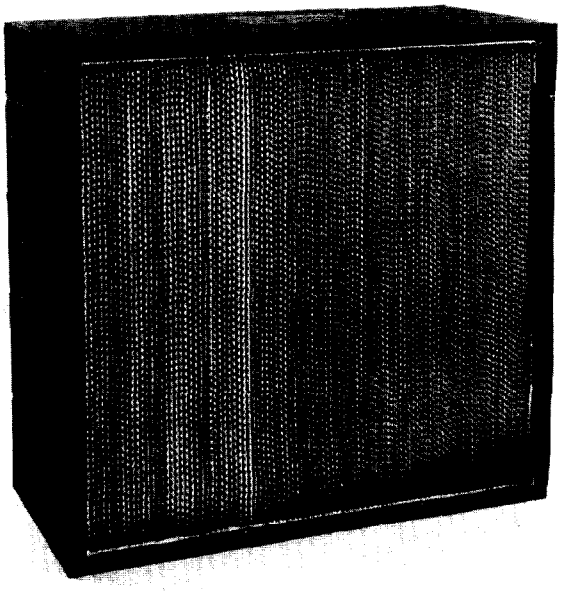

Figure 3B Spent filter - downstream and/ or clean side (Super-Pak).

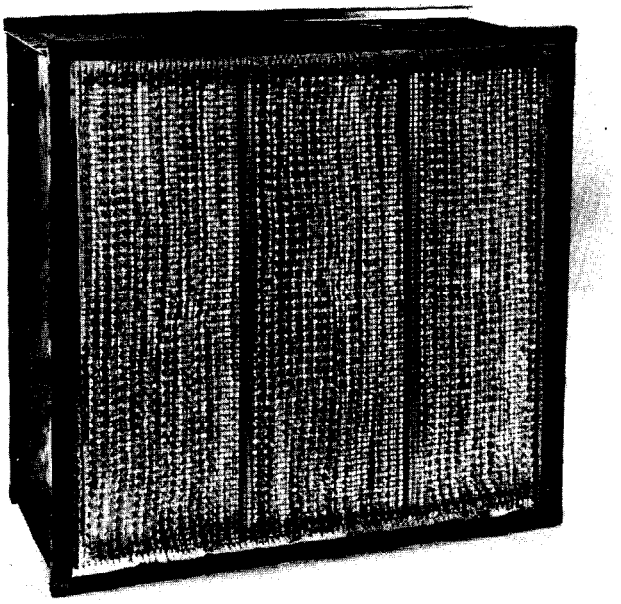

Figure 3C Spent filter - downstream and/ or clean side ("Super-Flow").

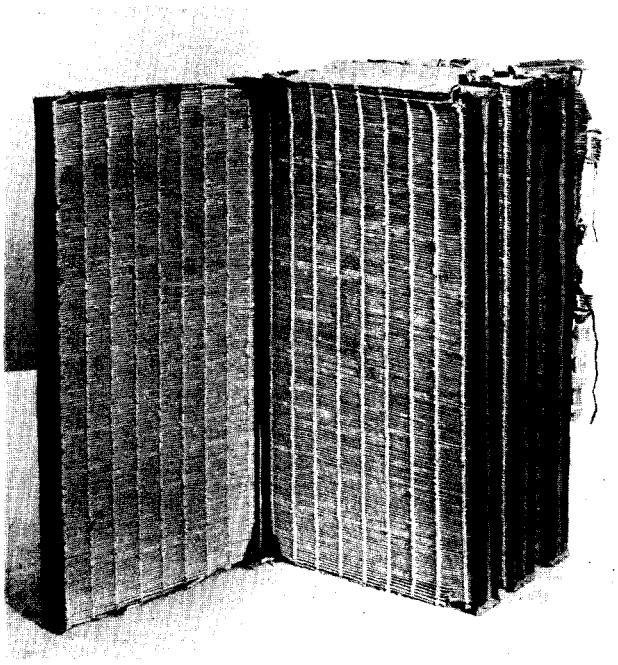

Figure 3D Spent filter - downstream and/ or clean side (Cassette).

Type Filter	Flow (CFM)	Media Area (Ft.^{2})	Media Vel. (FPM)	DOP % Eff.	Initial Pressure Drop (In. W.G.)	Final Pressure Drop (In. W.G.)	Dust Load (Grams)
Standard U.S. Design	1080	216	5	99.996	.92	3.00	1026
Super-Pak	1550	310	5	99.985	1.27	3.00	1140
"Super-Flow"	1250	250	5	99.985	1.03	3.00	840
Cassette	1950	390	5	99.995	1.10	3.00	1500
Cassette	2200	390	5.6	99.990	1.25	3.00	650
Cassette	1000	390	2.6	99.993	.42	.67	1050*

*Test still running.

Table I Atmospheric dust loading test results.

Atmospheric dust loading test results are shown on Table I and Figure 4. The Standard U.S. Design, Super-Pak and "Super-Flow" elements were tested at a filter media velocity of up to 5.6 FPM (1.70 meters per min.). The Cassette style was tested at 2.6, 5.0 and 5.6 FPM. The curves as shown are a best fit to the data obtained. Many reversible filter resistance changes were observed due to atmospheric conditions such as snow and rain which occurred during the test period. All tests were considered complete when the final filter resistance reached 3" (76.2 mm) water gage.

There is a marked difference in life when the Cassette filter is run at media velocities up to 5.6 FPM. At 5.0 FPM (1950 CFM) life is 10.2 months as compared to 3.9 months at 5.6 FPM (2200 CFM) or a factor of 2.6 to 1.0. The test at 2.6 FPM media velocity is not complete; however, the curves indicate life will be at the very least 7-10 times the life obtained at 5.6 FPM.

At media velocities of 5 FPM the "Super-Flow", Super-Pak, Cassette and Standard U.S. Design filters also show differences in life ranging from 8.8 months for the "Super-Flow" to 12.7 months for the U.S. Standard Design filter.

A visual examination of the spent filters was made. Figure 5 shows a section of the upstream side of the various filters. The Standard U.S. Design and Super-Pak were structurally sound. There was no evidence of pleat deformation. The "Super-Flow" showed pleat deformation with some sagging, nestling of filter folds, and sections of pleats adhering together. This results in loss of effective media area. The Cassette style filter also showed pleat deformation on the downstream side of the filter. The pleats had ballooned out which causes a corresponding reduction in filter media area.

The dust holding capacity of a filter depends on many factors including the following: initial pressure drop, type of filter media, media flow velocity or media area, type and particle size of dust filtered and environmental conditions. Filter configuration and design also play an important role.

In Table I the total dust load is listed for each filter tested. A comparison of the data on the filters run at 5 FPM media velocity shows that the U.S. Standard Design holds 1026 grams of dust. The Cassette filter held 1500 grams when tested at 5.0 FPM and only 650 grams when tested at 5.6 FPM. At 2.6 FPM it held 1050 grams even though the final pressure drop was only 0.67 inches water gage. This can be explained by the fact that the Cassette filter is subject to ballooning on the downstream side. This is a progressive phenomenon. As the filter loads the increasing pressure drop causes the two adjacent pleats of a fold to come into contact lowering the available media area. This condition is aggravated by increasing volume rates and adverse environmental conditions causing a loss in media tensile strength.

The "Super-Flow" filter which held 840 grams also showed pleat deformation because of configuration design. It appears that the filter media is not supported as well as it is in the U.S. Standard Design which employs aluminum separators.

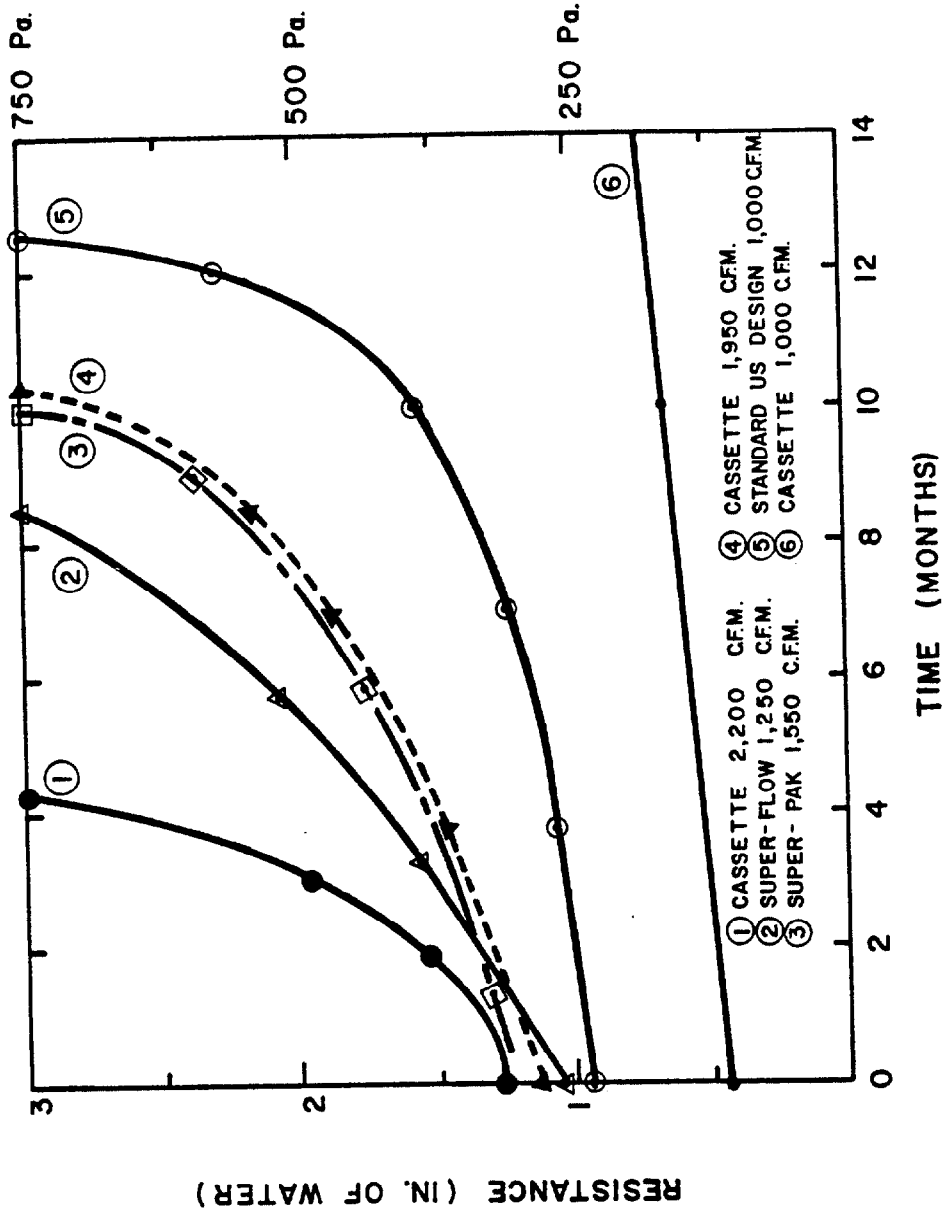

FIGURE 4 COMPARISON CURVES (RESISTANCE VS. TIME).

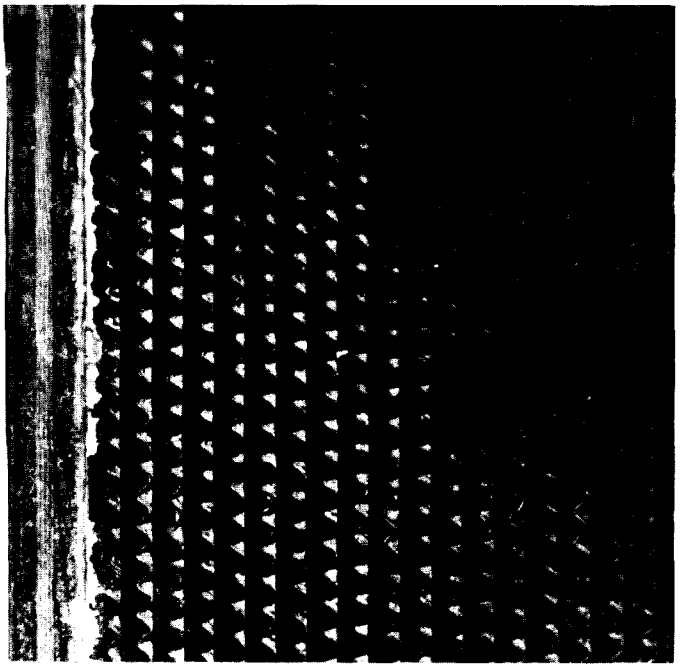

Figure 5A Spent filter - upstream and/or dirty side (Standard U.S. Design).

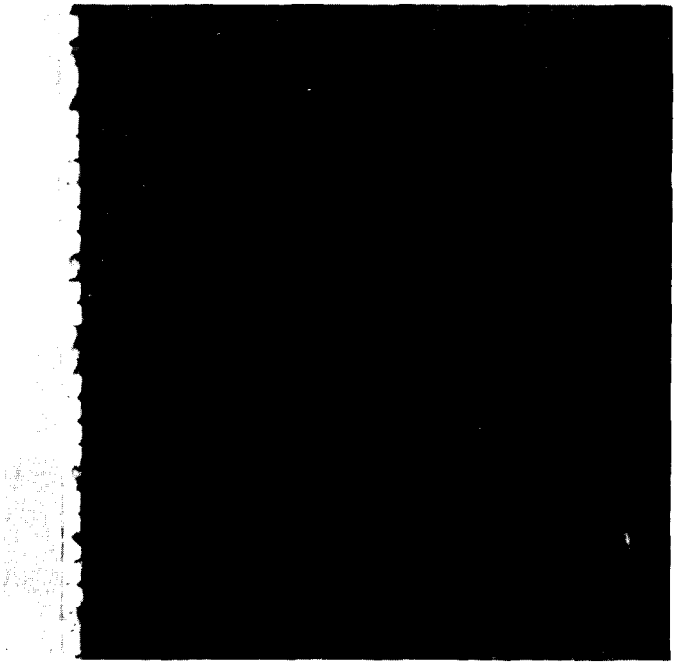

Figure 5B Spent filter - upstream and/ or dirty side (Super-Pak).

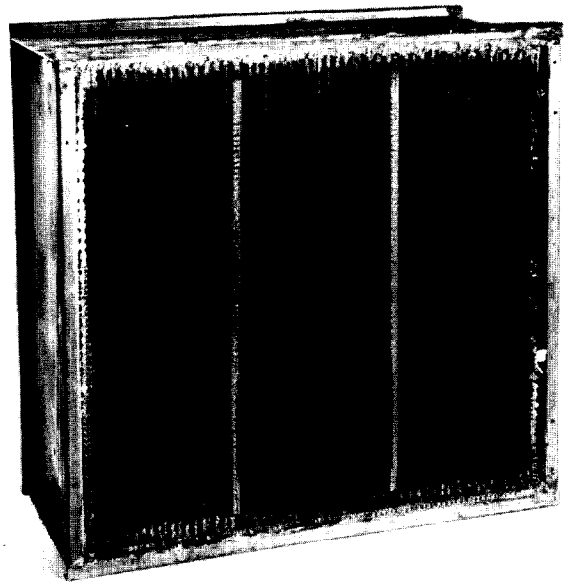

Figure 5C Spent filter - upstream and/ or dirty side ("Super-Flow").

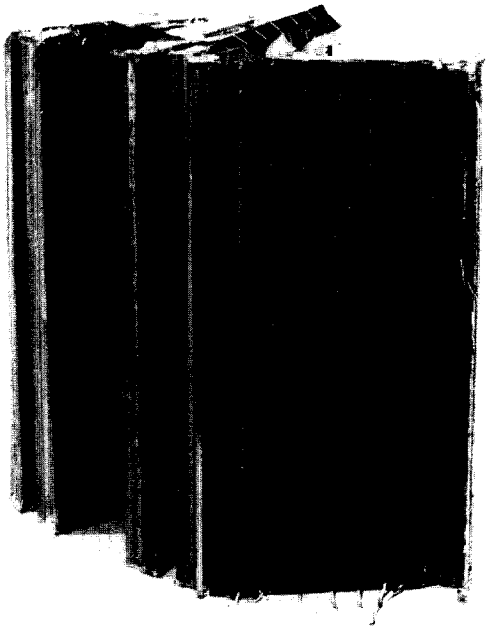

Figure 5D Spent filter - upstream and/ or dirty side (Cassette).

V. Performance Characteristics @ 1000 CFM

Frequently, it becomes desirable to operate filters below rated capacity. The advantages gained are longer filter life, reduced handling, and minimized space requirements for waste disposal.

The composite curves, Figure 6, show filter performance @ 1000 CFM. Curves (1), (3), and (4) - "Super-Flow", Super-Pak, Cassette Style, respectively were derived from the actual test data plotted in Figure 4 using the procedure outlined below. Curves (2) and (5) are the actual test data.

In an assembled filter the following equation represents the total clean pressure drop across the filter element.

$$\Delta P_t = \underbrace{\frac{\alpha_1 \text{ Vol.}}{A}}_{\text{Media Loss}} + \underbrace{\alpha_2 \text{ Vol.}^2}_{\text{K.E. Loss}} \qquad (1)$$

where:

ΔP_t = total pressure drop across filter

A = effective media area

Vol. = flow rate

α_1 α_2 = constants

The first term of the above equation is the media loss which is directly proportioned to the flow rate through the media. The second term is the kinetic energy loss which is created by the air entering, turning, and exiting from the filter element. For the flow ranges we are reporting, you normally can neglect the K.E. term for a good quality filter. Therefore, the total pressure drop (ΔP_t) is directly proportional to flow rate.

Non-linear conditions will exist in a filter design if you have an initial high K.E. loss, poorly supported media which results in an increase in α_2 with flow rate and compacting of the filter media which decreases the effective filtering media area. Furthermore, it should be noted that α_1 will increase as dust is collected on the filter media or pressure drop is directly proportional to dirty filter media.

If the dust challenge rate to the filter is essentially constant, which is the case in this program, then the pressure loss through the filter cartridge will be proportional to dust loading per unit filter media area or to time. Therefore, since the filter

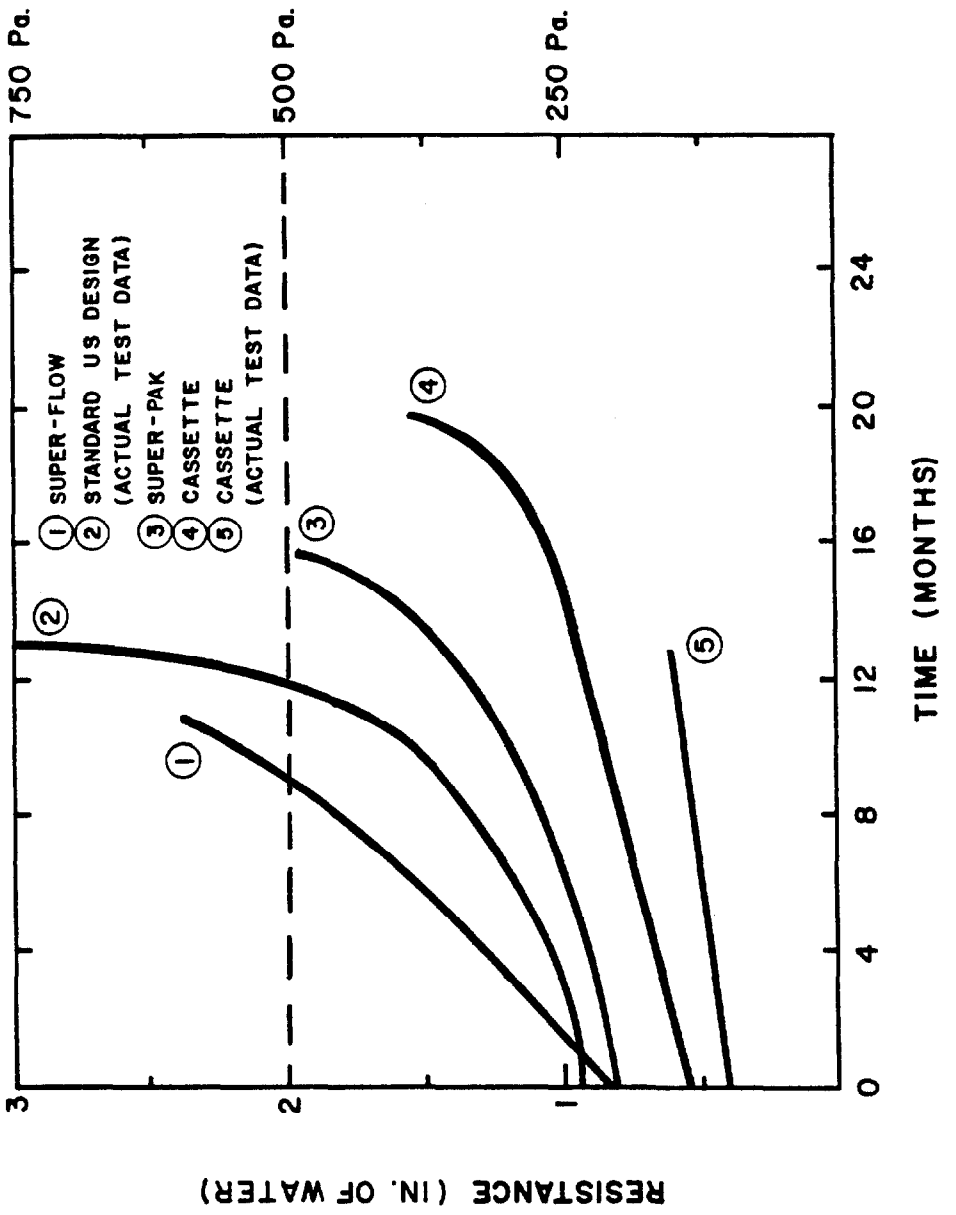

FIGURE 6 COMPARISON CURVES AT 1,000 CFM (RESISTANCE VS. TIME).

Filter Type	Actual Ordinance Points Taken from Figure 4		Calculated Performance Data @ 1000 CFM	
	t (Months)	ΔP (In. W.G.)	t (Months)	ΔP (In. W.G.)
"Super-Flow" Rated Flow - (1250 CFM)	0	1.04	0	0.832
	2	1.37	2.5	1.1
	5.5	2.0	6.88	1.6
	7	2.4	8.75	1.92
	8.5	3.0	10.6 ①	2.4 ②
Super-Pak and/or Mini Pleat Rated Flow - (1550 CFM)	0	1.1	0	0.564
	4	1.5	7.8	0.77
	7	1.8	13.65	0.92
	8	2.0	15.6	1.03
	10.2	3.0	19.9	1.54
Cassette Rated Flow - (1950 CFM)	0	1.1	0	0.564
	4	1.5	7.8	0.77
	7	1.8	13.65	0.92
	8	2.0	15.6	1.03
	10.2	3.0	19.9	1.54

① Calculated test data; i.e. $8.5 \times \frac{1250}{1000} = 10.6$ month

② Calculated test data; i.e. $3.0 \times \frac{1000}{1250} = 2.4$ in. W.G.

Table II Composite curves.

media area in a given filter element remains constant, one can use the above principal to construct filter performance at other flow conditions from a known filter loading curve. Note this procedure can only be used on well engineered filters. Table II tabulates performance data along with calculated data with examples on how the curves in Figure 6 were constructed.

It is evident from the composite curves that, if we use 2 inch or greater as the terminal pressure drop, filter life varies significantly between the various style filters when operating the filters at a reduced flow rate. Furthermore, comparing like filters (Figure 4 and Figure 6) you will observe the filter life increase for the "Super-Flow", Super-Pak, and Cassette filter is about 1.5, 2.5, and 4 times, respectively when operated at the reduced flow (1000 CFM).

VI. References

1. Dill, R.S., "A test method for air filters", National Bureau of Standards (1957), (ASHVE Transactions, Vol. 44, p. 379, 1938). ASHRAE 52-76, "Method of testing air-cleaning devices used in general ventilation for removing particulate matter", American Society of Heating, Refrigerating and Air Conditioning Engineers, Inc., United Engineering Center, 345 East 47th St., New York, NY 10017.

2. Military Specification MIL F-51068E, "Filter, particulate, high-efficiency, fire resistant".

3. U.S. Army, Edgewood Arsenal, Maryland, MIL-Q107-DOC136-300-175A, "Instruction manual for the installation, operation and maintenance of penetrometer filter testing, DOP, Q107".

PERFORMANCE OF 1000- AND 1800- CFM HEPA FILTERS ON LONG EXPOSURE TO LOW ATMOSPHERIC DUST LOADINGS. II

M.W. First and S.N. Rudnick
Harvard Air Cleaning Laboratory
Boston, Massachusetts

Abstract

Comparative tests were made to evaluate the performance characteristics of American- and European-design HEPA filters when exposed, for a number of years, to aerosols characteristic of nuclear and biohazard service. Although some of the European-design filters were operated at their rated airflow capacity of 1800 cfm, some were downrated to 1000 cfm to determine if their service life could be more than tripled compared to conventional 1000-cfm American-design HEPA filters, as filter theory predicts. Initial results indicate, however, that for the ambient aerosol used in this study, a European-design filter has a service life of only 1.6 times greater than an American-design filter when both operate at 1000 cfm. Further tests are in progress to verify this result.

Introduction

Comparative tests, which are a continuation of work reported previously[1], are in progress to evaluate the performance of American- and European-design HEPA filters when exposed continuously to ambient dust at about 200 feet above ground level. During 2½ years of testing, total suspended particulate matter at this location averaged 73 $\mu g/m^3$. American-design filters were operated at their 1000-cfm rated airflow capacity whereas European-design filters were operated either at their 1800-cfm rated airflow capacity or at 1000 cfm.

Prediction of HEPA Filter Life

An expression to predict L, the service life of an underrated European-design HEPA filter relative to that of an American-design filter when both operate at the rated airflow capacity of the American-design filter, is given by Equation 1:

$$L = \frac{\alpha^2(\beta H - H_o)}{\beta H - \alpha H_o} \qquad (1)$$

where α is the ratio of filter paper area in a European-design filter to that of an American-design filter, β is the ratio of rated airflow capacity of a European-design filter to that of an American-design filter, H is maximum acceptable pressure drop across the filter, and H_o is pressure drop of the clean European-design filter at its rated airflow capacity.

For the derivation of Equation 1, which can be found in the Appendix, pressure drop (ΔP) versus weight of collected dust (i.e., the performance curve) was assumed to be linear. Validity of this assumption depends primarily on dust composition and whether the air

passages between pleats bridge with dust. Rose and Rivers[2] found the performance curve to be nearly linear when filtering ASHRAE test dust without the lint component through HEPA filters. Flanders Filters, Inc.[3], however, published performance curves for HEPA filters cleaning ambient air from rural, urban, and industrial areas in which ΔP was concave downward when plotted versus dust weight whereas HEPA filter performance curves for fly ash with and without added lint given by Engle and Bauder[4] were concave upward.

An 1800-cfm rated European-design HEPA filter containing 1.8 times as much filter paper area as a 1000-cfm rated American-design HEPA filter and having a clean resistance at rated flow of 1 in.w.g. should have an extended service life at 1000 cfm relative to an American-design filter according to Equation 1 as follows:

Table I. Predicted service life of underrated European-design HEPA filter.

Maximum Allowable ΔP in.w.g.(H)	Relative Life (L)
1.5	6.1
2.0	4.7
3.0	4.0
4.0	3.7
5.0	3.6

Longer predicted service life for an underrated European-design filter, particularly when fan capacity is small, is attributable to lower dust deposit rate per unit area as well as lower filtration velocity through paper plus accumulated dust deposit.

Description of Aerosol

The concentration of atmospheric dust, i.e., total suspended particulate matter (TSP), sampled continuously in the vicinity of the HEPA filters with high volume air samplers[5] averaged 73 $\mu g/m^3$. Thirty-day average TSP concentrations, plotted in Figure 1, were somewhat lower during the initial period (1978) than more recently. This difference is attributed to street construction work over the past year and a half in the vicinity of the filter exposure stations.

A typical accumulation of dust on a European-design HEPA filter exposed for 9 months is shown in Figure 2. Fibrous material is evident despite the lack of human activity near the HEPA filters.

Results

Tests on 8 American- and European-design HEPA filters have been completed. The chronology of the tests is indicated on the TSP concentration plot (Figure 1), pressure drop versus time curves are plotted in Figure 3, and results are summarized in Table II. For comparison purposes, a pressure drop (ΔP) of 3 in.w.g., which is close to the maximum static pressure some of the blowers could generate and still maintain the desired airflow rate, was chosen as the

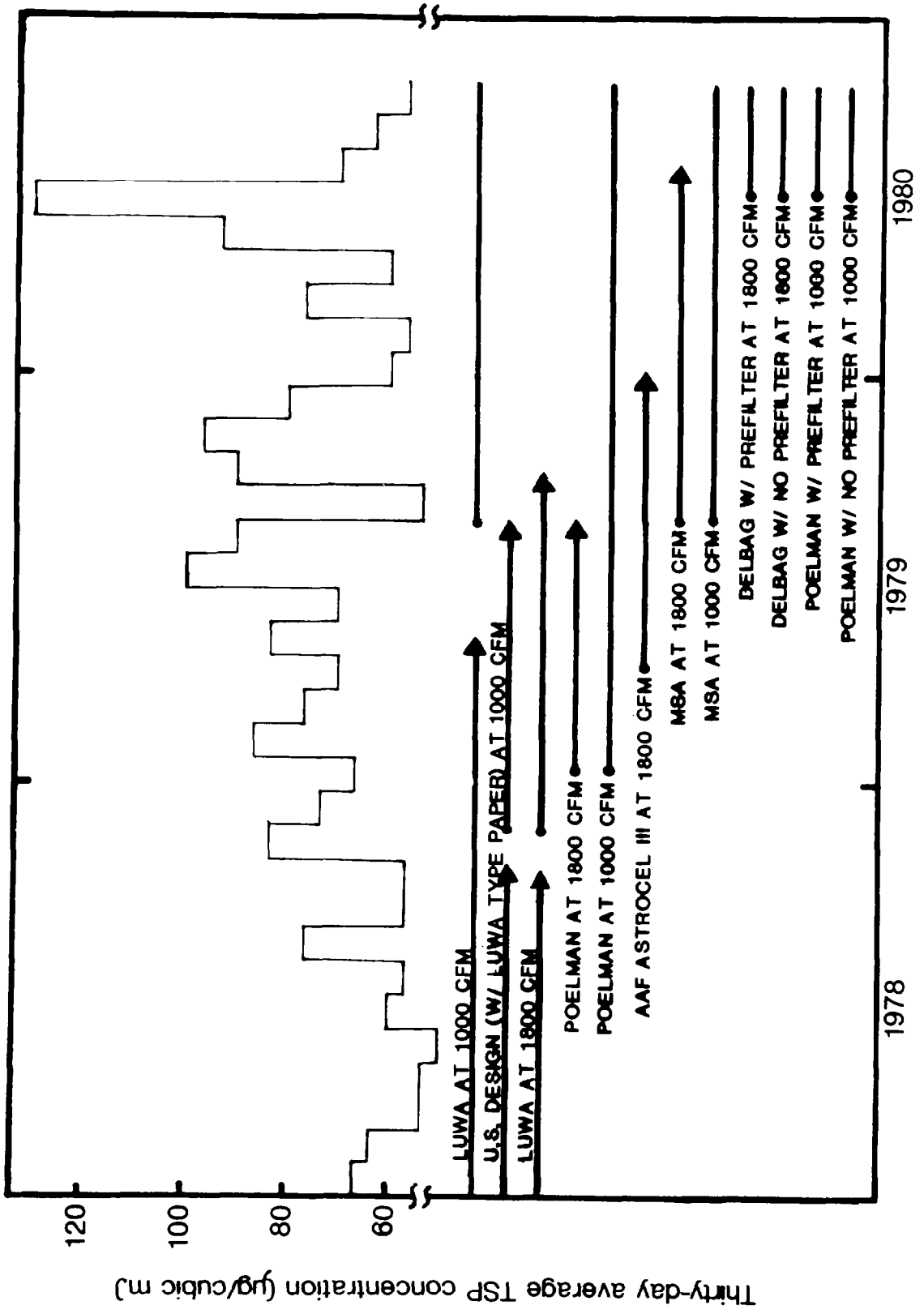

FIGURE 1. CHRONOLOGY OF TSP CONCENTRATION & HEPA FILTER TESTS

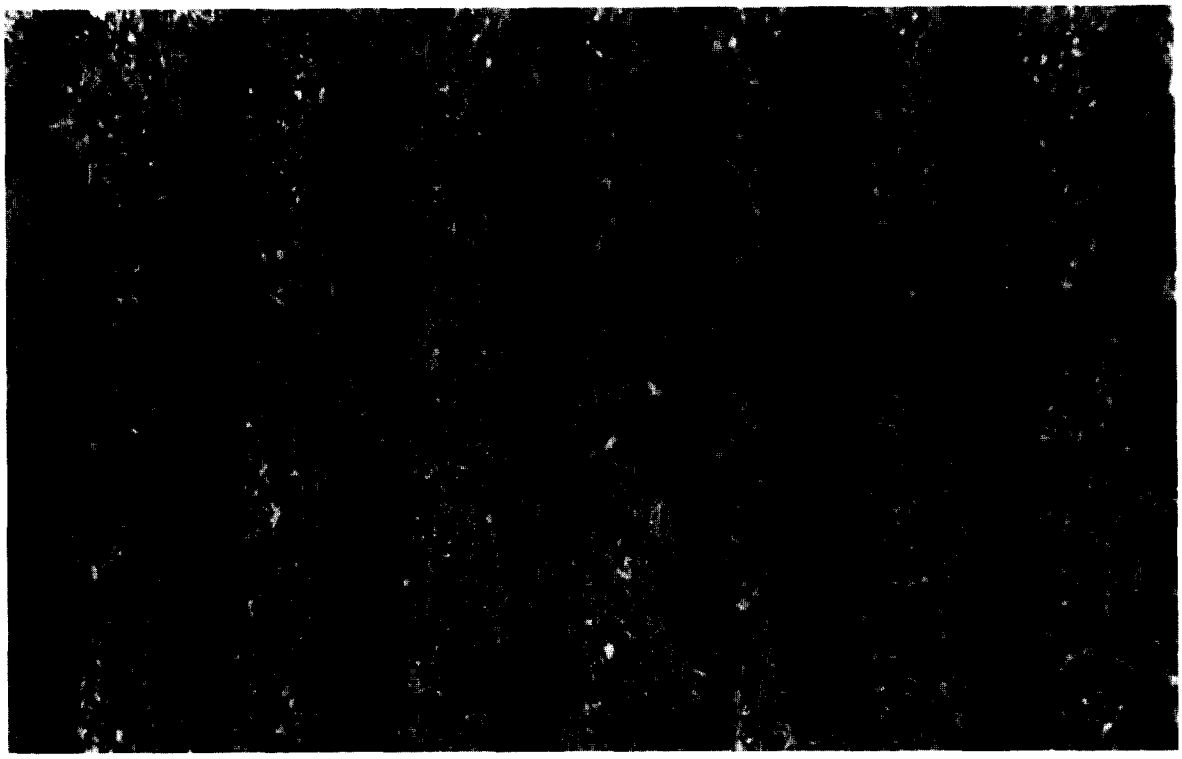

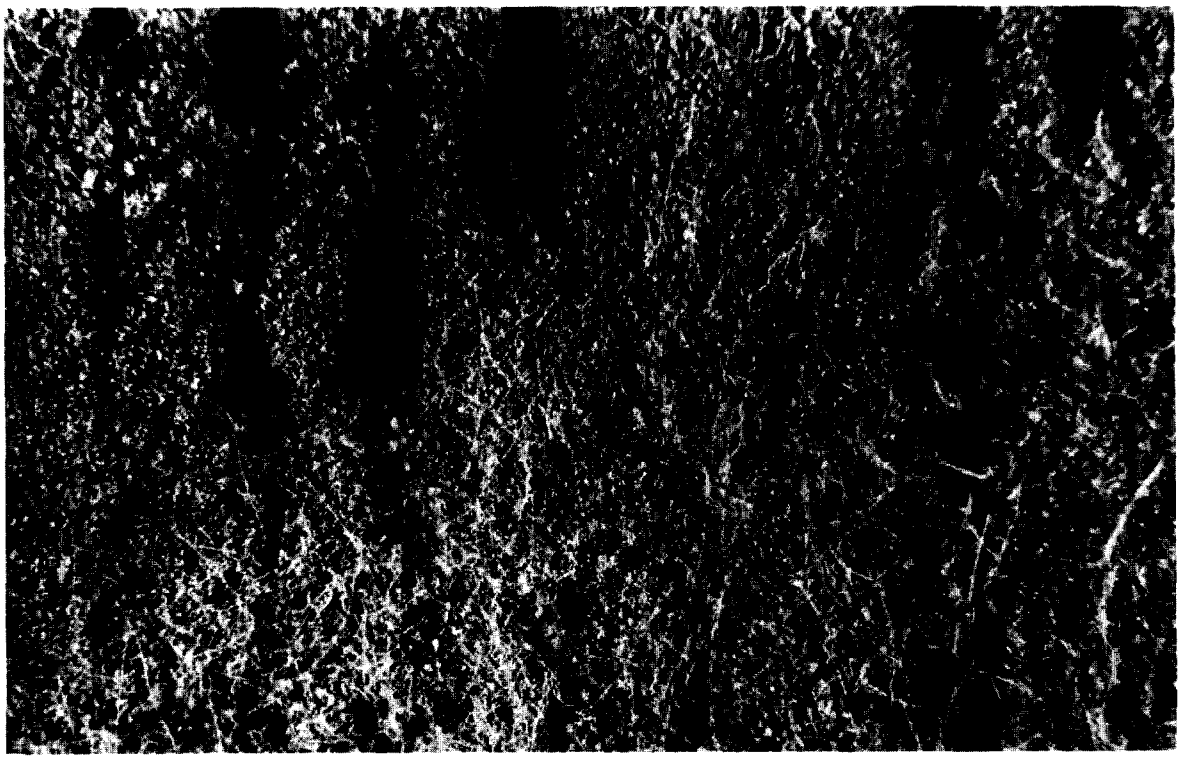

FIGURE 2. PHOTOGRAPH AT 7X MAGNIFICATION SHOWING DUST DEPOSIT BRIDGING PLEATS OF EUROPEAN-DESIGN HEPA FILTER THAT WAS SHUT DOWN BECAUSE OF EXCESSIVE AIRFLOW RESISTANCE. (TOP PHOTOGRAPH: TYPICAL AREA; BOTTOM PHOTOGRAPH: AREA TOWARD THE BACK OF V-SHAPED ENTRANCE PLENUM OF FILTER.)

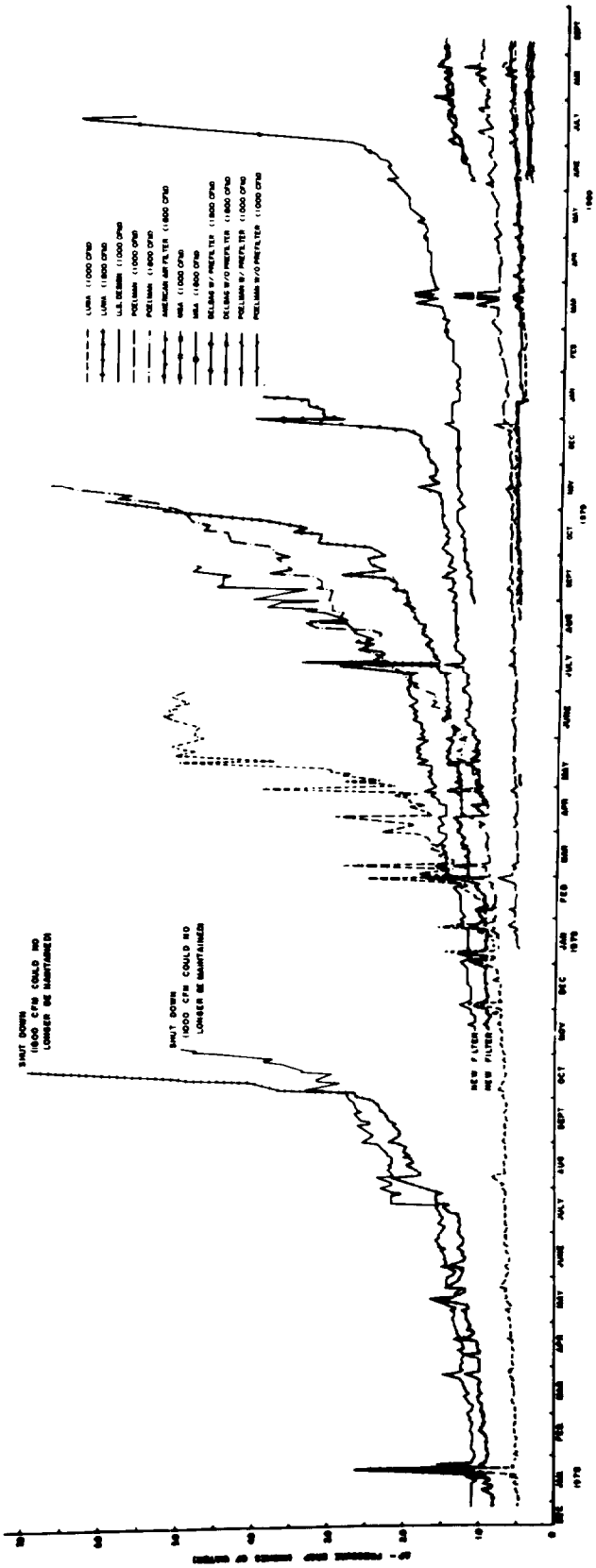

FIGURE 3. AIRFLOW RESISTANCE VARIATION WITH SERVICE TIME.

Table II. Summary of results.

HEPA Filter Brand	Airflow (cfm) Rated Capacity	Airflow (cfm) Test Rate	Startup Date	Initial Pressure Drop (in.w.g.)	Time to 3 in.w.g. (months)	Dust Weight (lb) 2 in. w.g.	Dust Weight (lb) 3 in. w.g.	Dust Weight (lb) 4 in. w.g.	Dust Weight (lb) 5 in. w.g.	Dust Weight (lb) 6 in. w.g.
American Design[a]	1000	1090	12/29/77	1.10	9.63	1.16	1.70	1.77	1.81	b
Luwa	1770	1000	12/29/77	0.49	16.3	2.87	2.95	3.02	3.19	b
Luwa	1770	1800	12/29/77	0.82	9.20	2.36	2.69	2.74	2.77	b
American Design[a,c]	1000	1090	11/17/78	1.10	9.07	1.72	2.14	2.23	b	b
Luwa[c]	1770	1800	11/17/78	0.92	10.6	3.63	4.03	4.25	4.33	b
Poelman	1770	1830	1/10/79	0.77	7.39	2.37	3.00	3.45	3.74	3.93
AAF	2000	2030	4/11/79	0.84	8.57	3.80	3.86	4.01	b	b
MSA	2000	1890	8/20/79	1.15	10.3	3.31	4.19	4.22	4.25	b

[a](with Luwa-type paper)
[b]not available
[c]replicated test

terminal ΔP for the filter's service life, although some filters were not shut down until they reached nearly 7 in.w.g. Where resistance figures at higher than 3 in.w.g. are available, they are also shown in Table II.

Two of the tests shown in Table II were replicated. The American-design HEPA filter using Luwa-type filter paper that went on line 29 December 1977 collected 1.70 lb of dust during 9.6 months of operation whereas an identical filter, also shown in Table II, was started up on 17 November 1978 and collected 26% more dust in 17 fewer days. This difference may be due to differences in particle size as a result of ground-level construction work, which is believed to be also responsible for high TSP concentrations and which, for the most part, occurred during the testing of the replication but not the original filter (see Figure 1). It would be expected that the larger the dust particles, the higher would be the dust-holding capacity of the filter[6]. The same reasoning applies to a similar result for the Luwa filters operated at their rated 1800-cfm airflow capacity. The second filter collected 50% more dust than the original (2.69 versus 4.03 lb) over a 15% longer test period before reaching 3 in.w.g. resistance. Other European-design HEPA filters that operated at 1800 cfm, i.e., Poelman, AAF, and MSA, had collected 3.00, 3.86, and 4.19 lb of dust, respectively, by the time they reached 3 in.w.g. As may be seen from Figure 1, they operated simultaneously over only part of their testing period except for the Poelman filter that was started up after the beginning of the second Luwa filter test at 1800 cfm and shut down before the end of this same test.

The longest-lived HEPA filter tested thus far was an 1800-cfm rated Luwa filter that operated at 1000 cfm. It went on-line 29 December 1977 and had collected 2.95 lb of dust when its ΔP reached 3 in.w.g. after 16.3 months of operation. The relative service life, L, of this underrated Luwa HEPA filter can be compared to that of the American-design HEPA filter because both used the same filter paper and operated at the rated airflow capacity of the American-design filter; i.e.,

$$L = 2.95 \text{ lb}/1.70 \text{ lb} = 1.74 \qquad (2)$$

based on the original test of the American-design filter, and

$$L = 2.95 \text{ lb}/2.14 \text{ lb} = 1.38 \qquad (3)$$

based on the repeat test. Because of the probable influence of differences in particle size as result of ground-level construction, the comparison should be made on American-design and Luwa filters that were operated simultaneously throughout, although this was not possible. As an alternative, the values for the two American-design filters from Figure 1 can be proportioned depending on the time each was operating simultaneously with the Luwa that ran at 1000 cfm. When this is done, it gives a service life, L, of 1.58.*

*1.70 lb (0.632) + 2.14 lb (0.368) = 1.86 lb
L = 2.95 lb/1.86 lb = 1.58

Discussion

When the performance curve, i.e., plot of ΔP versus dust mass, for either an American- or European-design HEPA filter is known, the performance curve for the other can be predicted at any airflow rate. For example, the experimental performance curve for the 1800-cfm rated Luwa filter that operated at 1000 cfm is plotted in Figure 4. It was linear during the initial two thirds of the test, and thereafter, ΔP increased exponentially; this type of behavior occurred for all HEPA filters tested thus far. Now, suppose that this filter had operated at 1800 cfm. Inasmuch as the relationship between ΔP and airflow velocity is linear for both the paper and dust deposit, a deposit that causes a 1.67 in.w.g. ΔP at 1000 cfm would result in a 3 in.w.g. ΔP at 1800 cfm (i.e., 3 in.w.g. x 1000 cfm/1800 cfm = 1.67 in.w.g.). If the structure of the dust deposit is assumed to be independent of filtration velocity,* this last statement would also be correct when the dust was filtered at 1800 cfm. Therefore, from Figure 4, at 1800 cfm, the Luwa filter would be expected to collect 2.67 lb of dust when its ΔP reached 3 in.w.g. This value is in good agreement with the original test on the Luwa filter operated at 1800 cfm, which collected 2.69 lb of dust at 3 in.w.g. ΔP, but not the repeat test filter that collected 4.03 lb of dust. This difference probably occurred because of an increase in ambient dust size as a result of ground-level construction work.

Consider now the 1000-cfm rated American-design HEPA filter that was fabricated from the same filter paper used in the Luwa HEPA filter. Inasmuch as the filtration velocity must not exceed approximately 5 fpm in order for the ΔP to be less than 1.0 in.w.g., the filter paper area would have to be reduced by a factor of 0.555 (i.e., 1000 cfm/1800 cfm = 0.555). Therefore, at 1000 cfm, the mass of dust collected at 3 in.w.g. would be expected to be that factor times the dust mass collected on a Luwa filter at 1800 cfm and 3 in. w.g. or 1.48 lb (i.e., 2.67 x 0.555 = 1.48 lb). During tests on American-design HEPA filters fabricated from Luwa-type paper, however, 1.70 lb dust was collected during the original test and 2.14 lb during the repeat test.

The service life (L) of an underrated Luwa filter compared to that of an American-design filter when both operate at the rated airflow capacity of the latter can now be predicted from a knowledge of the performance curve in Figure 4: i.e.,

$$L = 2.95 \text{ lb}/1.48 \text{ lb} = 1.99 \qquad (4)$$

Conclusions and Summary

The primary objective of the present work was to evaluate how often a European-design HEPA filter would require replacement if it were substituted for an American-design HEPA filter cleaning 1000 cfm of ambient air. Table III shows a comparison of experimental results

*In actuality, for a specified airflow velocity and dust mass, the lower the filtration velocity (i.e., velocity at which the dust is filtered), the lower the ΔP would be expected to be, although this dependency is probably very weak.(7)

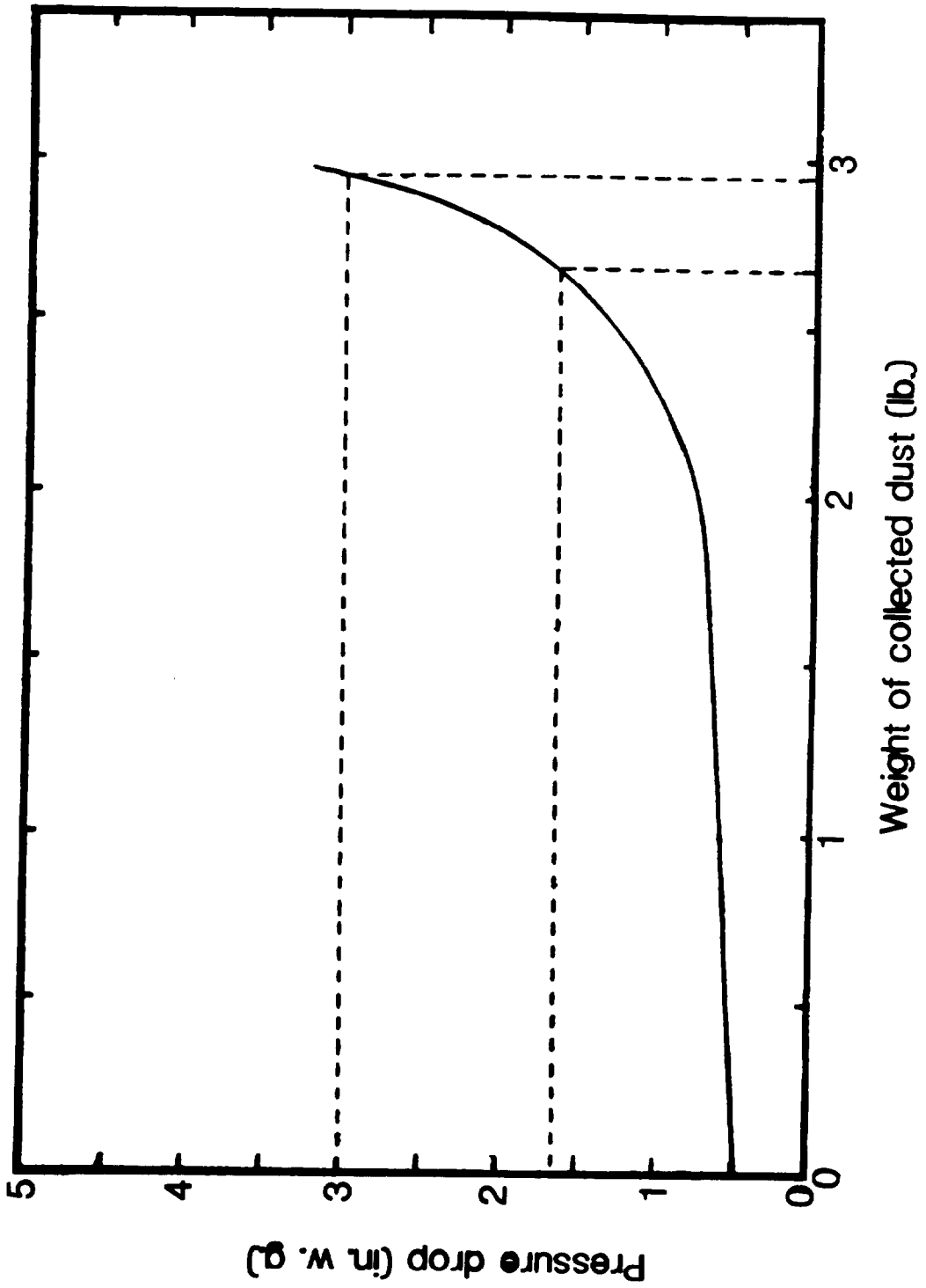

FIGURE 4. PERFORMANCE CURVE FOR LUWA FILTER AT 1000 CFM

obtained thus far and various predictions that can be made:

Table III. Service life of Luwa HEPA filter relative to American-design filter, both operated at 1000 cfm (L).

Experimental result	1.58
Predicted from performance curve of Luwa filter operated at 1000 cfm, i.e., Figure 4	1.99
Predicted from linear performance curve, i.e., Equation 1	3.96

Experimentally, a European-design HEPA filter operated at 1000 cfm was found to have a service life 1.6 times greater than an American-design HEPA filter at the same flow rate. Equation 1, which assumes a linear performance curve, would predict that the European-design filter lasts 4 times longer than the American-design filter. Although the performance curves were linear during the initial exposure period, the pressure drop thereafter increased rapidly and at an accelerating rate. Thus the lower filtration velocity and lower initial pressure drop of the Luwa filter when operated at 1000 cfm had little effect at the end of the filter's service life. Nevertheless, a factor of at least 1.8 was expected on the basis of the increase in filter paper area alone. Fibrous dust, however, tends to bridge the space between pleats, thus decreasing the filter's dust-holding capacity.(8) Because the European-design filter has smaller spaces between pleats, it may be more vulnerable to bridging by the fibrous component of ambient dust than the American-design filter. Relative to an American-design HEPA filter, the predicted service life of a Luwa HEPA filter based on its performance curve at 1000 cfm may have also been optimistic for the same reason.

Continuing Work

The HEPA filter testing program using ambient dust loadings is continuing; Table IV summarizes this work. The Luwa HEPA filter operating at 1000 cfm is a replication of a previous test; the Poelman and MSA HEPA filters operating at 1000 cfm are being tested to obtain comparisons with their performance at 1800 cfm, shown in Table II. These three filters have all performed better thus far than the only other European-design HEPA filters that we have tested at 1000-cfm, a Luwa filter whose performance curve is shown in Figure 4. Tests shown in Table IV are also being run with European-design Delbag HEPA filters operating at 1800 cfm with and without prefilters and European-design Poelman HEPA filters operating at 1000 cfm with and without prefilters. The prefilters are expected to expand significantly the life of these filters; this increase in life will be analyzed in the same manner as the filter's performance without prefilters.

Table IV. Operating HEPA filters.

Filter Brand	Rated Airflow Capacity (cfm)	Test Airflow Capacity (cfm)	Start-Up Date	Initial Pressure Drop (in.w.g.)	Pressure Drop in.w.g.	Dust Wt. (lb)
Poelman HEPA filter	1770	1000	1/10/79	0.50	1.15	4.23
Luwa HEPA filter	1770	1000	8/16/79	0.52	0.73	2.63
MSA HEPA filter	2000	1000	8/20/79	0.53	0.77	2.61
Delbag HEPA filter	1770	1800	6/3/80	1.13	1.62	0.95
Delbag HEPA filter plus prefilter[a]	1770	1800	6/3/80	1.17[b]+0.35[c]	1.62[b]+1.15[c]	0.95[d]
Poelman HEPA filter	1770	1000	6/4/80	0.45	0.48	0.52
Poelman HEPA filter plus prefilter[a]	1770	1000	6/4/80	0.51[b]+0.11[c]	0.53[b]+0.40[c]	0.52[d]

[a]Two-inch thick, polyester fiber pad; 40-denier (∿ 66 μm) fibers upstream and 4-denier (∿ 21 μm) fibers downstream

[b]Across HEPA filter

[c]Across prefilter

[d]Total for HEPA filter plus prefilter

APPENDIX

Effect of varying airflow rate or filter paper area in a HEPA filter: derivation of predicative equations

Nomenclature

a	area of filter paper, ft^2
A_x, A_y	filter paper area of HEPA filters X and Y, respectively, ft^2; $A_x > A_y$
H	maximum acceptable pressure drop across a HEPA filter, lb_f/ft^2
H_o	pressure drop through clean HEPA filter X at airflow rate Q_x, lb_f/ft^2
k_1	resistance coefficient for clean filter paper, ft^{-1}
k_2	specific resistance coefficient of dust deposit, ft/lb
m	mass of dust collected on filter paper, lb
M_x	mass of dust collected by HEPA filter X at airflow rate Q_x when pressure drop reaches H, lb
M'_x	mass of dust collected by HEPA filter X at airflow rate Q_y when pressure drop reaches H, lb
M_y	mass of dust collected by HEPA filter Y at airflow rate Q_y when pressure drop reaches H, lb
Q_x, Q_y	airflow rates through HEPA filters X and Y, respectively, ft^3/min (i.e., cfm); $Q_x > Q_y$
L	service life of HEPA filter X relative to HEPA filter Y when both are operated at airflow rate Q_y, dimensionless
V	filtration velocity, i.e., superficial velocity across the filter paper, ft/min (i.e., fpm)
α	A_x/A_y, dimensionless
β	Q_x/Q_y, dimensionless
ΔP	pressure drop, lb_f/ft^2
μ	gas viscosity, lb/ft·min

Derivation

Gas flow through a dust deposit on cloth or paper substrate is governed by D'Arcy's Law, which can be expressed as follows:[6]

$$\Delta P = k_1 \mu V + k_2 \mu V \frac{m}{a} \qquad \text{(A1)}$$

The first term on the right side of Equation A1 gives pressure drop across the clean substrate whereas the second term gives pressure drop resulting from the dust deposit. For HEPA filter X operated at airflow rate Q_x, when the maximum acceptable pressure drop is H, Equation A1 becomes

$$H = k_1 \mu \frac{Q_x}{A_x} + k_2 \mu \frac{Q_x}{A_x} \frac{M_x}{A_x} \tag{A2}$$

When the filter is clean, Equation A2 reduces to

$$H_o = k_1 \mu \frac{Q_x}{A_x} \tag{A3}$$

Combining Equations A2 and A3 by eliminating $k_1\mu$ gives an expression for the mass of dust collected on filter X at airflow rate Q_x and pressure drop H:

$$M_x = \frac{A_x^2 \ (H-H_o)}{k_2 \mu Q_x} \tag{A4}$$

When filter X is operated at airflow rate Q_y, which is less than Q_x, until reaching maximum acceptable pressure drop H, Equation A1 becomes

$$H = k_1 \mu \frac{Q_y}{A_x} + k_2 \mu \frac{M'_x}{A_x} \frac{Q_y}{A_x} \tag{A5}$$

The structure of the dust deposit, i.e., k_2, is assumed to be independent of filtration velocity V in Equation A6.* Combining Equations A3 and A5 by eliminating k_1 and μ gives an expression for the mass of dust collected on filter X at airflow rate Q_y and pressure drop H:

$$M'_x = \frac{A_x^2 \ (H-H_o/\beta)}{k_2 \mu Q_y} \tag{A6}$$

When the performance curve, i.e., plot of pressure drop versus mass of collected dust, is linear--that is, k_2 is constant--Equations A4 and A6 can be combined by eliminating k_2 and μ; this gives an expression for the mass of dust collected at airflow rate Q_y compared to that at Q_x for a specified maximum acceptable pressure drop H:

$$M'_x / M_x = (\beta H-H_o)/(H-H_o) \tag{A7}$$

Any consistent units of pressure may be used for H and H_o in Equation A7.

For example, if Q_x = 1800 cfm, Q_y = 1000 cfm, H = 3 in.w.g., and H_o = 1 in.w.g., then $M'_x / M_x = 2.2$; i.e., if 3 in.w.g. is the maximum acceptable measure pressure drop, 2.2 times as much dust should be collected on a European-design HEPA filter at 1000 cfm than at 1800 cfm.

When HEPA filter Y, which has a filter paper area A_y that is

*In actuality, the lower the filtration velocity (i.e., velocity at which the dust is filtered), the lower k_2 would be expected to be, although this dependency is probably very weak.[7]

less than A_x, is operated at airflow rate Q_y and maximum acceptable pressure drop H, Equation A1 becomes

$$H = k_1 \mu \frac{Q_y}{A_y} + k_2 \mu \frac{Q_y}{A_y} \frac{M_y}{A_y} \tag{A8}$$

Combining Equations A3 and A8 by eliminating $k_1\mu$ yields

$$M_y = \frac{A_y^2 \, [H - H_o(\alpha/\beta)]}{k_2 \mu Q_y} \tag{A9}$$

If the performance curve is assumed to be linear (i.e., k_2 is constant), then the service life (i.e., time until pressure drop reaches 3 in.w.g.) of HEPA filter X relative to HEPA filter Y, when both are operated at airflow rate Q_y, can be predicted by dividing Equation A6 by Equation A9:

$$L = M'_x / M_y = \frac{\alpha^2 (\beta H - H_o)}{\beta H - \alpha H_o} \tag{A10}$$

Any consistent units of pressure may be used for H and H_o in Equation A10.

For example, if Q_x = 1800 cfm, Q_y = 1000 cfm, H = 3 in.w.g., H_o = 1 in.w.g., A_x = 360 ft^2, and A_y = 200 ft^2, then L = 4.0; i.e., if 3 in.w.g. is the maximum acceptable pressure drop, an underrated European-design HEPA filter should last 4 times as long as an American-design HEPA filter when both operate at 1000 cfm.

Literature Cited

1. First, M.W. and Leith, D., "Performance of 1000 and 1800 cfm HEPA filters on long exposure to low atmospheric dust loadings," in Proceedings of the Fifteenth ERDA Air Cleaning Conference, Boston, MA, 7-10 August 1978, CONF-780819, NTIS, Springfield, VA, pp. 1185-90 (1979).

2. Rose, C.E. and Rivers, R.D., "Performance and environmental characteristics of a compact, high-capacity HEPA filter design," in Proceedings of the Fifteenth ERDA Air Cleaning Conference, Boston, MA, 7-10 August 1978, CONF-780819, NTIS, Springfield, VA, pp. 1176-84 (1979).

3. Flanders catalogue, Air Filtration Products, Flanders Filters, Inc., Washington, NC, p.1.25.

4. Engle, Jr., P.M. and Bauder, C.J., "Characteristics and application of high performance dry filters," ASHRAE J., 6(5):72-5(1964).

5. United States Environmental Protection Agency, "National primary and secondary ambient air quality standards," in Federal Register, 36(84), p. 8186, Washington, D C (1971).

6. Iinoya, K and Orr, Jr., C., "Filtration," in Air Pollution, Vol. IV, 3rd ed., A.C. Stern, Ed., Academic Press, New York, pp. 155-6 (1977).

7. Rudnick, S.N., Fundamental Factors Governing Specific Resistance of Filter Dust Cakes, Doctoral Dissertation, Harvard School of Public Health, Boston, MA, p. 106 (1978).

8. Burchsted, C.A.,Kahn, J.E., and Fuller, A.B., Nuclear Air Cleaning Handbook, ERDA 76-21, NTIS, Springfield, VA, p. 43 (1976).

Acknowledgement

This work was supported by the U.S. Department of Energy under contract number EY-76-S-02-3049.

DISCUSSION

GEER: I would like to ask if you analyzed those long fibers which appeared to be contributing to the bridging of the filters. We conducted a similar experiment many years ago on intake filters in a more open country setting and I do not remember any fibers like that.

FIRST: We did look at them critically and we examined them under electron microscopy and by other physical methods. I am afraid we don't know what they are or where they came from. We are at a complete loss to know how they got up to 200 feet.

GEER: Were the fibers human hair?

FIRST: It was not human hair because there is nobody ever up on that roof except our own people, who go up just for a brief time to change the daily filters for the total suspended particulate measurement. Absolutely no human contribution from the roof. Obviously, it is coming from the ground, but I do not know how. There must be a lot of fibers in the air that we are not aware of.

A PRELIMINARY ASSESSMENT OF THE DUST LOADING VERSUS PRESSURE DROP CHARACTERISTIC OF HIGH CAPACITY HEPA FILTERS

R. P. Pratt
U.K. Atomic Energy Authority
Harwell, England

Abstract

A design of High Efficiency Particulate Air (HEPA) filter offering enhanced flow capacity on conventional deep-pleat designs has been developed in Europe and is now available from several manufacturers. These filters offer significant reductions in the physical size of filtration installations and are also claimed to have an extended service life.

Dust loading versus pressure drop tests have been carried out on filters from two manufacturers using both ASHRAE and BS 2831 No. 2 test dusts at a flow rate of 3400 m^3/h and also downrated to 1700 m^3/h. Similar tests have been carried out on conventional deep-pleat design filters rated at 1700 m^3/h as a datum base for a comparison of performance for the two designs.

These initial results suggest that the high capacity filter might be used to advantage by plant designers in one of two ways. A significantly greater dust loading and hence filter life can be obtained by operating the filters at half their rated capacity. Alternatively the high flow rates can be used to reduce the size of a given installation but with a resulting reduction in the life of the filter.

Unexpectedly large differences were found between the filters from the two sources. This suggests that further work is required to compare products from all sources in order to optimise the potential savings from adoption of the new design.

I. Introduction

The standard HEPA (High Efficiency Particulate Air) filter used within the United Kingdom nuclear industry is of the conventional deep-pleat design rated at 1700 m^3/h (1000 cfm) with a pressure drop of 25 mm water gauge at start of life.

An alternative design has been developed by Sofiltra-Poelman, in France, which enables a greater area of filter media to be contained within the same physical dimensions as the deep-pleat filter, and hence offers a greater flow capacity for the same initial pressure drop. Thus the new design offers potentially smaller filter installations, fewer filters for ultimate disposal and hence significant cost savings over the conventional design(1).

Several manufacturers both in Europe and the USA are now producing high capacity filters similar to the Sofiltra-Poelman design and considerable interest is being aroused over their use.

The most crucial factor in the analysis of potential cost savings through the adoption of the high capacity filter lies in its dust loading versus pressure drop characteristic, and hence predicted life compared with the conventional filter.

A preliminary test programme has been carried out to determine the dust loading versus pressure drop characteristics of high capacity filters from two sources using standard test dusts, at a flow rate of 3400 m^3/h and also downrated to 1700 m^3/h. Similar tests were carried out on a conventional deep-pleat filter to give a reference datum from which to compare the performance of the high-

capacity filter.

II. Description of Filters Tested

The test programme was confined to two basic filter designs, the "deep-pleat" conventional design and the "high-capacity" design, and one physical size, 610 mm x 610 mm x 292 mm. Manufacturers' data on the three filter types tested are given in Table I.

Table I. Manufacturers' data on filters tested.

Parameter	Sofiltra	Luwa	Vokes
Filter type	1506-26	NS-30-ti	66-MAD-5-DS
Efficiency	99.99%	99.97%	99.95%
Area of paper	42 m^2	36 m^2	18.5 m^2
Temperature limit	200°C continuous	220°C continuous	250°C continuous; 500°C - 10 min.
Nominal pressure drop limit	100 mm H_2O	80 mm H_2O	150 mm H_2O no deterioration 250 mm H_2O burst pressure
Rated air flow	3000 m^3/h @ 25 mm H_2O	3000 m^3/h @ 25 mm H_2O	1700 m^3/h @ 27 mm H_2O
Pressure drop ~ flow	1000 m^3/h @ 7 mm H_2O 1800 m^3/h @ 13 mm H_2O 3000 m^3/h @ 25 mm H_2O	1800 m^3/h @ 15 mm H_2O 3000 m^3/h @ 25 mm H_2O	1000 m^3/h @ 15 mm H_2O 1700 m^3/h @ 25 mm H_2O -
Physical pleat size	18 mm deep x 3 mm pitch	25 mm deep x 2.5 mm pitch	285 mm deep x 5 mm pitch
Number of "packs"	16	12	-
Weight of filter	25 kg	12 kg (plastic case) 26 kg (steel case)	21 kg

Conventional Deep-Pleat Filter

This design is illustrated in Fig. 1. It consists of a continuous length of paper folded from front to rear of the filter case with corrugated spacers between each fold, forming a series of flow channels for the air. The 'pack' of folded paper and spacers is assembled and sealed into the filter case using conventional adhesives or a glass fibre mat packing for high temperature versions.

The particular filters tested were manufactured by Vokes Limited, type Nos. 66/MAD/5DS, to AESS 30/93402[2].

High Capacity Filter

These filters are assembled from panels of pleated paper arranged in a vee configuration within the filter case. The panels are machine made, and the spacing between the pleats controlled by threads or strips attached to the paper prior to

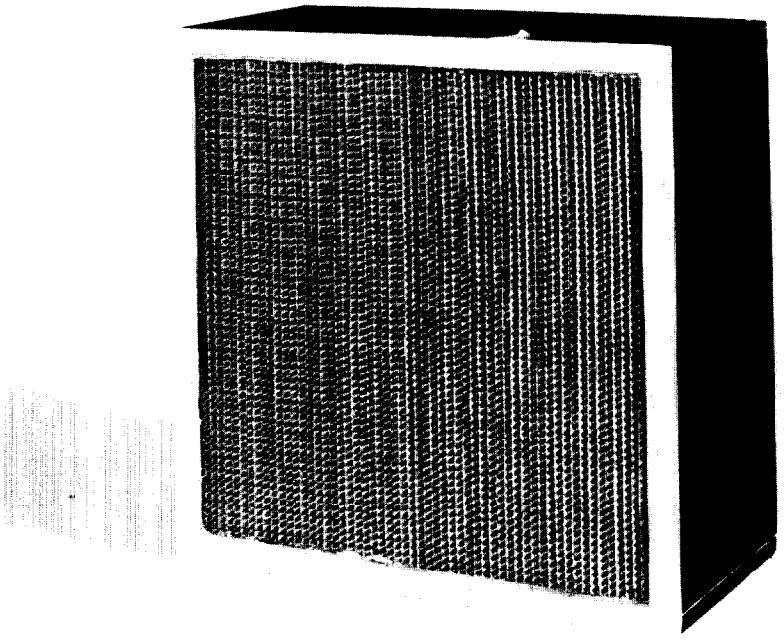

Figure 1. Conventional deep-pleat filter.

pleating. The pleated paper panels and support trays are fixed in the filter case using conventional adhesives. Pleat depths and spacings can vary with supplier, as can also the number of panels in the filter.

Filters from two manufacturers were tested, Sofiltra-Poelman type 1506-26, Fig. 2, and Luwa type NS-30-Ti, Fig. 3.

III. Test Programme

The dust loading tests were carried out in general accordance with BS 2831[3]. Tests were carried out at two flow rates, 3400 m^3/h and 1700 m^3/h and the flow rates were maintained constant throughout each test. Tests were carried out using two test dusts, ASHRAE[4] and BS 2831 No. 2. The ASHRAE test dust consists of a controlled blend of molocco black, cotton lint and quartz particles, whilst BS No. 2 dust consists solely of fused alumina particles of between 3.5μ and 7.0μ mean size. Dust concentrations during the test were approximately 200 mg/m^3 for BS No. 2 dust and 70 mg/m^3 for ASHRAE dust.

The efficiency of the filters was measured at intervals during each test using sodium flame photometry methods to monitor the integrity of the filter using increasing pressure drop conditions.

Details of the parameters for each test are given in Table II.

IV. Results

The results of the test programme are given in Table II and also shown graphically in Figs. 4-7.

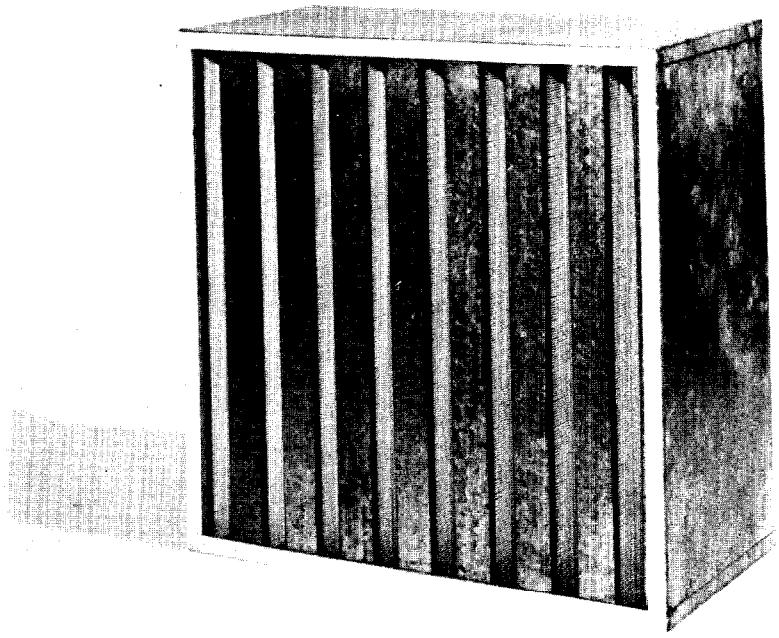

Figure 2. Sofiltra-Poelman high-capacity filter.

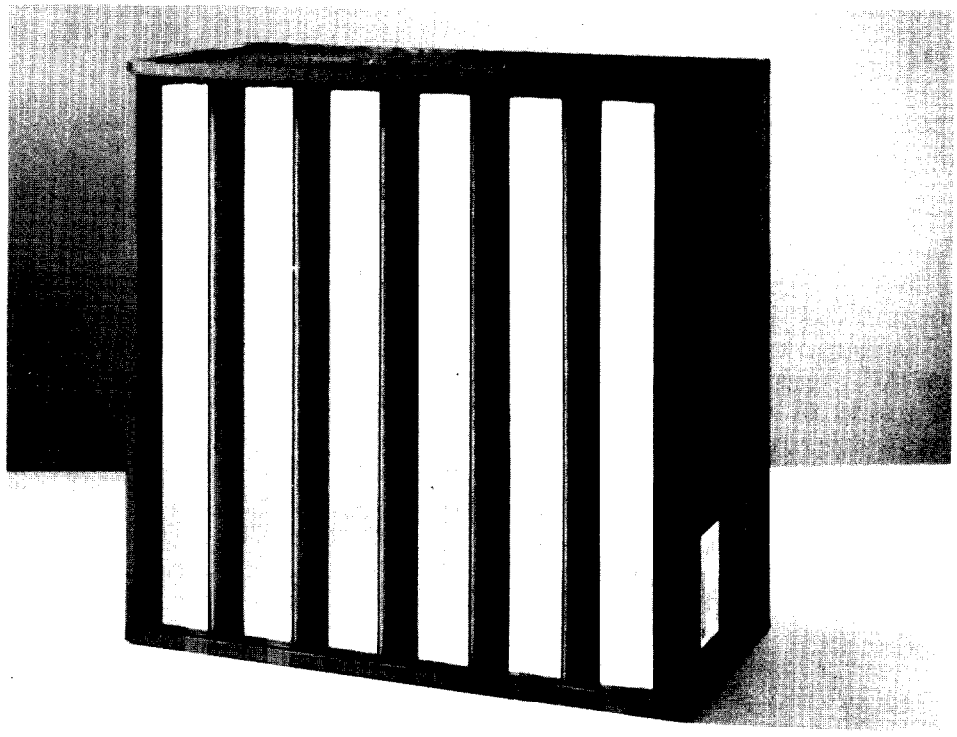

Figure 3. Luwa high-capacity filter.

Table II. Results of dust loading vs pressure drop tests.

	Dust Loading - kg							
Filter Type	Sofiltra	Vokes	Luwa	Vokes	Sofiltra	Luwa	Sofiltra	Luwa
Flow m^3/h	1700	1700	1700	1700	3400	3400	3400	3400
Test Dust	BS No. 2	BS No. 2	ASHRAE	ASHRAE	BS No. 2	BS No. 2	ASHRAE	ASHRAE
Pressure drop with zero dust loading mm H_2O	11.5	23.5	12	24.5	27.5	28.5	28	28.5
Pressure Drop mm H_2O								
25	8	0.5	.75	-	-	-	-	-
50	15	4.3	1.65	0.6	7.2	6.0	0.75	0.7
75	20	6.5	2.2	1.1	9.6	10.2	1.2	1.3
100	24	8.3	2.55	1.5	10.8	13.0	1.4	1.8
125	26.5	9.8	2.85	1.9	11.4	15.0	1.5	2.25
150	27.8	11.2	3.1	2.25	11.7	16.5	1.6	2.6
160	28.2	11.8	3.2	2.35	11.9	17.2	1.6	2.7
200	-	-	3.6	2.75	-	-	-	-
250	-	-	3.8	3.2	-	-	-	-
300	-	-	4.15	3.55	-	-	-	-
350	-	-	4.3	3.8	-	-	-	-

The test results for the conventional deep-pleat design and the high capacity designs down-rated to 1700 m^3/h, show the predictable higher dust holding of the latter due to its larger area of filter paper. This enhancement is however less marked with ASHRAE dust than BS No. 2 dust. The tests at the higher flow rate on the high capacity filters show that the Luwa filter holds significantly more of both BS No. 2 and ASHRAE dust than the Sofiltra filter at the same pressure differentials; eg, 17.2 kg compared with 11.9 kg of BS No. 2 dust and 2.70 kg compared with 1.60 kg of ASHRAE dust, at 160 mm H_2O. The distribution of dust through the flow channel of a high capacity filter is shown in Fig. 8.

The efficiency measurements taken during the tests revealed a weakness in the Sofiltra pleated panels. Three of the filters tested fell below the specified efficiency of 99.95% at pressure drops of 90 mm H_2O, whilst the fourth showed a similar fall at 100 mm H_2O. Examination of the panels after the test showed that the pleated paper had tended to tear approximately 20 mm from the adhesive and in line with the supporting tray, Fig. 9. Closer examination revealed that a reinforcing tape had been omitted from this region, leaving a longer-than-usual unsupported pleat length.

One Luwa unit showed a decline in efficiency to 99.95% at a pressure drop of 160 mm H_2O.

The Vokes filters remained within their specification throughout the tests.

V. Discussion

The results obtained from these tests show that dust loading capacity of both designs is very dependent upon the type of aerosol used, the dust loading with BS No. 2 dust being significantly greater than that with ASHRAE dust. However the graphs of dust loading versus pressure drop do show the characteristic shape reported by Professor First from tests using naturally occurring aerosols(5).

For the filtration of particulate matter similar in size distribution to BS No. 2 dust, the use of the high capacity filter could lead to a reduction in filter usage. Greater savings in operating costs could be achieved if the filters were downrated to 1700 m^3/h, but this would prevent the reduction in filter installation size offered by the new design.

The position with regard to the capture of aerosols similar to the ASHRAE test dust is not as clear. Neither the Luwa or Sofiltra units can offer a significantly higher dust holding capacity than the conventional design at their rated flows, and the only way in which a reduction in the number of filters used could be achieved would be through the use of the high capacity filter downrated to 1700 m^3/h.

The differences in performance of the two designs of high capacity filter was not expected and was not predictable on the basis of the physical parameters of the two designs. This suggests that the design could be optimised to increase its dust-holding capacity and hence useful life.

The lower initial pressure drop of the downrated high-capacity design could also be exploited in terms of reduced running costs for filter installations.

In order to quantify and optimise potential savings each plant would need to be considered separately, with factors such as predicted aerosol size distribution, capital and running costs, and the costs of storage or disposal of contaminated filters taken into account in the calculations.

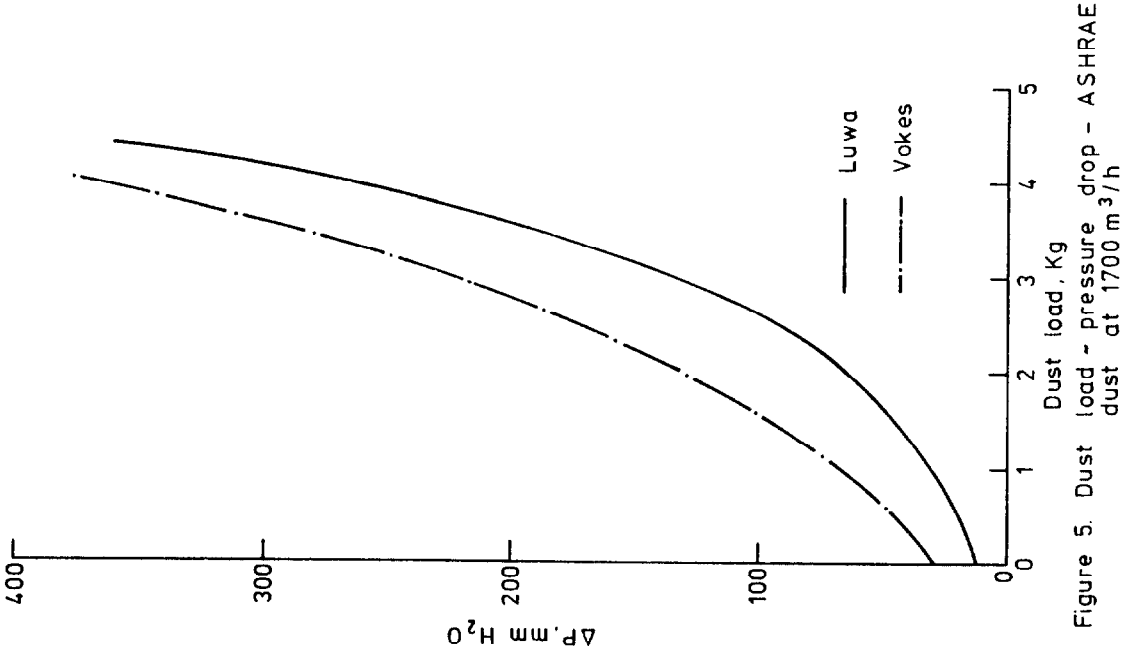

Figure 5. Dust load - pressure drop - ASHRAE dust at 1700 m³/h

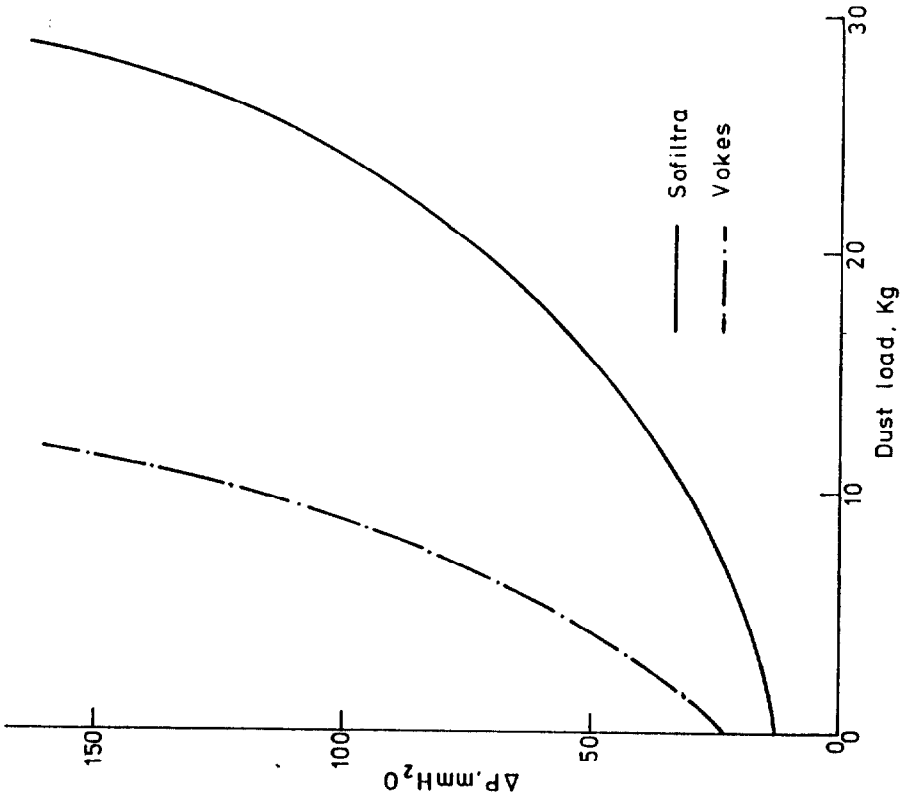

Figure 4. Dust - load - pressure drop - B.S. nos 2 dust at 1700 m³/h.

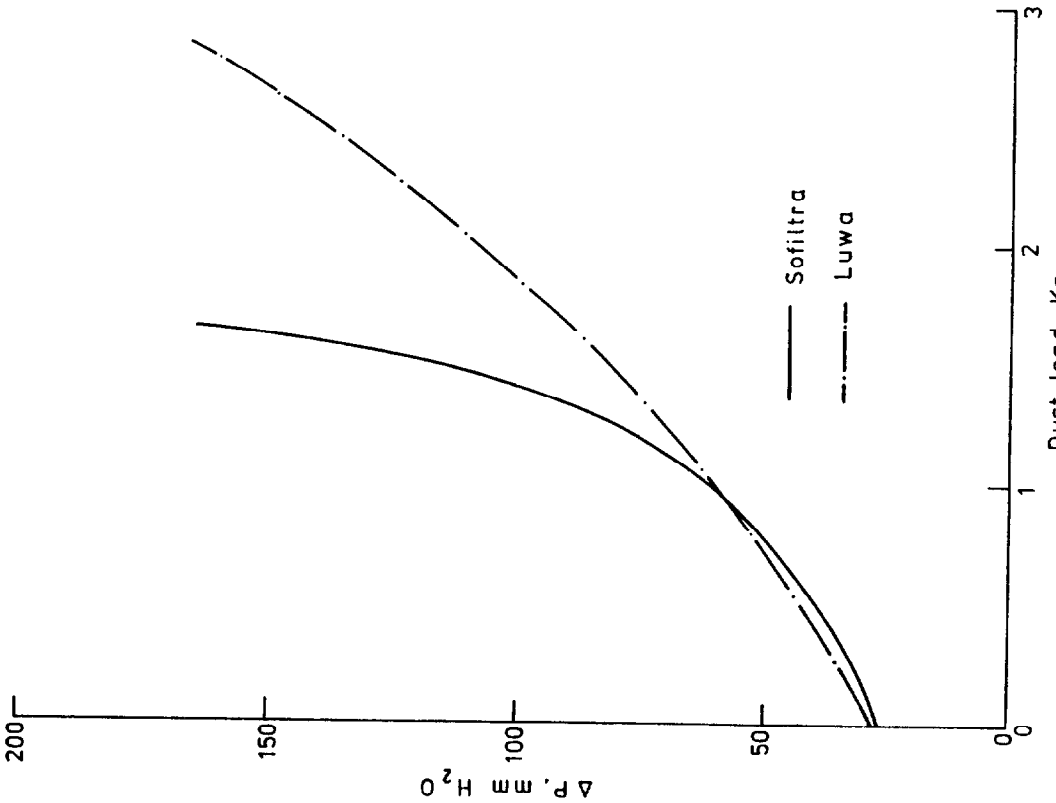

Figure 7. Dust load - pressure drop ASHRAE dust at 3400 m³/h

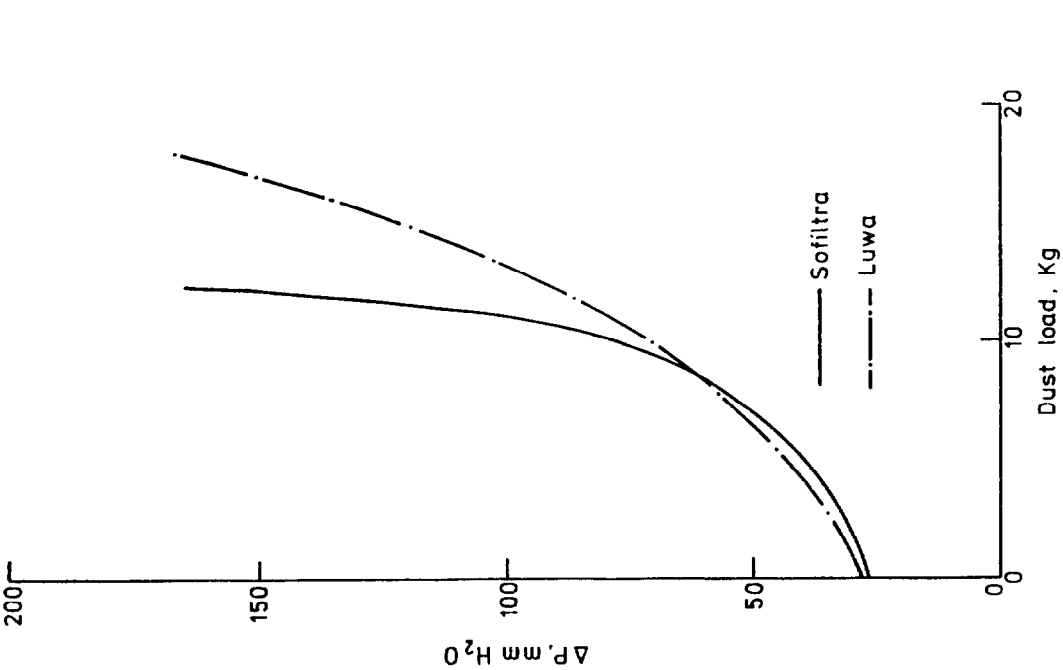

Figure 6. Dust load - pressure drop BS nos 2 dust at 3400 m³/h.

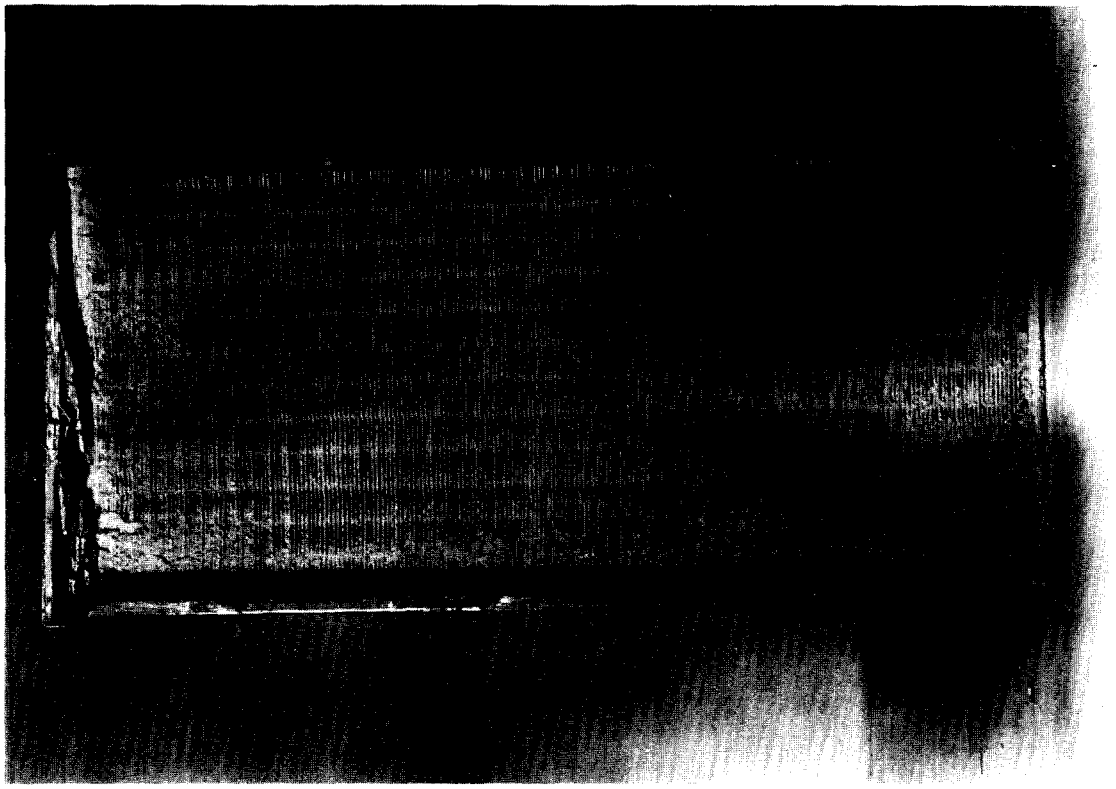

Figure 8. Dust distribution through a high-capacity filter flow channel.

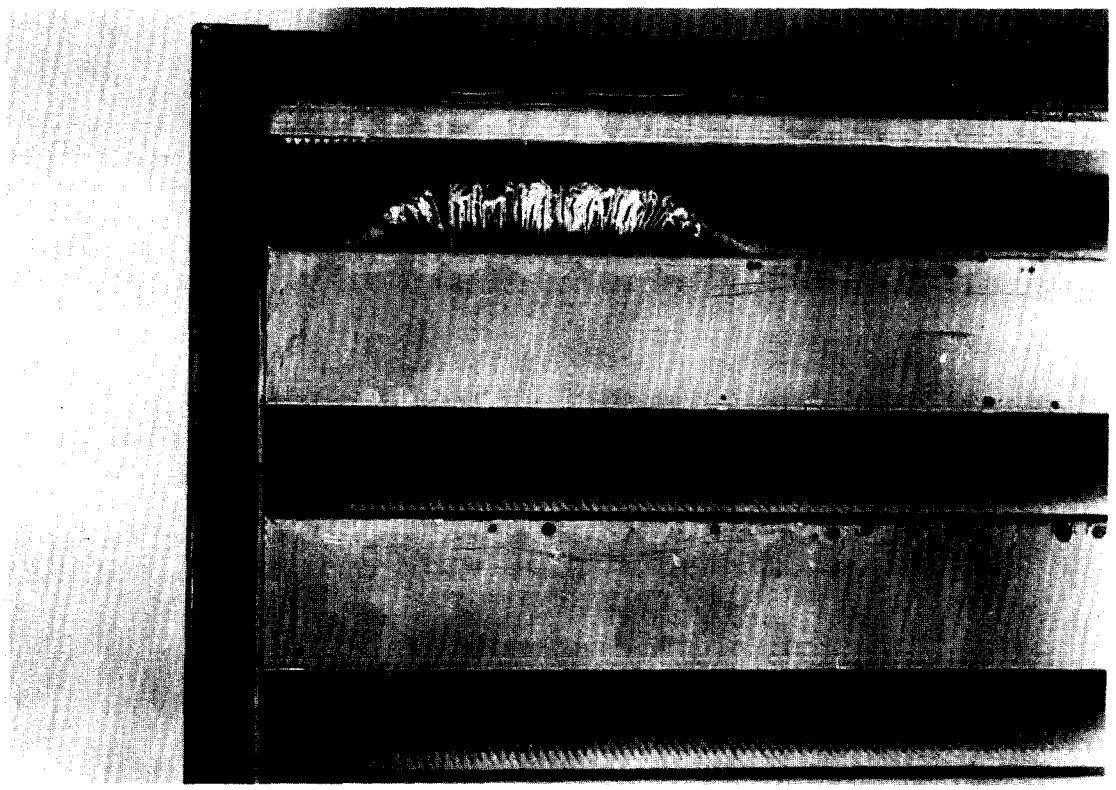

Figure 9. Damaged pleating on Sofiltra-Poelman filter.

The drop in efficiency found to occur in the Sofiltra filters has been discussed with the manufacturer. These discussions showed that, for production reasons, the reinforcing tapes were omitted close to the adhesive. Reassurances have been given that this will not occur on future production filters, and the manufacturer claims that the filter should stand the full 300 mm H_2O without failure.

It must be remembered that the results quoted were obtained from one filter only for each test and hence these results should be regarded as preliminary and therefore treated with caution, particularly where potential advantages are marginal.

An expanded test programme is under consideration which in addition to repeat tests to verify the results reported here, will include tests at intermediate flow rates and filters from other manufacturers.

It is hoped that the results obtained will enable plant designers and managers to minimise capital and operating costs through the selection of the most suitable filter for each application.

VI. Acknowledgements

I would like to thank Mr. J. M. Clarke and his colleagues at Chemical Defence Establishment, Porton, England for their assistance in carrying out the laboratory tests.

This work was carried out under the terms of reference of the Department of the Environment, UK Government.

VII. References

1. Bella, M., Steihl, H. H. and Sinhuber, D., "Extension of the maintenance cycle of HEPA filters by optimisation of their technical characteristics of filter and their construction", Delbag Luft filter - Berlin.

2. AESS 30/93402 - "Filter inserts high efficiency particulate air (HEPA) - non combustible glass fibre paper 25 to 500 litres per second".

3. BS 2831:1957 - "Methods of test for air filters used in air-conditioning and general ventilation".

4. ASHRAE 52:75 - "Method of testing air cleaning devices used in general ventilation for removing particulate matter".

5. First, M. W. and Rudnick, S. N., "Performance of 1000 and 2000 cfm HEPA filters on long exposure to low atmospheric dust loadings", Second World Filtration Congress, London 1979.

DISCUSSION

GILBERT: As I recall, Mr. Hoppitt, formerly of Vokes Air Filters, Limited, did some tests along this line. He performed his tests with ASHRAE dust without cotton linters. Did you have cotton linters in yours?

PRATT: I am aware of the work that Mr. Hoppitt did. Yes, we did use a standard ASHRAE dust with cotton lint present. I tried to do some extrapolation between the results of my work and his and it would appear that the lint had very little effect. If you look at the weights of dust collected on my filters, and from the calculated weight of the carbon black, you come up with very much the same results.

FIRST: When we designed our experiments, we very carefully ruled out the kind of experiment that you conducted on the basis of two considerations. One, the dust loading is far higher than we ever anticipate a HEPA filter will experience in normal operation. Second, we believed that the particle size you used was far larger than the filter would see in practice. I would be delighted if you would comment on that.

PRATT: I share your reservations. We also were concerned that we were going to get results which were not exactly applicable. To this end, I tried to get some information from our nuclear plant operations. I asked what sort of particle size distribution they were likely to get in their ducts. I would suggest that if you try to get the same sort of information in the US, you probably will not be any luckier than I was. The only comment I would make is that I would, with respect, suggest that your natural aerosol is probably as uncharacteristic as the sort of thing you would find in cell vents and offgas lines as is my test dust.

HAYN: Which concentration of ASHRAE dust do you use for your loading tests?

PRATT: We use 70 mg/m^3.

CLEANABLE SINTERED METAL FILTERS IN HOT OFF-GAS SYSTEMS

G. A. Schurr
E. I. du Pont de Nemours & Co., Inc.
Wilmington, Delaware

ABSTRACT

Filters with sintered metal elements, arranged as tube bundles with backflush air cleaning, are the equivalent of bag filters for high-temperature, harsh environments. They are virtually the only alternative for high-temperature off-gas systems where a renewable, highly efficient particle trap is required. Tests were conducted which show that the sintered metal elements installed in a filter system provide effective powder collection in high-temperature atmospheres over thousands of cleaning cycles.

Such a sintered metal filter system is now installed on the experimental defense waste calciner at the Savannah River Laboratory. The experimental results included in this paper were used as the basis for its design.

Introduction

An experimental defense waste calciner, installed at Savannah River Plant, is a prototype test unit for drying low-level radiation defense waste slurries. The resultant dry powders - primarily metal oxides - are then vitrified in a glass matrix through a melt process. The calciner off-gas system doubles in function to disengage a portion of the dry powders while evacuating the water vapor and atomizing air. This dual function makes it imperative that the first stage filtration be both cleanable and able to operate in a high-temperature, corrosive environment.

Initial work, conducted at the Battelle Pacific Northwest Laboratory, demonstrated the viability of sintered metal filter elements equipped with a back-pulse cleaning capability. These elements are constructed from Inconel metal powders to meet the environmental requirements of the calciner.

Experiments were conducted in operating and cleaning sintered metal elements to guide their selection for the off-gas system. The experiments also helped establish operating procedures directed toward maximizing the effective life of the system.

Experimental Apparatus

The experimental test facility is shown schematically in Figure 1. Included is a feed system for injecting test powders into the filter, a housing and holder for two sintered metal filter elements, a reverse-flow air system for cleaning the sintered metal elements, and the accessory instrumentation.

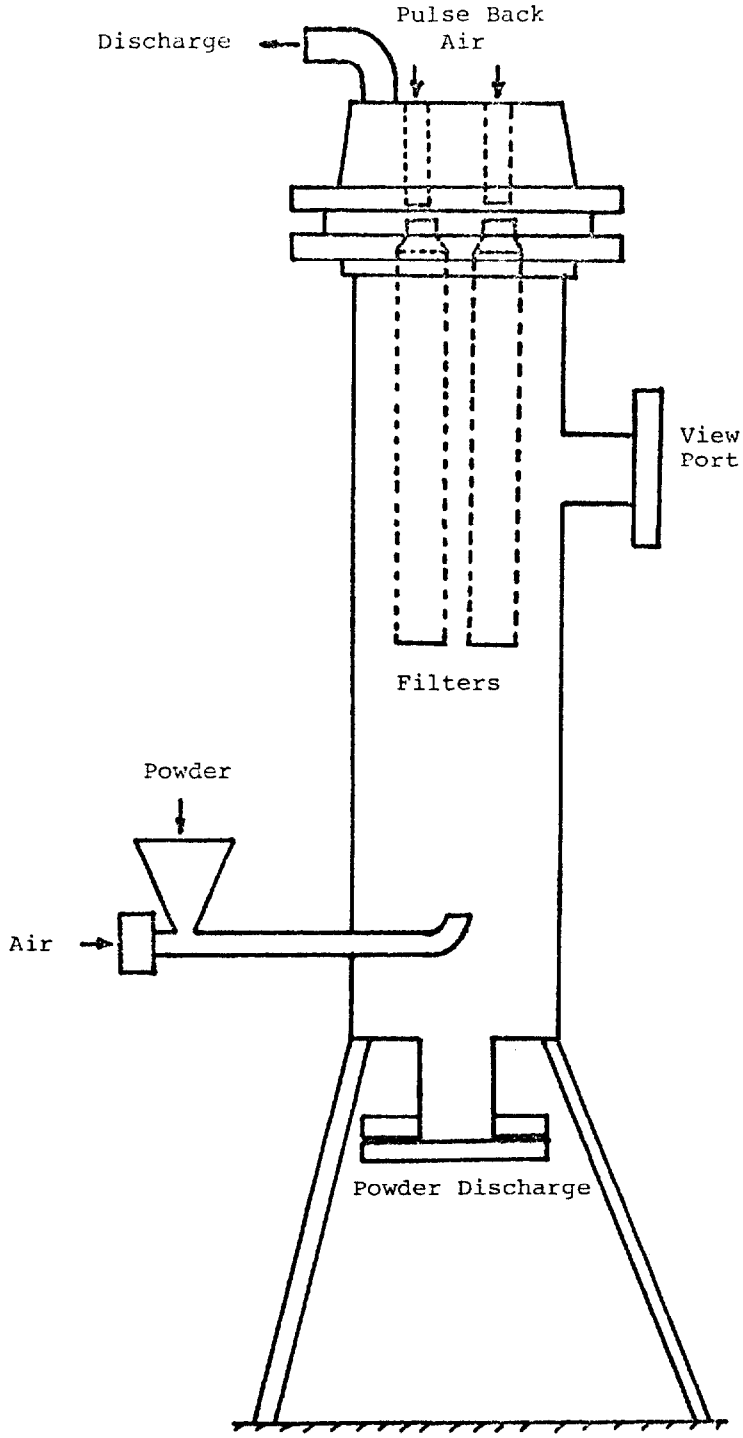

FIGURE 1 - SCHEMATIC OF FILTER TEST APPARATUS

The filter chamber is 6" diameter with a 14" disengaging zone below the elements. A reservoir is located at the bottom of the chamber for collecting settled and back-cleaned powder. A 3" flange with viewing window is provided at the filter level. The chamber is designed to hold two, 2" diameter by 16" long filter elements, each supplied with a built-in venturi nozzle. The filter elements are mounted directly on top of the filter chamber. The

off-gas vents through a 2" pipe. Jets for reverse air flow are built into the head of the chamber, aligned with the center line of the filter elements. The spacing between the jet and the venturi section of the filter is adjustable.

Test powder is fed into the filter chamber through an air injector system which is designed to disperse the powder as it is conveyed into the filter chamber. The gas flow is metered through the injector nozzle orifice. Solids feed rate is controlled by solids metering into the injector suction.

The pulse-back air filter cleaning system includes quick-opening solenoid valves operating off a high-pressure air manifold. These valves control the air flow through 0.21" nozzles directed to the centerline of the filter venturi section. The pulse-back air is taken directly from the house high-pressure air supply. An electronic timer controls the solenoid valves. It has a range of pulse duration from 0.1 second to greater than 10 seconds, with an adjustable period between pulses. The start of a pulse cycle can be controlled manually or automatically with the timer. The filters can be cleaned either singly or together. This pulse-back air is not heated.

The pressure in the filter chamber and the pressure drop across the filter elements is measured through fast-response pressure transducers and a strip chart recorder. The pressure transducers have a temperature limit of 120°C. In experiments where higher temperatures are encountered in the test chamber, water manometers are used.

The gas for conveying the powder into the filter system is steam, air, or mixtures of both. The gas feedline passes through a superheater which has a temperature limit of 650°C.

The selection of the filter element is based upon the process requirements. The experimental defense waste calciner requires that the elements have a fine pore size. This is to limit penetration of the powders that are expected, and to preserve the life of the filter. A high permeability is desirable to minimize the number of filter elements required for a given volume of off-gas. Filter elements rated at 10 microns by the isopropanol bubble-point test method were selected for the tests. These filters were supplied by Mott Metallurgical Co.

The filter elements were made of sintered metal construction using Inconel metal powder. They have stainless steel venturi elements. A schematic of a filter cross-section is shown in Figure 2. The two filter elements were spaced on 2" centers. This provided a 1" free space between the filter elements.

Calcine Powder

The powder used in these tests was obtained from Pacific Northwest Laboratory. It is a mixed metal oxide which simulates the composition of the waste materials expected to be calcined in a production unit. The size of the powder was characterized

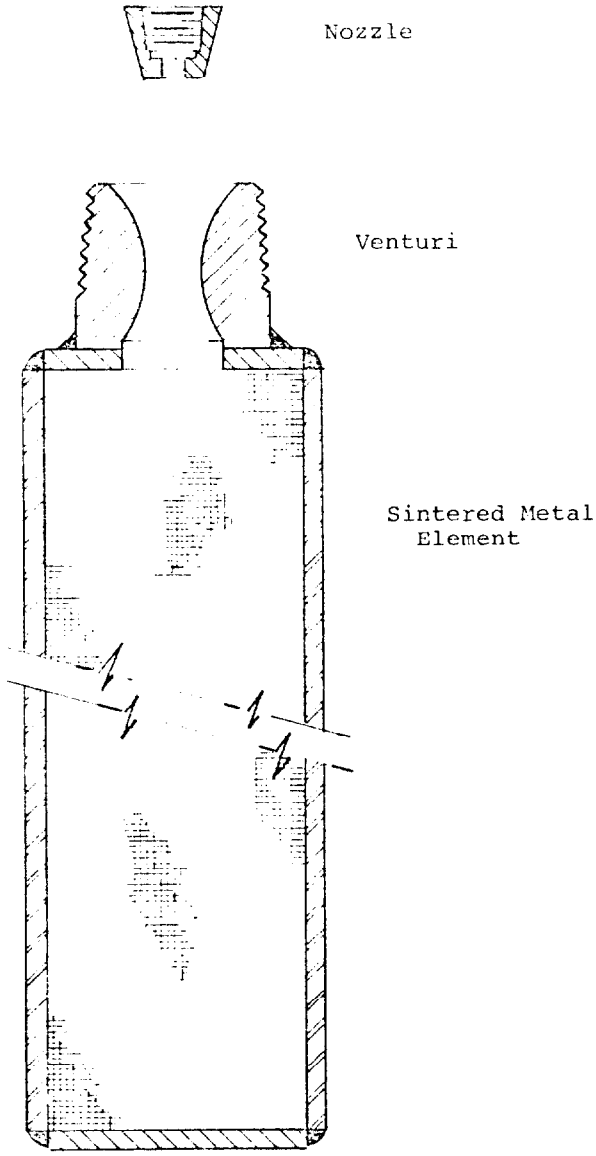

Figure 2 - Filter Element

with a Coulter Counter. The size distribution is shown in Figure 3. The powder has a bulk density of 0.63 g/cc and a true density of 3.1 g/cc.

Experiments

The cleanability of the filter influences the long-term permeability of the sintered metal, and is the prime factor that influences filter life. It is, in turn, influenced by the surface porosity, initial precoating, solids build-up, and face velocity of the gas stream to the filter. The experiments described evaluated the effect of these factors for one filter porosity. The permeability is determined in the tests by measuring the pressure drop across the elements - a higher pressure drop meaning lower permeability.

The filter elements include a built-in venturi section. The pressure drop across the element is thus the sum of resistances through the porous element and flow through the venturi. The pressure drop through the venturi nozzle remains constant for identical gas flows since it is not in the particle stream and stays clean. The pressure drop through the elements in air, as determined in these tests before precoating is shown in Figure 4. A test was also made with 385°C superheated steam. A pressure drop of 6.6" W.G. was measured at a face velocity of 4 ft/min.

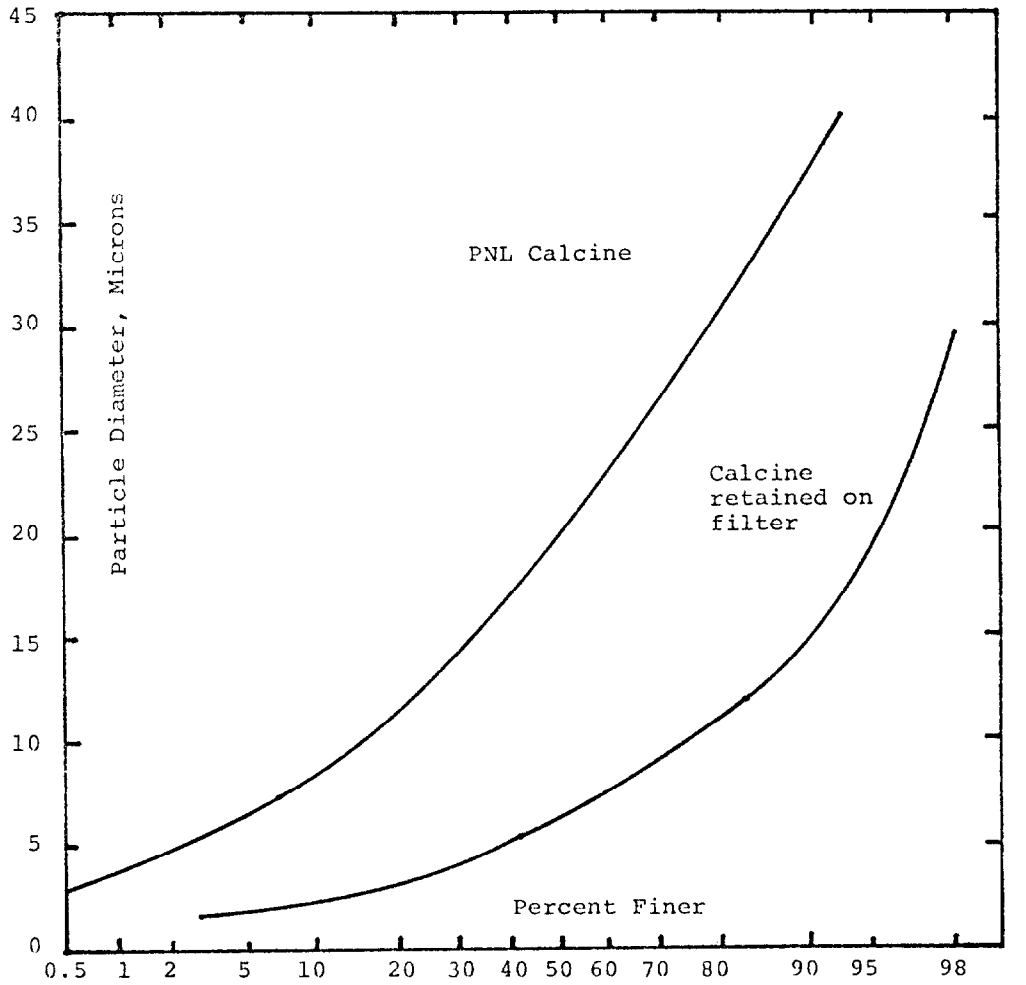

FIGURE 3 - PARTICLE SIZE DISTRIBUTION OF CALCINE POWDER

Precoat

In all experiments new or cleaned filter elements were precoated with the calcine powder. Face velocities were kept below 1.5 ft/min during this procedure. This minimized the likelihood of deep penetration of fine particles into the filter pores. Conversely, it also meant only the finest fraction of the calcine powder reached the filter.

The precoating resulted in a reproducible, one time increase in the pressure drop of the filter element. This is shown in

Figure 5. The pressure drop of the precoated elements proved to be a good reference base. Even after "plugged" filters were rejuvenated by dissolving calcine in a nitric acid bath and recoating, the reference pressure drop remained constant within ±5%.

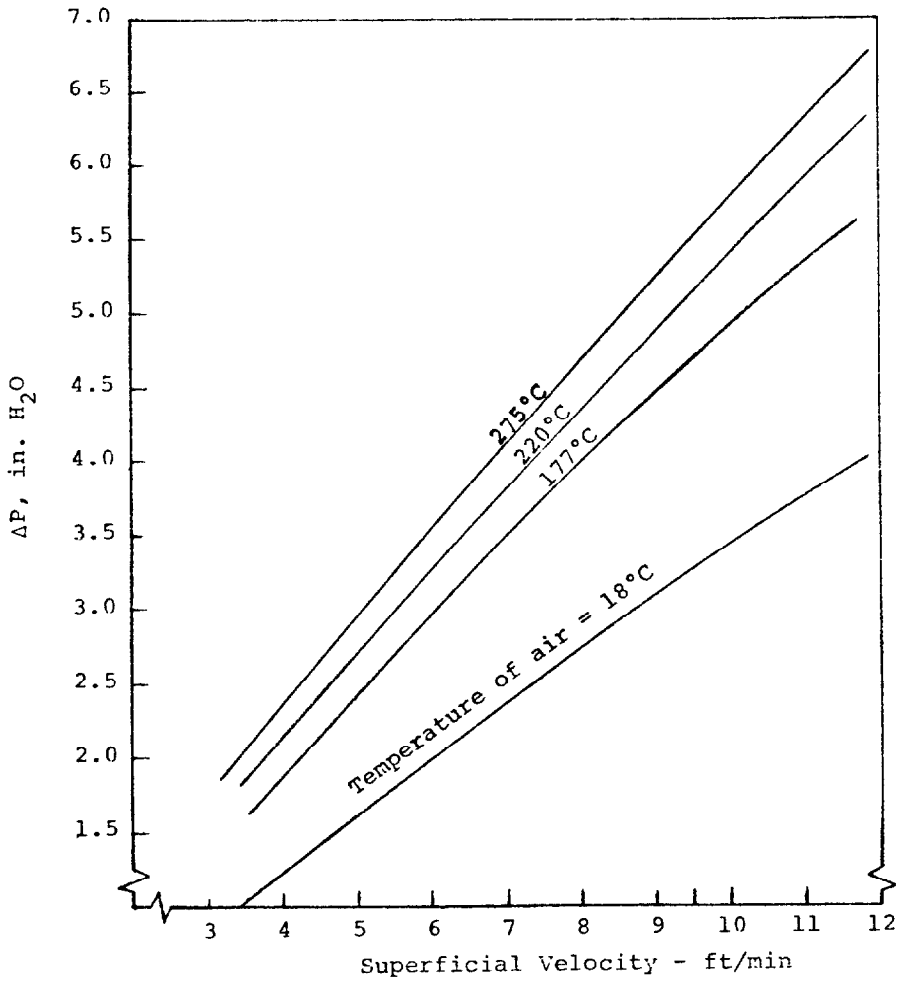

FIGURE 4 - PRESSURE DROP AS A FUNCTION OF VELOCITY FOR 10μm SINTERED METAL FILTER

Pulse-Back Cleaning

A pulse-back cleaning cycle is a reverse flow of air through the orifice nozzle directed to the centerline of the venturri throat. In all tests, the nozzle was spaced 6 mm from the element. The venturi throat is 19 mm in diameter.

One hundred psig air was supplied to the nozzles. The quick activating valves were set at a 0.4 second time interval between the start to open - start to close sequence. The two filters were pulsed together, ie, the controller operated the valves simultaneously.

The 0.4 second pulse duration is the "normal" cleaning cycle. In a long cleaning cycle, the reverse pulse is maintained

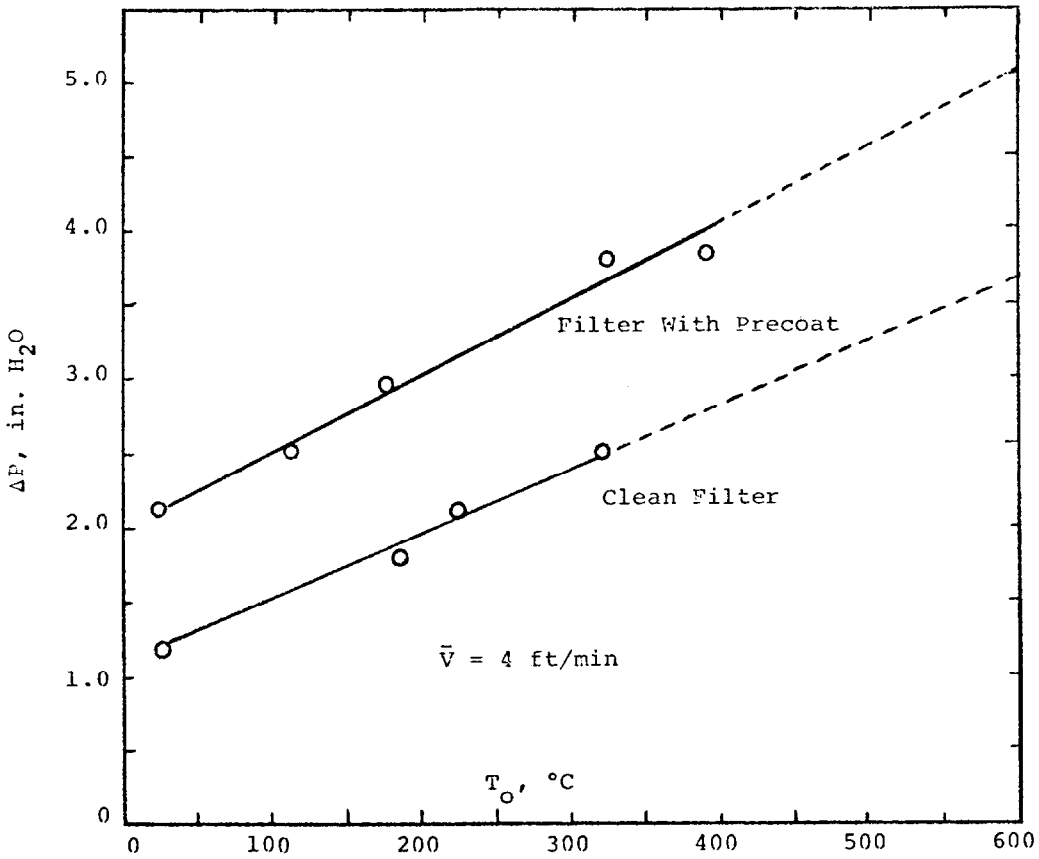

FIGURE 5 - PRESSURE DROP AS A FUNCTION OF GAS TEMPERATURE. 10μm RATED SINTERED METAL FILTER

for five seconds. A counter on the timer recorded the number of cleaning cycles.

In each test, the calcine powder was metered to the feed injector to give a dust loading of 3 grams/ACFM gas. The coarsest powder settled into the chamber. For all tests, the face velocity to the filters was kept at 4 ft/min. Pressure drops across the filter elements were measured with a pressure transducer at the reported face velocities when no powder was entering the filter chamber.

It was found that 30 minutes of powder feed was required to build a filter cake of 0.25-0.5mm depth. At this filter loading, the cleaning cycle removed the surface dust mostly as fragments of filter cake. A pressure increase of 7.5" H_2O at 4 ft/min velocity across the filter was needed to form a coherent filter cake. A cleaning cycle with less dust on the elements removed a cloud of discrete particles, many of which re-entrained upon flow reversal.

Observation showed that, while most dust is blown off the filter surface after pulse-back, a thin coating remains. Some of this coating was collected and analyzed by the Coulter Counter for size distribution. It is finer than the feed material; see Figure 3.

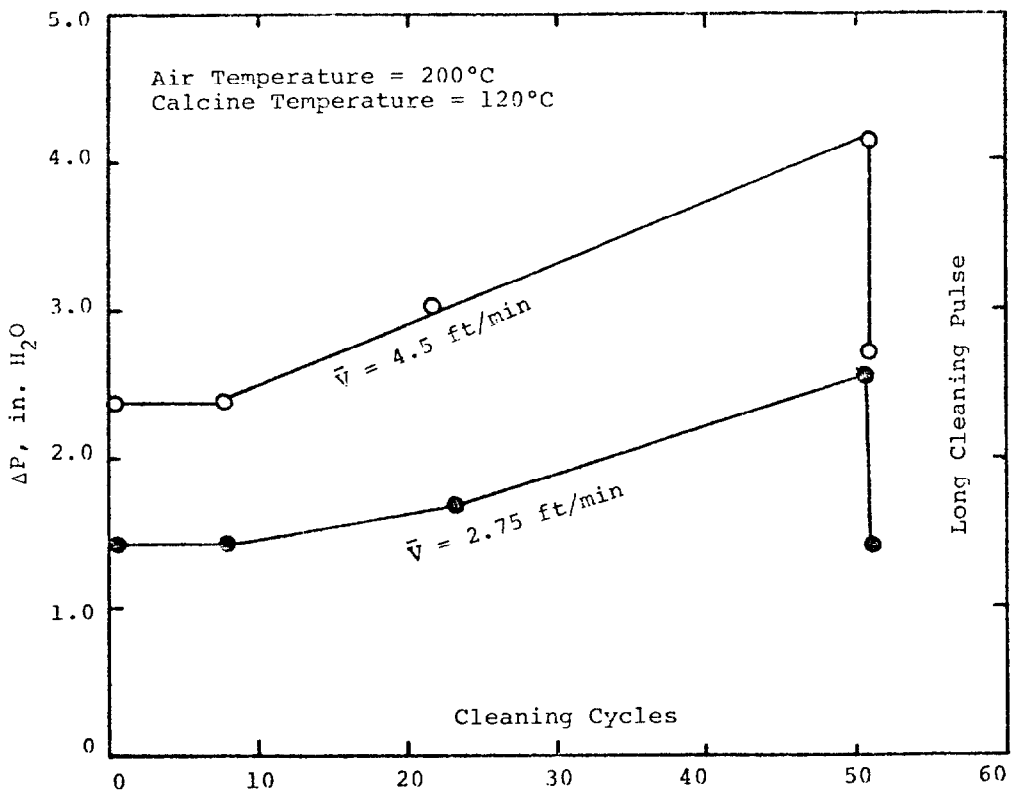

FIGURE 6 - PRESSURE RISE VERSUS CLEANING CYCLES FOR HOT AIR AND HEATED CALCINE. FILTER CAKE DEVELOPED BEFORE CLEANING.

Figures 6 and 7 show the pressure drop history over 65 cleaning cycles. Figure 6 is for a case in which the conveying air temperature was 200°C and the calcine had been preheated to 120°C. Figure 7 is for a case in which the temperature of both the conveying air and the calcine were 18°C. In both cases, the pressure drop increased more or less linearly with the number of cycles, but the rate of increase varied with face velocity: the higher the velocity, the more rapid the increase in Δp. At the end of 65 cycles, however, a long pulse restored Δp to the starting level.

The effect of the filter cake build-up was investigated by running long-term tests at pulse-back frequencies of one minute (dusting condition) and 30 minutes (coherent filter cake discharge) over many cycles. A calcine temperature of 120°C and air temperature of 200°C was maintained. Pulse-back air is at 18-20°C. The results are shown in Figure 8.

Allowing a filter cake to form before cleaning resulted in a slow pressure rise through 1,070 cleaning cycles. A periodic long pulse recovered some additional permeability. Frequent pulsing with dusting increases pressure drop much faster.

The development of a cohesive filter cake appears important to protect the sintered elements from particle penetration which reduces permeability irreversibly. Longer reverse flow cycles clean more efficiently than short pulses.

The results shown in Figure 8 lead to the following conclusions:

- The frequent pulsing cycle in which dusting occurs causes a more rapid rise of pressure drop than does cleaning after a filter cake is established on the filter surface.
- A long reverse flow cleaning cycle is more effective than a short pulse.
- The flow resistance depends on the face velocity. The pressure drop is a power function of the face velocity.

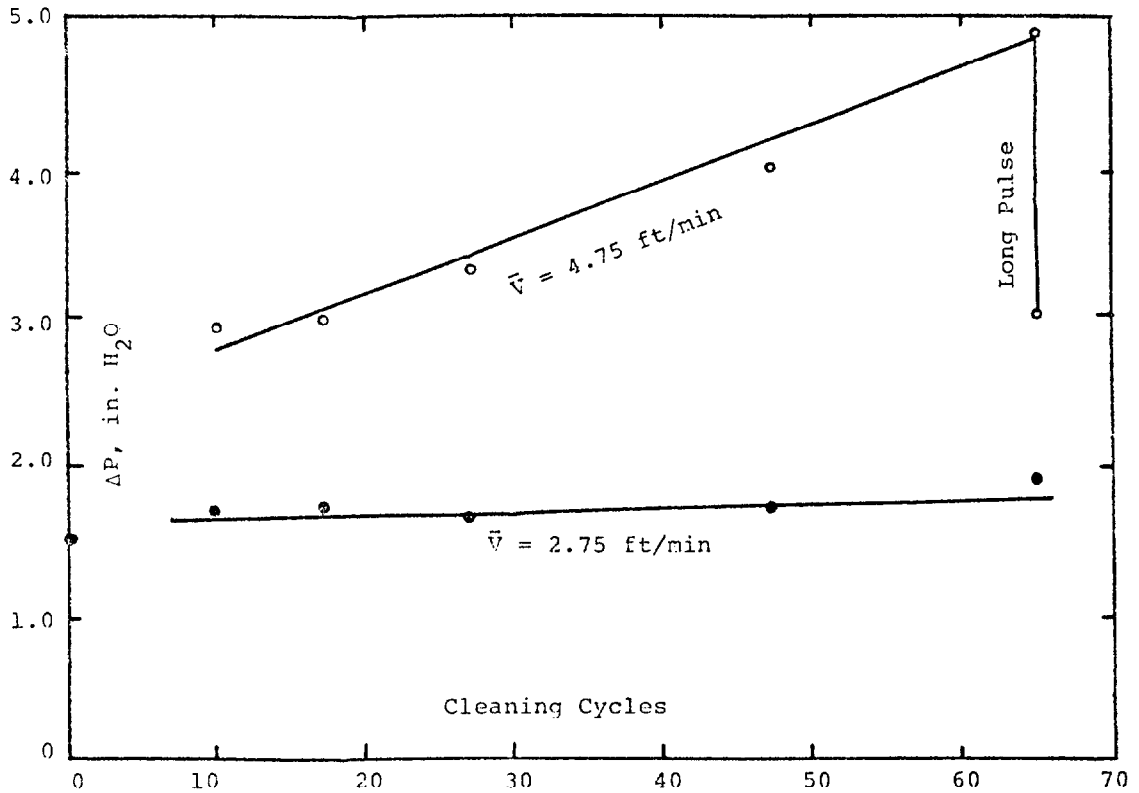

FIGURE 7 - PRESSURE RISE VERSUS CLEANING CYCLES - AIR AND CALCINE AT AMBIENT TEMPERATURE. FILTER CAKE DEVELOPED BEFORE CLEANING.

Filter Efficiency

A polydisperse DOP aerosol with a mean diameter of 0.7 μm was used to test relative efficiency of these filter elements when new, with a precoat, and with greater than 0.25 mm filter cake on the surface. The results are:

Filter Condition	% Efficiency
Clean-unused	64.0
Clean-with precoat	92.0
With filter cake	>99.98

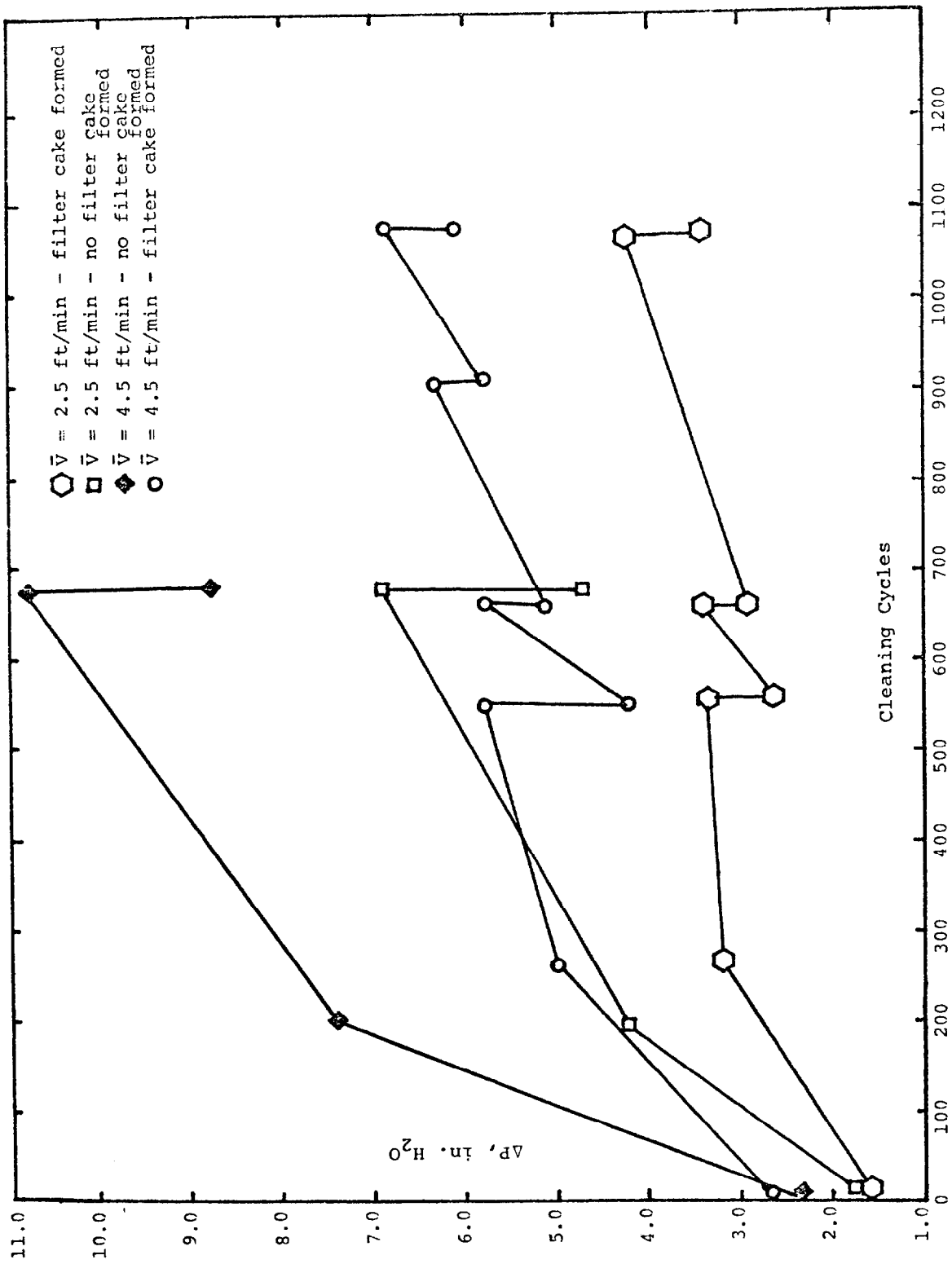

FIGURE 8 - PRESSURE DROP AS FUNCTION OF MANY CLEANING CYCLES

Filter Operation

The experimental defense waste calciner has 142 filter elements. Each element is 2" in diameter and 72" long. These are arranged in 13 banks - each bank of filters to be cleaned simultaneously. The preferred cleaning operation is to allow the filter cake to build on all the filters until the pressure drop reaches a value where a coherent cake discharge is assumed. Then each bank can be cleaned in rapid sequence.

The optimum procedure has a major drawback in that up to 50% of the total spray dryer output is expected to collect on the filters. If they are all cleaned in rapid sequence, a slug of material will be returned to the melter. This is an obvious deterrent to steady state continuous operation. The alternative is to clean each bank singly so that only 1/13 of the collected powder is discharged at any one time. This reduces the instantaneous slug of powder to something more manageable. The negative aspect is that a greater portion of the total flow will then pass through the cleaned filters until the pressure drop is equalized.

The higher face velocity on the filter will increase the likelihood of deep penetration into the surface pores, making reverse flow cleaning less effective.

The data presented illustrate the advantages of designing the filter system with enough surface area to permit operating at face velocities below 2.5 ft/min. The advantages include:

- Preservation of filter permeability over more cleaning cycles.
- Reduction in powder load on the filters due to lower entrainment velocity.
- Greater flexibility in adjusting timing cleaning sequence.

HIGH EFFICIENCY PARTICULATE REMOVAL WITH SINTERED METAL FILTERS*

B.E. Kirstein, W.J. Paplawsky, and D.T. Pence
Science Applications, Inc.
4030 Sorrento Valley Boulevard
San Diego, California 92121

T.G. Hedahl
EG&G Idaho, Inc.
P.O. Box 1625
Idaho Falls, Idaho 83415

Abstract

Because of their particle removal efficiencies and durability, sintered metal filters have been chosen for HEPA filter protection in the off-gas treatment system for the proposed Idaho National Engineering Laboratory Transuranic Waste Treatment Facility. Process evaluation of sintered metal filters indicated a lack of sufficient process design data to assume trouble-free operation. Subsequent pilot-scale testing was performed with fly ash as the test particulate. The test results showed that the sintered metal filters can have an efficiency greater than 0.9999999 for the specific test conditions used. Stable pressure drop characteristics were observed in pulsed and reversed flow blowback modes of operation. Over 4900 hours of operation were obtained with operating conditions ranging up to approximately 90°C and 24 volume percent water vapor in the gas stream.

1. Introduction

1.1 Transuranic Waste Treatment Facility

During the past 26 years, thousands of tons of nuclear waste contaminated with transuranic (TRU) elements have been stored or buried at the Idaho National Engineering Laboratory (INEL). This waste, composed of both combustible and noncombustible materials, may be retrieved, processed, and shipped to a federal repository for permanent disposal. An attractive method for processing this waste is to convert it by means of a high-temperature slagging pyrolysis incinerator (SPI) process into an inert, basalt-like solid which encapsulates the TRU elements. The SPI has been selected as a processing method to be incorporated into the INEL Transuranic Waste Treatment Facility (TWTF). The major process operations in the TWTF will be waste receiving, waste preparation, incineration, slag handling, and off-gas treatment. The Waste Processing Building will incorporate the latest available technology in waste handling, fissile material assaying, criticality control instrumentation, off-gas cleanup, remote operation/maintenance, and decontamination. Process equipment generally will be operated remotely using both local and central controls.

---

*Work performed under USDOE Contract EY-76-C-07-1570

A mixture of TRU waste and contaminated soil will be fed to the incinerator system (see Figure 1.1) with sufficient supplemental fuel to produce slag. The gasifier, a vertical shaft furnace similar to municipal solid waste incinerators, will burn the combustible material in the waste. The noncombustible waste will be incorporated in a molten slag at the bottom of the gasifier which will flow to a slag processing system. The gaseous products of combustion, including some particulate, will pass from the gasifier to the secondary combustion chamber for complete combustion of the gasifier off gases and combustible particulate. High temperatures in the secondary combustion chamber will cause most noncombustible particulate in the off-gas stream to fuse and collect at the bottom of the chamber where it will be removed as slag also.

A key to guaranteeing safety and environmental acceptability for the TWTF is an efficient off-gas treatment system. The off-gas treatment system for the TWTF must establish effective control of radioactive and other potentially harmful airborne materials. Various off-gas treatment technologies were evaluated with respect to fine particle recovery for use in TWTF. A detailed evaluation of the material balance of the incinerator off-gas stream indicated that high efficiency particulate air (HEPA) filters alone would become overloaded and plug after approximately one-half hour of operation. Therefore, some type of continuous particulate recovery equipment would be required in the off-gas treatment system. The removal efficiencies of venturi scrubbers fall off rapidly for particles with aerodynamic diameters below about 1 micrometer (μmA) which makes their use impractical for this application. Electrostatic precipitators (ESP) also do not appear to have sufficient fine particulate removal efficiencies, and the design of an ESP requires far more information about the incinerator particulate than is available. Bag filters also do not have a sufficient fine particulate recovery efficiency for this application and, further, pose other safety problems for a secure radioactive materials off-gas treatment system. A dry off-gas treatment system utilizing sintered metal filters (SMFs) was selected for development and design, based on SMFs high particulate removal efficiency, reduced maintenance (possibly in a remote environmental), and absence of any secondary contaminated liquid waste. However, the lack of adequate design information for SMFs necessitated a pilot-scale test program to verify reported fine particulate recovery efficiencies and operating conditions. The description of this program is presented in the sections that follow.

A conceptual design of the TWTF and associated process systems was completed in May 1980.[1] Based on subsequent design evaluations, the dry system appears to be the most favorable for TWTF, although different systems could also satisfactorily control the off-gas particulates with an increase in the HEPA filters change-out rate.

The conceptually designed off-gas treatment system interfaces with the waste heat boiler system with the receipt of hot off gas from the fire tube section of the boiler. The treated off gas is discharged through the building HVAC exhaust system final HEPA filters. The major components included in this system are (a) spray dryers and their associated chemical feed system; (b) sintered metal filters; (c) NO_x catalytical reduction reactor and associated heat exchangers; (d) HEPA filters; (e) induced draft fans; and (f) ash handling system, pelletizer, and transport system. All equipment, except the induced draft fans, are remotely operated and maintained.

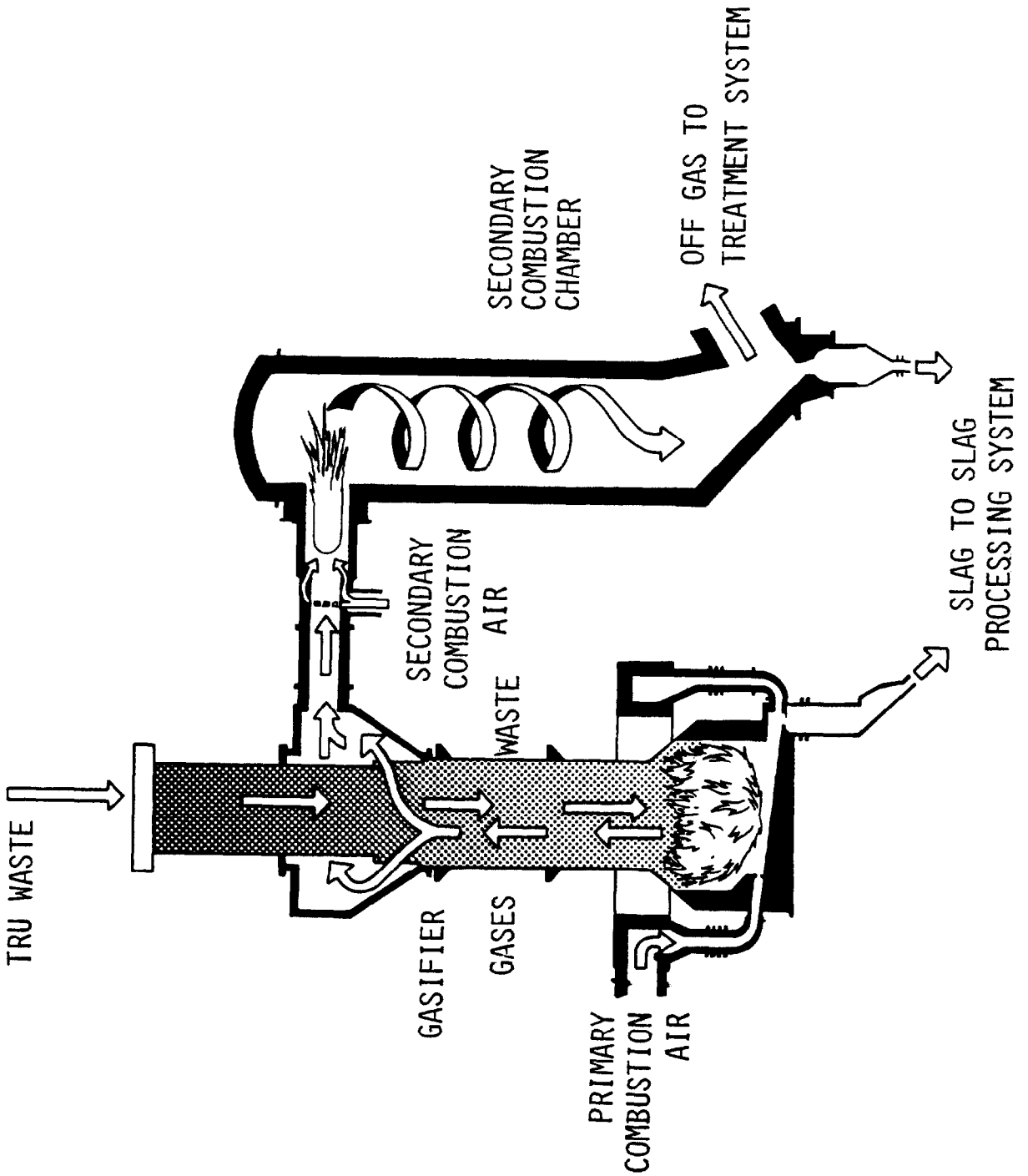

FIGURE 1.1. SLAGGING PYROLYSIS INCINERATOR SYSTEM.

SAI-80BK-29

The first system component is a spray dryer, where the SO_2, SO_3, and HCl in the gas are removed by reaction with an atomized aqueous solution of soda ash, forming a dried particulate of sodium sulphite, sodium sulphate, and sodium chloride. The flow rate of aqueous solution is controlled to maintain dry particulate solids and an unsaturated exit gas under all normal operating conditions. The coarser fraction of the fly ash from the incinerator and the sodium salt particulate found in the spray dryer are captured below the spray dryer vessel for delivery to the ash handling system. The evaporation of water from the droplets of soda ash solution in the spray dryer cools the off gas from approximately 350°C (660°F) to a temperature between 121 and 177°C (250 and 350°F). The off gas together with the finer fraction of the fly ash and sodium salt particulate, leaves the spray dryer and is routed to the sintered metal filters (SMFs). The SMFs removed >99.99% of the remaining particulate from the off gas. The particulate collected on the filter element is removed by pulses of compressed air, and collected in hoppers for delivery to the ash handling system. The filtered off gas leaves the SMFs and is then routed to the NO_X converter.

The NO_X converter system consists of a heat exchanger and a selective catalytic reduction reactor. The off gas enters the heat exchanger, where its temperature is raised to approximately 400°C (750°F). It then enters the selective catalytic reduction reactor, where the NO_X is reduced to elemental nitrogen and water by reaction with ammonia in the presence of a selective catalyst. The off gas then returns to the heat exchanger, where its heat is transferred to the incoming gas and its temperature is reduced to about 177°C (350°F). A supplementary electric type heater is furnished to add heat to the gas entering the selective catalytic reduction reactor during periods of low NO_X concentration. At other times, the exothermic NO_X-NH_3 reaction will provide adequate heat to maintain catalyst temperature within the proper operating range. The off gas leaves the NO_X converter and is routed to the HEPA filter system.

The HEPA filter system consists of two banks in series of high-temperature nuclear-grade HEPA filters in a common housing. The purpose of the HEPA filter system is to form a final barrier to the escape of radioactive particulate from the off-gas treatment system. The housing is arranged for in-place dioctylphthalate (DOP) testing of the filter elements. From the HEPA filters system, the cleaned and treated off gas is routed to an induced draft fan. The induced draft fan generates the necessary suction to maintain setpoint draft in the incinerator system. The fan is a centrifugal type, with volume control arranged to respond automatically to a pressure signal from the incinerator control system. From the induced draft fan, the off gas is routed to the building HVAC Zone I final filter system.

The ash handling system collects the particulates from the spray dryer and SMF hoppers through pneumatic feeders, and conveys the particulate pneumatically to a central receiver. Exhaust air is returned to the off-gas treatment system between the spray dryer and the SMFs. The central receiver is equipped with a vent filter to prevent the re-entrainment of collected particulate back into the off-gas treatment system. The lower end of the receiver forms a hopper for the storage of the particulate delivered to it. The hopper outlet is equipped with a gravity operated material handling type flap valve. After a period of operation, system vacuum is broken, the flap valve opens, the collected particulate drops to the pelletizer. The pelletizer consists of a surge bin, a combination mixer-extruder, and a surface type dryer. The purpose of the pelletizer is to form the collected particulate into dried pellets strong enough to withstand

injection into the incinerator slag casting tundish. A surge bin stores particulate from the ash handling receiver and delivers it by gravity feed to the mixer-extruder, which mixes the particulate with water and a suitable binder and forces it through an extrusion die, forming cylindrical pellets. A rotary arm cuts the pellets from the die and allows them to drop into the dryer. The dryer consists of one or more electrically heated conveyor screws in a suitable trough. The dried pellets are then recycled to the incinerator slag casting tundish for encapsulation into the slag.

1.2 Background of Sintered Metal Filters

The use of sintered metal filters (SMFs) to remove particulate from a gas stream has been practiced for over 25 years.[2] Yet in this time, quantitative design equations have not been developed nor has a satisfactory explanation been given of how the filters operate without plugging over long operating times. These filters have been used in a variety of nuclear applications that are only partially documented with respect to operating conditions. Typically, particulate removal efficiencies will be stated without presented information on the particulate size distribution; or the size distribution of particulates that were presumed to pass through the filters will be presented with virtually no characterization. Also, experience has been reported on the pressure drop performance, again without information on the incoming particulate size distribution. Industrial experience with SMFs is virtually nonexistent in the literature. While it is known that there are industrial users, limited contact with these users reveals their desire not to advertise certain aspects of their manufacturing processes. In the presentation that follows, experimental results are provided describing the operation of sintered metal filters to remove fly ash from a gas (air) stream where the primary objective was to obtain stable operation with respect to pressure drop and to obtain high particle removal efficiencies. These results were then used in the conceptual design of an off-gas treatment system for a radioactive processing facility that uses a slagging pyrolysis incinerator as described in Section 1.1.

1.3 Description of Sintered Metal Filters

In a typical application, the sintered metal filters (SMFs) are installed in a vessel as shown in Figure 1.2. SMFs are rigid barrier filters resembling bag filters in use and operation. Particulate-laden gas enters the filter vessel usually below the filters or by way of an impact plate that prevents direct jetting of the inlet gas on the filters. The gas passes through the filters leaving the particulate deposited on the filter surface. The cleaned gas is collected in a manifold for further processing or release. Without removing the filter cake, the pressure drop across the filters will steadily increase. For long-term operation, SMFs must be periodically cleaned or they will eventually plug. The filters are cleaned by a reverse flow of clean gas, either in a pulse or continous mode. When the pressure drop after filter cleaning exceeds the capacity of the process equipment, the filters are usually considered plugged. There are many different definitions of plugging, such as completely blinded off for any applied pressure; however, for the discussion here, a plugged filter is meant to refer to a continued rise in pressure drop with respect to the cleaning operation, and not neccessarily a no-flow situation.

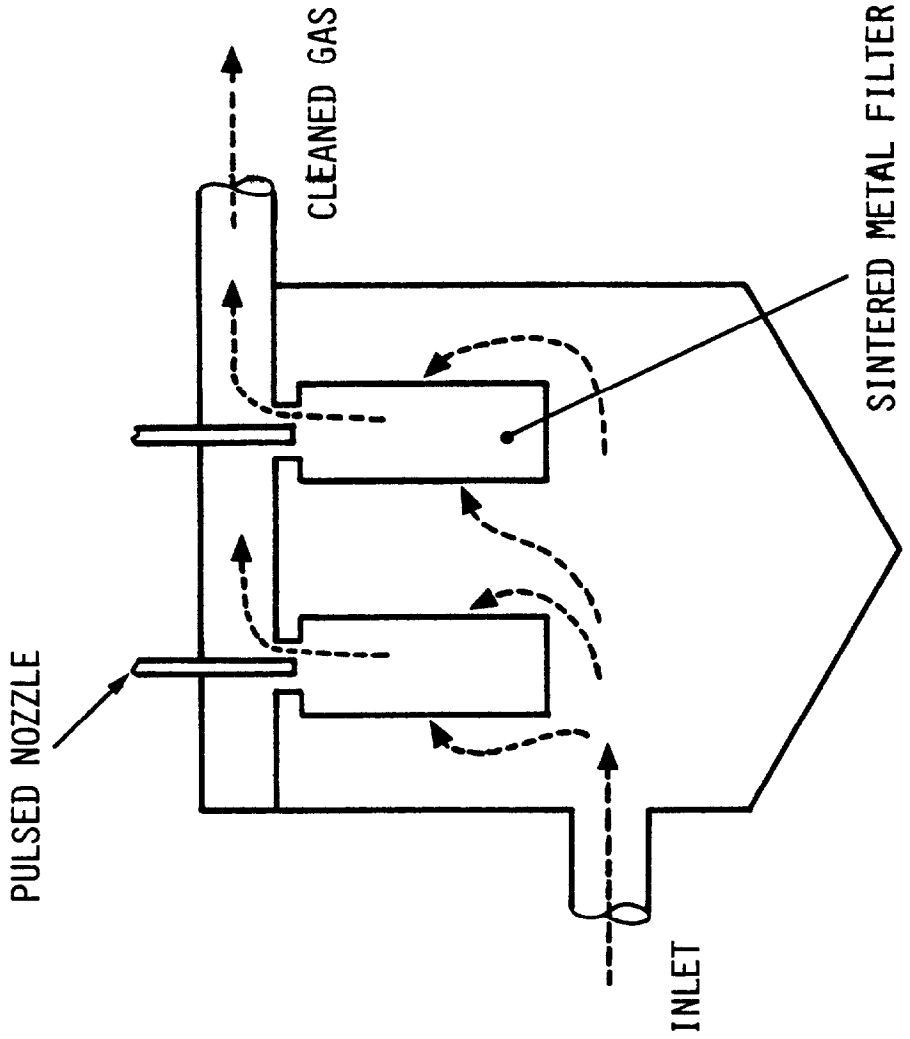

FIGURE 1.2. POROUS SINTERED METAL FILTERS IN PARTICULATE RECOVERY APPLICATION IN GAS STREAM.

SAI-80BK-23

The filters are manufactured by sintering a powdered metal, which can be stainless steel or other alloys, in the form of a thin sheet. Basically the metal powder of a certain particle size range is evenly spread on a flat surface at the desired thickness, sintered, then cooled. The resulting sheet is then rolled into a cylinder and the seam welded. Attaching a blind cap at one end and a pipe connection of some kind at the other completes the construction. Filters can also be produced with no weld seam if desired,[3] and a variety of shapes can be fabricated. The pore size distribution of the filter is determined by the particle size(s) that comprise the starting powder and the detailed fabrication procedure. The nominal pore sizes advertised are from 0.5 to 40 microns, but the determinations of these sizes is not always indicative of the smallest particle that can penetrate the filter; therefore, some filters are rated according to an absolute and nominal particle size that can be removed.[4]

1.4 Process Design Using Sintered Metal Filters

There are no satisfactory design equations that describe the application of sintered metal filters for the recovery of particulate from a gas stream; only design practices. A set of design equations would describe the filter efficiency as a function of the pore size distribution of the filter, the incoming particulate size distribution, and superficial gas velocity. The design equations would also describe the pressure drop during filter loading and immediately after the filters were cleaned. It is necessary to know the presure drop relationships in order to size fans for an entire process system design. The final result of the design equations would yield a set of operating parameters for nonplugging operation. The most common concern about the use of SMFs is the operating time before plugging occurs.

The design practices are not specifically a function of particulate size distribution except that the pore size of the filter should be smaller than most of the particulate. The superficial velocity that is verbally recommended is usually 1.2 to 2.1 m/min (4 to 7 ft/min) or sometimes even less, even though pressure drop versus superficial velocity for clean filters is advertised at considerably greater velocities.[3,4]

The method of filter cleaning, which is referred to as blowback, can be either of the pulsed type similar to that used for bag filters or continuous reverse flow. There has been a rather extensive amount of work published on the pulsed blowback method[5-7] while the reverse flow blowback method has received very little attention.[2] In the pulsed blowback method, a tube or nozzle is directed to the filter exit as illustrated in Figure 1.2. When the pressure drop across the filter has reached a predetermined value, or when a specified elapsed operating time has occurred, a high pressure source of gas is applied to the nozzle for approximately 0.4 s. This pulse of gas stops the forward flow of gas through the filter and by some mechanisms dislodges some or most of the filter cake. The high pressure gas source is usually at 100 psig. In the reverse flow blowback method of cleaning, a reverse flow of gas is maintained for a few seconds. The reverse superficial gas velocity should be one-half to one times the forward velocity.[2]

It should be emphasized that a number of filters can be placed in a single vessel and each filter or a fraction of the filters can be cleaned while the others remain in operation. Thus, the use of the filters in this manner yields

a process that continuously removes particulate from a gas stream, much in the same manner that bag houses operate. However, each blowback method requires considerably different hardware, and the specific method used appears to be a function of the size of the installation in terms of the number of filters. There appears to be no single source of information which describes the advantages of one blowback method over the other with respect to filter efficiency, pressure drop, and non-plugging operation.

The theory of operation of porous SMFs is described in the open literature only in a very fragmented way. A correct theory of operation would be expected to lead to appropriate design equations or detailed design practices. However, the theory of operations presented appears to be superficial in some cases, explaining how the filters will plug,[8] rather than how they may exhibit stable operation.

A sintered metal filter should not be compared to a high efficiency particulate air filter, commonly referred to as a HEPA filter. A HEPA filter has a very high particulate removal efficiency in its clean state and is loaded with particulate only once and disposed of. In contrast, a SMF has a high particulate removal efficiency when loaded with particulate and is not disposed of after being loaded once. The SMF appears to obtain its high efficiency and non-plugging operation from a thin permanent cake that is formed and remains even after blowback. This thin permanent cake is believed to protect the metal portion of the filter from permanently plugging.

Specific experience with SMFs ranges from descriptions of plugged filter operations at one extreme[6] to hundreds and thousands of hours of trouble-free operation with efficiencies so great that they are not easily measured;[9,10] and hence, for that application the efficiency was considered essentially absolute.[9] In this case, the observed efficiency determination was made by examining downstream piping from a radioactive fluidized bed operation for contamination.

Sometimes the efficiencies are only briefly noted as in Reference 11 where a particulate removal efficiency of 0.99999 is given. A high removal efficiency with no plugging has even been observed in a system where the approach velocities ranged from 3 to 4.3 m/min (10 to 14 ft/min) with pressure drops approximately 14 kPa (2 psi).[12]

2. Experimental Program to Test Sintered Metal Filters

2.1 Purpose

The primary objective of the SMF test program was to verify the applicability of the filters in the INEL Transuranic Waste Treatment Facility off-gas treatment system. Two criteria that were considered necessary for applying SMFs were particulate removal efficiency and stable pressure drop. The particulate size distribution used in the tests had to match or be finer than that expected from the slagging pyrolysis incinerator. The pressure drop requirements were stable operation at as low a pressure drop as practicable. A further objective was to test both blowback methods to determine any advantage of one over the other with respect to obtaining the primary objectives.

2.2 Experimental Apparatus

The experimental apparatus initially used for testing the SMFs in a pulsed-blowback mode is shown in Figure 2.1. The apparatus was designed to deliver a constant volumetric flow rate of gas to the filter vessel. The main gas flow from the blower was split into a vent and a process flow. A venturi tube located near the filter vessel served as the flow rate indicator which supplied a differential pressure signal to a two-mode proportional plus reset pneumatic controller. The output of the controller positioned the vent valve to maintain the venturi tube differential pressure setpoint.

The pulsed-blowback hardware is shown in Figure 2.2. This hardware is not as sophisticated as some described in the literature,[3,5] but experience [12] indicated it would be successful. The blowback logic initiated the blowback pulses when the pressure drop had attained a predetermined value. This value was arbitrarily chosen because there was no information available on the expected pressure drop after blowback. Two filters were blown back at a time with a 20-second pause between pulses until all filters were pulsed. No tests were conducted where the blowback was initiated on a time cycle.

The experimental apparatus used for testing the SMF in a sustained reverse flow blowback mode is depicted in Figure 2.3. The main process stream and fly ash injector are the same as Figure 2.1. The reverse flow air was supplied by a secondary system. During normal operation while the SMFs were loading, valve A in Figure 2.3 was open and valve B closed. The reverse-air blower was operated continuously, and the required volumetric flow rate of reverse air for blowing back the porous SMF was controlled and vented through the pressure control valve. The pressure control valve was adjusted so that the pressure drop across it was approximately the same as that across the SMF during blowback. By making this pressure adjustment, the flow control valve did not have to hunt for a new position the instant blowback started.

When the pressure drop across the porous SMF had attained a predetermined value, the sustained reverse flow blowback sequence was started. Valve A would close, valve B open, and another valve in series with the pressure control valve would also close. This flow configuration was applied to two SMFs at a time for approximately 3 seconds. The other sets of filters were then sequentially blown back at 30-second intervals.

Six filters were installed in the filter vessel. Each filter was 0.91 m (3 ft) long by 6.8 cm (2-3/4 in.) OD by 0.15 cm (1/16 in.) wall. One set of six filters was obtained from Pall Trinity Micro Corporation,[4] grade H and an another set of six filters was obtained from Mott Metallurgical Corporation,[3] filtration grade 2 micrometers.

The test particulate used was fly ash. Fly ash was chosen because it generally appeared to have a particulate size distribution similar to that expected from the slagging pyrolysis incinerator. The fly ash was injected into the pressurized process gas stream as shown in Figures 2.1 and 2.4. Redispersal of the fly ash was obtained by subjecting it to a jet of gas issuing from a 0.317 cm (1/8 in.) OD tube with a 0.081 cm (0.032 in.) ID with a pressure drop greater than 310 kPa (45 psi). The fly ash was augered into the injector with a standard solids feeder.

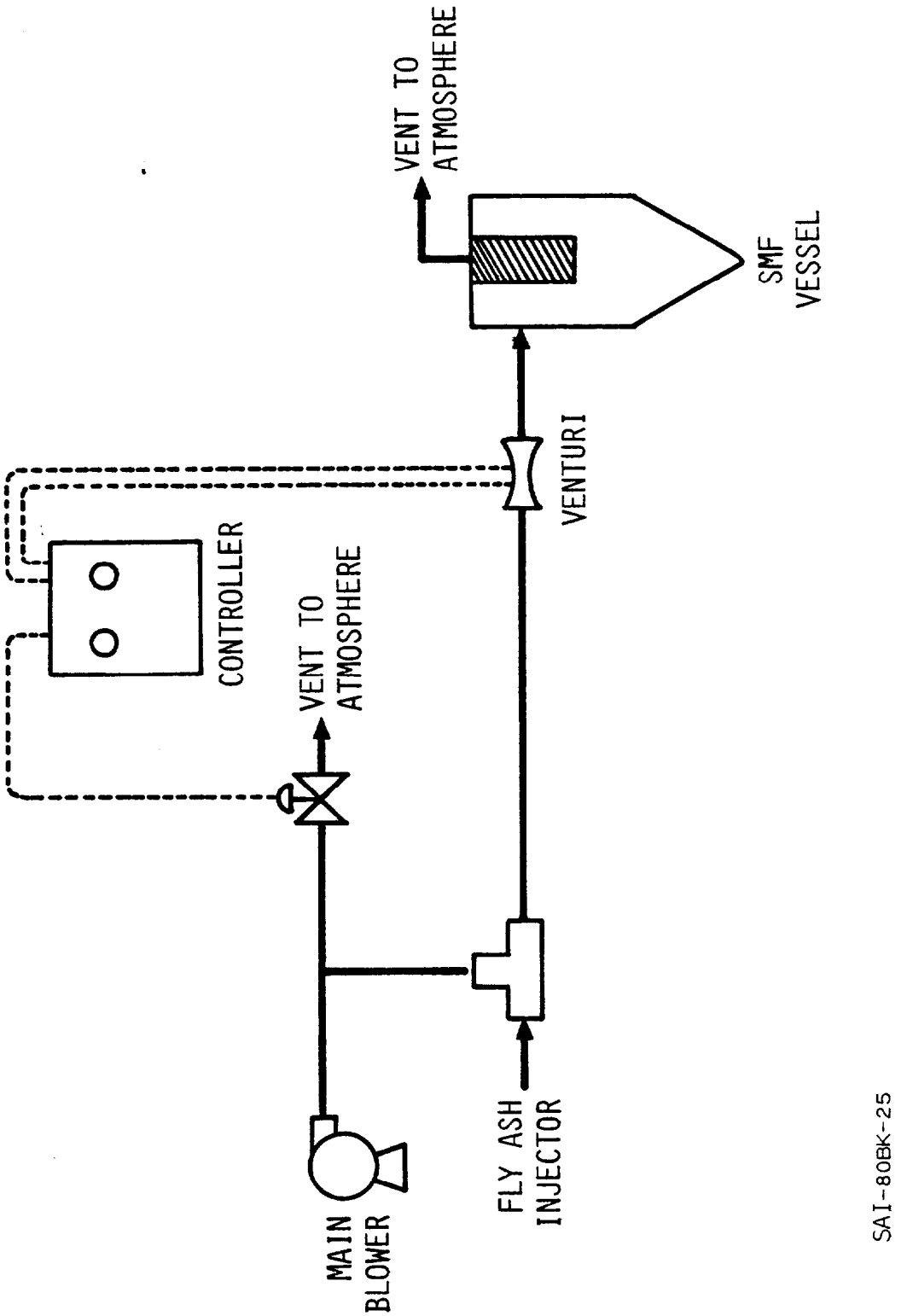

FIGURE 2.1. FLOW SYSTEM FOR PULSED BLOWBACK POROUS SINTERED METAL FILTER TESTING.

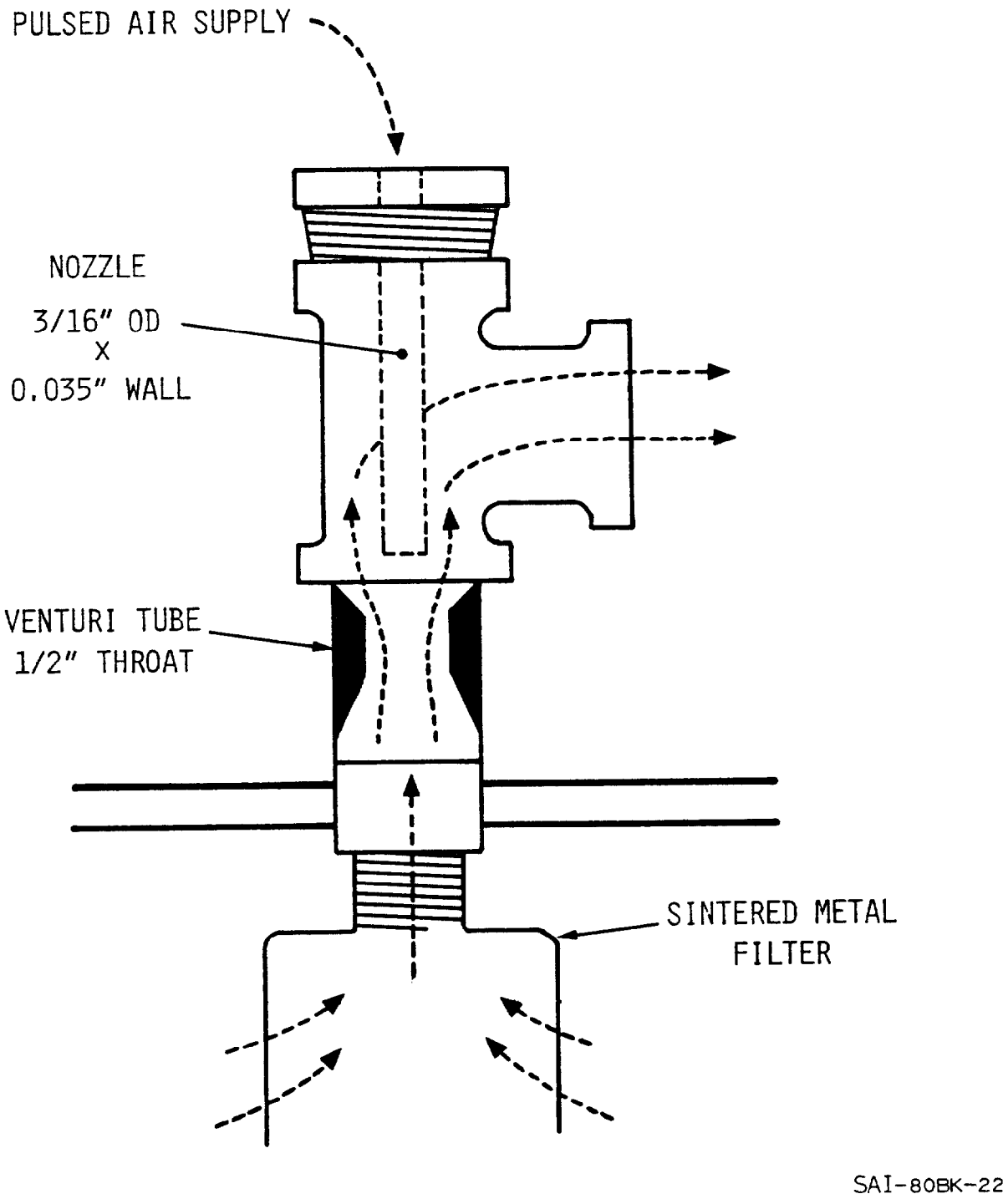

FIGURE 2.2. PULSED BLOWBACK ASSEMBLY.

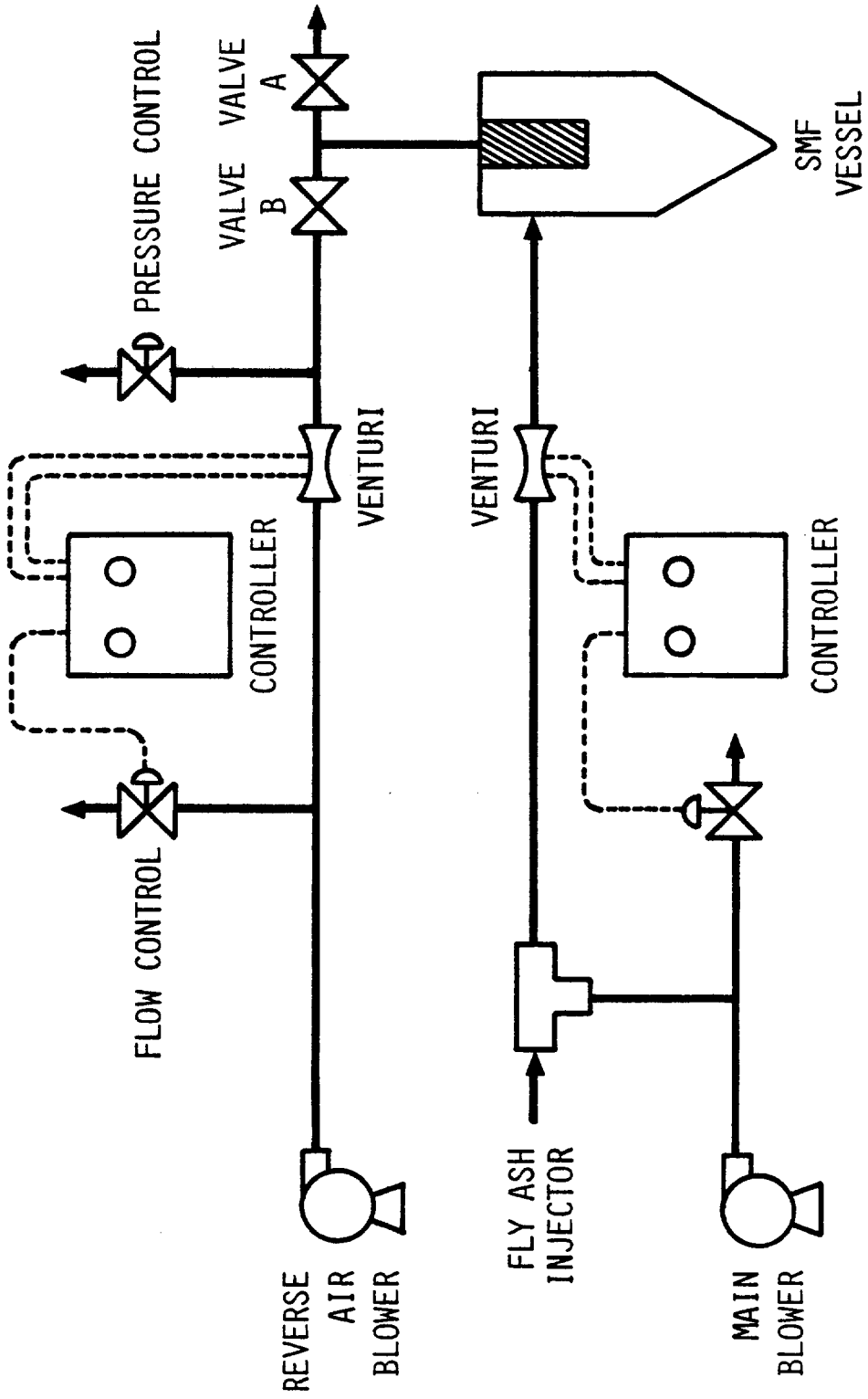

SAI-80BK-24

FIGURE 2.3. FLOW SYSTEM FOR SUSTAINED REVERSED FLOW BLOWBACK POROUS SINTERED METAL FILTER TESTING.

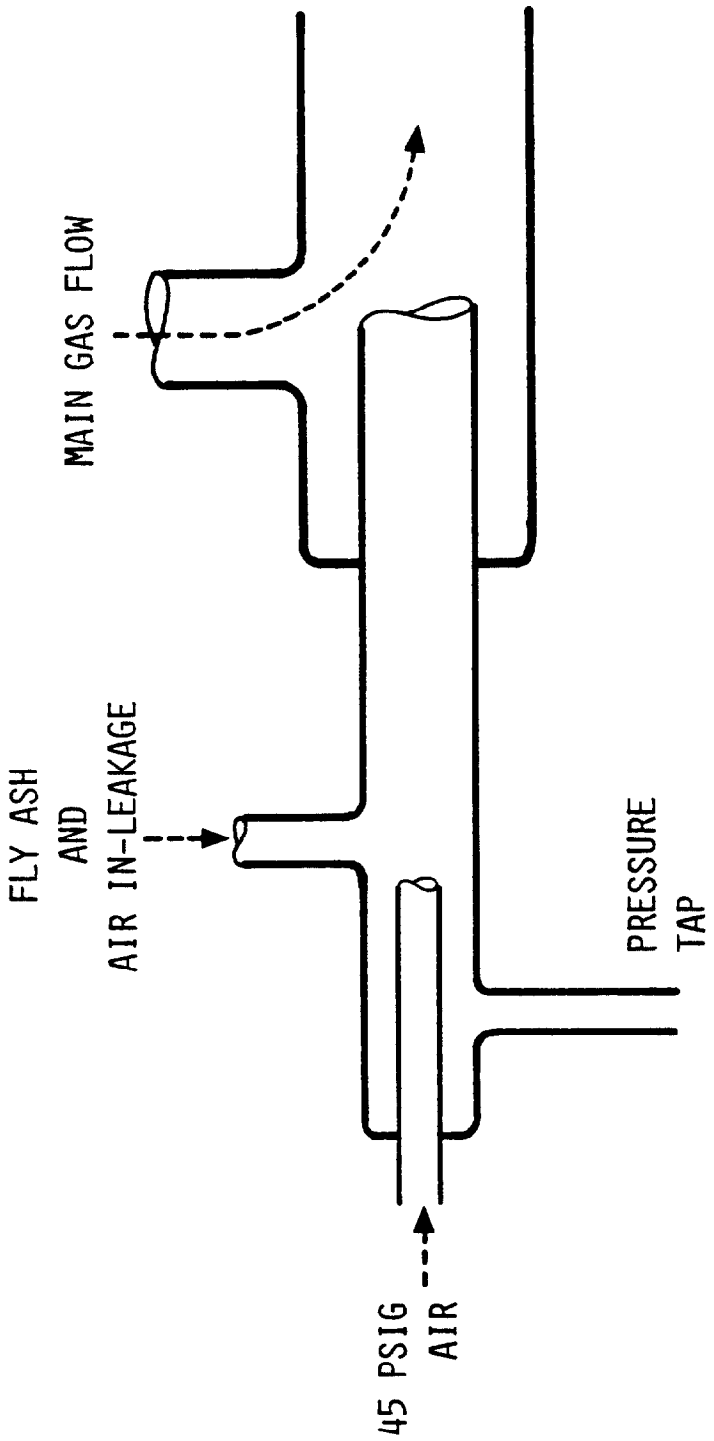

SAI-80BK-27

FIGURE 2.4. FLY ASH EJECTOR.

Efficiency measurements were made with a particulate sampler placed downstream from the filter vessel. The particulate sampler consisted of two 47-mm in-line filter holders in series which were connected to a constant volume pump. The sample probe was placed in the center of the downstream pipe. The filter closest to the process stream, called the A filter, was expected to gain mass due to particulate which had passed through the SMFs. The second filter which filtered the sample gas after the A filter, was called the B filter. The purpose of the B filter was a control to yield information on handling errors in mass determinations and possibly information on the efficiency of the A filter.

The filters used were Gelman Spectro - grade 47-mm filters with a reported efficiency of 99.95% for 0.3 micrometer diameter particles. This efficiency is generally attainable when the superficial velocity is in the range of 1.6 to 3.1 m/min (5 to 10 ft/min). The superficial velocities used for these 47-mm filters in the SMF test program were in the range of 10 m/min (32 ft/min) where the efficiency is estimated to be about 99.9%.[13]

In order to observe the operation of the sampling filters, a pressure gauge was installed at the outlet of the B filter holder. Since the sample volume was obtained through the use of a constant volume pump, any particulate removal of of the A and B filters could be observed during operation by a change in pressure drop across them for the constant volumetric flow rate. Also, observing a pressure drop across the A and B filters gave the assurance that a flow of gas through them was occurring.

2.3 Test Program[14,15]

2.3.1 Particulate Size Distribution and Loading

The particulate size distribution and loading of the redispersed fly ash reaching the SMFs were measured by sampling after the filter vessel when no filters were installed. The reason for obtaining these measurements in this manner was that the filter vessel had an efficiency for particulate removal of about 60% for the fly ash used. The filter efficiencies reported here are based on these downstream measurements to assure that artifically high results are not reported.

The particulate size distributions obtained by cascade impactor measurements[16] after the filter vessel are presented in Figure 2.5 along with the expected distribution from the slagging pyrolysis incinerator. This figure shows that the redispered fly ash that reached the SMFs was finer than the incinerator particles below 10 μmA.

Total particulate loadings were obtained with in-line filters as previously described. Again the particle loadings were obtained after the filter vessel with no filters installed. The particulate loadings were in the range of 3 g/Nm^3 with a fly ash injection rate of 10 g/min into a gas flow rate of 1.25 Nm^3/min.

During the final stages of SMF testing 5 wt% red iron oxide paint pigment in the fly ash was used as the test particulate. The iron oxide was added to increase the percentage of fines, and cascade impactor measurements indicated that the iron oxide increased the sub-1.2 μmA fraction by approximately 80%.

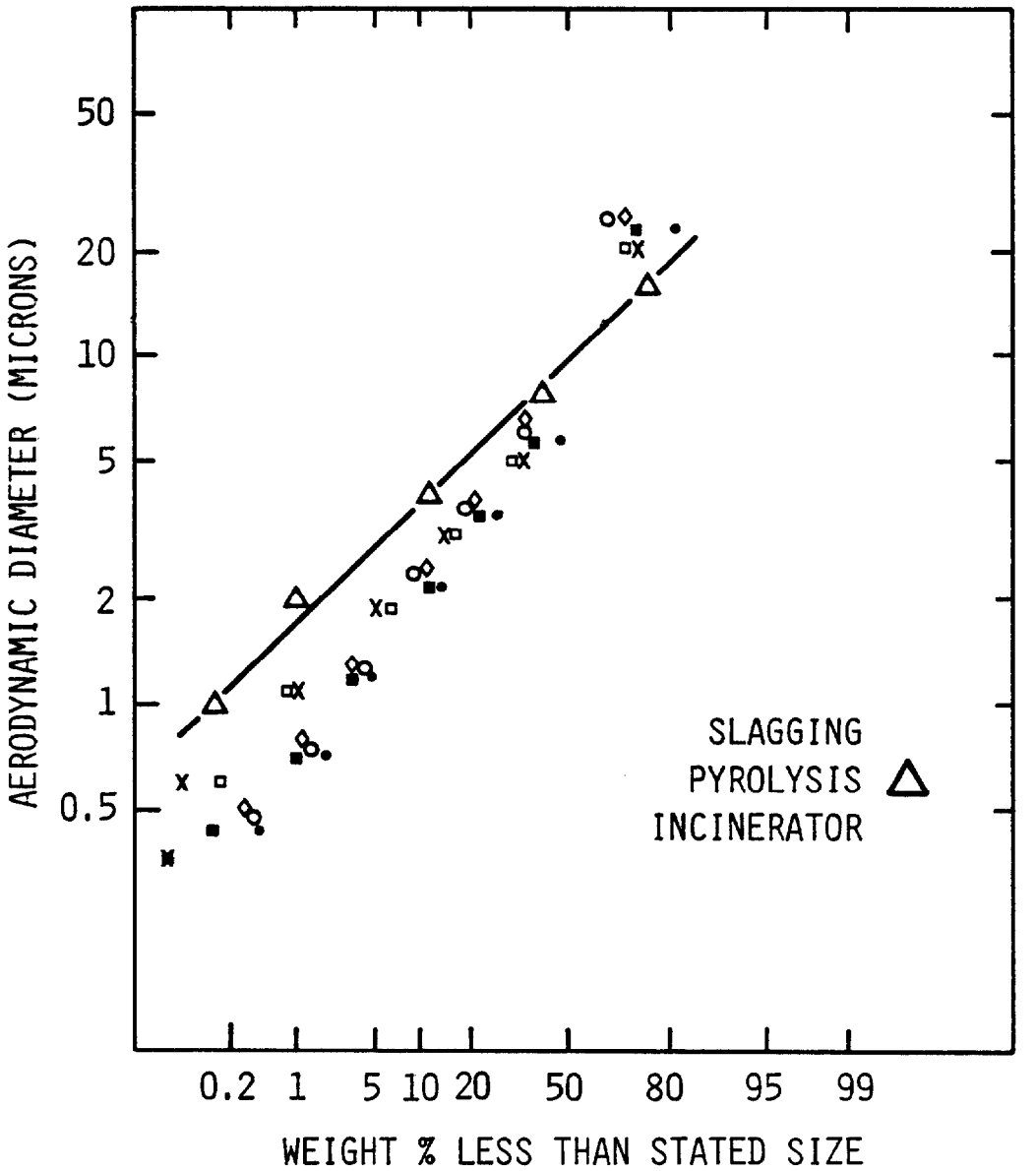

SAI-80BK-26

FIGURE 2.5. PARTICULATE SIZE DISTRIBUTION OF REDISPERSED FLY ASH.

2.3.2 Sintered Metal Filter Efficiencies

The SMF filter efficiencies for both sets of filters were determined in a total of 15 tests. Two of these tests in the pulsed-blowback mode were for over 280 hours and yielded the highest estimates of particulate removal efficiency. The data from these two tests are presented in Table 2.1 and show efficiencies greater than 99.99999% for fly ash removal on a mass basis. The Run Number identification in the first column of Table 2.1 denotes an A and B in-line filter measurement. The A measurement was the filter used to sample the gas-particulate flow, and the B measurement was the filter in series behind A as previously described. In each long-term test, no mass change was observed on the A-B filters. Since no mass change could be observed on these filters, a mass collected of 0.1 mg was assumed. The value of 0.1 mg is based on numerous experiments in the laboratory on filter handling procedures and repeated mass determinations. In other tests with reverse flow blowback some discoloration of the A filter was observed, but the mass gain was not measurable. This discoloration was determined to be due to the unfiltered blowback air. In the tests with iron oxide plus fly ash no red discoloration of the sampling filters was observed.

The conditions of the two tests conducted for over 200 hours were a superficial velocity of 1.16 m/min (3.8 ft/min) with a pulsed-blowback initiation pressure drop of 6.25 kPa (25 in. WC). The gas was air at ambient temperature and humidity and the temperature in the filter vessel was approximately 40^{0}C (104^{0}F). These conditions are referred to as the base conditions.

Thirteen additional SMF tests at other conditions were made that had gas-particulate sampling times less than 200 hours. Since no mass gain on the sampling filters was observed, with one exception, the 0.1 mg gain was assumed. These tests yield efficiencies on the order of 99.999%. The one exception where a mass change was observed on the A filter, but not the B filter, was attributed to the downstream piping being contaminated with fly ash due to previous cascade impactor measurements. Subsequent recleaning of the piping resulted in no mass increase of the sampling filters.

While sampling with the A-B filters the suction pressure immediately after the B filter was monitored. From the beginning to the end of a test this pressure was essentially constant to within 0.12 kPa (0.5 in. WC) indicating that no gross loading of particulate was occurring.

A determination of the absolute particulate removal efficiency of the SMFs was not possible with the hardware and techniques used. Only bounded estimates could be obtained for the particulate source used.

2.3.3 Pressure Drop Characteristics

The porous SMF pressure drop immediately after blowback is called the recovery pressure drop. For stable operation this pressure drop must remain well below the blowback initiation pressure drop. The recovery pressure drop after every blowback in the tests described here was recorded. In the pulsed-blowback mode where the initiation pressure drop was 6.25 kPa (25 in. WC) the recovery pressure drop appears to stabilize at 3.75 to 4.25 kPa (15 to 17 in. WC).

TABLE 2.1. SINTERED METAL FILTER PARTICULATE REMOVAL EFFICIENCIES

Gas Flow to SMFs: 73.8 Nm^3/h

Fly Ash Feed Rate: 10 g/min

Sampling Rate: 1.62 Nm^3/h

RUN #	SAMPLING TIME (h)	MASS COLLECTED (mg)	ESTIMATED MASS COLLECTED (mg)	SMF EFFICIENCY[a]
23a	282	(-0.06)	0.1	0.99999991
23b		(-0.14)		
30a	440	(-0.19)	0.1	0.99999994
30b		(+0.08)		

[a]Based on 1/3 fly ash feed rate

Over 100 blowback cycles were required to attain apparently stable operation. These test results do not indicate infinitely stable pressure drop characteristics; however, the data for over 400 cycles on two different sets of filters did not indicate an increasing trend in the recovery pressure drop.

Reverse flow blowback tests were conducted at the base condition. Initially, the reverse flow superficial velocity was one-half the forward velocity and resulted in a recovery pressure drop only slightly below the initiation pressure drop. Increasing the reverse flow superficial velocity to 1.2 m/min (3.8 ft/min) resulted in a recovery pressure drop of 4.5 kPa (18 in. WC) for over 250 cycles.

Other tests conducted on pressure drop characterizations include variation of the blowback initiation pressure drop, increased superficial velocity, particulate size distribution change, and temperature and humidity changes of the process air stream. Changing the pulse blowback initiation pressure drop had no observable effect on the recovery pressure drop at the base conditions. However, increasing the superficial velocity did result in an increase in the recovery pressure drop. Returning to the base condition after increasing the superficial velocity did not result in a return to the prior recovery pressure drop. From this result it appears that the porosity and/or thickness of the permanent cake on the filter are determined by the highest superficial velocity. Changing the particulate size distribution with iron oxide as previously noted had no effect on the recovery pressure drop compared to the base condition.

Probably the most significant tests with respect to pressure drop characteristics were performed with conditions of high humidity and temperature. By injecting steam into the air process stream, a gas composition containing approximately 24 volume percent water vapor was obtained. The process stream was heated to approximately 90°C (194°F) to maintain a dry system. These conditions resulted in a rapid increase in the recovery pressure drop from 4.5 kPa (18 in. WC) at the base condition to greater than 5.2 kPa (21 in. WC). Temperature alone was the variable that affected the recovery pressure drop. This was determined by allowing the system to stabilize with steam injection, then stopping the steam injection, and finally shutting down the process heater. There was no change in the recovery pressure drop when the steam was stopped, but the recovery pressure drop decreased to 3.9 kPa (15.5 in. WC) as the air stream cooled down after the process heater was shut down. Repeated applications and removal of heat appeared to indicate that the change in pressure drop is reversible. This pressure drop change with respect to temperature appears to be due to a change in porosity and viscosity, and has been quantified for a clean SMF.[3]

2.4 Observations on Cake Release

The filter vessel was fabricated with an extra 4-inch flanged opening located at approximately the midpoint of the installed SMFs. This observation window revealed some details on cake formation and release that have not been reported before.

Both sets of filters were intially tested in the pulsed-blowback mode. With both sets of filters, a stable permanent cake was not formed until approximately the 100th cycle operating at the base condition. During the first 20 blowback

cycles, the cake was completely released at the instant of blowback leaving a slightly fly ash-colored SMF surface. At the instant of blowback, the cake would appear to expand slightly with vertical fissures and then fall. However, after 20 cycles patches of fly ash were adhering to the SMF surface at the instant of blowback while fly ash was still being lost from the surface of these patches. By the 100th cycle the entire filter surface had a permanent cake formed, and the cake was being dislodged as many very small pieces, leaving a mottled appearance to the permanent cake. The release of these many small pieces did not come from the entire surface of the filter cake but from only a small fraction of the surface. It appeared that if a certain area released cake on one blowback pulse it did not do so on the next blowback pulse because there was never a permanent pattern recognized on the cake immediately after blowback.

An effort was made to measure the cake thickness by examining the filters when removed from the vessel. Based on measurements of the cake just before blowback, the cake thickness was estimated to be approximately 0.076 cm (0.030 in.). Upon further handling of the SMFs removed from these tests, it was discovered that a definite outer layer of filter cake could be easily removed from the filter by holding the filter vertically, and gently tapping the blind end with a metallic object. Upon tapping the filter in this manner, cracks would be formed in the cake; and once a small patch fell off, the entire cake would peel off under the influence of gravity over a period of a few seconds. In order to stop the entire cake from peeling, the filter was turned 90^0 to a horizontal position. The cake thus residing on the "top" now could be examined. Figure 2.6 is an example of these observations. In this figure the undisturbed cake is at the top and a small verticle (on the figure) crack can be seen in the middle. Actually there are three layers evident in this figure with the middle layer being the dark section to the right, and the permanent layer being the light section below. The two outer layers in Figure 2.6 fell off the SMF when it was gently rotated 180^0. The permanent layer is not of uniform thickness and estimated to be approximately 0.002 cm (0.005 in.) thick.

These observations present evidence for the existence of the permanent filter cake and other layers of cake which are easily removed. From these observations, it is clear that the filter cake is not of uniform structure with respect to strength properties. This immediately suggests the possibility of a structural cake such as that illustrated in Figure 2.7. In this figure the permanent layer is illustrated by the smaller particles residing next to the SMF surface, with the outer layer that is removed during blowback composed mainly of the larger particles in the distribution. The smallest particles can migrate through the outer layer because of the packing void of the larger particles. For the situation shown in Figure 2.7, the cake would be expected to fracture at the boundary of the large and small particulate at the instant of blowback. The existence of layers with different particulate size distributions is easy to visualize. Assuming this is the case, the small particles are capable of compressing more and the layer becomes stronger, also, van der Waal's forces would be expected to contribute to greater cake strength. As a result, the outer cake is bonded weakly relative to the inner cake and is released at blowback. Of course, in order to have a complete explanation of cake behavior, a description of the self-limiting growth of the inner layer must be developed. If the particulate size distribution is bounded on the lower end, then the permanent cake can provide absolute filtering and prevents particulate migration into the metal of

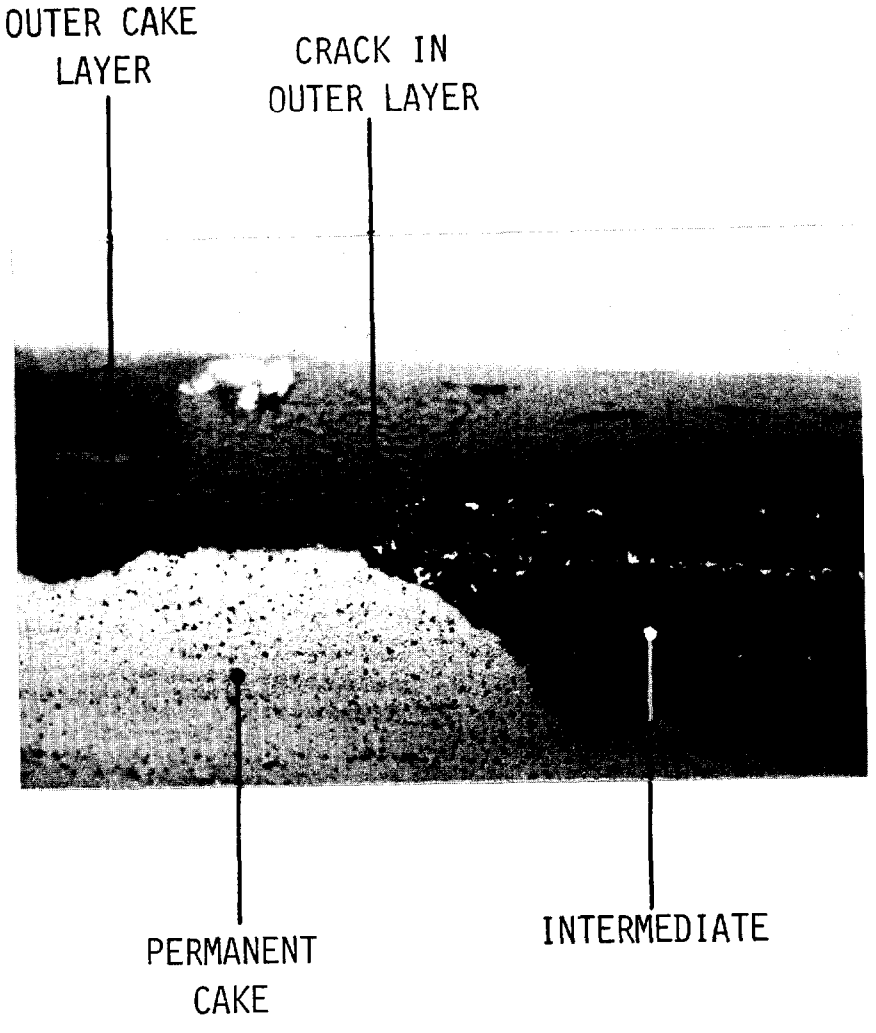

FIGURE 2.6. SINTERED METAL FILTER WITH VARIOUS LAYERS OF FILTER CAKE.

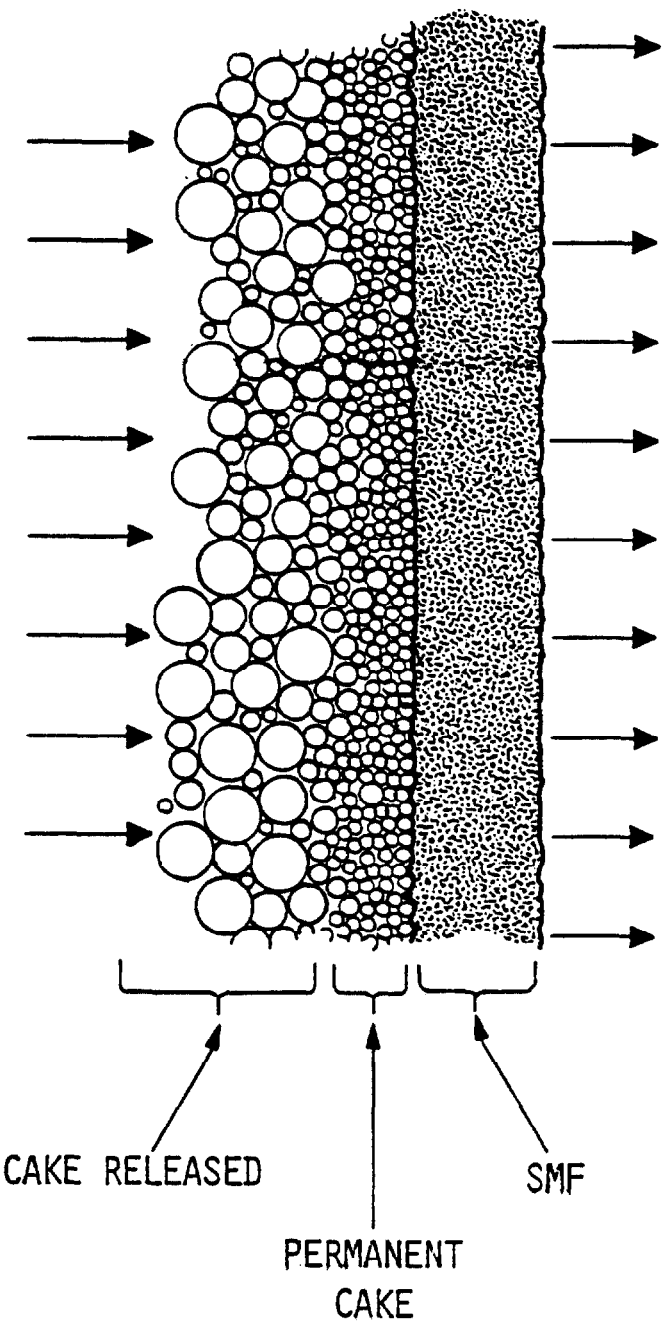

SAI-80BK-21

FIGURE 2.7. ILLUSTRATION OF HYPOTHETICAL CAKE STRUCTURE ON SMF.

the SMF. Reinstalling used filters whose surface had been swept clean resulted in essentially the same pressure drop as in the new unused condition at a superficial velocity of 1.16 cm/min (3.9 ft/min). This observation was made only once and supports the hypothesis of a thin permanent cake which provides the high particle removal efficiency.

Experimental evidence for a hypothesis on the mechanisms involved in SMF operation has not been obtained beyond the observations presented here. However, other fields of science and technology are concerned with similar problems on how particulate for a given particulate size distribution pack,[17,18] fractionate[19] and behave with respect to strength properties.[20]

3. Conclusions

3.1 Particulate Removal Efficiencies

The SMF particulate removal efficiencies reported here were obtained from a specific experiment. The efficiency of the SMFs are absolute in the sense that no measurable particulate were ever collected downstream from the filter vessel. The estimated efficiencies are on the order of 99.99999% based on the minimum assumed mass gain of downstream collection filters. This estimate is limited by the efficiency of the collection filters themselves which were HEPA filters. Other detection methods for particulate passing through the SMFs could very well yield a different result, but the detection method used in these experiments is similar to the intended application of HEPA filter protection. The efficiencies reported here are only for the particulate size distribution used and should not be interpreted or applied in any other sense.

3.2 Pressure Drop Characteristics

The pressure drop across the SMFs appeared to stabilize after an initial startup period. The pressure drop of interest is the recovery pressure drop that occurs immediately after blowback. It is not possible to demonstrate non-plugging operation in an absolute sense, but only over the time frame of an actual test. The pressure drop characteristics reported here are only for the specific conditions and fly ash tested. Over 4900 hours of operation with over 5100 blowbacks were conducted on SMFs with no apparent plugging observed.

3.3 Mechanisms of SMF Operation

The mechanism by which the filtered particulate behave with respect to the observations of the filter cake reported here is not presently known. However, observations are now reported that can yield clues with respect to the operating mechanism of SMFs, or more correctly, rigid barrier filters. Undoubtedly, knowledge from many fields of science and technology will be required to fully understand and predict the performance of rigid barrier filters through a complete set of design equations.

3.4 Other Applications of SMF

A process design engineer is reluctant to use a unit operation that is not well understood. In the case of SMFs, there are very few large applications of thousands of square feet of sintered metal filters because of not only the cost,

but also a lack of design equations. On the other hand, there are numerous applications involving hundreds of square feet of sintered metal filters where the relative size involved presents a smaller risk to the user. At the present it appears that data and design information are emerging that will make rigid barrier filters usable in such systems as incinerator flue gas filtration, extreme temperature environments, and where extremely high particulate removal efficiencies are required on a continuous-use basis.

References

1. Volume 1, Conceptual Design Report: Design Description for the Slagging Pyrolysis Incinerator Project, prepared for the United States Department of Energy Slagging Pyrolysis Incinerator Project Office, Idaho Operations Office, Idaho Falls, Idaho, by the Ralph M. Parson Company, Report number 5942-SPI-05 (May 1980).

2. D.B. Pall, "Filtration of Fluid Catalyst Fines From Effluent Gases", Ind. & E.C., Vol. 45, No. 6, p. 1197-1202 (June 1953).

3. Introduction to Engineering Controlled Porosity Products, Catalog No. 1000, Mott Metallurgical Corporation, Farmington, Conn.

4. The Pall Porous Metals Filter Guide, PSS-700a, Pall Trinity Micro Corporation, Cortland, New York (September 1978).

5. E.L. Carls and N.M. Levitz, "Blowback of Sintered-Metal Filters: A Review of Tests and Operating Experience", ANL-7392, Argonne National Laboratory (January 1968).

6. H.S. Meyer, "Rover Process Verification Studies-Sintered Metal Filters Blowback System", ICP-1165, Idaho Chemicals Program, Idaho National Engineering Laboratory (August 1978).

7. W.J. Bjorklund, "Development and Use of Sintered Metal Filters with Fluidized Bed and Spray Calcination of Simulated High-Level Waste", BNWL-2074, Battelle Pacific Northwest Laboratories, Richland, Washington (July 1976).

8. E.A. Zenz and H. Krockta, "The Shallow Expandable Bed-A Versatile Processing Tool", AIChE Symposium Series, Vol. 67, No. 116 (1971).

9. W.S. Rickman, personal communication, General Atomic Company, San Diego, California (September 1980).

10. O.D. Erlandson, personal communication, General Atomic Company, San Diego California (September 1980).

11. Nuclear Regulatory Commission SNM-1097, Docket number 70-1113, attachment 1, (December 1979).

12. B.E. Kirstein, personal communication, Science Applications, Inc., San Diego, California (November 1978).

13. C.A. Burchsted, et.al., Nuclear Air Cleaning Handbook, EPDA 76-21 (March 1976).

14. B.E. Kirstein, et.al., R&D for an Off-Gas Treatment System for a Slagging Pyrolysis Radioactive Waste Incinerator, Final Report for Phase III, prepared for EG&G Idaho, Inc., Idaho Falls, Idaho, prepared by Science Applications, Inc., San Diego, California (June 1979).

15. B.E. Kirstein, et.al., R&D for an Off-Gas Treatment System for a Slagging Pyrolysis Radioactive Waste Incinerator, Final Report for Phase IV, prepared for EG&G Idaho, Inc., Idaho Falls, Idaho, prepared by Science Applications, Inc., San Diego, California (February 1980).

16. Instruction Manual: Series 220 Source Cascade Impactor, Sierra Instruments, Inc.

17. S.D. Wicksell, "The Corpuscle Problem: A Mathematical Study of a Biometric Problem", Biometrics XVII, p. 84 (1975).

18. Particle Workshop, Loughborough University of Technology, Department of Chemical Engineering (March 29-April 12, 1971).

19. W.C. Krumbein, "Thin-Section Analysis of Indurated Sediments" Journal of Geology, Vol. 43, p. 482 (1935).

20. A.W. Jenike, "Storage and Flow of Solids", Bulletin of the University of Utah, Vol. 53, No. 26 (November 1964).

DISCUSSION

BERGMAN: I would like to add some further comments to those of the last two speakers concerning the performance of sintered metal filters. I especially want to emphasize the point made by Dr. Kirstein that sintered metal filters are not in the same class of high-efficiency filters as HEPA filters. Figure 1 shows a plot of the efficiency vs. particle diameter for a clean sintered metal filter. The sintered metal filter and test conditions were comparable to those in Dr. Kirstein's paper. Although the face velocity in our tests was 6.6 cm/s instead of 2 cm/s, this difference has a negligible effect on the efficiency curve. The major points to be made in Figure 1 are that the minimum efficiency of the sintered metal filter is below 70% and that the efficiency increases rapidly with increasing particle size. One of the primary reasons for the unusually high efficiencies reported in Dr. Kirstein's paper is the large particle size used in their efficiency tests. The other point that I would like to emphasize is the dramatic increase in efficiency that occurs during filter clogging. Although we have not done clogging tests on sintered metal filters, comparable tests with glass fiber filters can illustrate the increased efficiency. Figure 2 shows the efficiency

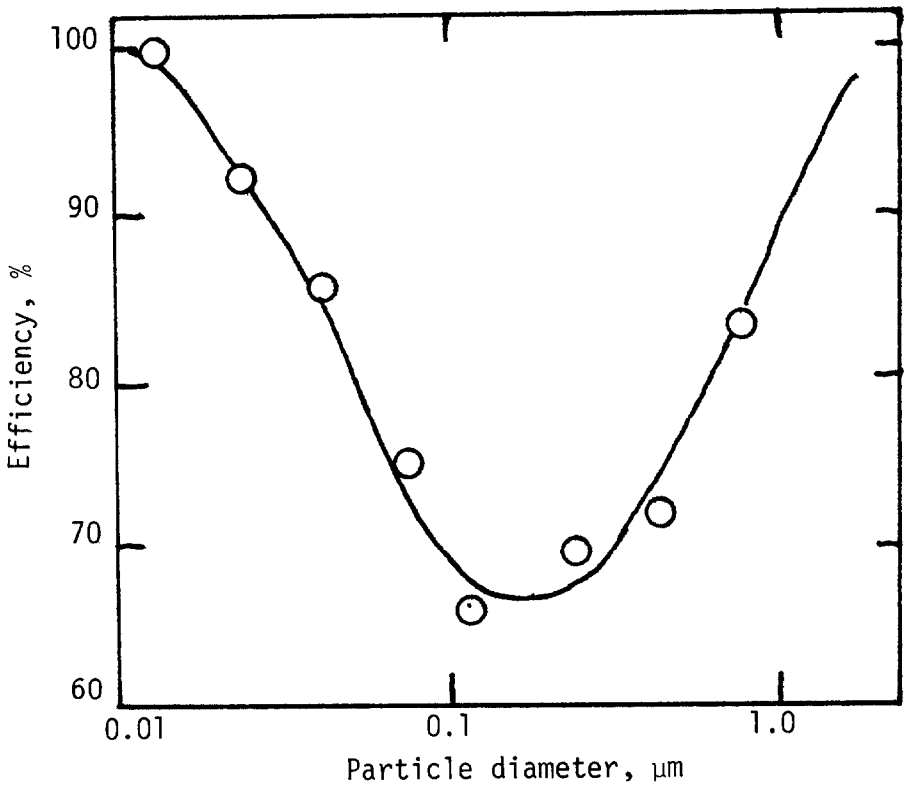

Figure 1. Filter efficiency of a clean sintered metal filter as a function of particle diameter when measured at a face velocity of 6.6 cm/s and using sodium chloride aerosols. The corresponding pressure drop was 5.2 in. w.g. The filter medium was a 1/16 in. thick flat sheet of porous stainless steel having a nominal 0.4 μm particle removal rating in air.

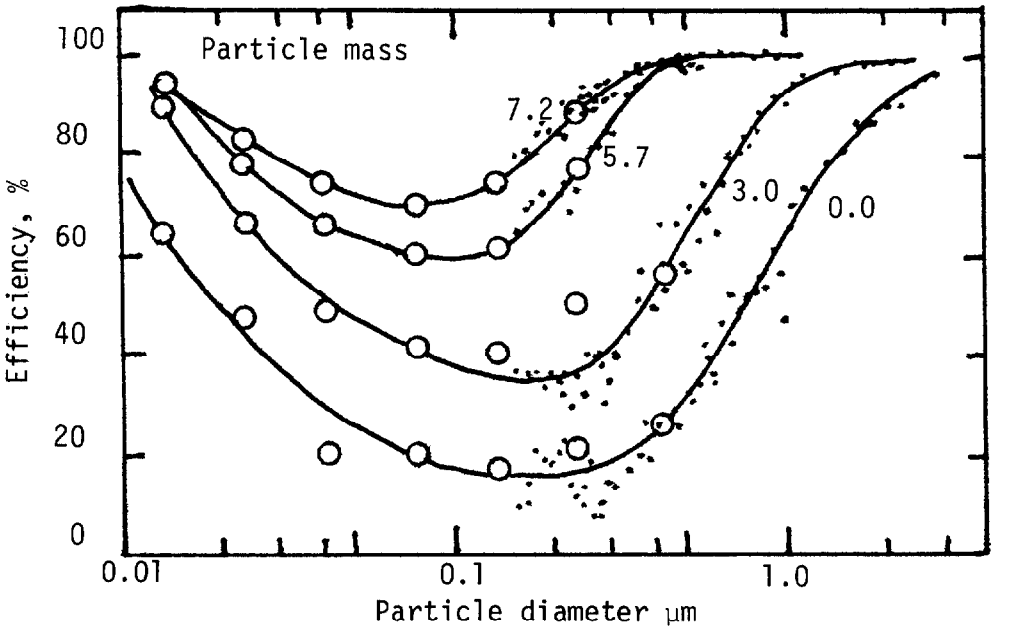

Figure 2. Filter efficiency of a glass fiber filter as a function of particle diameter during filter clogging when measured at a face velocity of 66 cm/s. The numbers next to the curves give the mass of sodium chloride trapped on the filter. The pressure drop across the filter increased from 0.6 to 5.2 in. w.g. as the particle mass increased from 0.0 to 7.2 g.

of a glass fiber filter as a function of particle diameter during filter clogging. Each of the curves represent the efficiency after the filter has trapped a given mass of sodium chloride aerosol. The particle mass captured by the filter is indicated next to each curve, with the 0.0 curve representing the clean filter. Note the rapid increase in filter efficiency with increasing clogging, especially for the larger particle sizes. Thus, the extremely high efficiencies reported for sintered metal filters having a particle deposit are primarily due to the particulate cake rather than the filter itself.

GILBERT: Dr. Kirstein, what was the material from which your sintered metal was made?

KIRSTEIN: Stainless steel.

INTERIM SUMMARY OF SESSION CHAIRMAN:

We had three papers today on loading of various designs of high efficiency filters. I think the results were quite similar in most of the cases, except that the loading of the filters exposed at HACL had a factor not present in the other tests, namely, the road repair of the street which gave an extra high dust load. It reached about 73 $\mu g/m^3$. Each laboratory, it appears, will continue to conduct tests.

In the latter two papers we have the use of sintered metal filters, very much in the shape of a bag filter. In Dr. Schurr's case, he used a reverse pulse, and found that the cleaning cycle pulse was very important. In Dr. Kirstein's case, he operated not on a time cycle, but on a pressure cycle to clean the filters of fly ash.

DPSPU 80-30-11
September 8, 1980

PERFORMANCE OF SAND FILTERS FOR THE SEPARATIONS AREAS AT THE SAVANNAH RIVER PLANT*

D. A. Orth
Savannah River Laboratory

G. H. Sykes and J. M. McKibben
Savannah River Plant

E. I. du Pont de Nemours & Co.
Aiken, SC 29808

Abstract

Two new large sand filters, 30.5 by 100 m, were constructed and put into service at the Savannah River Plant (SRP) in 1975 and 1976. These units were designed to provide final filtration of process air -- one for each of the two separations areas. Eventual flow will be 4,950 m^3/min (205,000 scfm) on each unit when all facilities are connected. They were built as replacements for the original sand filters that began operation in 1954 and 1955. The new filters have been operated in parallel with the old units following partial failure of the old units from acid attack and erosion of the concrete support structure for the sand beds. The design of the new units was based on extensive tests at SRP on characteristics of different sands (reported in the 14th Air Cleaning Conference). The performance of the new filters meets criteria for pressure drop, flow capacity, and efficiency. The efficiencies measured by DOP test are greater than 99.98% (limit of accurate measurement).

Parallel operation reduces air velocity through the beds, which increases efficiency. Partial collapses with subsequent repair continue to occur in the old units, which will be removed from service if deterioration becomes excessive.

A characteristic of sand filter performance has been low apparent efficiency at low input; efficiency increases as the activity input rises. This is attributed to a small entrainment

* The information contained in this paper was developed during the course of work under Contract No. DE-AC09-76SR00001 with the U.S. Department of Energy.

release from the large amount of activity already sorbed on the filter; this release controls and lowers the calculated efficiency at low input. An analysis of efficiency as a function of input activity projects efficiencies greater than 99.99% for large inputs that might be characteristic of large internal accidents. The data indicate that DOP efficiencies can be used in hazards analyses to determine accident consequences. Routine evaluation of filter releases can be used for surveillance to establish that performance is normal at other times.

Introduction

Deep-bed sand filters have provided the final filtration of process air from the two SRP fuel processing plants since startup in 1954. Two new sand filters were built to supplement the original filters and have operated in parallel with the old ones for 4 years. The original filters and their performance have been described previously as well as the extensive work to provide a design basis for the new ones[1-4]. The new filters were built as a result of acid attack and erosion on the concrete support structures of the old filters that allowed localized collapse and thinning of the beds with consequent activity releases. The old filters were repaired at the time, so there were no large continuing releases.

The real problem in design was to ensure that the new filters began operating with performance equal to the old filters, excluding the failures. This meant the new units had to perform much better at startup than the original units, which had a startup efficiency of only about 99.7 to 99.8%. They improved greatly over the years, presumably by compaction and dust accumulation that increased the efficiency to match or excel HEPA standards. Clearly in this day of heightened environmental concern it would have been embarrassing to install large new filters and simultaneously increase releases. The objective of high initial efficiency was met, so indeed it is possible to engineer a pile of sand to deliver a required performance.

Conclusions

The new SRP sand filters confirm that such units can be constructed for high efficiency at initial operation. The goal of the engineering test program to characterize and supply sands that would give high efficiences without excessive pressure drop also was attained.

Efficiencies of the units as measured by input and output α and β,γ activity are a function of input activity level, and the interpretation that the output is determined both by true efficiency plus some small release from the activity inventory on the filter still appears valid. The efficiency as measured by DOP test does correspond to the efficiency attained with large activity inputs; hence, DOP tests should be an adequate basis for hazards analysis for the releases following large internal accidents in facilities

equipped with sand filters. The input-output activity measurements also show a marked increase in efficiency with time. Continuing surveillance of input and output, with allowance for the small factor of release from filter inventory of activity, can provide continuing information on the integrity of the filter.

Radiation measurements within both the new and old beds show that the activity peak is gradually moving lower rather than rising. In conjunction with the evidence of simultaneously increased efficiency, this behavior reinforces previous conclusions that filter life is not limited by migration and breakthrough of activity.

Pressure drop in the other three filters is not increasing in the way that it did on the old F-filter, where possible explanations have included concrete dust and acid attack on minerals present in the sand. Current performance would indicate that excessive pressure drop also is not a life-limiting item in filters that are properly constructed and operated.

Filter Service

Sand filters in F and H Areas are in similar, but not identical, service. The F-Area separations plant primarily processes irradiated ^{238}U to separate ^{239}Pu, with some special work on the higher transuranium elements. The H-Area separations plant primarily processes enriched uranium fuels from SRP and from a wide variety of research and experimental reactors. The H-Area plant also processes irradiated ^{237}Np to separate ^{238}Pu. The ^{238}Pu processing operations and differences in cooling times following irradiation have placed heavier burdens on the H-filter with respect to filtration of α and β,γ activity. The input to the sand filters also has been reduced with time as a result of upgrading the filtration system on the vessel vent systems that serve the process tanks within the separations plants. The vessel vents have been major contributors to the sand filter inputs in the past. The improvement does not directly affect efficiency but does reduce the amount of activity released for a given efficiency and does influence the activity inventory in the sand bed, which indirectly affects efficiency. Finally, the F-filter has a higher volumetric air load from some extra facilities, and the extra load can influence efficiency according to the design tests. The composite result is that the F-filter has a lower output but also a somewhat lower efficiency.

Filter History

The general chronology of the SRP sand filters is covered in previous papers, but a brief summary is useful for reference. Fuel processing operations started in F Area in 1954 and H Area in 1955. The two filters increased in efficiency steadily with time, as measured by decreased release of activity, but the best filter, F, also has a continuing increase in pressure drop. The failures referred to previously happened in 1969 on H-filter and 1971 on

F-filter. Supplementary filter supports were installed but these still permitted small losses of sand from the bed and occasional small releases.

During this period excessive pressure drop on the F-filter required removal of the top foot of the 3-ft sand layer, and a decrease in efficiency was noted. The first DOP tests were made on the filters at this time and gave 99.98% efficiency for H-filter and 99.96% for F-filter. The design of new filters proceeded during this period, and the new F-filter was put into service in December 1975 and the H-filter in April 1976.

Although they can be isolated and taken out of use, the old filters have been left in service to decrease the air flow velocity through the sand, because of the test work that showed significant dependence of efficiency on flow. The DOP tests on the combined filters at startup of the new filters showed 99.98 to 99.99% efficiency in both areas. A lower efficiency was measured at one particular later period in the F-filter as a result of problems in the old filter (see later discussion). The old filters will be isolated if they cannot be maintained in reasonable working condition.

Air Flow Measurements -- F Area

When the new sand filter was put into service in F Area in parallel with the old sand filter, several different types of flow measurements were made to establish a data base for subsequent studies.

The division of air flow between the two filters was determined by measuring air flows through the three plenum exit ports on the new filter and the total air flow from both filters in the exit air tunnel. A total of 90,000 cfm was flowing through the new filter, and the total air flow was 150,000 cfm. Therefore, 60,000 cfm was flowing through the old filter.

Linear air velocity up through the sand filter was measured on a 90-point grid in the new filter (figure 1). The flow was found to be uniform throughout the filter within the uncertainty of the measurement. Uniform flow is highly desirable for long-term life and efficiency of the filter.

A low velocity anemometer was obtained to make the measurements. This instrument has a range of 0 to 30 cm/sec with an accuracy, as stated by the manufacturer, of ±1 cm/sec over the range of 0 to 20 cm/sec. Air velocities are measured with an external probe and are read directly from the instrument in centimeters per second.

The anemometer probe was mounted in the center of a 1- x 1- x 2-ft windshield (figure 2), approximately 4 in. above the surface of the sand. The windshield reduced interference from turbulence and crosscurrents, allowing a more accurate measurement of the vertical airflow from the sand bed.

Preliminary tests with the new anemometer indicated that at an air flow of about 1 cm/sec, the manufacturer's calibration was high by a factor of about 2 or 3. Therefore, it was necessary to recalibrate the anemometer in the very low flow range.

An apparatus to calibrate the anemometer over the range of flow rates expected in the sand filter was designed and built. The design was based on Euler's equation for liquid displacement by gravity from an open vessel. Euler's equation in it simpliest form is:

$$V = k\sqrt{h} \qquad (1)$$

where: V = inlet or outlet velocity, cm/sec
h = height of liquid, cm
k = constant, cm (0.5)/sec

This states that the inlet or outlet velocity (V) is proportional to the square root of the height of liquid (h) in the vessel. Since the height of liquid and the inlet and outlet velocities are continuously changing, this formula is unsuited for an exact determination of V. However, by choosing a vessel with the appropriate dimensions so that the height of liquid will remain essentially constant over a short time period, the small change can be ignored and the velocity assumed constant.

Figure 3 is a schematic diagram of the calibration apparatus. The vessel was filled with water to a predetermined height (h) and then allowed to drain into a graduated cylinder for a measured time. The time interval and liquid level are preselected so that the inlet velocity would be essentially constant. The linear velocity of the air entering the vessel was calculated from the known volume of liquid displaced during the time interval and the diameter of the inlet tube. To increase the accuracy of calibration over the desired flow range, two different sizes of inlet tubes were used. The calculated linear velocities and the corresponding instrument readings were taken while the volume of liquid was being displaced. A calibration graph based on these measurements was constructed (figure 4) and used to determine the linear velocity for each grid point in the sand filter.

The linear velocities measured at the surface of the sand bed ranged from 1.39 to 2.30 cm/sec. The average linear velocity (mean) was 1.82 cm/sec and the mode was 1.80 cm/sec through the new filter with a standard deviation of 0.21 cm/sec. The theoretical predicted velocity was 1.3 cm/sec, based on the measured flow and sand bed area.

The data, shown in table I and figure 5, indicate that the velocity profile at the surface of the sand bed is essentially uniform with no significant systematic gradients or localized areas of high or low flow.

The filters exhibit normal pressure drop behavior to date. The resistance of the sand beds to air flow determines the fan power requirements to maintain desired total flow through the ventilation system; hence, a significant variable. As noted in previous papers, excessive pressure drop on the old F-filter necessitated the removal of 1 ft of the sand bed in 1972. The present parallel filter systems do show the summer-winter variation in flow that has been typical since plant startup. The H-filter system pressure drop is holding steady,but there is some indication of a continued increase in the F-filter system. This last does not mean that the new filter is increasing in resistance but may indicate just a continuing increase in flow resistance on the old filter. The new filters were built with several groups of pressure taps in the beds, and measurements on the new F-filter show a low pressure drop through the sand layers.

Table I. Grid points with corresponding linear velocities.

Grid Point	Linear Velocity, cm/sec	Grid Point	Linear Velocity, cm/sec	Grid Point	Linear Velocity, cm/sec
1	1.80	31	1.80	61	1.80
2	2.30	32	2.02	62	1.60
3	2.30	33	1.80	63	1.92
4	1.60	34	1.80	64	1.80
5	1.60	35	2.30	65	1.80
6	1.80	36	1.60	66	1.50
7	1.80	37	1.60	67	1.60
8	1.60	38	1.80	68	1.72
9	2.02	39	1.80	69	2.02
10	1.72	40	2.30	70	1.80
11	1.80	41	1.80	71	1.80
12	1.50	42	2.02	72	1.80
13	1.50	43	a,c	73	1.80
14	1.60	44	1.80	74	1.39
15	a,b	45	a,b	75	a,b
16	a,b	46	2,b	76	a,b
17	1.92	47	1.39	77	1.60
18	1.72	48	2,c	78	1.72
19	1.60	49	1.72	79	1.80
20	1.80	50	1.80	80	1.80
21	1.60	51	1.80	81	1.72
22	1.80	52	1.60	82	1.80
23	1.80	53	1.80	83	1.80
24	1.80	54	1.80	84	1.92
25	2.02	55	2.15	85	2.02
26	2.30	56	2.15	86	1.80
27	1.92	57	1.80	87	2.02
28	2.02	58	1.72	88	2.30
29	2.02	59	1.80	89	2.15
30	1.60	60	1.80	90	2.30 ± 0.13

[a] Could not measure because of turbulence.
[b] At exit ports.
[c] Beneath personnel entry port.

Radiation Profiles

Recent radiation profiles through the parallel old and new filters are shown in figure 6. The profiles through the new sand filters parallel the early results on the original ones, 25 years ago, with the radiation peaking near the coarse sand/fine sand interface. We would expect the radiation peak to move down slowly with time as particulate matter accumulates so that eventually the peak will be at the gravel/sand interface as in the old filters.

As noted in previous work, there is no tendency for upward movement and eventual breakthrough of activity. The radiation level on the old filters has decayed significantly since parallel operation commenced, as a result of the lowered input. At various times in the past, shorter-cooled feed materials and poorer prefiltration of the process vessel vent stream have given radiation levels over 1 R in the peaks. These radiation data are gathered in periodic meansurments in the 10 monitoring tubes in the old filter and 9 monitoring tubes in the new, and the plotted data represent averages at a given level for all the tubes.

The range of values at a given level serves as an independent check on uniformity of air flow, because any area with above-normal flow would be expected to collect higher activity as well. The radiation maps of the two new filters are quite uniform except for one end of the F-filter, where air free of β,γ activity enters from an alpha-processing facility.

Filter Efficiency Analysis

It is always comforting if the efficiency of the filters as measured by DOP test corresponds to the actual retention of α and β,γ radioactive particles, because then the results of standard test conditions can be used in safety analyses. The following subsections discuss the efficiencies as projected by analysis of performance. The results indicate to us that real efficiency is at least as good as the DOP tests.

Limiting Efficiency Projection

The simple observation is that calculated efficiency for filtration of α and β,γ activity still is strongly dependent upon input, being better as input increases. Additionally, the calculated efficiency does appear to be improving with time on the new-old filter combination, as previously observed on the old filter alone. The proposal advanced in the past to explain the increased efficiency as input increased, as well as the pattern of response to large inputs, is that two mechanisms were operating. Some fraction goes through the filter in accordance with true efficiency,while another fraction represents re-entrainment from the large inventory of activity on the filter, as supported by specific radionuclide measurements (see later discussion). Further, the inventory is at risk for only a limited period before it is covered with dust and chemicals or otherwise fixed in place. Superimposed on these factors

is the effect of decay of short-lived fission products in the inventory. The proposed explanation still appears valid.

The data collected over 4 years since the new filters have been in service can be illustrated in several ways. Simple chronological plots of input, output, and calculated penetration (1-efficiency) for β,γ and α activity on both units are shown in figures 7 through 10. The wide swing in input activities reflects different processing programs in the facilities; and α and β,γ input vary independently, particularly in H Area because of the independent operation of the facility for enriched uranium recovery from reactor fuel and for ^{238}Pu recovery from irradiated ^{237}Np. On these graphs, the variation in output activity has a damped response to the input activity. The calculated penetration is seen to be a damped but almost exactly reflected image of the input activity. There is an apparent trend to lower penetration (increased efficiency) for the same input over the time period.

The data also can be plotted to show the relation between penetration and input as in figures 11 and 12 for the H-filter, and the increasing penetration with time also is apparent in the comparison of 1979 and 1980 data with the older data.

Accepting that our model of filter performance is correct, the current performance of the H-Area filter system would indicate that the first-flight penetration is certainly less than 0.02% (efficiency greater than 99.98%) and that it may well be less than 0.01% (efficiency greater than 99.99%).

An incident that occurred in March 1980 provided data to support this conclusion. A small process leak of a concentrated solution of ^{243}Am and ^{244}Cm caused high activity levels of these radionuclides in the sand filter inlet air. Analyses indicated that 5,781 mCi of these isotopes were in the sand filter inlet, but only 0.546 mCi in the air discharged from the stack -- an efficiency of 99.99%. These data are particularly relevant because there was no significant inventory of these isotopes on the filter when the incident occurred.

A natural concern is that a large increase in inventory from the large in-plant accident would raise the background release level so that the integrated release will be less than the projected high efficiency, even accepting our model. However, the historical response to past large inputs, the rate of return to a nominal background, and the tiny fraction that the background release is of estimated inventory still all argue that any continuing release fraction beyond the approximately 0.01% of the original input of a large in-plant accident will be small except in very extreme cases.

Probability vs. Penetration Analysis

An alternative analysis of filter efficiency has been made in an effort to assess probability of performance for application to hazards analyses; i.e., what is the probability that a specified filtration efficiency would be attained? A basic conclusion is that a

meaningful result is difficult to derive in these cases where efficiency appears to be a function of activity input. An indiscriminate summation of historical data may assume that a low efficiency calculated at the time of low input has an equal probability of occurring at high input. Further, the changes in physical condition of the filters with time and our responses to the failures must be considered. There were the periods of filter failure and the removal of 1 ft of sand from the F-filter because of high pressure drop. Also, when the first filter failures occurred, there were low efficiencies for varying periods of time before the cause was recognized and the filters repaired. If data from all of these periods are incorporated and the effect of input activity on efficiency is ignored, the penetration vs. probability groups project a substantial probability that filtration efficiency will be low with corresponding larger external effects from in-plant accidents.

This type of analysis indicated only moderate efficiencies even since the new filters were put online. Figure 13 is sucn a penetration vs. probability graph for the combined α and β,γ performance of the new H-filter system. It indicates a little less than 50% probability that the efficiency will be as high as 99.98%, and about a 10% probability that the efficiency will be less than 99.9%. This result is diametrically opposed to the conclusions of the analysis in terms of input activity where large inputs all are projected to have efficiencies approaching or greater than 99.99%.

Some better estimates of probabilities of performance can be obtained if data are grouped by input activity. Even here, the continuing improvement argues that only recent data be used. Also, the different responses require that α and β,γ be considered separately. Data for the β,γ performance of the new H-filter were discussed in relation to figure 9, which illustrates very good efficiencies in the region above 10,000 mCi/mo input. These data, also analyzed in figure 13, give greater than 80% probability that efficiency would be greater than 99.97%. The shallow slope also projects a very small probability (about 0.005) that efficiency would be as low as 99.96%. Consideration of just the last 1-1/2 years actually gives basically the same slope and 0.005 probability projection of efficiencies of 99.96% for input activities as low as 2,500 mCi/mo, with a fair probability that efficiency would be better than 99.99%. In the same manner, high probabilities of high efficiencies are indicated for high inputs of alpha activity.

Surveillance

In the 1976 report[4], a simple graph of filter output vs. input was indicated to be a means to detect abnormal operation before the filters were challenged by some large in-plant accident. An envelope can be drawn on this type of graph to define acceptable performance in terms of the "inventory release" and first-flight efficiency. It appears that the technique is still valid and would have alerted us to some abnormal conditions in the F-filter sooner than actually transpired.

The H-filters handle much more activity than the F-filter, and the old H-filter had recurrent crater-forming slumps that gave short-term increases in output activity. Hence, a crater detection system was installed in H Area, and constant attention was paid to even small increases in activity released, with quick inspection and repair of any craters. Both the input and output in F Area were smaller, and slumps were relatively infrequent so no detection system or convenient method of inspection were installed.

There were no large releases from F Area, but an excess over normal release was noted in November 1979, which lead to a DOP test that gave 99.22% efficiency as compared with the greater than 99.98% expected. An entry was made into the old filter, and four shallow craters were found and repaired. A review of 1978 and 1979 data showed a major period and perhaps a minor period when performance for alpha filtration deviated from the envelope of expected performance, as shown in figure 14. The major deviation from July 1978 to November 1978 is quite apparent on the graph. A chronological plot of the excess release shows a smooth rise that peaks in September 1978. After the fact, we would guess that these months represent the periods of crater formation.

The evidence of an excursion in alpha release from a slumping incident (but little evidence of β,γ release) corresponds to other episodes and is perhaps the most significant result. A reasonable explanation is that the alpha inventory on the filter is always growing, and a small fraction is mobilized when the bed is disturbed, but the β,γ inventory at risk reflects decay of the short-lived fission products and now actually is decreasing with time on the old filter.

References

1. Sykes, G. H., and J. A. Harper, "Design and operation of a large sand bed for air filtration," Treatment of Air Borne Radioactive Wastes (IAEA Symposium), CONF 680811-13 (1968).

2. Schurr, G. A., D. B. Zippler, and D. C. Guyton, "Deep-bed filter performance tests," 12th AEC Air Cleaning Conference (1972).

3. Schurr, G. A., and J. E. Johnston, "Characterizing sand grains to optimize filter performance," 13th USAEC Air Cleaning Conference (1974).

4. Orth, D. A., G. H. Sykes, and G. A. Schurr, "The SRP sand filter: more than a pile of sand," 14th ERDA Air Cleaning Conference (1976).

5. Davis, W. T. "Airflow velocity profile through the new F-Area sand filter," DPSPU 78-11-21 (1979).

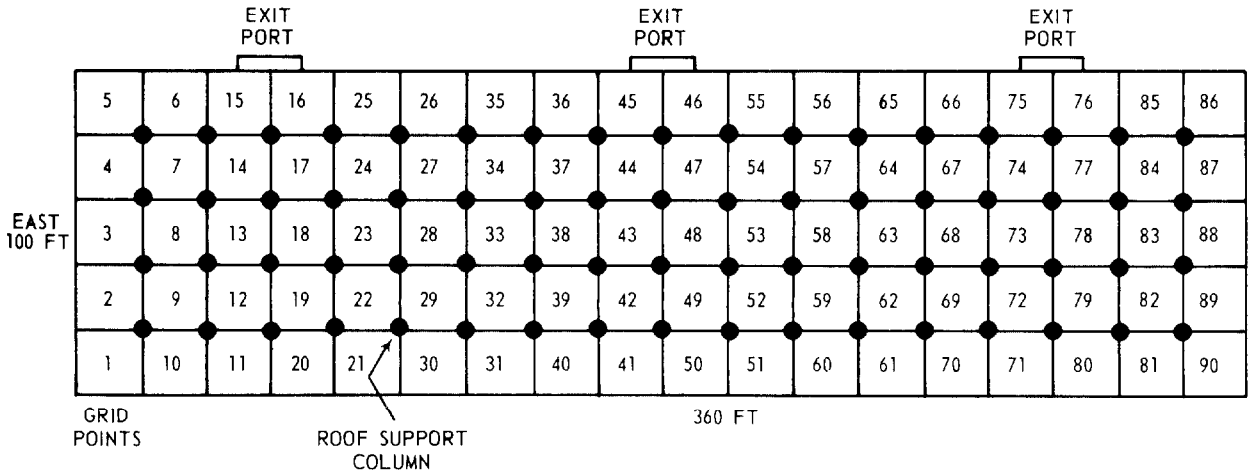

FIGURE 1. NEW F-AREA SAND FILTER

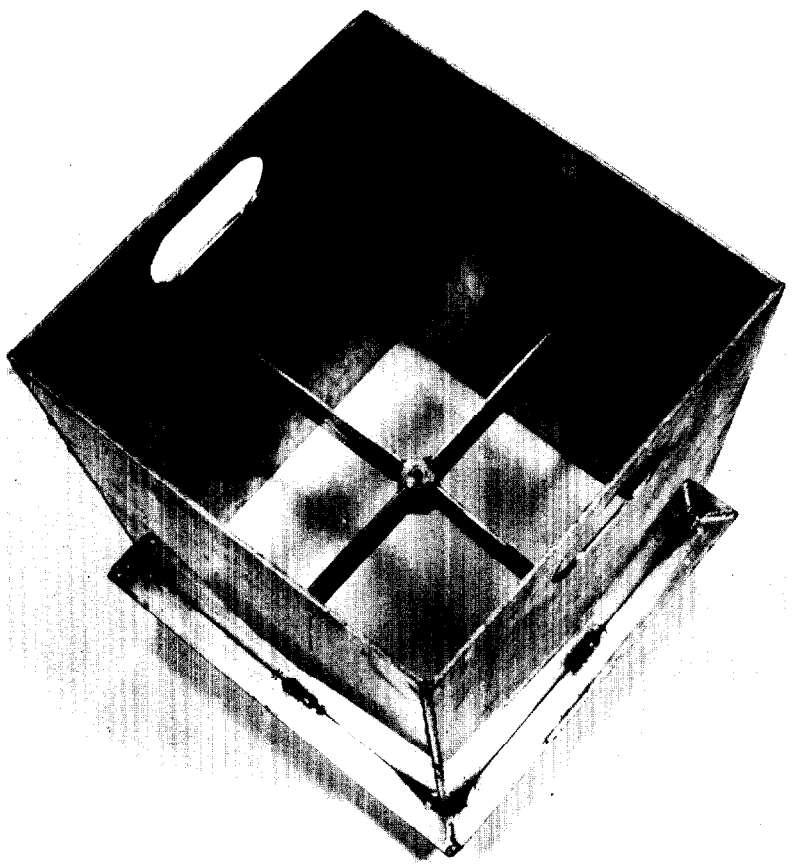

FIGURE 2. WIND SHIELD

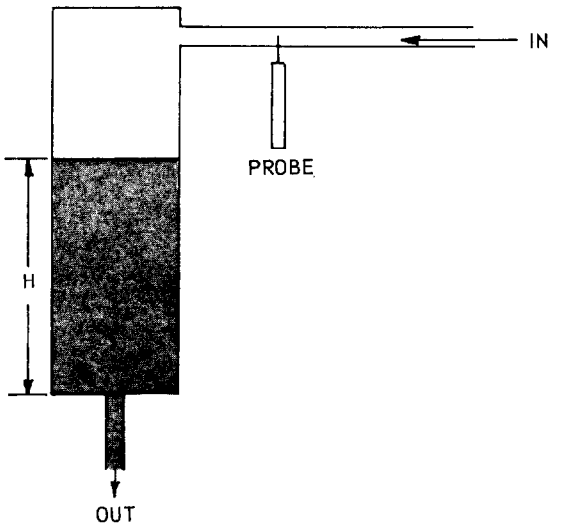

FIGURE 3. CALIBRATION EQUIPMENT

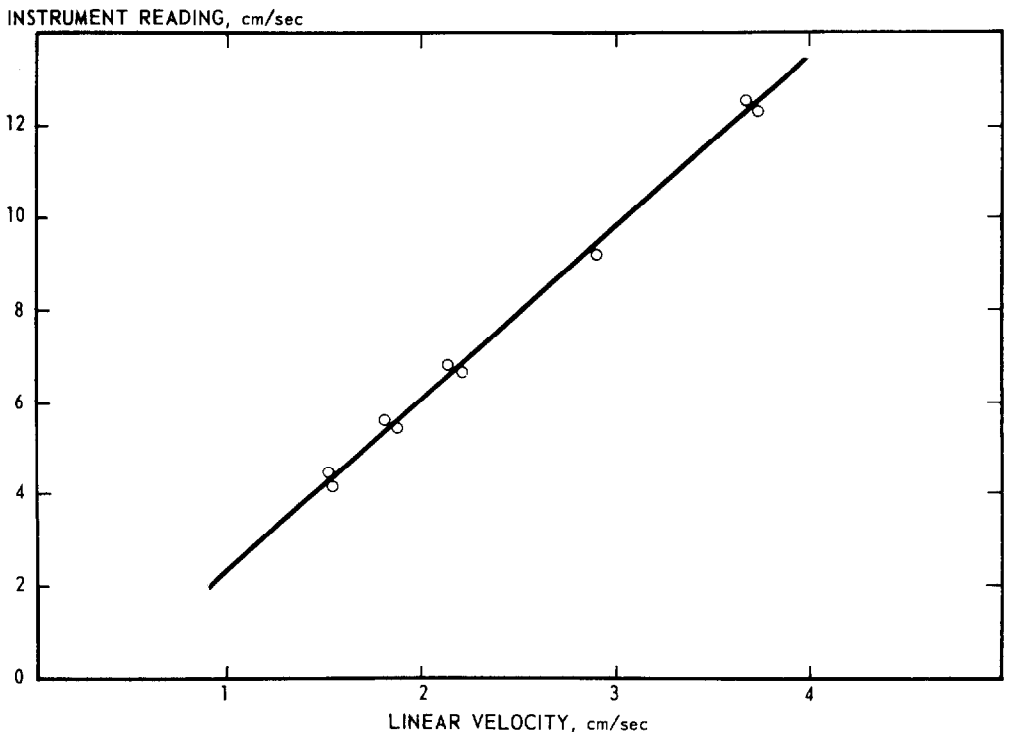

FIGURE 4. CALIBRATION CURVE DISA MODEL 55D81
LOW VELOCITY ANEMOMETER

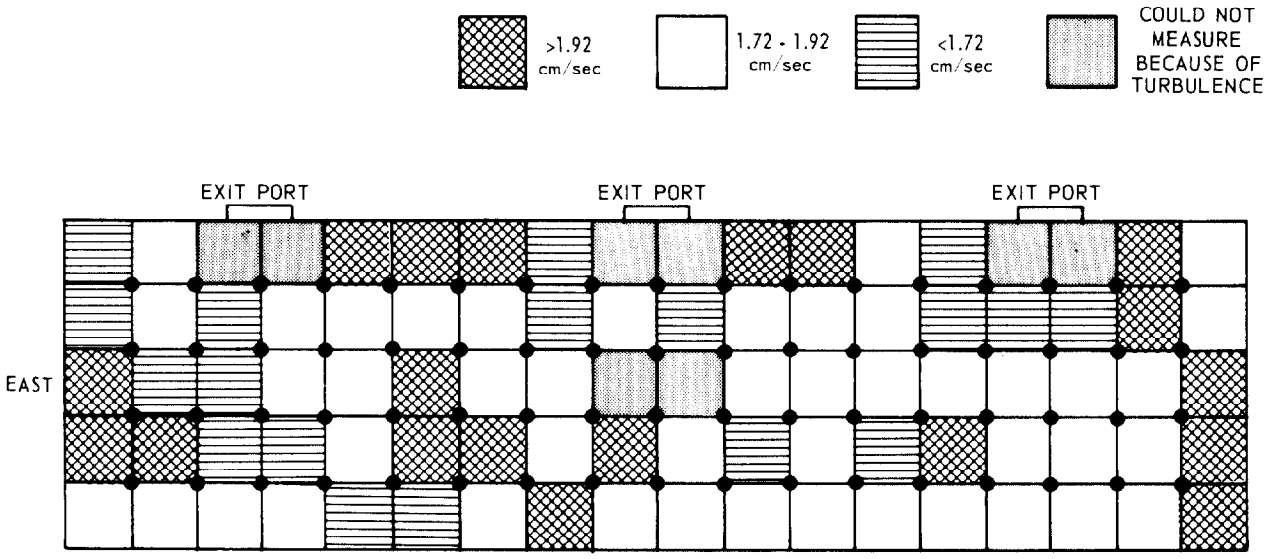

FIGURE 5. AIRFLOW VELOCITY PROFILE

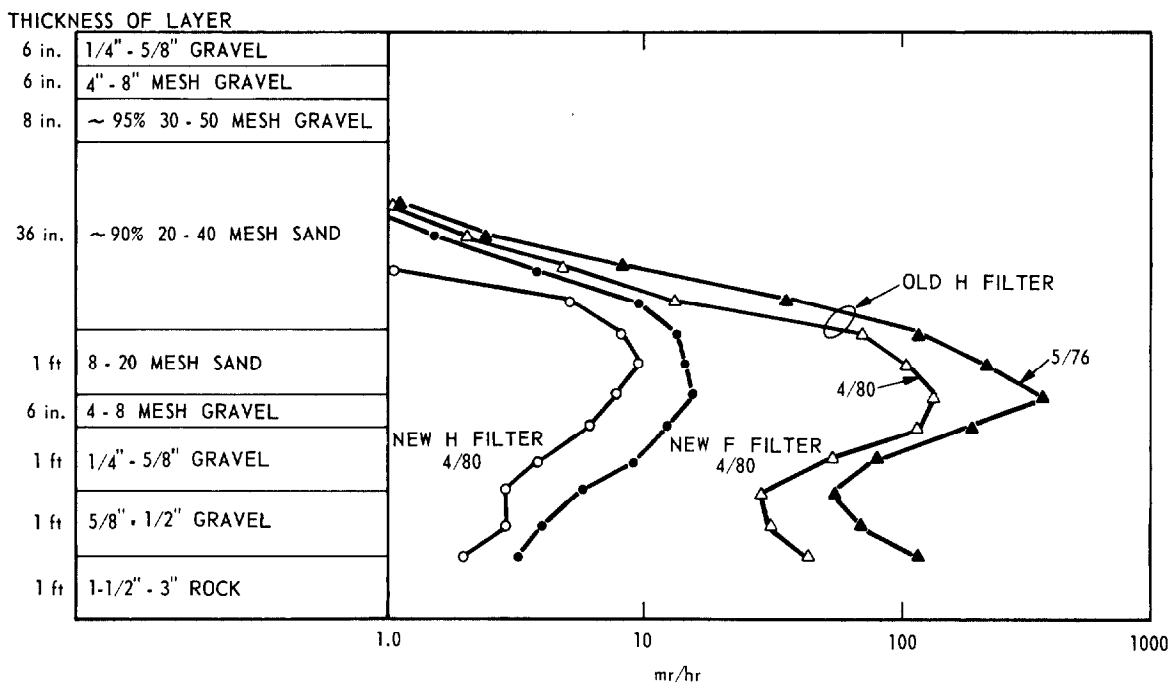

FIGURE 6. RADIATION PROFILES

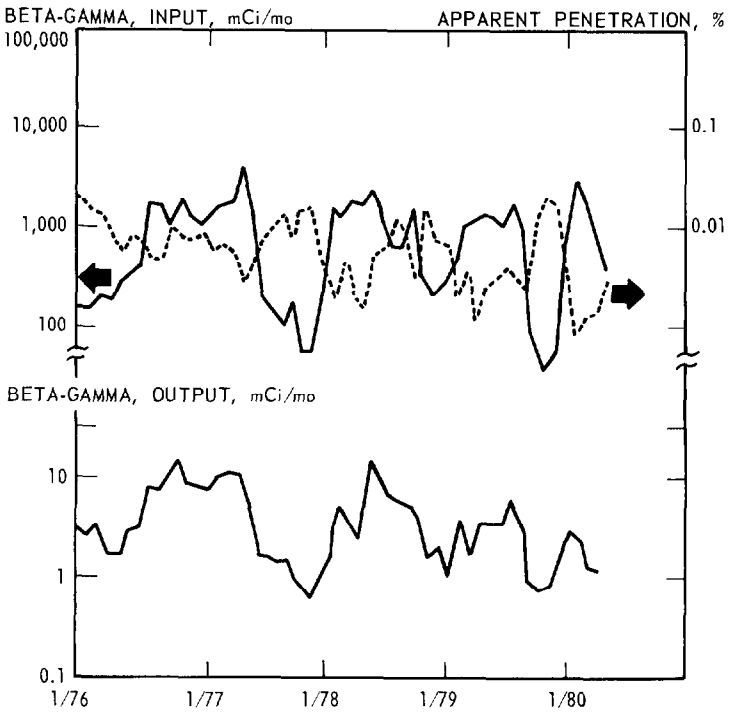

FIGURE 7. PERFORMANCE SINCE NEW SAND FILTER CONNECTION - F FILTER BETA-GAMMA ACTIVITY

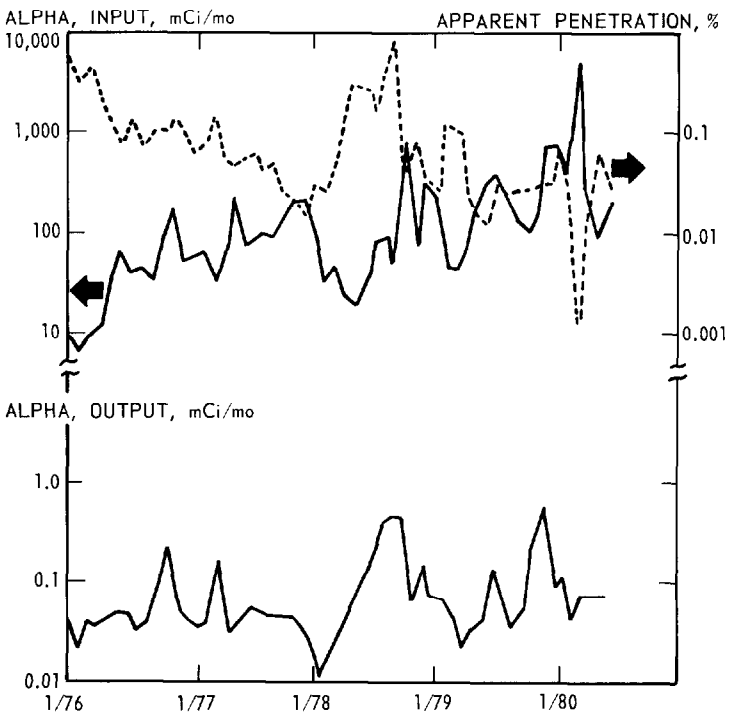

FIGURE 8. PERFORMANCE SINCE NEW SAND FILTER CONNECTION - F FILTER ALPHA ACTIVITY

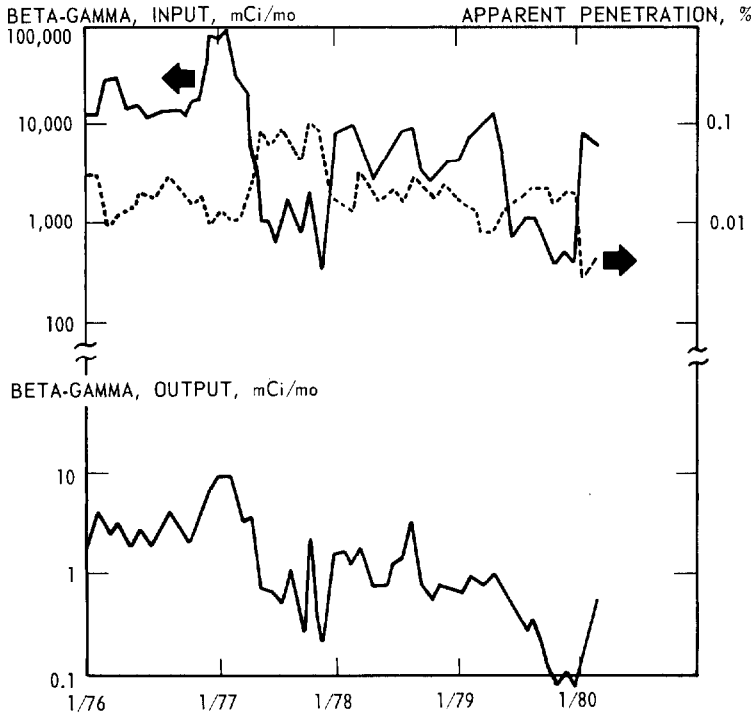

FIGURE 9. PERFORMANCE SINCE NEW SAND FILTER CONNECTION - H FILTER BETA-GAMMA ACTIVITY

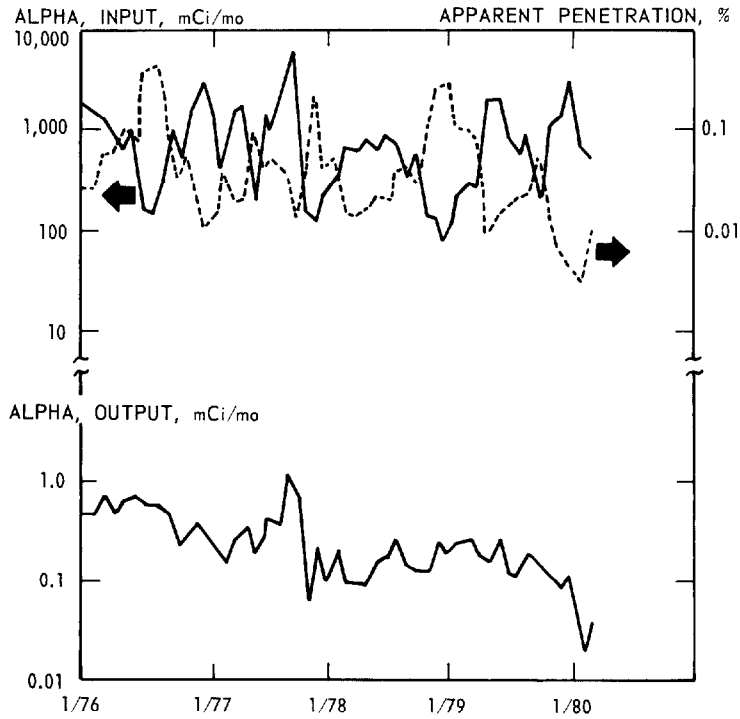

FIGURE 10. PERFORMANCE SINCE NEW SAND FILTER CONNECTION - H FILTER ALPHA ACTIVITY

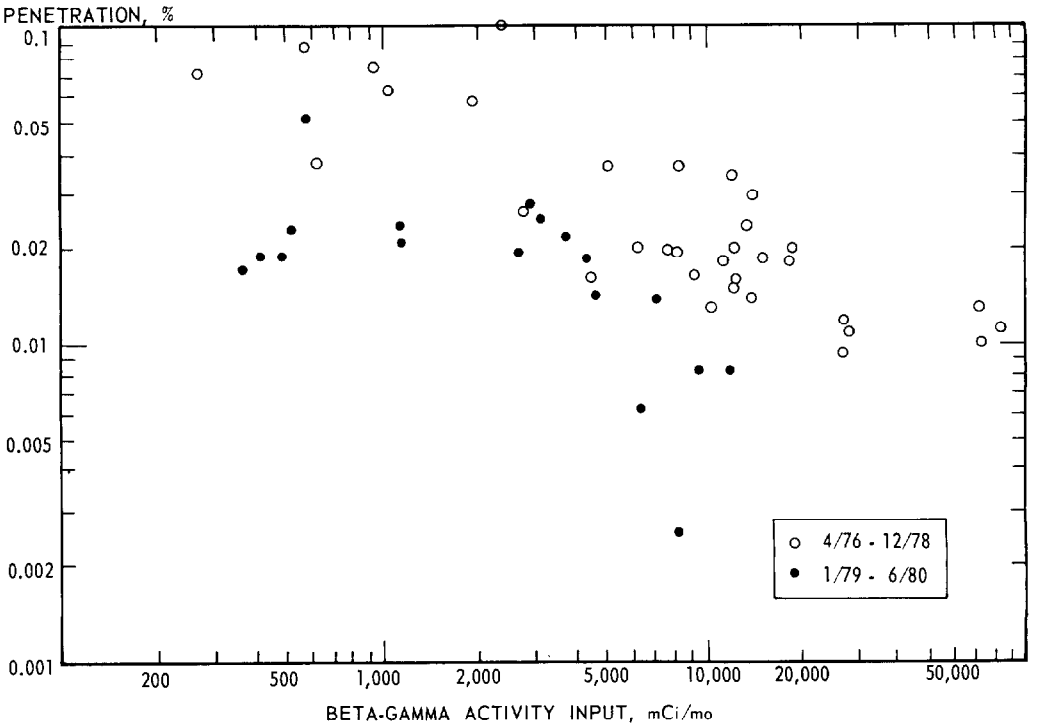

FIGURE 11. NEW H FILTER; BETA-GAMMA INPUT AND FRACTIONAL PENETRATION

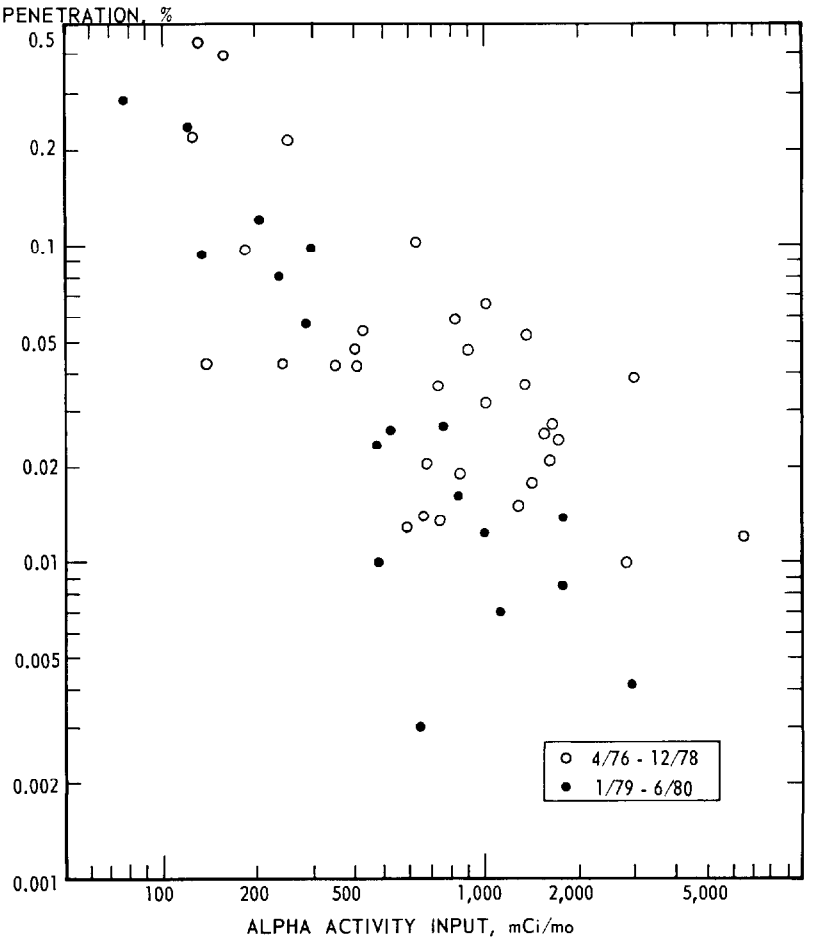

FIGURE 12. NEW H FILTER; ALPHA INPUT AND FRACTIONAL PENETRATION

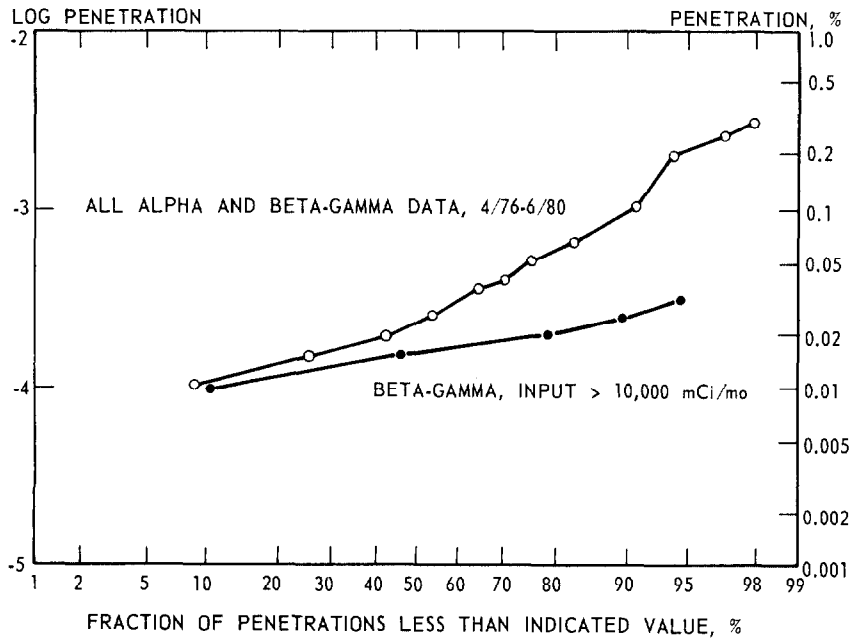

FIGURE 13. NEW H FILTER, DISTRIBUTION OF ALPHA AND BETA-GAMMA PENETRATION DATA

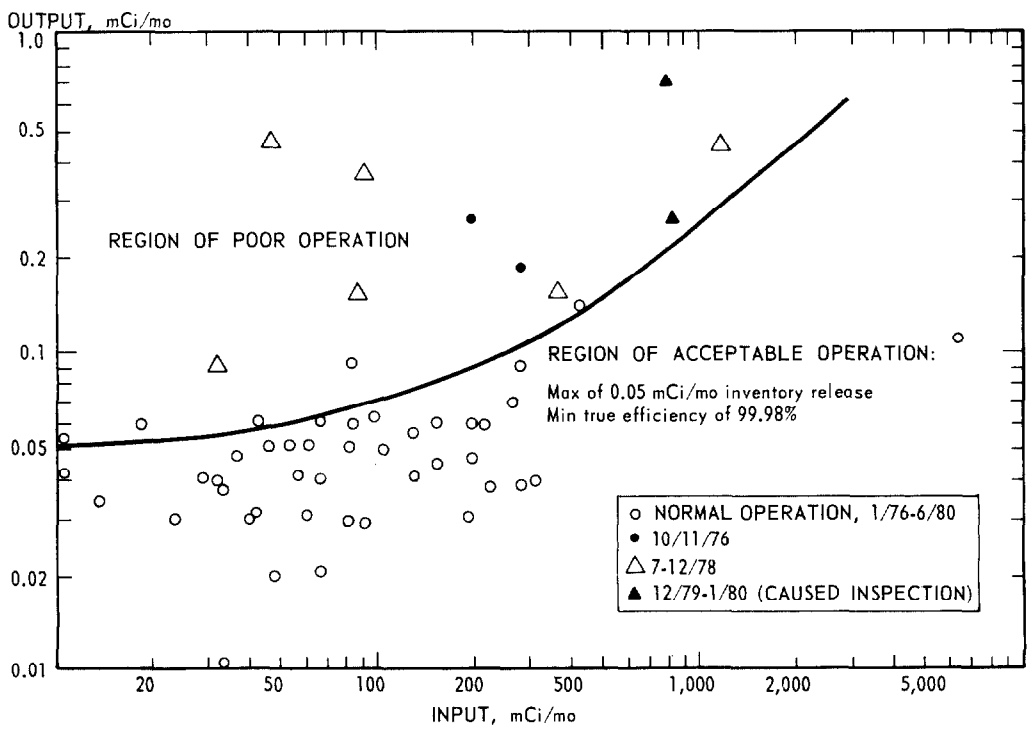

FIGURE 14. F FILTER, ALPHA INPUT AND OUTPUT

DISCUSSION

ORTH: The pressure drop across our sand filters at a nominal superficial velocity of around 5 fpm (2.5 cm/s) is of the order of 8 in.w.g.; that is,through the entire assembly. As I indicated, the pressure drop has gone up on one of the filters over time. There is a detailed discussion of pressure drop in our paper from the 1976 Air Cleaning Conference.

HERRMANN: What do you have before the sand filters? Do you have HEPA filters before the sand filters?

ORTH: The sand filters are taking canyon process air directly out of the processing canyons. This is the largest air volume. There is also some flow from the vessel vent system serving individual vessels. That air first goes through a packed bed-scrubber arrangement which is not a HEPA filter. The combined vessel vent air plus the bulk air from the canyons then goes through the sand filter.

CHEEVER: After removing one foot of sand, was the pressure drop then about what would have been predicted at start-up?

ORTH: As we did not make measurements of the equivalent of one foot less of standard configuration at start-up, the answer is, "We do not know." But pressure drop did go back down to about the same as the other filter, which now had a foot more of sand.

GEER: I would be interested to know if you have ever compared the life cycle cost of a large sand filter installation with a comparable multistage HEPA system of the same capacity.

ORTH: That was part of the design basis. Some of that information was touched on by Schurr during a round table discussion on "Design of Air Cleaning Systems for Pn Facilities" at the 12th Air Cleaning Conference in 1972. The answer is, "Yes, we considered it." We cannot yet factor in disposal costs for the sand filter, since we are not sure what they will be. The sand filter costs somewhat more to install than the HEPA filter but, in the view of my management, the overall long-term, i.e., twenty to thirty year, operating costs taking into account replacing HEPA filters and their disposal costs favors the sand filter. Also, the inherent accident protection that you get with the sand filter is outstanding. If you try to get equivalent accident protection with HEPA filters that you think you will get with sand filters, it would not be just a train of HEPA filters, it would be a lot more equipment.

GEER: How do you plan to dispose of sand filters eventually?

ORTH: That is a subject of some discussion. I think it would take more time to answer than I want to take right here. We have considered the matter and it is not easy.

GEER: In Colorado, we promised our governor we would not bury anything. Therefore, we would have to move it.

ORTH: We realize you have a problem at Rocky Flats.

SODIUM FIRE AEROSOL LOADING CAPACITY OF SEVERAL SAND AND GRAVEL FILTERS

J. R. Barreca and J. D. McCormack
Westinghouse Hanford Company
Hanford Engineering Development Laboratory
Richland, Washington

Abstract

Improved specific loading capacity for sodium fire aerosols was the objective of a sand and gravel test series. The aerosol capacity and related differential pressure of eight aggregate filters is presented. A maximum specific aerosol capacity, for dry aerosol, of 2.4 kg (Na) m^{-2} was obtained. This filter was loaded to a final differential pressure of 2.6 kPa. The average superficial face velocity was 0.5 cm/sec and the average efficiency was 99.8%. The test results indicate that filter capacity increases with aerosol moisture content and with decreasing superficial velocity.

I. Introduction

Sand bed filters have been suggested as components of sodium cooled reactor emergency air cleaning systems(1). As filters of sodium fire aerosols they have been found to be both efficient and resistant to chemical damage(2). They are also passive devices with demonstrated reliability in the nuclear industry(3). However, their mass loading capacity is low and for use in emergency air cleaning systems, very large filters are required. To reduce their size and cost, the specific mass loading capacity must be increased. The objective of the work described in this report was to devise sand bed filters with increased capacity for aerosols of interest for sodium cooled reactors.

II. Experimental Arrangement

A diagram of the filter testing system is shown in Figure 1. The source of sodium hydroxide/oxide aerosol varied throughout the test series. In the first and fourth tests, a concrete room (300 m^3) served as an aging chamber for the aerosol, and a pool fire was the principal method of generation. An 850 m^3 steel vessel, the Containment Systems Test Facility, was used to contain aerosol produced by sodium spray fires during tests 2, 3, 5, and 7. In the sixth test, a sodium vapor generator was used to produce high concentration aerosol in a 1.4 m^3 steel vessel.

The aerosol source was connected by a 10 cm diameter duct (usually less than 2 meters in length) to the inlet of an experimental filter. The test filter consisted of up to ten, 15 cm high, 51 cm diameter, sieves which were filled with aggregate. These trays with gaskets were bolted together to form a column or stack (see Figures 2 and 3). A gap of approximately 1 cm usually separated the top aggregate surface in a sieve from the support screen of the sieve above it. Pressure taps allowed monitoring of the differential

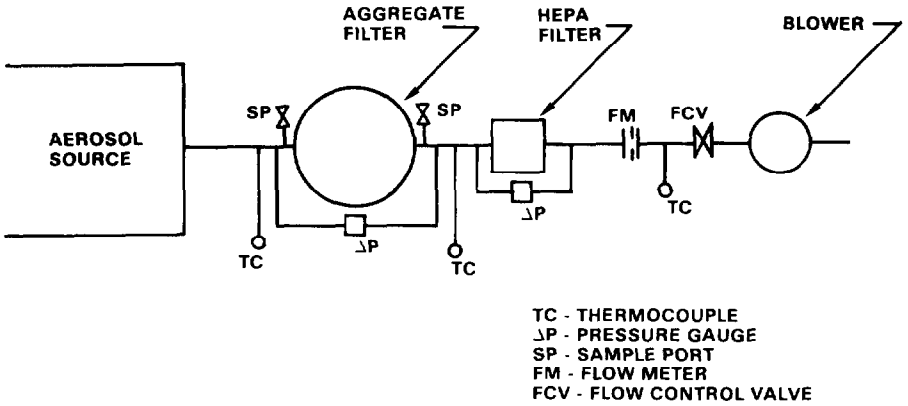

FIGURE 1. Filter Test Schematic.

FIGURE 2. Aggregate Filter Stack.

pressure across each tray. Sample ports in the stack inlet and outlet plenums allowed aerosol concentration and particle size sampling. Thermocouples extending into the plenums were used to monitor air stream temperatures.

In all tests except the first, a 31-cm x 31-cm x 31-cm HEPA filter was coupled to the aggregate filter exit plenum. After completion of the test, the HEPA filter from each stack was washed and the water was analyzed for sodium. The results of such analysis together with the total sodium as aerosol found in the stack was used to determine overall filter efficiency.

During each test the air flow was monitored and kept constant. For the low flow rate tests, a rotameter and positive displacement pump were used. In the higher flow rate tests an orifice meter and blower were employed. Flow rate, total pressure drop and the temperatures were logged in digital form.

III. Test Aggregates and Aggregate Arrangement

In the first five tests, six particle size groups of rounded filter gravel were used. For the sixth and seventh test, the group containing the largest particle size was regraded into two groups. The size distribution of five of the seven groups is shown in Figure 4. Also shown in Figure 4 are the size distributions of the two filter sand groups used throughout the test series. The porosity of both the sand and the gravel size groups and their average particle size is given in Table I. Since porosity changes with the amount of settling, the values given should be considered representative rather than exact.

TABLE I. Size and Porosity of Test Aggregates

Aggregate Group	Mean Aggregate Diameter, mm	Porosity
A	0.7	0.39
B	1.3	0.37
C	3.4	0.35
D	9.5	0.37
E	12.7	0.36
F	25.0	0.40
G	28.3	0.38
	63.5	0.41
	88.9	0.41

Other than the largest size of gravel, none of the aggregate groups were mixed. The aggregate arrangement in all filter stacks for which an increase in total stack differential pressure was achieved, is shown in Table II (tray No.1 is the top of the stack). Each sieve was filled to a depth of approximately 13 cm.

FIGURE 3. Filter Stack Aggregate Trays.

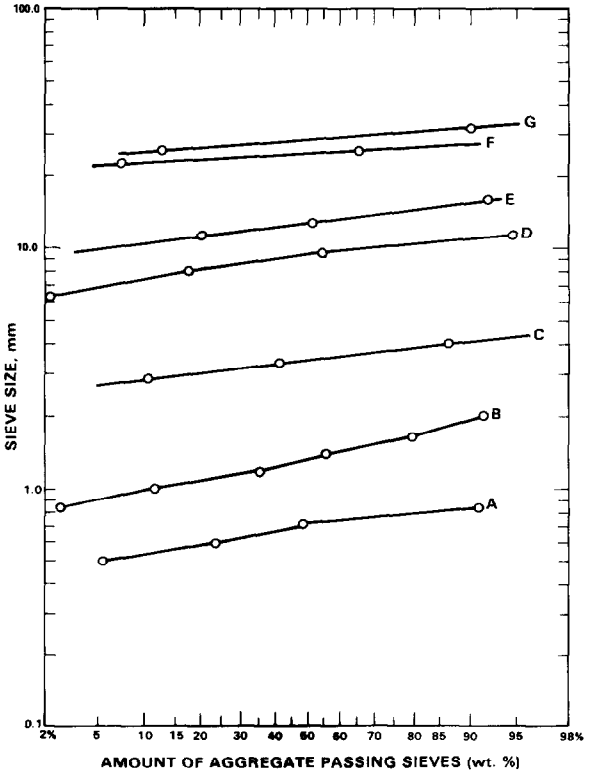

FIGURE 4. Aggregate Size Distribution.

TABLE II. Stack Aggregate Distribution by Average Aggregate Size

Sieve No.	Mean Aggregate Diameter, mm							
	Stack 1-1[a]	Stack 1-2[a]	Stack 4-1	Stack 4-2	Stack 5-2	Stack 6-1	Stack 7-1	Stack 7-2
	Inlet	Inlet						
1	28.3	28.3	0.7	0.7	0.7	0.7	0.7	0.7
2	28.3	12.7	1.3	1.3	0.7	1.3	0.7	0.7
3	12.7	12.7	3.4	3.4	1.3	3.4	1.3	1.3
4	12.7	9.5	25.0	25.0	1.3	9.5	3.4	3.4
5	9.5	9.5	28.3	28.3	3.4	12.7	9.5	9.5
6	9.5	3.4	28.3	28.3	9.5	25.0	12.7	12.7
7	3.4	3.4	76.2	76.2	12.7	28.3	25.0	25.0
8	3.4	1.3	76.2	76.2	25.0	63.5	28.3	28.3
9	1.3	0.7	----	----	28.3	88.9	63.5	63.5
10	0.7	0.7	----	----	76.2	88.9	88.9	88.9
			Inlet	Inlet	Inlet	Inlet	Inlet	Inlet

(a) Downflow. All others are upflow

IV. Test Procedure

After assembly, each filter stack was checked for leakage. Leakage was reduced to less than 5% of the intended flow rate at the maximum total stack differential pressure. The stack to be tested was connected as in Figure 1. The flow was directed up through the stacks except in the first test where the air flow was downward. Flow was established when the aerosol concentration was near 1.5 g Na/m^3. The flow rate was held nearly constant throughout the test period. After flow termination the stack was disconnected, sealed and another stack connected. Three stacks could be used during each test, but difficulties with aerosol production limited the number of stacks usually tested. After each test, the trays of aggregate were individually washed. Flame spectrometer analysis of the wash water was used to determine the amount of sodium on each tray. The aerosol used in these tests included Na_2O_2, NaOH, Na_2CO_3 and their hydrates, with an average sodium content of 50%. Thus, mass expressed as Na should be multiplied by a factor of two to obtain total mass.

V. Experimental Results and Discussion

Aerosol Conditions

Of the tests in Table II, Stack 5 was the only one in which steam was added to the aerosol. The aerosol in Stack 6 was very dry. Its bulk density was 0.075 g (aerosol)/cm^3 and its sodium fraction was 0.56. Aerosol concentration in Stack 6 was also the highest with an average value near 10 g (Na)/m^3 in the inlet plenum compared with 2-3 g (Na)/m^3 in the other tests. The aerosol aerodynamic mass median diameter in the inlet plenum generally averaged between 2 and 3 micrometers throughout the test series. The dominant aerosol chemical

form in most tests was sodium hydroxide.

Distribution of Aerosol in the Filters

In the process of disassembling the stacks, aerosol was observed on the top surface of the gravel but not on the bottom surface in most of the stacks. This top surface coating was particularly noticeable in stack 6-1. In this stack the coating was measured to be nearly 1 cm thick on the three largest aggregates and was observable on the 12.7-mm gravel. In stack 7-1, aerosol was observed on the bottom of the 12.7-mm aggregate and on the top surface of the 88.9-mm gravel.

The distribution of aerosol, as sodium, throughout the stacks is given in Table III. Since the flow direction was downward in the stacks 1-1 and 1-2, inlet plenum sodium was deposited on the top tray. In all other stacks, the sodium deposited in the inlet plenum was not included in the fractions shown in Table III. The ratio of aerosol mass, as sodium, in the inlet plenum to that in the aggregate for the remaining (upflow) stacks ranged from 0.12 to 0.38. By comparing the distribution in stack 7-1 with 1-1, the effect of flow direction on aerosol distribution can be perceived. The deposited aerosol cake which forms on the inlet surface of a downflow bed can remove aerosol[4]. In this series of tests, aggregate arrangements which produced uniform tray-wise aerosol distribution were sought. The upward flow favors uniform tray distribution.

TABLE III. Fraction of Total Sodium in Each Tray

	Fraction of Sodium Recovered From Stack							
Sieve No.	Stack 1-1	Stack 1-2	Stack 4-1	Stack 4-2	Stack 5-2	Stack 6-1	Stack 7-1	Stack 7-2
1	0.396[a]	0.553[a]	0.007	0.021	0.088	0.013	0.042	0.066
2	0.085	0.308	0.017	0.030	0.202	0.049	0.151	0.149
3	0.317	0.048	0.636	0.451	0.149	0.071	0.288	0.113
4	0.021	0.025	0.056	0.075	0.304	0.078	0.322	0.325
5	0.018	0.013	0.044	0.048	0.176	0.194	0.063	0.057
6	0.015	0.019	0.081	0.090	0.024	0.092	0.032	0.057
7	0.024	0.009	0.047	0.092	0.024	0.189	0.023	0.050
8	0.016	0.009	0.112	0.195	0.012	0.086	0.018	0.063
9	0.032	0.012	-----	-----	0.012	0.093	0.030	0.064
10	0.076	0.004	-----	-----	0.008	0.135	0.029	0.057
Total	1.000	1.000	1.000	1.000	1.000	1.000	1.000	1.000
Inlet Plenum	-----	-----	0.38	0.28	0.30	0.16	(b)	0.12

(a) Down flow. These values include settled material from inlet.

(b) Data lost.

The effect of face velocity on the distribution of deposited aerosol can be observed by comparing stack 6-1 with 7-1 in Table III. The face velocities in 6-1 and 7-1 were 0.5 and 5.8 cm/sec, respectively. Apparently, penetration through the same size aggregate increases with increasing face velocity. In effect the range of useful aggregate sizes decreases with increasing velocity. If mass loading capacity is compared on the basis of area rather than volume, and capacity increases with uniformity of aerosol distribution, then increased face velocity results in decreased capacity due to the decrease in useful aggregate range.

A summary of test results is given in Table IV. The stack loadings are reported at a value of 1.5 times initial differential pressure. This value was chosen because typically the stack differential pressure began to increase sharply after reaching this value.

The effect of aerosol moisture content on loading capacity can be seen in Table IV by comparing stack 5-2 (wet aerosol), with 7-1 (dry aerosol). Wet aerosols have higher bulk densities and hence require a reduced storage space in the bed. If differential pressure increases with decreasing void volume, and capacity is expressed in terms of aerosol mass, then the increased capacity with increased bulk aerosol density, due to moisture, should be expected. The bulk density of the aerosol used in stack 6-1 was low (0.075 g aerosol/cm^3) compared with that of the moist aerosol in stack 5-2 ($\sim$ 1 g/cm^3). Because the dry aerosol is a more challenging case, the specific loading capacity of stack 6-1 is considered to be the best value obtained in the test series. Approximately 12% of the aggregate void volume in this stack was filled with aerosol.

Efficiency was not considered as important as aerosol capacity in these tests. The average aerosol removal efficiencies in Table IV reflect this fact. Improved efficiency should result from the use of more sand trays or a finer sand layer. The relatively high efficiency in stack 6-1 seems to reflect the previously discussed dependence of penetration on superficial velocity rather than aggregate size differences.

VI. Conclusions

The mass loading capacity of aggregate beds for sodium fire aerosols was investigated. This work shows that by optimizing the aggregate distribution to increase uniformity of aerosol deposition and by using a low superficial velocity ($\sim$ 0.5 cm/s) a specific aerosol capacity of 2.4 kg Na/m^2 can be obtained for dry aerosols. This is twice the highest value previously reported[5]. The corresponding final differential pressure at this loading was 2.6 kPa. Using this specific loading capacity, an aggregate filter designed to hold 5000 kg of dry NaOH would require a cross-sectional bed area of 1200 m^2 (35 m per side). Such a filter would operate at an air flow of 6 m^3/s (12,700 cfm). The test results also suggest that bed velocity and loading can be "traded off", thus allowing optimization of the filter for the particular flow and loading requirement.

TABLE IV. Collected Mass and Pressure Drop Summary

Test and Stack No.	1-1	1-2	4-1	4-2	5-2	6-1	7-1	7-2
Average superficial velocity, cm/sec	4.7	0.5	6.5	2.4	7.0	0.5	5.8	2.0
Initial Stack ΔP, kPa	0.6	0.1	1.3	0.3	1.6	0.1	1.6	0.5
Final Stack ΔP, kPa	3.2	0.4	6.1	6.7	4.7	2.6	6.0	5.8
Specific loading capacity at 1.5 initial ΔP, kg Na/m^2	0.25	0.39	0.06	0.07	3.57	1.66	0.14	0.30
Specific loading capacity at final ΔP, kg Na/m^2	0.43	0.44	0.26	0.13	3.71	2.36	0.31	0.51
Stack Efficiency, %	---	---	94.04	88.51	94.71	99.77	97.23	95.20

VII. References

1. J. D. McCormack, R. K. Hilliard, A. K. Postma, and L. D. Muhlestein, "An Evaluation of Alternative Air Cleaning Systems for Emergency Use in LMFBR Plants," Proceedings of the 14th ERDA Air Cleaning Conference, CONF-760822, pg 989, February 1977.

2. L. Böhm, S. Jordan, W. Schikarski, "The Off-Gas Filter System of SNR-300," Proceedings of the 13th AEC Air Cleaning Conference, CONF-740807, pg 620, VI, August 1974.

3. R. A. Juvinall, R. W. Kessie, and M. J. Steindler, "Sand-bed Filtration of Aerosols: A Review of Published Information on Their Use in Industrial and Atomic Energy Facilities," ANL-7863, June 1970.

4. L. Böhm, S. Jordan, "On the Filtration of Sodium Oxide Aerosols by Multilayer Sand Bed Filters," J. Aerosol Sci., 7, pg 311, (1976).

5. A. Alexas, S. Jordan, and W. Lindner, "Filtration of Sodium-Fire Aerosols," Nuclear Technology, Vol. 42, pg 320, March 1979.

DISCUSSION

SCHURR: I missed the point on how you determine breakthrough in terms of your aerosol holding capacity. I wonder if you could review that. You said that you had aerosol holding capacity of about 12% of the void volume, but I missed in your presentation how you determined breakthrough and capacity.

BARRECA: Capacity was determined by the differential pressure at the end of the test. The differential pressure was stated in that one slide at something like 2.6 kPa.

CONSTANTINO: I do not see the pressure drop for the sand filters in comparison with the HEPA filters. Would you please comment on that?

BARRECA: The pressure drop stated in my paper was for the sand filter only, not across the HEPA filter. Am I answering the right question?

CONSTANTINO: No, I do not see it. What was the pressure drop compared to HEPA filter pressure drop?

BARRECA: Pressure drop as a function of flow is in Table IV in the preprint of my paper.

INFLUENCE OF THERMOPHORESIS ON PARTICLE REMOVAL IN A MOVING GRANULAR BED FILTER AND HEAT EXCHANGER

S.N. Rudnick, M.W. First, and J.M. Price
Harvard Air Cleaning Laboratory
Boston, Massachusetts

Abstract

Bench-scale investigations were made to determine the influence of thermophoresis on particle removal in a moving granular bed filter. A continuous flow of 2-mm diameter ceramic granules at ambient temperature entered the top of the filter and moved slowly downward under the influence of gravity countercurrent to the gas stream. At an inlet gas temperature of 240°C, gas mass velocity of 0.12 kg/(s·m^2), and granule velocities up to 0.015 cm/s, clean bed collection efficieny for a submicrometer sodium chloride aerosol was found to increase the more the gas was cooled, indicating that thermophoretic forces were playing a measurable role in particle collection.

Introduction

Moving granular bed filters (MGBF) have the potential to serve the dual purpose of steady-state heat exchange and filtration. They are uniquely adaptable for high temperature work because of their large interfacial surface area per unit volume and because they can be constructed entirely from refractory materials. Many nuclear applications, such as calcination and vitrification[1], require gas cooling and cleaning before final decontamination by HEPA filters, because these filters are sensitive to heat and limited in dust-holding capacity. For some processes, a MGBF offers the additional possibility that the granular material can be selected so that it can be used elsewhere, such as the frit component in a nuclear waste vitrifier, and thus eliminate one radioactive waste for separate disposal.

A MGBF consists of a column of granules that moves slowly downward under the influence of gravity while an aerosol flows simultaneously through the intergranular voids. Although gas flow may be cocurrent, countercurrent, or crossflow to the direction of granule movement, the countercurrent mode is preferred for maximizing heat transfer. Upward gas flow in a countercurrent MGB filter, however, impedes the downward motion of the granules and can produce a cessation of granule motion or, in the extreme case, the granules may fluidize. Nevertheless, the countercurrent mode appears to be the most attractive for the present work.

During this experimental investigation, special emphasis was placed on testing whether a continuous flow of cold granules, used for gas cooling as well as aerosol filtration, would give improved collection of submicrometer particles by the mechanism of thermophoresis, which is enhanced when the thermal gradient between gas and granules is increased. An intergranular dust deposit was not allowed to form because it would have increased heat transfer resistance, thereby reducing the temperature gradient in the intergranular voids. This would have diminished the importance of thermophoresis as a particle removal mechanism.

Thermophoretic Deposition in Granular Beds

Published information on thermophoretic deposition in granular beds is sparse. Ranz[2] devised a dimensionless group that he used as a measure of the relative importance of thermophoretic forces in granular beds. This dimensionless group, the ratio of the thermophoretic force to fluid resistance, is given in Equation 1.

$$\frac{9\pi}{2} \frac{k_g}{(2k_g + k_p)} \frac{D\mu^2 z}{\rho T v} \frac{dT}{dx} \qquad (1)$$

where

k_g = gas thermal conductivity, J/(m·s·K)
k_p = particle thermal conductivity, J/(m·s·K)
D = particle diameter, m
μ = gas viscosity, Pa·s
ρ = gas density, kg/m^3
z = particle mobility, s/kg
v = superficial velocity, m/s
T = absolute temperature, K
x = distance in direction of thermal gradient, m

Ranz stated that "whenever this group has a value greater than about 0.1, the thermophoretic force is significant for particle motion." Based on ambient air and 1.0-μm diameter particles, he concluded that "a significant value of the dimensionless group cannot be obtained unless conditions such as ice cold collectors of 10^{-2} cm diameter in 100°C aerosols are employed. Such physical systems," he said, "are conceivable but are of doubtful practicability."

Strauss[3], describing work done in his doctoral dissertation[4], was more optimistic; he wrote, "It has also been suggested that thermal precipitation may play a part in the deposition of particles from a hot gas when this is passed through a cold packed bed. The passages in the bed are narrow and so even a temperature difference of 50°C may give rise to a temperature gradient of 10°C/mm in the passages. Calculations show that this would result in deposition of 98.8 percent of particles of 0.1-μm diameter in a 0.2-m deep bed at 500°C." Strauss[5] later said that his calculations, which were based on a capillary model, may be inappropriate for thermophoretic deposition in granular beds. Strauss and Lancaster[6] also considered the well-mixed model used in electrostatic precipitator design for predicting thermophoretic deposition; it is as follows:

$$\eta = 1 - \exp(A\ W/V) \qquad (2)$$

where

η = particle collection efficiency, dimensionless
A = collector surface area, m^2
W = particle drift velocity, m/s
V = volumetric flow rate, m^3/s

Unfortunately, neither Ranz nor Strauss supported their work with experimental studies and a search of Chemical Abstracts and Engineering Abstracts for the years 1940 through 1977 failed to turn up other references to thermophoretic deposition in granular beds.

Experimental Apparatus

Experimental apparatus, shown in Figure 1, consisted of three parts: high temperature tunnel, salt aerosol generator, and bench-scale-sized MGBF. The high temperature tunnel was an insulated 2.5-m long steel duct with 10x10-cm cross section in which air was heated with an oxyacetylene torch. Blower, flow-regulating damper, and orifice flowmeter provided the desired airflow rate. The temperature in the tunnel was monitored with a bimetallic thermometer and controlled by manual adjustment of the oxyacetylene torch. A portion of the tunnel atmosphere was introduced into the filter by a separate blower. Because of the large heat capacity of the tunnel and filter, about 4 hours were required to reach thermal equilibrium. During this period, no salt was aerosolized.

In the MGBF, granules stored in an upper funnel-shaped hopper moved into and slowly progressed downward by gravity through a 5-cm diameter, 10-cm deep column in which the granules functioned as filtering and heat exchange medium. The granules discharged through a funnel-shaped port before spilling into a hopper. Granule flow rate was controlled by a rotating drum covered with a thin layer of corregated aluminum and located below the discharge port. The size of the corregations was slightly greater than the granule diameter. The drum was driven by a variable speed DC motor, which allowed the granule flow rate to be adjusted.

Aerosol from the high temperature tunnel flowed into a 10-cm diameter, 4-cm high plenum concentric with the granule-filled column and then through a 30-mesh woven wire screen (which required frequent cleaning) before entering the granular filter bed crosscurrent to the flow of the granules. After entry, the aerosol passed upward countercurrent to the slowly moving granules and left the filter through another screen and plenum identical to the inlet. Exit airflow rate was measured with a calibrated venturi flowmeter after the air was cooled to ambient temperature and water condensate from the fuel gas combustion removed. The temperatures of the inlet and outlet gas streams were measured with thermocouples located in their respective plenums. Significant heat was lost to the surroundings from the gas on passing from inlet to outlet plenum despite 5-cm of ceramic-fiber insulation.

Granules

Arlcite ceramic beads were selected for this service because of their high density (3.25 g/cm^3), to resist bridging and fluidization; their refractory nature, to withstand heat shock; and their spheroidal shape, to assure good flow properties. They are available in 8/12-mesh size from Electro Refractories and Abrasives Division of Ferro Corporation in East Liverpool, OH. Average bead diameter is 2.11 mm with a coefficient of variation equal to 8.6%. They have a pososity of 40% while flowing through the MGBF, a thermal conductivity at 20°C of 14 J/(s·m·K), and a specific heat of 920 J/(kg·K).

Test Aerosol

Vaporized salt (sodium chloride) was used for these tests be-

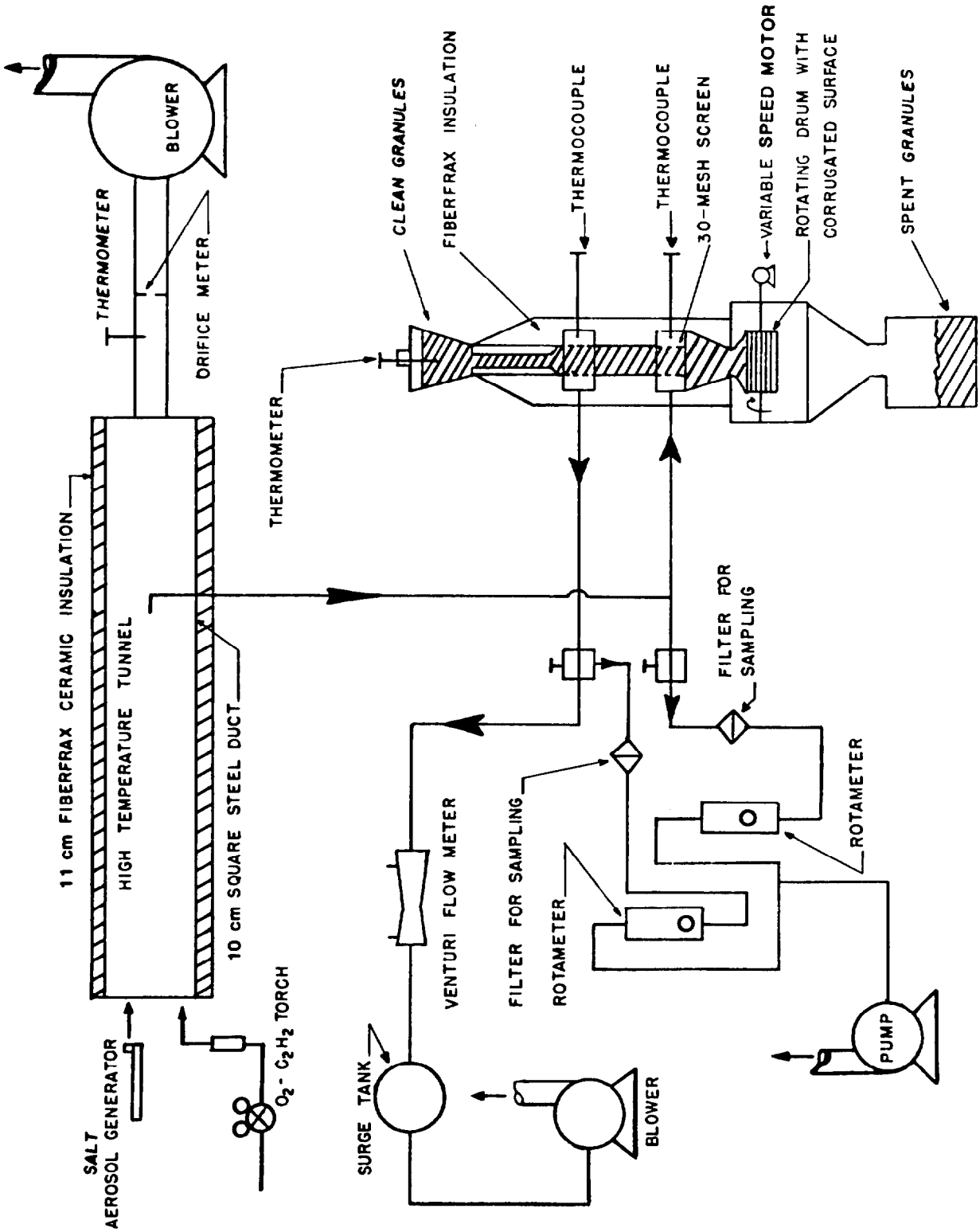

FIGURE 1. HIGH TEMPERATURE MOVING GRANULAR BED FILTER

cause it has a negligible vapor pressure at the experimental temperature and can be aerosolized to yield particles with a count median diameter close to 0.1 μm — a size responsive to thermophoretic forces. The salt aerosol generator that was used is patterned after a British design[7]. It uses a variable speed motor to feed a rod of salt through the center of a specially modified oxypropane-fed ring burner. The upstream and downstream salt aerosols were sampled simultaneously through membrane filters, which were placed as close to the MGBF as feasible to minimize deposition in the sampling lines. The sampled gases were cooled to ambient temperature, condensate removed, and flow rates measured with rotameters. The membrane filters were soaked in distilled/deionized water. Salt aerosol penetration was measured by two methods: atomic absorption spectrometry and chloride ion specific electrode. Salt concentrations were generally too low and sampling time too short to utilize gravimetric methods.

Results and Conclusions

By varying granule velocity in the MGBF while operating at constant gas mass velocity, constant inlet gas temperature, and constant inlet granule temperature, the temperature gradient between gas and granules could be altered. Thus, when granule velocity was increased, the resultant increase in temperature gradient was expected to produce an improvement in particle collection efficiency because thermophoretic forces would play an increasingly more important role as a particle removal mechanism. Gas phase temperature drop was correlated with particle penetration because the gas phase mechanisms by which a gas is cooled in a moving granular bed are the same as those that cause particle removal by thermophoresis; i.e., both phenomena rely on temperature gradient as the driving force for transfer and both occur simultaneously. Transferred heat can be thought of as an integrated result of the gas phase temperature field, which would affect thermophoretic deposition in a way similar to heat transfer. The extent of particle removal by thermophoresis should, therefore, be related to the sensible heat loss of the gas, which is directly proportional to its temperature drop resulting from passage through the moving granular bed.

To establish whether thermophoretic forces contribute significantly to particle collection efficiency, a series of runs was made in a countercurrent MGBF at a superficial gas mass velocity of 0.12 $kg/(s \cdot m^2)$, i.e., 10 cm/s at STP, and 238° inlet gas temperature while feeding ambient temperature granules at 7 velocities up to 0.015 cm/s. Each run required at least a full day's operation to reach steady state.

The experimental results are given in Table I. The excellent agreement between samples A and B indicates that the sampling and analytical procedures were reproducible. That thermophoretic forces improve particle collection efficiency can be seen from Figure 2, which shows that penetration (Pt) of submicrometer salt particles decreased as granule velocity (G) increased ($\%Pt = 70.7 - 985G$). Although the data show considerable scatter, the inverse correlation of penetration with granule velocity is significant at greater than 95% confidence (but less than 99% confidence). Similarly, penetration decreased as gas tem-

Table I. Results on collection of salt aerosol by thermophoretic forces.

Granule Velocity cm/s	Weight % Penetration			Gas Temperature °C	
	Sample A	Sample B	Average	Inlet	Outlet
0.016	53.0%	56.8%	54.9%	235	88
0.011	60.6	60.1	60.3	239	90
0.0080	55.4	56.0	55.7	240	118
0.0070	72.9	68.5	70.7	240	127
0.0045	67.8	67.6	67.7	236	140
0.00090	69.2	67.6	68.4	236	169
Fixed Bed	70.7	70.4	70.6	238	178

perature drop (ΔT) increased, as shown in Figure 3 ($\%Pt = 80.2 - 0.150\Delta T$). Again, the inverse linear correlation of penetration with gas temperature drop is significant at greater than 95% confidence (but less than 99% confidence).

The net increase in particle removal efficiency attributable to thermophoretic forces, however, is actually greater than that indicated in Figures 2 and 3 because the average gas temperature was lower in those runs in which the granule velocity was higher. Hence, diffusional deposition, which increases with increasing temperature, played a less important role as the granule velocity was raised. This is true despite the increase in aerosol residence time at lower average temperature. The magnitude of this decline in efficiency resulting from lower average gas temperature at higher granule rates can be estimated from data for isothermal runs. Isothermal experiments were conducted,but the results were unclear because of experimental difficulties.

Future Work

Although the present study shows that thermophoretic deposition plays a measurable role in a MGBF and heat exchanger, further experimental studies are necessary to demonstrate the particle-collecting potential of this device. In particular, experimental studies should be done at higher granule velocities and higher inlet gas temperatures than reported here. Data at isothermal conditions are also necessary if thermophoretic deposition is to be quantified more adequately. The MGBF shown in Figure 1 is not suitable for further studies because of various inadequacies (e.g., poor insulation and particle deposition on inlet screen) and because of temperature limitations and vulnerability to corrosion. For these reasons, a new pilot-plant-sized experimental filter and high temperature tunnel were constructed. The filter, shown schematically in Figure 4, was made from 310 stainless steel so that it could withstand mildly corrosive atmospheres up to a temperature of 1000°C. It has additional advantages over the previous design as follows: (a) no inlet or exit screens, (b) a nonfunneling granule discharge port plus turntable for granule flow control, which should give plug flow of granules[8], (c) more extensive and reliable temperature monitoring of the gas stream, and (d) improved insulation for adiabatic operation. The tube bringing clean granules from the hopper to the filtering section

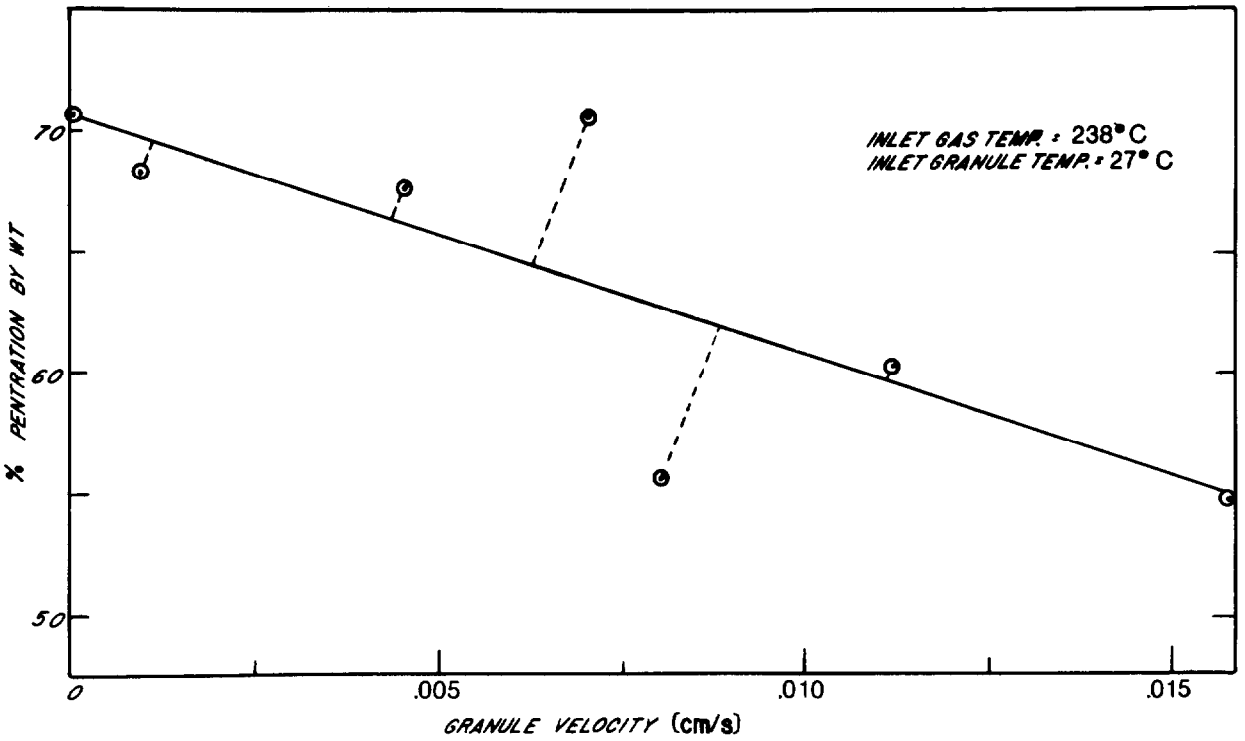

FIGURE 2. SALT AEROSOL PENETRATION VS GRANULE VELOCITY

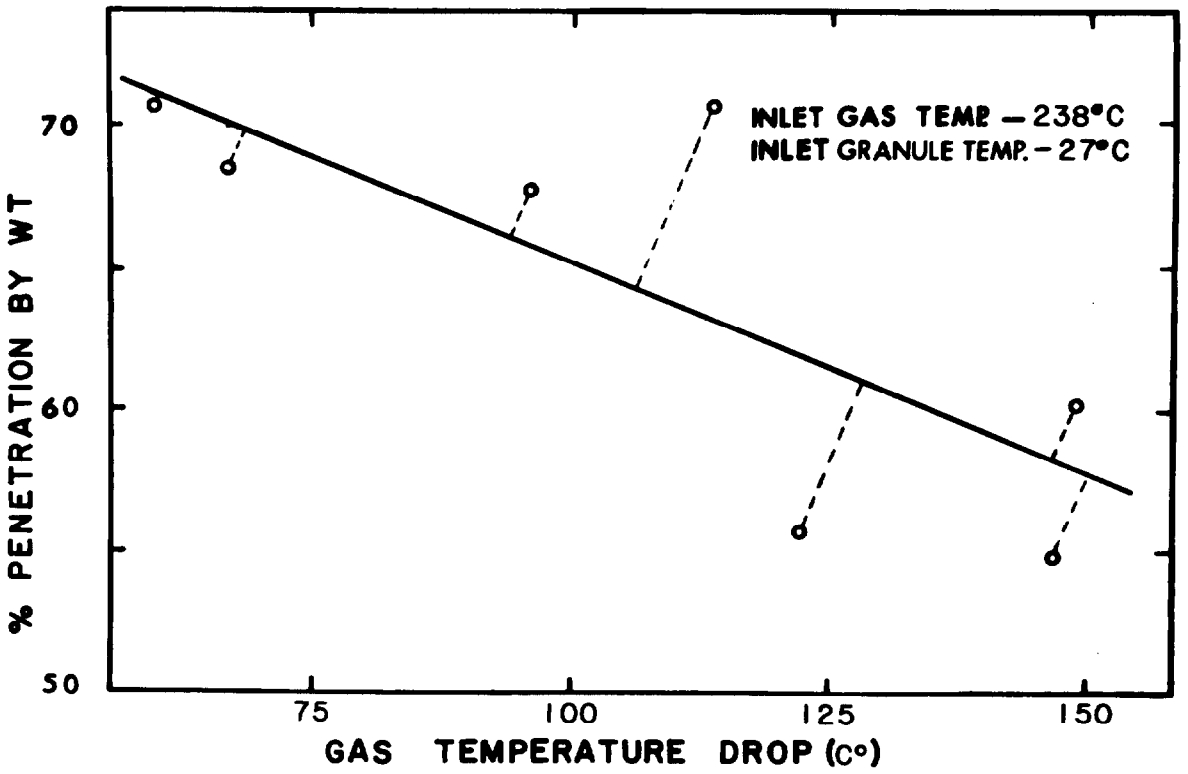

FIGURE 3. SALT AEROSOL PENETRATION VS GAS TEMPERATURE DROP

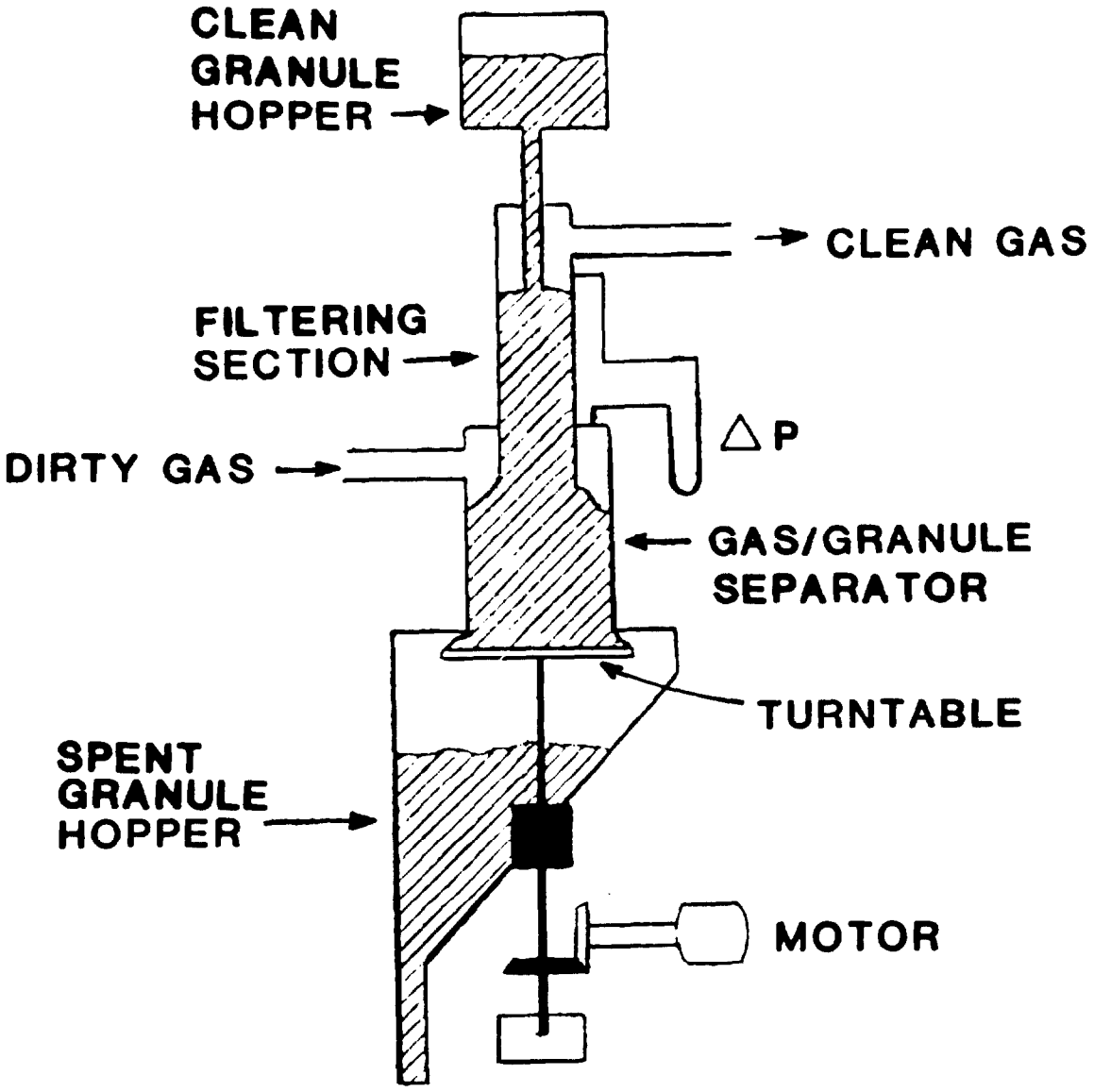

FIGURE 4. NEW DESIGN OF MOVING GRANULAR BED FILTER

also has insulation on its interior and exterior to prevent premature heat transfer from gas to granules.

Acknowledgement

This work was supported by the U.S. Department of Energy under contract number EY-76-S-02-3049.

Literature Cited

1. Bonner, W.F., Blair, H.T., and Romero, L.S., Spray Solidification of Nuclear Waste, ERDA Contract E(45-1)-1830, Battelle Pacific Northwest Laboratories, Richland, WA, August 1976.

2. Ranz, W.E., The Impaction of Aerosol Particles on Cylindrical and Spherical Collectors, U.S.A.E.C. Report SO-1004, March 1951.

3. Strauss, W., Industrial Gas Cleaning, 2nd ed., Pergamon Press, Oxford, England, 1975, p. 508.

4. Strauss, W., Doctoral Dissertation, Sheffield University, 1959, pp. 92-6.

5. Strauss, W., Letter to Dr. D.W. Underhill, September 1977.

6. Strauss, W. and Lancaster, B.W., "Prediction of gas cleaning methods at high temperatures and pressures," Atmos. Environ. 2: 134(1968).

7. Edwards, J. and Kinnear, D.I., "Flame generation of sodium chloride aerosol for filter testing," in Proceedings of the 13th AEC Air Cleaning Conference, CONF-740807, NTIS, Springfield, VA, 1975, pp. 552-64.

8. Takahashi, H. and Yanai, H., "Flow profile and void fraction of granular solids in a moving bed," Powder Technol. 7:205(1973).

DISCUSSION

DORMAN: I seem to remember that a good many years ago, I made some wild guesses and rather crude calculations and came to the conclusion that thermophoresis was not very important, but I think that this paper proves me wrong and we must agree that thermophoresis has some effect.

PENBERTHY: I noted that you said that you are using bead material which is 40% porosity. Was that largely alumina?

FIRST: Yes, it is a ceramic bead. The porosity I am talking about is between the granules as they flow down the column. The beads themselves are very hard and not porous at all.

PENBERTHY: I am wondering about the possible use of a different kind of a granule, one that would be naturally porous, such as volcanic pumice. This has the possibility, since it contains multivalent components such as iron, that it may exert a different influence. I come from the State of Washington. We have just received a new supply and I thought perhaps you might build markets for it.

FIRST: If you will indicate a supplier of pumice beads, we will give it a try.

DEVELOPMENT OF ACID-RESISTANT HEPA FILTER COMPONENTS

K. Terada, R. W. Woodard, and O. I. Buttedahl
Rockwell International
Energy Systems Group
Rocky Flats Plant
Golden, Colorado

Work Funded by the Department of Energy

Abstract

Laboratory and in-service tests of various HEPA filter media and separators were conducted to establish their relative resistances to HNO_3-HF vapors. Filter medium of glass fiber with Nomex® additive and aluminum separators with a epoxy-vinyl coating have performed quite well in the acid environment in the laboratory, and in prototype-filters placed in service in a plenum at Rocky Flats. Proprietary filters with new design and/or components were also tested in service with generally good results.

I. Introduction

This program was undertaken to reduce the volume of contaminated waste HEPA filters by prolonging their service lives. At Rocky Flats, replacement of HEPA filters is frequently necessitated due to loss of efficiency caused by chemical degradation of the filter. The two most corrosive chemicals entering the filter plenums are HNO_3 and HF which are used in the dissolution process of plutonium. Realistically one cannot expect to find materials completely inert to these acids yet meet the other requirements of filter components. However, any improvement in the acid resistance of HEPA filters is worthwhile.

The primary emphasis of this work has been on increasing the acid resistance of the medium component of HEPA filters. The basic ingredient of the medium is glass fiber which until recently, also contained about 5% asbestos. It was decided to retain glass fiber as the major ingredient because of its availability, its cost, and its noncombustibility, and focus on the problem of its susceptibility to attack by HF. This problem was studied in two ways. They were: (1) protect the medium with an acid-resistant coating and (2) add an acid-resistant fiber to the glass fiber matrix. The rationale of the first approach is obvious. The advantage of an additive for acid resistance has been demonstrated in tests with asbestos.[1,2]

The omission of asbestos from HEPA filters by most manufacturers because of potential carcinogenic hazards added the task of developing a replacement of the asbestos separators. Various materials were tested in the laboratory as well as in in-service prototype filters. Filters of new designs that do not utilize separators or have glass fiber strings to separate minipleated medium have also been evaluated in service.

Laboratory tests were conducted in a test chamber where filter media were subjected to airflow equivalent to 1000 cfm in a 2x2x1-foot (size 5) HEPA filter.(1) The relative humidity in the air was maintained at about 50% and the HF and HNO_3 concentrations were varied between 0.5 to 5 and 20 to 200 ppm respectively. Filtration efficiencies and air resistances of the acid exposed media were measured with the Q-127 or Q-76 filter test equipment manufactured by Air Techniques, Inc., Baltimore, Maryland.

II. New HEPA Filter Components

New Filter Media

The hypothetical basis of this effort to develop new media is that the loss of filtration efficiency is primarily due to HF attack. While HF attacks all glass fibers, the most susceptible are the fibers with the smallest diameters because of their greatest surface area-to-mass ratio. The objective then is to protect the fine fibers by coating them or to incorporate HF resistant fine fibers in the medium as a relacement for asbestos.

Glass Fiber Coatings

The study of the effect of coatings on glass fibers consisted of testing coated glass fiber media handsheets in the acid test chamber to determine whether their acid resistances were significantly greater than on uncoated reference handsheets. Applications were primarily by spraying the coating dissolved in a solvent but in some cases, the handsheets were immersed in the solution. Parylene N® (Union Carbide), a xylene polymer resin, was applied as a vapor under vacuum. Appropriate thicknesses of the coatings were determined empirically by their effect on the acid resistance, penetration, and flammability of the handsheets. The materials tested were silicones, Saran® (Dow Chemical Company), wax, and Parylene. The first three materials did not show any significant improvement in acid resistance. The Parylene-coated handsheets were not tested for acid resistance because they were very flammable.

Asbestos Substitutes

The properties of asbestos used in filter medium were considered to establish criteria for the selection of candidate fibrous materials for testing and evaluation as additives to glass fibers.

Scanning electron microscopy shows asbestos fibers span a wide range of sizes and contain a fair percentage with diameters of 0.2 micrometers or less (Figure 1). The presence of the fine fibers ingrained in the media produces a very tight filter. This is reflected in the fact that a filter handsheet made entirely of crocidolite asbestos had a pressure drop of 46 mm H_2O, while those made of glass fibers with 5% asbestos typically have pressure drops of about 35 mm H_2O when measured under identical conditions in the Q-127 test apparatus.

The superior acid resistance of filters containing asbestos compared to all glass fiber filters is shown by the increase in acid resistance as the asbestos concentration is raised.(2) Asbestos apparently provides acid resistance by reinforcing the glass fibers being corroded, especially the smaller fibers.

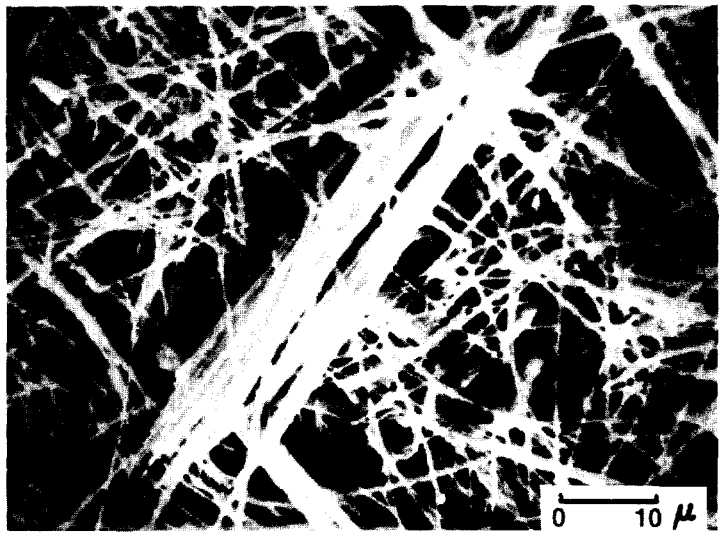

FIGURE 1. SEM PHOTO OF CROCIDOLITE ASBESTOS FIBERS

Accordingly, the substitute materials sought should: (1) have acid resistance, (2) be commercially available at an acceptable price, (3) have fiber diameters ranging down to 0.2 micrometers and (4) be environmentally nonhazardous. Temperature resistance is desirable but not essential as the filters will be exposed to elevated temperatures only in case of fire and even the loss of all the additive fibers would probably not decrease the filtration efficiency below the 97% minimum efficiency specified under such conditions.

Identification of fibers meeting these criteria have produced only a limited number of candidates. The criteria most difficult to meet was the submicron size requirement. A number of manufacturers were approached about development work to produce fine fibers but the cost of the project and the market size for the fine fibers discouraged their interest.

Fiberfrax® (Carborundum Corporation) was one of the candidates which appeared to meet the size requirements but it proved to have less acid resistance than glass fibers and contained large quantities of "shot". One of the most promising additive materials is Nomex® (Du Pont), a polyamide. During the early stages of the manufacture of Nomex fiber, a product containing a mixture of fibers of different diameters is formed and these are used to make Nomex paper. This paper can be resuspended in a slurry and added to glass fibers to make filter media. It blends quite well with glass fibers. Du Pont Nomex paper, Type 411, was found to be most suitable for this purpose and handsheets prepared with it met the tensile, penetration, thickness, and resistance criteria. Evaluation of the acid resistance of the handsheets in a test chamber indicated it was comparable to that with asbestos additive. At about that time a paper manufacturer made an experimental run of medium containing about 5% Nomex additive and 2% binder and asked Rocky Flats to evaluate its acid resistance in its acid vapor test chamber. The results of the tests are shown in Figures 2 and 3. Acid resistance tests of experimental medium containing about 5% Nomex and 5% binder and waterproofing are now in progress.

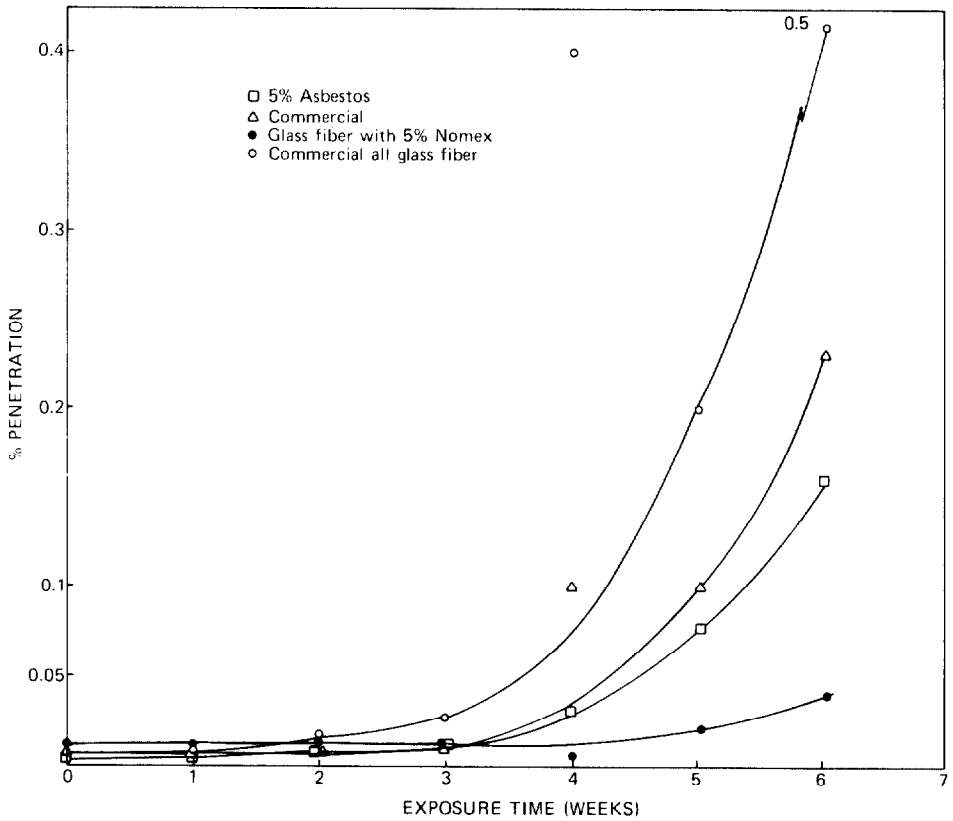

FIGURE 2. FILTER MEDIA ACID EXPOSURE TEST DATA I

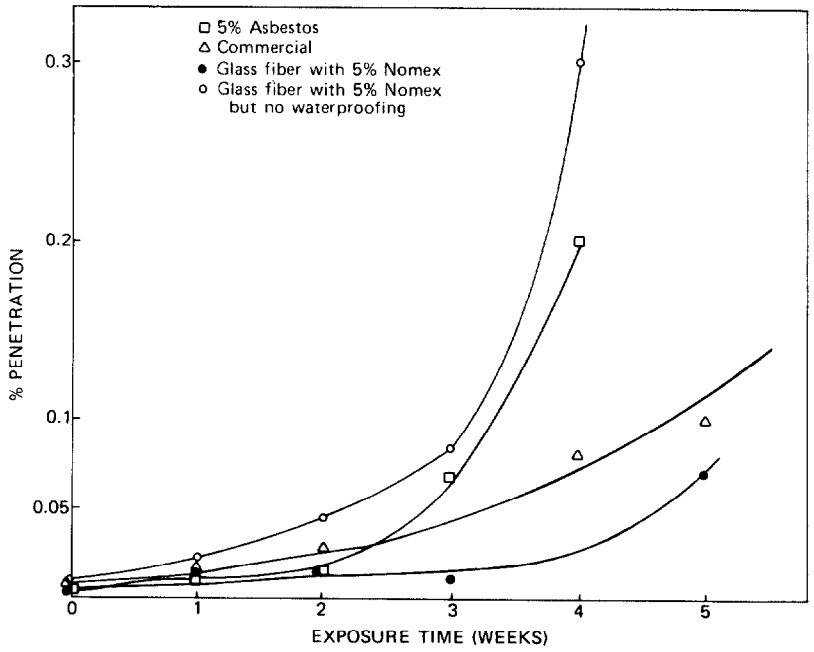

FIGURE 3. FILTER MEDIA ACID EXPOSURE TEST DATA II

The effect of higher concentrations of organics is being studied because some tests have indicated that binders and waterproofing in commercial media increase acid resistance. Since this medium contains organic content higher than the 7% specified in MIL 51079C, a high temperature test was conducted on two prototype filters containing this medium. The test consisted of passing 371°C (700°F) air through the filter at 1,000 cfm for 5 minutes (UL 586). This treatment should not lower the filtration efficiency below 97%. The filtration efficiencies after the heat treatment were 99.97 and 99.99% at 1,000 cfm. Figure 4 shows one of these filters after the test.

Another material which shows good potential is Kevlar® (Du Pont). Although it is not produced in submicron sizes, Kevlar fibers can be shredded so that many of the fibers are reduced to the submicron range (Figure 5). The size distribution can apparently be controlled by the amount of shredding. It has higher thermal resistance than Nomex as shown in the thermogravimetric (TGA) curve (Figure 6). The TGA curve shows that the beginning of decomposition of Nomex is at about 400°C, whereas Kevlar begins to decompose at about 500°C.

A test of relative chemical resistance to a solution of 7N HNO_3 and 0.1N HF for 120 hours indicate Kevlar is superior to Nomex in acid resistance. In the acid immersion test, Kevlar lost 1/2% by weight, while Nomex and Johns-Manville microfiber Type 106 lost 1 and 22% respectively. Physically, the yellow Kevlar turned golden brown while Nomex ranged from dark brown to almost black and became brittle. The glass fibers became significantly more fragile. Multiple internal reflectance infrared spectroscopy of the fiber surfaces showed that oxidation and nitration of Nomex occurred but no significant change was detectable on the Kevlar surface. Thermogravimetric analysis of the acid treated organic fibers revealed the decomposition temperature of both Nomex and Kevlar decreased from 350 to 330°C and from 470 to 410°C respectively.

Effects of radiation on Nomex, Kevlar, and glass fiber - 5% asbestos were tested by exposing one-inch strips of handsheet to gamma radiation. Although in actual usage alpha radiation is by far dominant, radiologists consider the effects of alpha and gamma radiation to be essentially equivalent in this type of study.

After the first day of irradiation, Nomex and Kevlar turned slightly brown but subsequently exhibited very little visible change. Figure 7 shows the radiation effects on tensile strength. Of the three materials, only Nomex exhibited some loss of tensile strength.

New Separator Materials

Since most filter manufacturers have ceased using asbestos separators, and separatorless filters are still being evaluated at present, substitute separator materials were investigated.

Metal Separators

Metal separators of steel and aluminum have high temperature resistance but low chemical resistance.

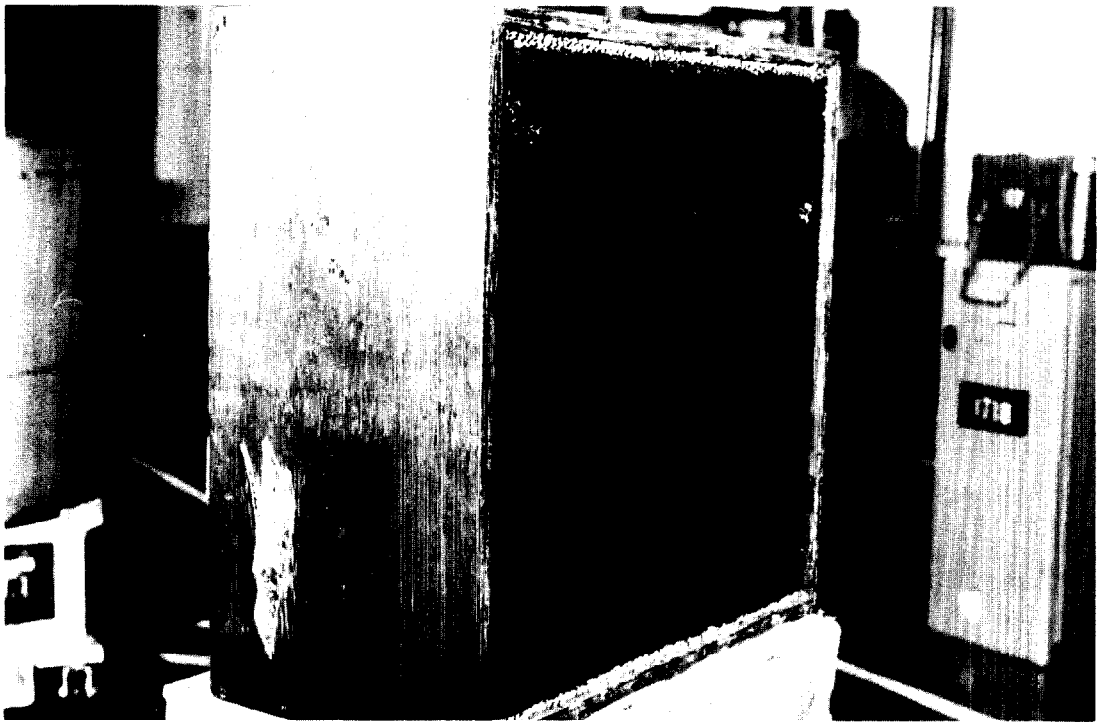

FIGURE 4. HEPA FILTER WITH COATED ALUMINUM SEPARATORS AND MEDIUM CONTAINING NOMEX - AFTER HOT AIR TEST

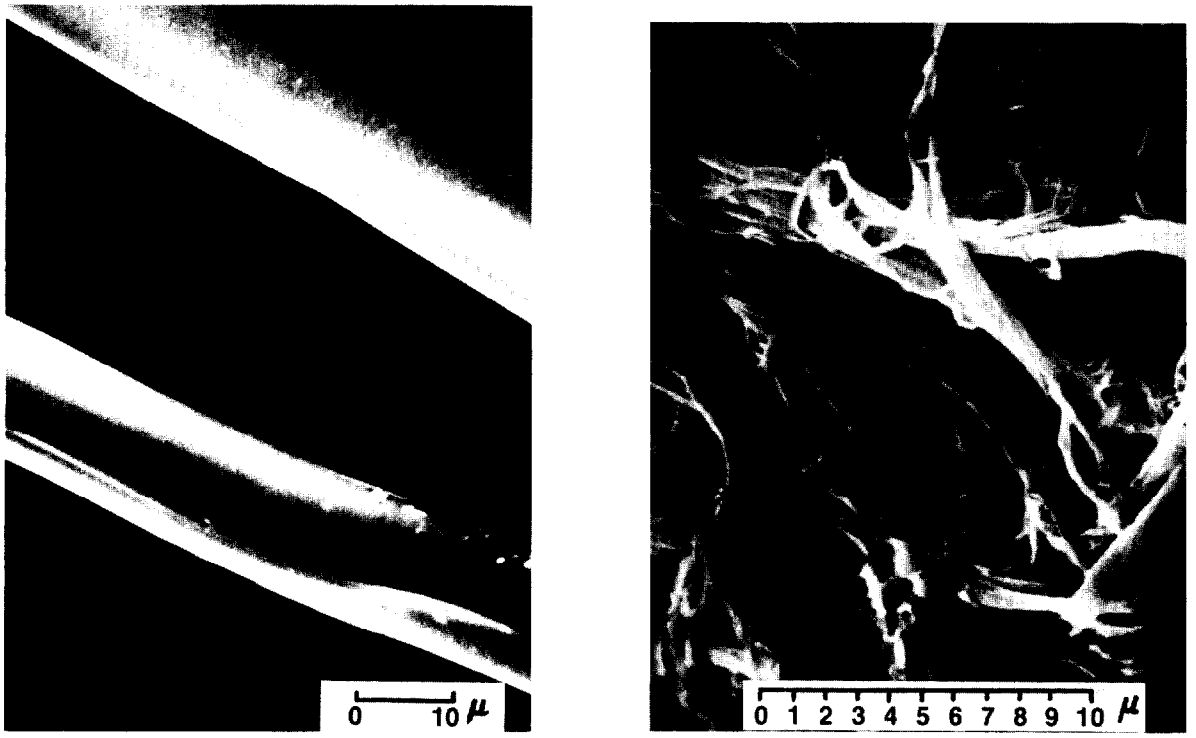

FIGURE 5. KEVLAR FIBERS. UNSHREDDED (LEFT) AND SHREDDED (RIGHT)

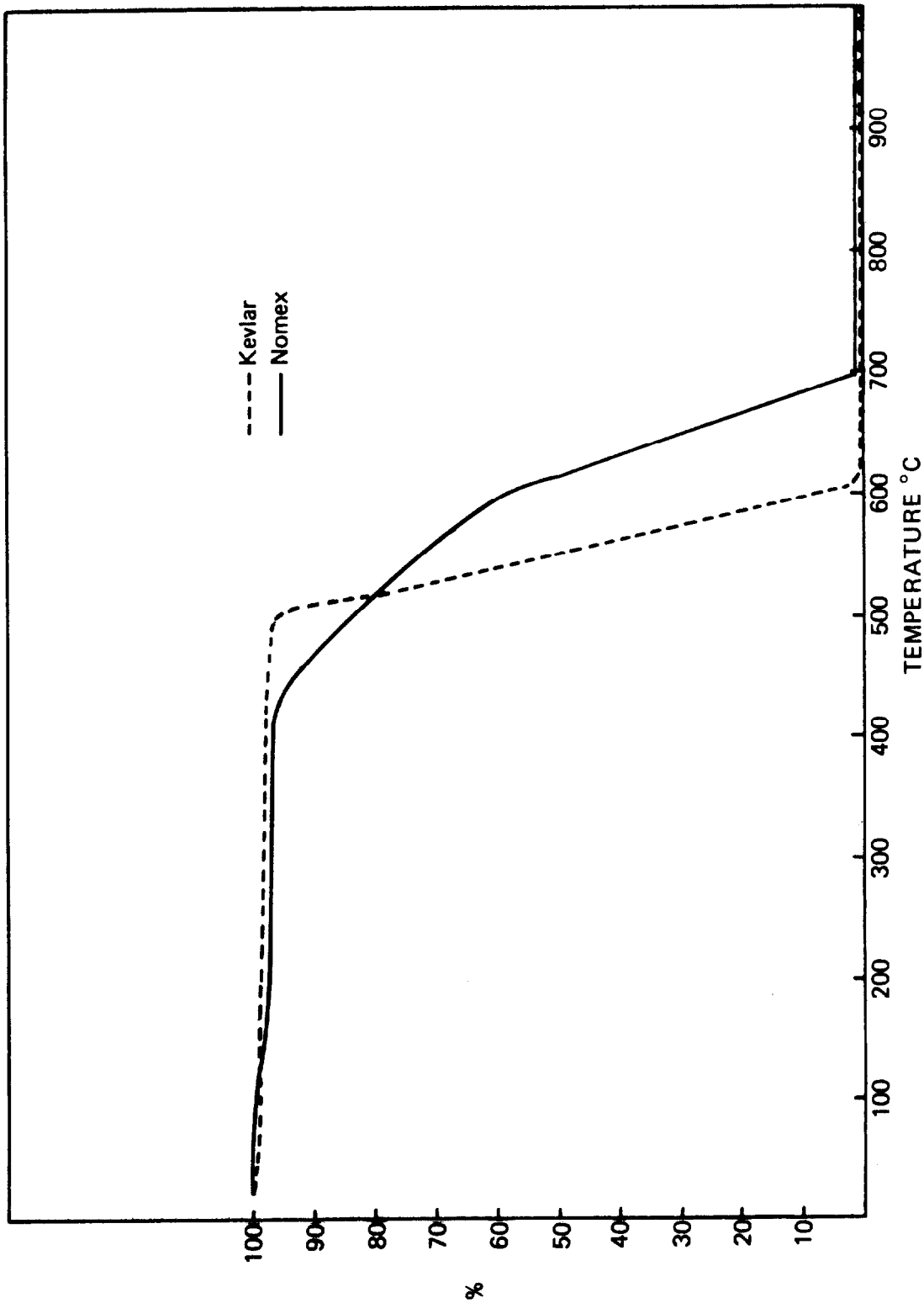

FIGURE 6. THERMOGRAVIMETRIC ANALYSIS OF NOMEX AND KEVLAR

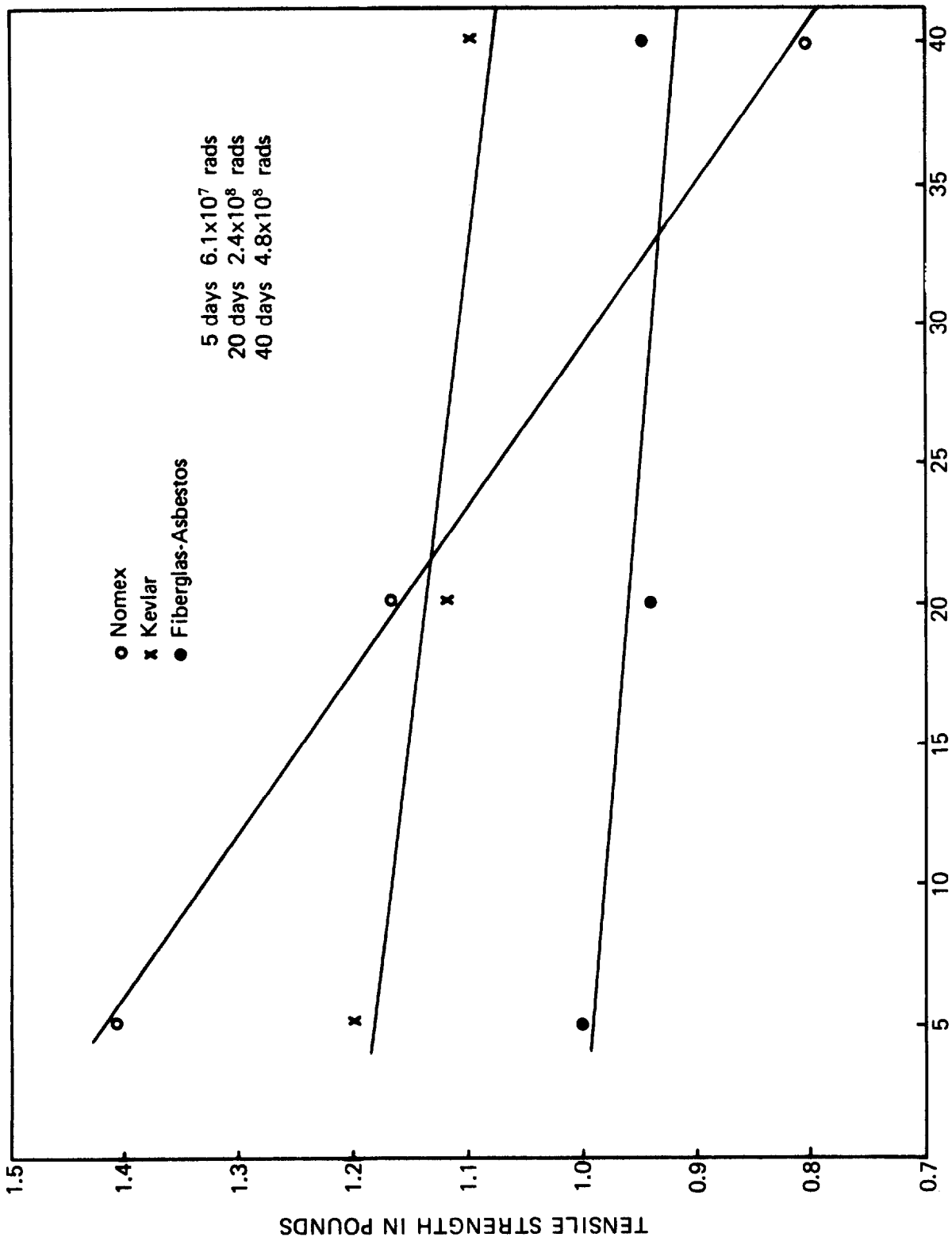

FIGURE 7. RADIATION EFFECT ON TENSILE STRENGTH OF FILTER MEDIA FIBERS

Stainless steel should function quite well but the cost of this material is about $450 per size 5 HEPA (2 x 2 x 1') filter using 12.5 micrometers thick sheets. The steel becomes cheaper as thickness is increased. For 50-micrometer sheets the material cost decreases to about $175 per filter, but the weight of the separators increases to about 12.7 Kg per filter. The asbestos separators for each filter weigh approximately 4.5 Kg. Current cost of size 5 HEPA filters is about $100 each.

Composite Material Separators

Composite materials such as coated aluminum and glass fiber with a reinforcing polymer show the best potential for fabrication of separators. Aluminum laminated with Kapton® (Du Pont), a polyimide film, exhibited excellent thermal and chemical properties but the cost exceeded even that for stainless steel. Subsequently, coatings on aluminum whose temperature resistances are below 371°C were tested. Aluminum laminated with PVC failed the high temperature test because of a flammable solvent used in the adhesive. Epoxy and epoxy copolymer coatings to 2.5 to 5 micrometer thicknesses are not stable at 371°C, but are functional. The filter (Figure 4) which was subjected to the high temperature test contained aluminum separators coated with an epoxy-vinyl copolymer. The coating had darkened but remained intact and displayed no evidence of separation from the aluminum.

Exposure of the coated aluminum to HNO_3-HF atmosphere showed excellent stability. After several weeks the effect of the acid exposure becomes evident at the unprotected edges of the aluminum where a few millimeters of the coating is separated from the aluminum.

A major advantage of epoxy-coated aluminum is that it is readily available. Thus far, prototype filters of two HEPA filter manufacturers with their own sources of coated aluminum were subjected to the high temperature test and passed.

Glass fiber separators are also being evaluated. One manufacturer currently has the capability of marketing a filter using glass fiber separators, but the separators are so thick that the amount of medium that can be incorporated in the filter is reduced. Consequently the filter area is reduced to such an extent that the pressure drop exceeds the maximum allowed.

Using glass fiber mats of about 0.4 mm thickness, various binders such as sodium silicate, polyester, silicones, and polyimide were tried to stiffen the glass fibers into a corrugated separator. A polyimide stiffener has yielded the best results to date. Figure 8 shows corrugated glass fiber-polyimide separators fabricated in the laboratory. The darkened corner of the lower right sample was caused by exposure to a match flame for a few seconds. It was not flammable. A disadvantage of polyimide is that it must be dissolved in an organic solvent such as dimethyl formamide or toluene as it is incompatible with water. Also after application to the glass fiber sheet it must be cured at elevated temperatures. The samples shown were cured at 180°C for 30 minutes. The curing time can be reduced by using higher temperatures.

Currently other polymeric resins and processes which present fewer manufacturing constraints are being investigated.

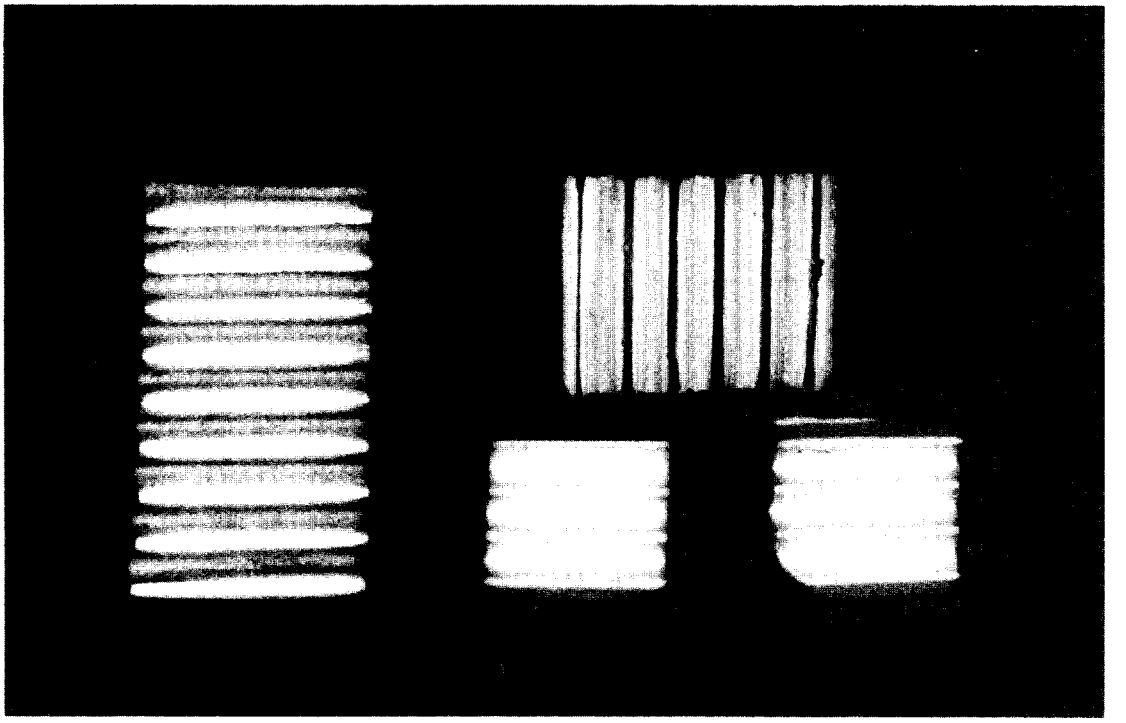

FIGURE 8. GLASS FIBER SEPARATORS WITH POLYIMIDE STIFFENER

III. Laboratory Hot Air Test

Hot air resistance tests of size 5 HEPA filters on a routine basis to evaluate new filter components are cumbersome and can result in the generation of considerable amounts of smoke and heat as once occurred during the test with PVC laminated aluminum separators. In an effort to minimize the number of large scale tests, a small apparatus was set up to screen the prospective new components (Figure 9). A simulated "filter" is fitted in a wire mesh holder for free passage of air. This inserted into the test "plenum" when the air reaches 371°C. With a medium area of about 335 square centimeters, a flow rate of 1.8 cfm is equivalent to 1,000 cfm for a size 5 filter. Figures 10 and 11 show the PVC-aluminum laminate had partially melted and the epoxy-vinyl coated aluminum had darkened but remained intact. The thermocouple within the "filter" showed an exotherm whose temperature rose from 371 to 880°C for the laminate and to only 391°C with the coated aluminum separators. These results are in agreement with those obtained in the full scale tests.

IV. In-Service Filter Testing

In-service tests were conducted in the first stage of plenum FU-2B into which air is exhausted from Production Chemical Recovery Glove Box lines.[1] This is the plenum in which filters are subjected to the most corrosive acid atmosphere at Rocky Flats. Filters tested in the plenum are either commercial or prototypes with either new components and/or design. Before being placed in the plenum, their air and temperature resistances and penetrations are determined. Failure of the penetration or resistance tests by these filters would not compromise the filtration system as air passing through this plenum goes through eight stages of filtration before being exhausted to the atmosphere.

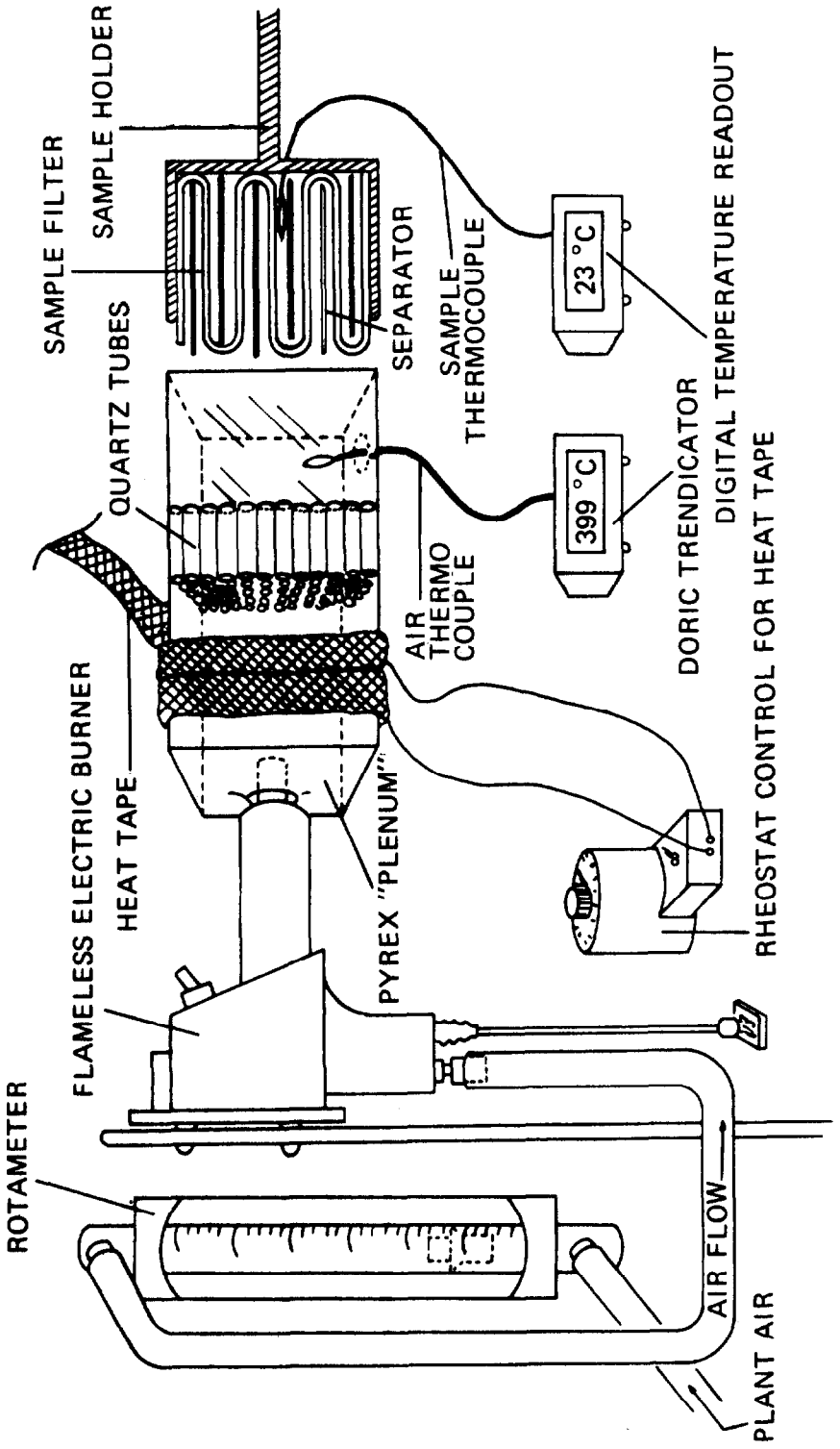

FIGURE 9. LABORATORY HOT AIR TEST APPARATUS

FIGURE 10. PVC-ALUMINUM AFTER LABORATORY HOT AIR TEST

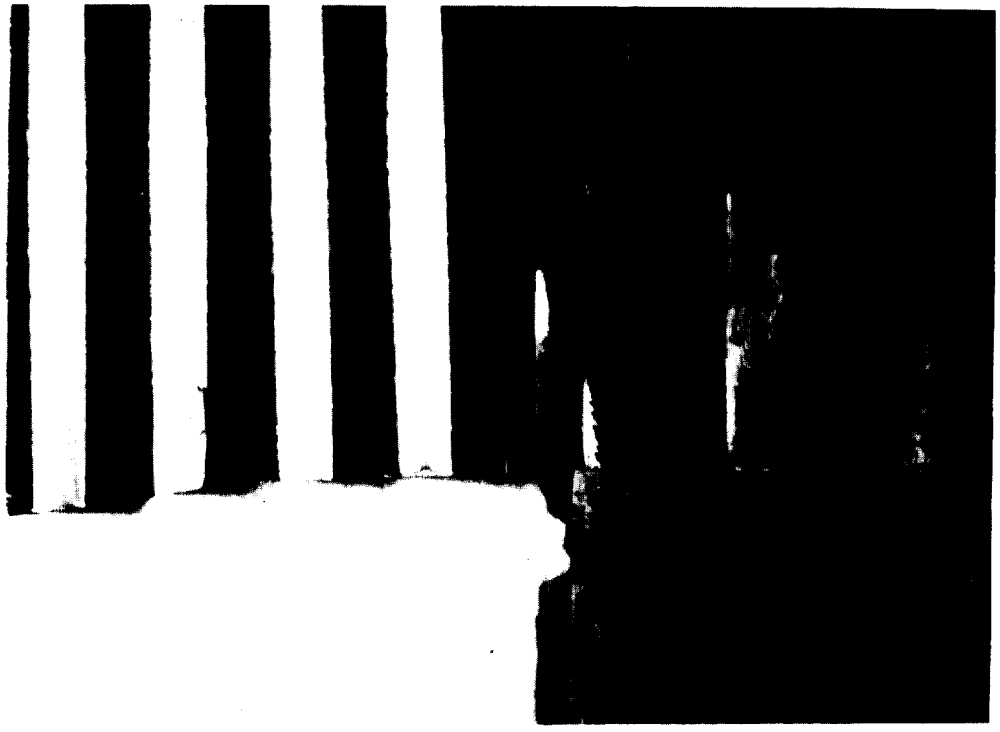

FIGURE 11. EPOXY-VINYL SEPARATORS (TOP) AND Y-100 MEDIUM (BOTTOM) BEFORE AND AFTER LABORATORY HOT AIR TEST

Tests of Experimental and New Commercial Filters

Separatorless Filters

Thirty-six Flanders Super-Flow® (Flanders Filter Company) filters with Y-100 medium have been tested. All but one have performed satisfactorily. The filter which failed is shown in Figure 12. A section of the medium has collapsed. The other fifteen Super-Flow filters being evaluated simultaneously in the same stage did not exhibit any evidence of failure.

Two MSA minipleated filters with Dexter 1236 medium (coated with polyphenylene oxide) performed with mixed results. One filter performed quite well but the other suffered considerable damage by the time it was removed (Figure 13). However, it should be stressed that this particular filter was left in the plenum for 8 months. During the periods this filter was in service, normal filter change times were 4 to 6 months.

Filters with Aluminum Separators (and medium containing Nomex additive)

A total of eight filters with coated aluminum separators were tested. Five were supplied by ALFCO and the remainder by Cambridge Filter Company. The coated aluminum was obtained by these firms through their own suppliers. For comparison purposes, filters with uncoated aluminum separators were placed adjacent to these filters.

After 6 months service, the filters were replaced. Figures 14 and 15 show the difference in acid resistance between the coated and uncoated aluminum. The upstream edges of the uncoated aluminum separators were destroyed 1 to 3 inches into the medium. Beyond that, for several additional inches the aluminum separators had been corroded to where they were not functional as separators. The downstream edges of the uncoated aluminum separators displayed a thin crust of salt which was probably $Al(NO_3).9H_2O$. The coated separators appeared clean and unaffected except for 2-3 mm from the edge where the coating was separated from the aluminum. Parts of the medium-separator components from these filters were studied for gas generation.

Filters with aluminum separators are about 7 Kg lighter than those with asbestos separators and, after service, their weight gain can be as much as 7 Kg less. During service filters with chrysotile asbestos separators gain weight primarily from nitric acid attack on asbestos to form $Mg(NO_3)_2.6H_2O$. In addition, during periods of high humidity, the hygroscopic magnesium salt tends to deliquesce and drips from the filters. The lighter filters are a considerable aid to the filter-change crew who must handle them in confined spaces while clad in supplied air suits. The lighter filters also tend to decrease installation damage.

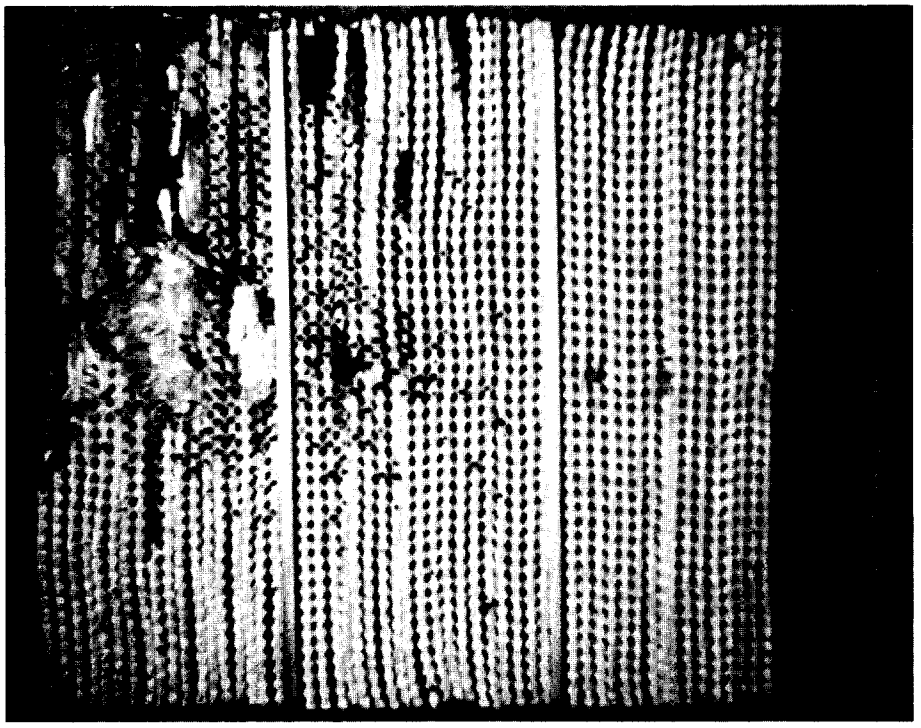

FIGURE 12. SUPER-FLOW FILTER WITH PARTIALLY COLLAPSED MEDIUM

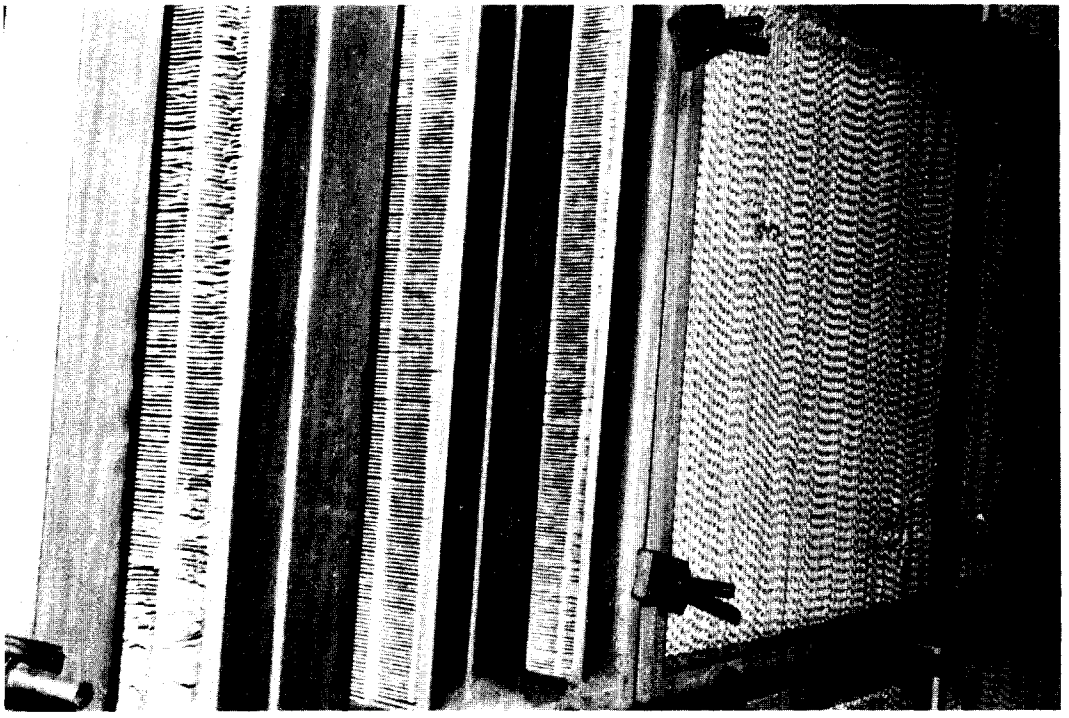

FIGURE 13. MINIPLEATED FILTER AFTER EXTENDED SERVICE

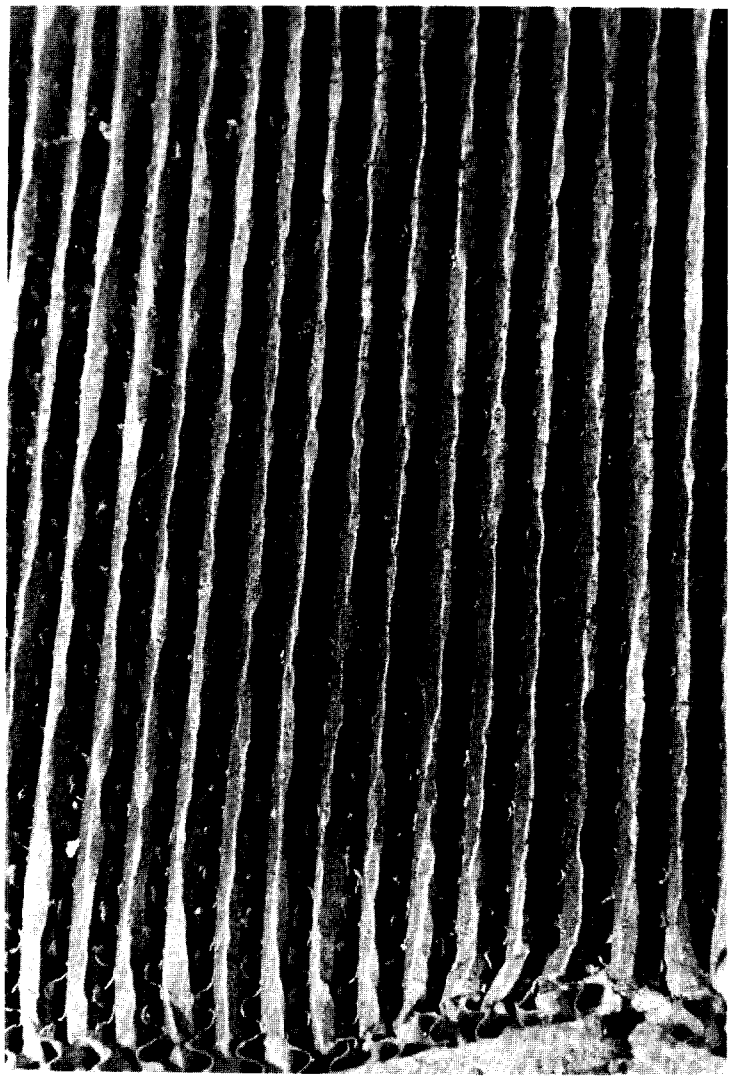

FIGURE 14. UPSTREAM FACE OF FILTER WITH UNCOATED ALUMINUM SEPARATORS (LEFT)

FIGURE 15. UPSTREAM FACE OF FILTER WITH COATED ALUMINUM SEPARATORS (BELOW)

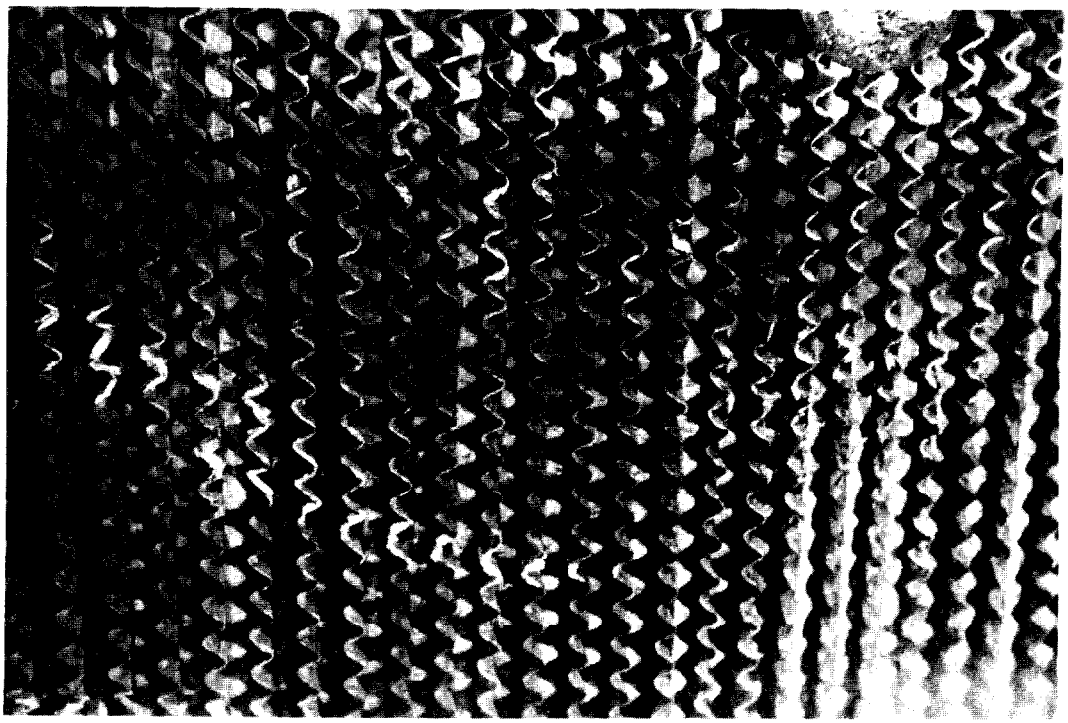

In-Place DOP Tests of Spent Filters

The filters described above were placed in the first stage of the plenum along with filters containing 5% asbestos medium and asbestos separators, which have been the standard filters used at Rocky Flats, as a control. The first stage consists of 30 filters which were usually DOP aerosol tested just before they were replaced. Because the DOP generators that were used were incapable of producing the huge quantities of DOP smoke required for 100% concentration, a lower concentration of 10-20% was used. Particle detection was by means of a probe connected to a forward light scattering photometer located outside the plenum. The probe was moved across the face of the filter by a member of the filter change crew in the plenum wearing a supplied air suit. Voice communication between the exterior and interior of the plenum was by radio and port holes provided visual contact.

Table I lists the filters that were placed in the first stage of plenum FU-2B in the past 2 years, date tested, and the number that failed the DOP test at the end of their service life.

Most of the filters, at the time of their replacement, still retained their filtration efficiency. Therefore, the test results do not identify which media have superior acid resistance. Two steps will be taken in the future to accomplish this objective.

The first step will be to increase the DOP concentration in the plenum during the test from about 15% to 100%. A thermal generator with a greater DOP aerosol generating capacity will be used to replace or supplement the two air operated aerosol generators currently being used. The increased DOP concentration will result in greater sensitivity in the tests and will help differentiate between filters which have retained their efficiencies from those that are marginal but not seriously degraded.

The second step will be to increase the service life of the filters by allowing greater degradation of the filters. The DOP test results indicate that many of the filters could have been left in service. Timing of the filter change is usually on the basis of physical appearance of the filters and the duration they have been in service.

If necessary, selected filters of the second stage will be temporarily removed in order to DOP test the corresponding first stage filters. This will help establish the optimum time to obtain in-service data on the comparative acid resistance of filter media. Measuring the loss of filtration efficiency of the first stage requires the removal of the second stage since they are installed back-to-back.

Study of Components of Spent Filters

Gas Generation by Acid Attack on Aluminum Separators

A potential problem is the effect of acid on the aluminum separators in spent filters during long-term transuranic waste storage. The question was: "What kind and how much gas would be generated?" In an effort to gain some

TABLE I. IN-PLACE DOP TETS OF SPENT FILTERS

Date Installed	Date DOP Tested	5% Asbestos	Super-flow	MSA	ALFCO	Cambridge	Other
September 1978	November 1978	15	14*	1			
November 1978	May 1979	23(1)	6	(c)			
May 1979	November 1979	19(1)	4	1	2		4(a)
November 1979	August 1980	19	4		3	3	1(b)

LEGEND:

5% Asbestos - Fiberglas-5% asbestos medium with asbestos separators

Superflow - Flanders separatorless filter with Y-100 medium

MSA - MSA minipleated filter with Dexter 1236 medium

ALFCO - Filter with coated Al separators and glass fiber medium (installed May '79) or glass fiber-Nomex medium (installed Nov. '79)

Cambridge - Filter with coated Al separators and glass fiber-Nomex medium

Other
(a) Filter with uncoated Al separators and glass fiber medium
(b) Flanders filter with glass fiber separators and Y-100 medium
Digits within the parentheses indicate the number of filters which had leaky medium.

*Medium in one filter partially collapsed (see Figure 12).

(c) Left in service.

insight on the scope of this question, when spent filters with aluminum separators were removed from the in-service tests described in this report, parts of the filters were placed in steel containers equipped with pressure gauges and gas sampling ports. Approximately 10% of the media-separator combination was removed from filters containing coated and uncoated aluminum separators. Changes in pressure and composition of the container atmosphere were monitored periodically and the results are listed in Tables II and III. The pressure in the container with the uncoated separators decreased with the oxygen concentration. When the oxygen was depleted, the NO_x concentration began to increase. Apparently the overall reactions are the oxidation of aluminum first by the oxygen, then subsequently by the nitrate to form NO_x. After about 8 months, the pressure in the container with the uncoated aluminum separators rose 45% above its initial pressure while that with the coated aluminum showed no change. Currently there are studies to determine ways in which NO_x could be absorbed or combined and whether this would be sufficient to prevent overpressurization.

Scanning Electron Microscopy of Spent Media

Samples of glass fiber-asbestos, Y-100 and Dexter 1236 media were taken from filters replaced in May 1979 and photographed in a scanning electron microscope. Figures 16 through 18 show the upstream and downstream sides of the media at 1000X. The difference in the amount of filtered material on the upstream and downstream side is greatest with the Y-100 and was probably due to being in a central location of the plenum where air flow is greatest. The upstream side of the Dexter 1236 which came from the minipleated MSA filter which was in service for 8 months does not show this accumulation of particles possibly because of the greater surface area available in filters of this configuration.

V. Summary and Conclusions

Efforts to develop acid-resistant components which will prolong the life of HEPA filters have progressed along the lines of locating improved substitutes for asbestos. In the case of the media, Nomex as an additive appears to have chemical resistance at least equal to that of asbestos. Present tests are directed toward determining whether it is better, and if so, how much better? Handsheets with Kevlar microfibers as additives have demonstrated the feasibility of using this material which has better chemical and physical properties than Nomex.

Separators of aluminum coated with a epoxy-vinyl copolymer have performed quite well in service. Gas generation resulting from acid attack of the aluminum has not been a problem, but methods of eliminating this potential are being studied. Glass fiber separators should serve quite well, but since no manufacturer seems interested in this development, some laboratory work has been conducted. Polyimide resin seems to function quite well, but large scale fabrication may be impractical. Other stiffening agents such as ceramic adhesives and high temperature organic resins are being considered.

In-service tests of prototype and commercial filters show them to be comparable in chemical reactivity to the standard asbestos-containing filters. Their service lives thus far appear to be equal. The weight of a spent size 5 HEPA filter, as transuranic waste, can be reduced by as much as 14 Kg when coated aluminum separators are used in place of asbestos separators.

TABLE II

UNCOATED FILTER-SEPARATOR PRESSURE AND GAS ANALYSIS RESULTS

(SAMPLE #22)

Time (days)	Pressure (torr)	H_2	N_2	O_2	Ar	CO_2	NO_x	Hydrocarbons
0	636	0.0	78.2	20.6	0.9	0.3	0.0	trace
26	621	0.0	80.2	18.6	1.0	0.2	0.0	trace
48	604	0.0	80.9	17.8	1.0	0.8	0.0	trace
83	597	0.2	85.3	13.1	1.0	0.4	0.0	trace
179[a]		0.1	93.6	3.3	1.4	1.5	0.1	trace
217	634	0.5	93.0	0.0	1.3	1.6	3.6	trace
235	925	0.6	82.7	0.0	0.7	1.2	14.8	trace

[a] Pressure not recorded at this time.

TABLE III

COATED FILTER-SEPARATOR PRESSURE AND GAS ANALYSIS RESULTS

(SAMPLE #16)

Time (days)	Pressure (torr)	H_2	N_2	O_2	Ar	CO_2	NO_x	Hydrocarbons
0	630	0.0	77.4	21.4	1.0	0.2	0.0	trace
26	627	0.0	77.6	21.2	1.0	0.2	0.0	trace
48	625	0.0	78.1	20.6	1.0	0.3	0.0	trace
83	625	0.0	79.1	19.7	1.0	0.2	0.0	trace
179[a]		0.0	79.1	19.5	1.0	0.3	0.0	trace
217	625	0.0	78.0	19.5	1.1	0.6	0.0	trace
235	925	0.0	79.4	18.9	1.1	0.6	0.0	trace

[a] Pressure not recorded at this time.

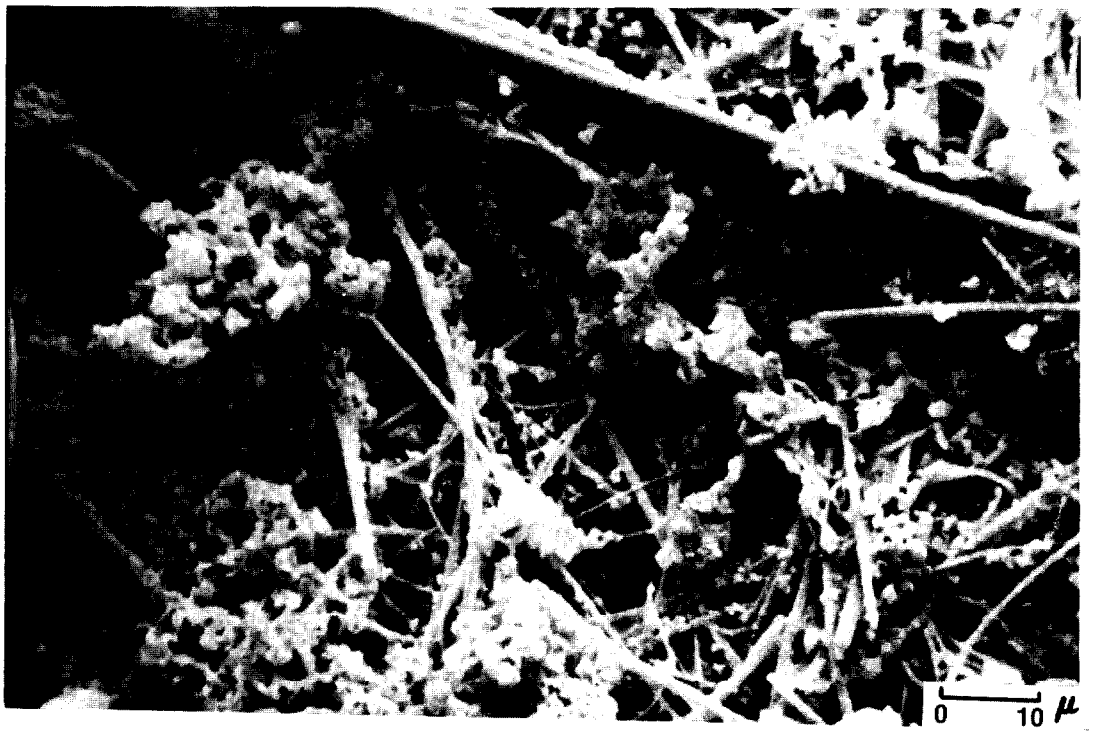

FIGURE 16. GLASS-ASBESTOS MEDIUM-UPSTREAM (TOP), DOWNSTREAM (BOTTOM)

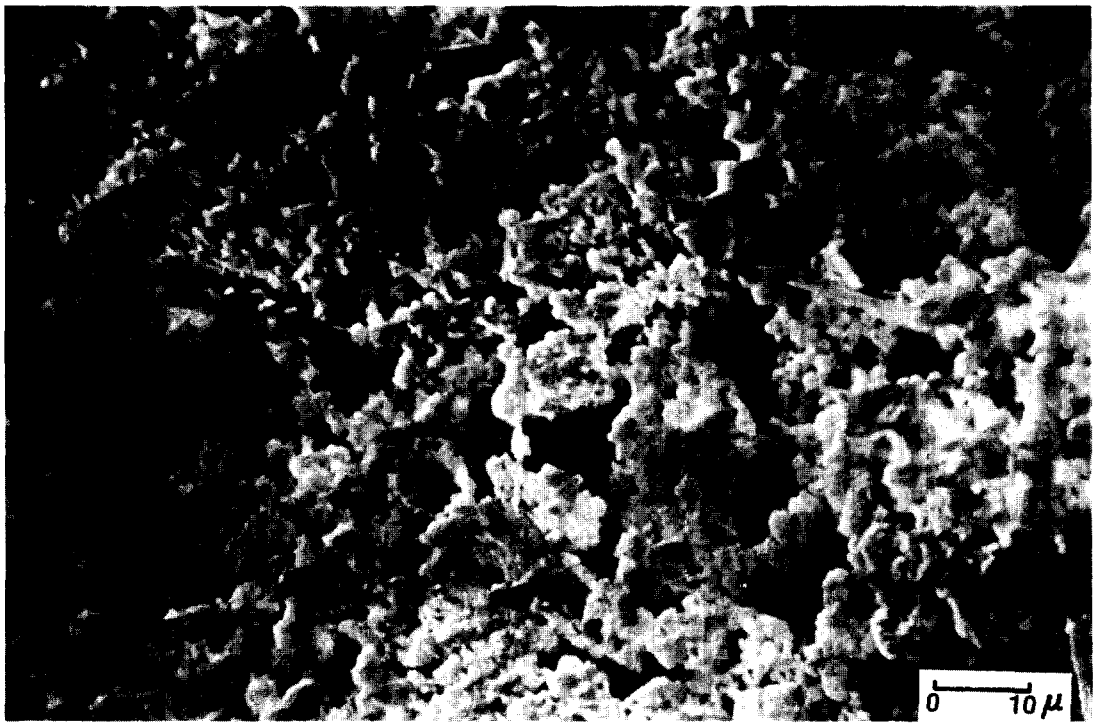

FIGURE 17. Y-100 MEDIUM-UPSTREAM (TOP), DOWNSTREAM (BOTTOM)

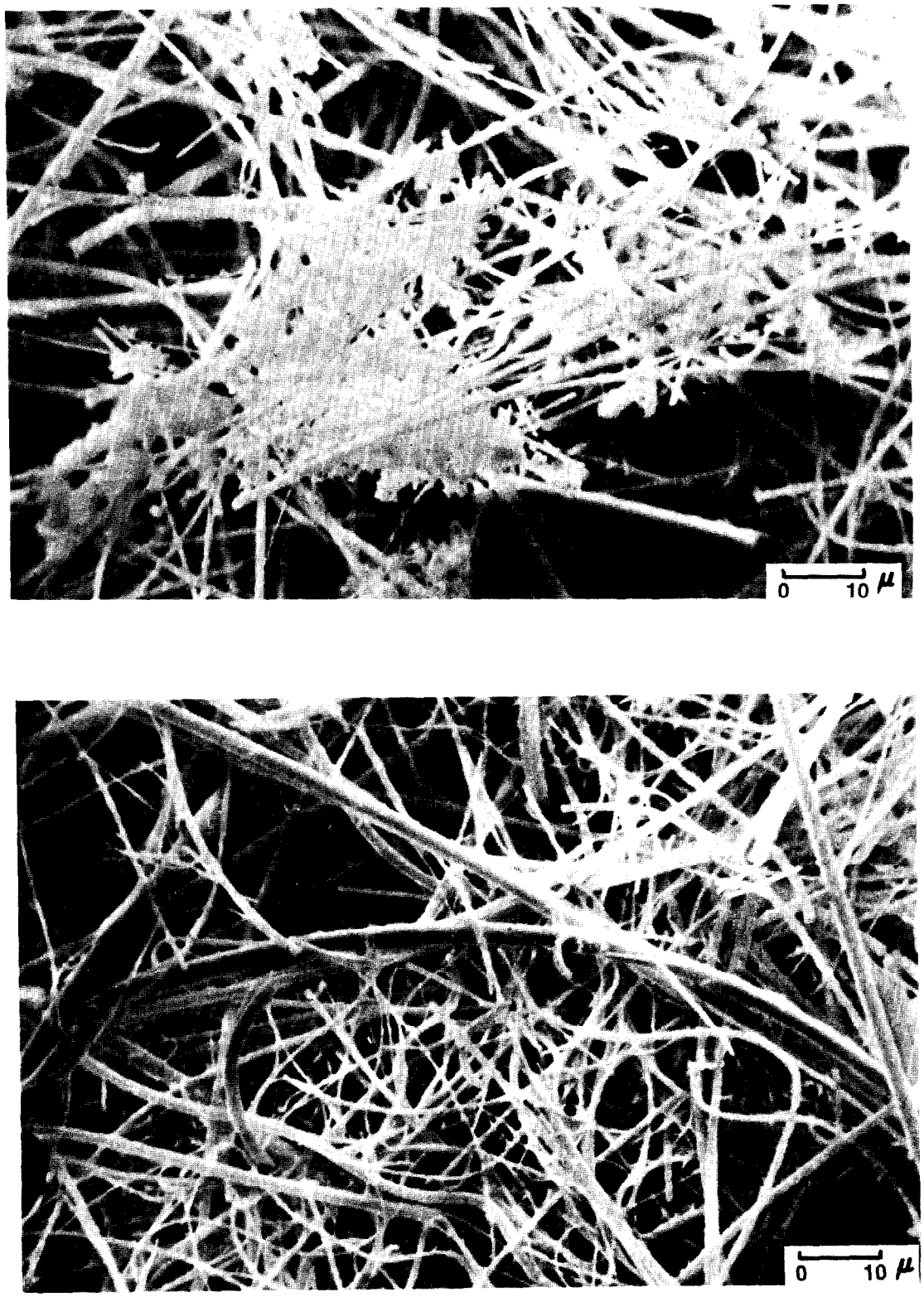

FIGURE 18. DEXTER 1236 UPSTREAM (TOP), DOWNSTREAM (BOTTOM)

VI. Acknowledgments

The authors wish to thank P. A. Hyman, D. I. Hunter, and E. L. Damico of the Analytical Laboratory, V. K. Grotzky and J. F. Capes of the Electron Optics Laboratory, W. D. Gilbert and F. W. Wittich of the Filter Certification Laboratory for their technical assistance, and R. J. Merlini for his helpful suggestions and advice.

VII. References

1. R. W. Woodard, K. Terada, and O. I. Buttedahl, "Studies on Prolonging HEPA Filter Service in Chemical Applications," CONF-780819, p. 1100. Proceedings of the Fifteenth DOE Nuclear Air Cleaning Conference, August 1978.

2. W. L. Belvin, M. A. Krimmel, H. C. Schwalbe, and E. N. Gleaton, "Development of New Fluoride Resistant HEPA Filter Medium," TID 26649, Herty Foundation, Savannah, Georgia, August 1975.

DISCUSSION

BOHANNON: Can you tell me who is the manufacturer of the Nomex-containing medium?

TERADA: Hollingsworth and Vose.

BURCHSTED: Can you tell me who the manufacturer of the filter was, and also, can you tell me whether the properties of the medium conform to the requirements of MIL-F-51079? That is, the military specification for HEPA filter medium?

TERADA: The filter manufacturers were Aluminum Filter Company in Santa Barbara, California, and Cambridge. They made the prototype filters. As for the specification, are you talking about the organic composition?

BURCHSTED: The organic composition, the tensile strength, the moisture resistance, the thickness, radiation resistance, etc.

TERADA: We have not run moisture and radiation tests, but the organic concentration is about 7%. Tensile stress tests have been run and air resistance, also. They met the specifications.

SHOULDER: I notice in the slide that it appeared that you used a standard wood filter frame. I am wondering if you looked into other materials, as well as the bonding material between the media and the frame?

TERADA: No, those matters are not within the scope of what we are doing. We are looking for materials which will increase the acid resistance of the HEPA filter medium. And thus far, at Rocky

Flats, we really have not had much problem with the frame and the adhesive.

SHOULDER: Would your test equipment be capable of testing the frame and the bonding material?

TERADA: We have not tested these components, but we could. I am not sure how good the results would be, but it is possible.

SHOULDER: Where is your test facility located?

TERADA: It is at Rocky Flats in one of the laboratories.

PARSONS: I just wanted to state that the material that was in the filters tested at Rocky Flats was irradiated and does meet the military specification referred to by Mr. Burchsted, except that the organic content (combustible material) is over 7%.

BOHANNON: When you spoke of the coated aluminum, was that from one supplier or is it available from many aluminum suppliers?

TERADA: At least one of our filter suppliers, the Aluminum Filter Company, has declined to tell us who the supplier was. You might ask Cambridge Filter Corporation. They might tell you.

HAYN: We heard in the morning session about metal fibers and HEPA filters. Why do you not use recleanable HEPA filters made of metal fiber fleeces?

TERADA: We are looking at the possibility of using pre-filters which are cleanable.

HAYN: But now you can buy commercial metal fiber fleeces which have HEPA filter capabilities. They have been tested with aerosols used in HEPA filter testing.

TERADA: I do not know anything about that filter material.

DORMAN: Could you tell me who supplies these fleeces, Dr. Hayn?

HAYN: We have made tests with metal fiber fleeces using sodium chloride aerosols generated by a standard British generator. We measured an efficiency about 99.97% with these aerosols using metal fiber fleeces. These fleeces are made from sintered metal fibers with a fiber diameter of about 4 microns. The metal fiber fleeces are produced by Bekaert in Belgium.

ELECTROFIBROUS PREFILTERS FOR USE IN NUCLEAR VENTILATION SYSTEMS*

By

W. Bergman, W.D. Kuhl, W.L. Russel, R.D. Taylor, H.D. Hebard, A.H. Biermann, N.J. Alvares, D.G. Beason, and B.Y. Lum

Lawrence Livermore National Laboratory (LLNL), Livermore, California

Abstract

We have established a comprehensive program for the U.S. Department of Energy to develop electrofibrous prefilters to extend the life of High Efficiency Particulate Air (HEPA) filters that are used in the nuclear industry. We have selected the electrofibrous filter because, compared to the mechanical fibrous filter, it has a higher efficiency and longer lifetime. Two different electrofibrous filters have been developed for use in nuclear ventilation systems. One prototype is a stationary prefilter while the other is a rolling prefilter. Both prefilters use the same basic filtering technique in which a fibrous filter medium is sandwiched between a high voltage electrode and a ground electrode, both electrodes having a sufficient open area to offer minimum air resistance. The applied voltage on the electrodes generates an electric field that polarizes the filter fibers, which then attract suspended particles via electrostatic forces. Since a finite time is required for this electrostatic attraction, the filter media and electrodes have been pleated to provide a sufficiently long particle residence time.

The stationary electrofibrous prefilter has the same dimensions (610 x 610 x 305 mm) as commercially available mechanical filters that are used in ventilation systems. However, the additional requirement of high voltage on the electrodes has greatly increased the complexity of the electrofibrous prefilter. Laboratory tests using DOP and NaCl aerosols in a modified ASHRAE filter test apparatus have shown that the electrofibrous prefilter increases in efficiency from 40 to 90% as 10 kV is applied to the electrode.

The special requirement of protecting the HEPA filter from a high concentration of smoke aerosols during fire conditions led to the development of the rolling, electrofibrous prefilter. We established the feasibility of this concept in a series of tests using commercially available rolling prefilters that were modified for removing smoke aerosols. Although the rolling prefilter concept is not a cost effective measure for the sole purpose of protecting HEPA filters from smoke aerosols, it became cost effective when used primarily for protecting the HEPA filters from normal production aerosols. The same piece of equipment is then used for both normal operating conditions as well as emergency fire conditions. Several prototype electrofibrous rolling prefilters were designed, built and evaluated. The filter evaluations were conducted using NaCl and DOP aerosols as well as smoke aerosols.

*This work was performed under the auspices of the U. S. Department of Energy by Lawrence Livermore Laboratory under contract No. W-7405-ENG-48.

I. INTRODUCTION

The HEPA filters used in the nuclear industry to remove radioactive airborne contaminants are extremely effective and practical devices and will continue to be so despite the large number of new control devices presently available. However, HEPA filters generate a significant volume of radioactive waste and are costly to purchase and operate. The actual cost of materials and labor to buy, change, test, and dispose of a HEPA filter is several times its initial purchase price. In an effort to reduce the HEPA's operational cost and the volume of radioactive waste it generates, the Nuclear Fuel Cycle and Waste Management Division of DOE has contracted with LLNL to develop an enhanced filtration system that will extend the service life of HEPA filters. The approach selected by LLNL consists of using an electrofibrous prefilter to take the load off the HEPA filter, since it appears to have a greater potential for success than other methods, such as scrubbers and electrostatic precipitators.

The electrofibrous filter represents the best technology for removing airborne particles. Compared to a conventional fibrous filter, the electrofibrous filter has a much higher efficiency and significantly lower pressure drop at the same level of particle loading. This dramatic increase in filter performance due to the added electrical forces has recently created a world-wide interest in this field. A symposium on Fibers, Electrostatics and Filters that was held in Princeton, New Jersey in November 1979, illustrated the diversity of techniques used to generate electrofibrous filters(1).

The concepts used in our electrofibrous prefilter are not new. Electrostatics have been used to improve the performance of fibrous filters since 1930. Although the electrofibrous filters can have a number of different configurations, all are based on either charging or polarizing the filter fibers. This generates an electrical force between the fibers and particles and results in a large increase in the filter efficiency and filter life. The primary methods for generating electrofibrous filters include precharging the aerosols, polarizing the filter media with electric fields, a combination of these two methods and permanently charging the fibers. These methods have been reviewed previously(2).

LLNL has established a comprehensive program to conduct theoretical modelling, small-scale laboratory experiments, prototype development and field evaluations of electrofibrous prefilters. The objective of our theory and laboratory experiments is to understand the mechanical and electrical filtration mechanisms for both clean and clogged filters in sufficient detail to optimize the electrofibrous filter. Although we have not yet completed this optimization study, we have identified the important parameters in the prototye design and have established general design criteria.

Using these design criteria, we have been developing prototype electrofibrous prefilters for use in radioactive gloved boxes and in nuclear ventilation systems. The design and field evaluation of our prototype filters for gloved box applications have been reported elsewhere(3). In this report we will present the design criteria and our preliminary evaluation of prototype electrofibrous prefilters for nuclear ventilation systems.

II. Design Concept for Electrofibrous Filter

The design concept for the electrofibrous filter that we selected was based upon applying an external electric field across a fibrous filter. The filter medium in this design concept is considered to be disposable and will be replaced

with new medium rather than being cleaned. This concept was selected over the other approaches for electrifying the filter medium because it had the best potential for success in the nuclear industry. The basic components of the electrofibrous filter described in this report are illustrated in Fig. 1. A fibrous filter medium is sandwiched between two perforated electrodes separated by a spacer. By applying high voltage to one electrode and grounding the other, an electric field is generated across the filter medium that polarizes the filter fibers. The polarized fibers are responsible for the increased filter efficiency. An important property of this electrofibrous filter is its extremely low power requirements. The 200 mm x 200 mm element shown in Fig. 1 uses less than 5 mW of electrical power when 10 kV is applied across the electrodes. However, because of the high voltage used in this filter, it can not be used in an explosive environment. Although a spark across the electrodes is extremely rare, it does occur under malfunction conditions and should be considered in potential applications. The potential fire hazard from this low energy spark is very small.

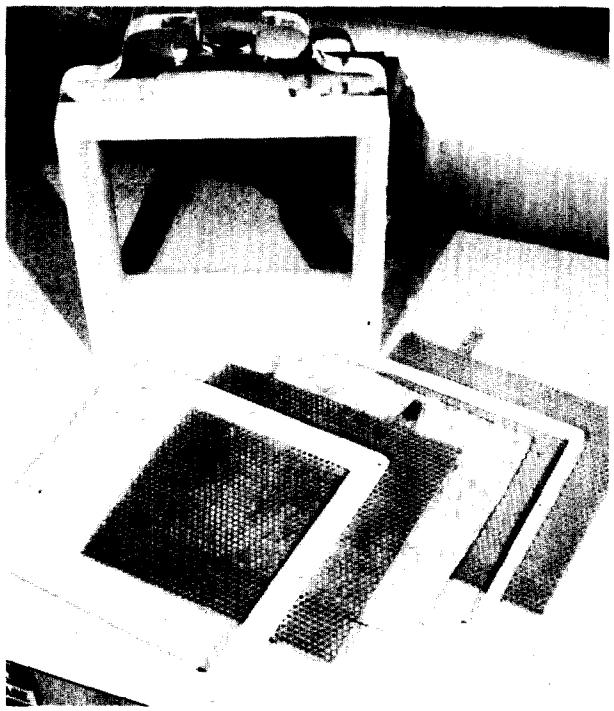

Figure 1

Components of electrofibrous prefilter.

Other concepts for electrofibrous filters were also considered but did not appear practical for our application. Electrofibrous filters that were generated by precharging incoming aerosols with a corona discharge presented a potential fire hazard that would severely restrict their application. However this approach appears to be very applicable in noncombustible environments. Prototype electrofibrous filters have been developed by precharging aerosols with a corona discharge prior to filtration in both cloth and deep bed filters[4,5]. The Apitron Division of American Precision Industries, Inc. (Charlotte, North Carolina) has a commercially available bag house filter that incorporates a corona charger upstream of standard cloth bags.

Another class of electrofibrous filters that was eliminated from our consideration is the permanently charged filters. These filters are very attractive since they have the improved filter performance due to electrification without the need for additional charging devices. When we began our program in 1976, the only permanently charged electrofibrous filter that was available was the Hansen filter[6]. This filter is basically a wool pad in which small,

charged particles of resin are scattered over the surface of the wool fibers. The resin particles become highly charged due to frictional charging during the manufacturing process in which the wool-resin mixture is combed on a textile carding machine. Since the resin particles have a high resistivity, they can retain the charge for long periods of time. These highly charged resin particles can attract aerosols through electrostatic forces and are responsible for the high efficiency of Hansen filters. Unfortunately, the resin particles can be discharged when exposed to ionizing radiation, concentrated organic solvents, or excessive heat. When this happens, the Hansen filter becomes a very poor filter. Because of the potential discharging problem and the flammability of the wool fibers, we did not believe that the Hansen filter could be used in nuclear ventilation systems.

However, a new generation of permanently charged filters that are based on electrets appears to significantly reduce the problem with the flammability and discharging of the filter. With further improvements either underway or planned, the electret filter will be a viable candidate for use in nuclear ventilation systems. Electrets are the electrical counterparts of magnets and are formed by heating and cooling a polymer in an intense electric field. The pioneering work of van Turnhout and his colleagues have led to the practical application of electrets in fibrous filters[7,8]. They have developed a new continuous charging method that allows the mass production of electret fibers. The N. V. Verto Company (Rotterdam, The Netherlands) has used this method to produce electret filters and began marketing the filter medium in 1979.

III. Theory of Electrofibrous Filter

Developing an accurate theory of the electrofibrous filter is an important part of our filtration program. This theory will be used to optimize the design of our prototype electrofibrous filters. Since a detailed description of the theory was already published, we shall briefly review the essential features of the theory[2,9,10]. The dominant characteristics of the electrofibrous filter that must be theoretically explained are (1) the higher efficiency and (2) the longer filter life when compared to a conventional fibrous filter. The increased filter efficiency due to the applied electric field was previously shown in Fig. 1.

When an external electric field is first applied to the filter, the only capture mechanism is due to the forces between a polarized fiber and a polarized or charged particle. The electric field instantly polarizes the fiber, which then attracts both charged and polarized particles. The charged particles that deposit on the fiber then gradually build up a fiber charge which introduces the second mechanism. This mechanism is based on the force between charged fibers and charged or polarized particles. The increased filter efficiency is thus due to a time independent attraction between polarized fibers and aerosols, and a time dependent attraction between charged fibers and aerosols. An equilibrium charge is established on the fiber in a dynamic process of charge accumulation due to the particle deposits and charge dissipation due to the fiber conductivity. Other researchers have not considered the time dependent mechanism involving fiber charge and could therefore not explain many experimental findings.

Figure 2 illustrates the two particle capture mechanisms that are responsible for increasing the filter efficiency. The larger and smaller circles represent the cross sections of the fibers and the charged particles respectively. The solid lines are the electrical lines of force, while the dashed lines are the particle trajectories for the two capture mechanisms. These capture mechanisms are due to the interaction between a polarized fiber and a charged particle, and

the interaction between a charged fiber and a charged particle. The same basic mechanisms are also valid for uncharged particles, in which case, we must replace the charged particles with polarized particles.

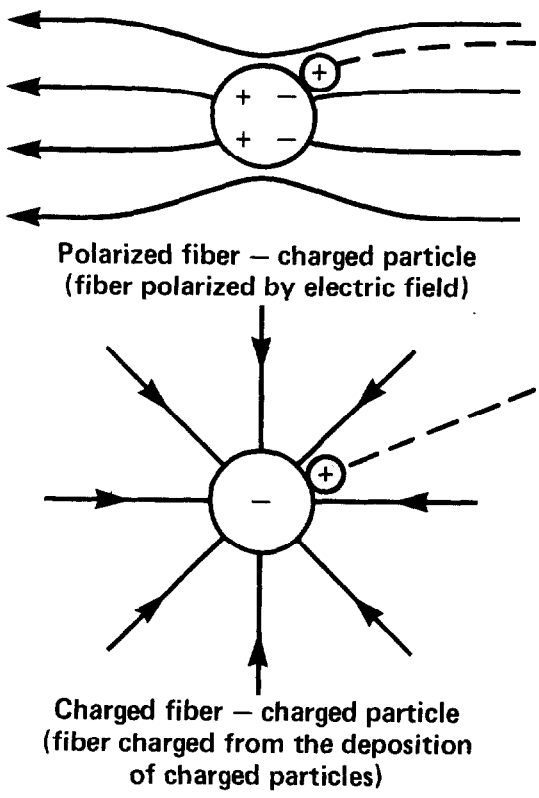

Figure 2

Electrical capture mechanisms responsible for the increased filter efficiency.

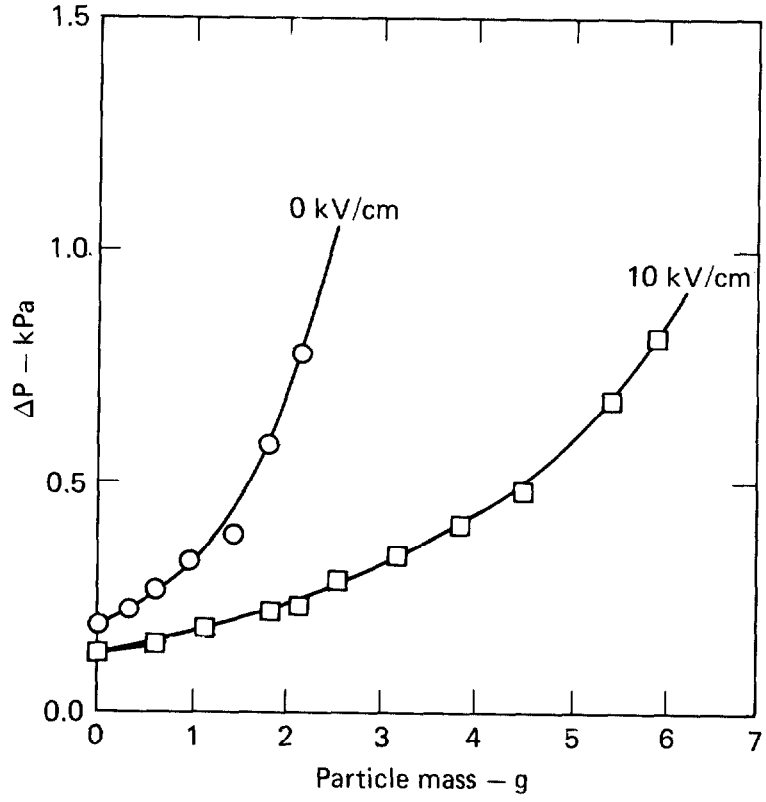

Figure 3

The applied electric field increases the filter service life.

The second characteristic of electrofibrous filters is the increased service life when compared to a conventional fibrous filter. Fig. 3 shows the pressure drop across two similar filters operated with and without an electric field during filter clogging. The filter operating with an applied electric field has a considerable extension in service life compared to the conventional filter. This extension in filter life is due to changes in the particle deposition around individual fibers on a microscopic scale and changes in the particle deposition through the filter bed on a macroscopic scale. Both of the changes in the particle deposition are a direct consequence of the increased collection efficiency of the individual fibers.

The extension in filter life due to the macroscopic change in particle deposits is primarily due to the variation in the fiber packing density within a filter. Lamb et al[11] have shown that the fiber packing density within most filters vary greatly, the outer surface having a much lower density than the interior portion. In the absence of an electric field, the particles penetrate to a region within the filter where the packing density is higher, therefore forming a heavy deposit within the filter volume. This type of deposit is shown schematically in Fig. 4A. However, with an electric field, the particles are

captured by fibers on the front face of the filter, where more particle deposits can be accommodated because the fiber packing density is very low. The increased fiber efficiency due to the electric field is responsible for the enhanced particle collection on the front face of the filter. Fig. 4 shows that the particle deposits on the front face of the filter form a more open structure (Fig. 4B) than the deposits within the filter volume (Fig. 4A).

On a microscopic scale, the effect of the applied electric field is to extend the period in which the particle deposits are in the first stage of filter clogging. Payatakes has characterized filter clogging as a sequential process in which the morphology of particle deposits goes through four major stages[12]. In the first stage particles deposit directly on the fiber and form a random covering of isolated particles. In the second stage, particles deposit preferentially on previously deposited particles and form extended particle chains called dendrites. This stage of filter clogging is illustrated in Fig. 5A where the large and small circles represent the fiber and particle deposits respectively. The dendrites intermesh with neighboring dendrites in the third stage and bridge between neighboring fibers in the fourth and final stage of filter clogging. With a superimposed electric field, the increased collection efficiency results in a more dense and uniform surface coverage during the early stages of filter clogging as shown in Fig. 5B. The electrical forces cause particles to deposit on the downstream side of the fiber and fill in the open spaces on the upstream side that were inaccessible to mechanical capture. Thus for the same quantity of particles trapped on a fiber, the deposits formed due to electrical capture are in stage 1 (Fig. 5B) while the deposits formed due to mechanical capture are in stage 2 (Fig. 5A). The lower air resistance of the deposits in stage 1 accounts for the decreased pressure drop when filters are operated with an electric field.

A B

Figure 4

Schematic of the filter cross section showing the particle deposits (A) without an electric field and (B) with an electric field.

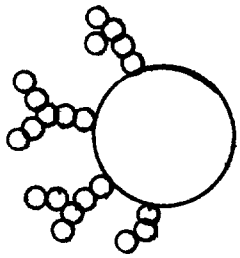

A

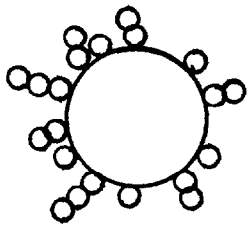

B

Figure 5

Schematic of particle deposits on a fiber (A) without an electric field and (B) with an electric field.

IV. Design Criteria for Prototype Electrofibrous Filters

The design of a prototype electrofibrous filter for nuclear ventilation systems requires making a number of decisions on key filter parameters. The criteria used for making these decisions are summarized in Table I.

Table I. Design criteria for electrofibrous filters

Design parameter	Criterion
Physical dimensions	610 x 610 x 305 mm
Resistance	less than 250 Pa
Face velocity	minimum value
Filter medium	minimum flammability minimum conductivity minimum fiber packing density minimum compressibility minimum water adsorption
High voltage electrodes	maximum open area good structural support for filter medium good electrical contact with medium optimum electric field orientation good insulation from ground high electrical resistance
High voltage power supply	maximum d.c. voltage automatic shut down during overload
Efficiency	maximum value
Dust holding capacity	maximum value
Cost	minimum value
Waste volume	minimum value
Medium replacement	minimum effort
Electrical safety	minimum hazard

We have not been able to assign specific crieria to the different parameters because most of the parameters are interdependent and require and optimization study. For example, decreasing the fiber packing density of the filter medium will increase the dust holding capacity, but will also decrease the filter efficiency and resistance. We plan to conduct this optimization study in the near future using our theoretical models of electrofibrous filters[2,9,10]. Although we have not yet established the optimum design criteria, we were able to select approximate parameter values that would result in a satisfactory filter design, although by no means optimum. The selection of these parameter values was based on choosing a reasonable value for the most important parameters first and then adjusting the remaining parameters according to the criteria in Table I wherever possible.

The starting point for the filter design is the physical dimensions and the maximum resistance of the prototype filter, which we have chosen to be the same as the standard HEPA filter. These dimensions and filter resistance have become an international standard in high efficiency filtration systems. Maintaining the same parameter values would allow the electrofibrous prefilter to be evaluated and used in any existing filter holder for HEPA filters.

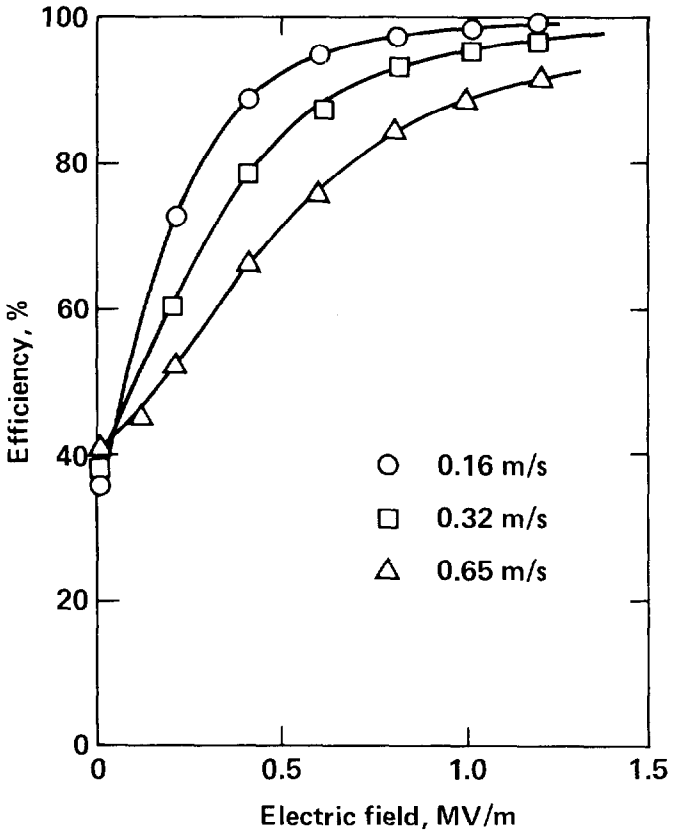

Figure 6

Filter efficiency as a function of electric field for two layers of AF-18 tested at different flow velocities.

After the physical dimensions, the most important design parameter is the filter face velocity, which should have a minimum value. A lower face velocity will decrease the filter resistance and increase the filter efficiency and dust holding capacity. Figure 6 illustrates the increased filter efficiency for electrofibrous filters due to a decreased face velocity. This figure shows the efficiency as a function of the applied electric field for the same filter operated at three different face velocities. A lower face velocity produces a higher filter efficiency because the electrical forces have a longer time to attract particles to the filter fibers. The most common technique for decreasing the face velocity is to increase the filtering area by pleating the filtering element; the number of pleats being governed by the thickness of the filtering element and the ease of replacing the filter medium.

The next important design parameter to be resolved is the selection of a filter medium that meets the criteria listed in Table I. The criterion for a maximum resistance of 250 Pa eliminated the fabric media that is typically used in bag house filters. These filters generally have resistances that greatly exceed our criterion. We, therefore, selected the deep bed fibrous media for our electrofibrous filters. The medium should be nonflammable to avoid potential fires in the ventilation system. It should have a minimum conductivity to prevent short circuiting the high voltage electrodes. A medium with lower conductivity also increases the filter collection efficiency due to the charged fiber mechanism shown in Fig. 2. Filters with high conductivity will not be able to maintain a large fiber charge because the charge will bleed away. Unfortunately real materials do not generally meet both of these criteria. For example, glass fibers are nonflammable but are moderately conductive. In contrast, plastic fibers have very low conductivities, but are flammable.

The criterion for the filter medium to have a minimum fiber packing density was established to increase the filter dust holding capacity. Lamb et al have shown that electrofibrous filters with a low fiber packing density have a significantly lower increase in pressure drop during filter clogging than filters with a high fiber packing density[11]. Unfortunately, this lower pressure drop increase is obtained at the expense of a decreased filter efficiency. This undesirable effect can be minimized by designing a filter medium with a graduated fiber packing density. Most filter media already have a significant gradation in the fiber packing density because of the manufacturing techniques used to make the media. Lamb et al have shown that this gradation is a major factor contributing to the lower pressure drop of

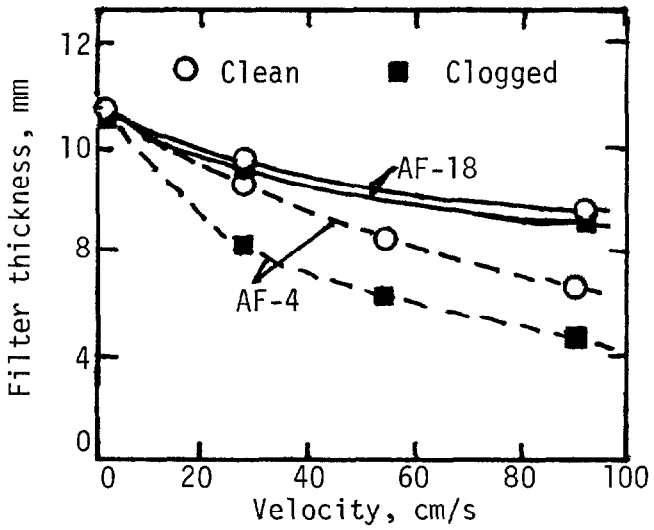

Figure 7

Filter thickness as a function of air flow velocity for clean and clogged AF-4 and AF-18 filters.

electrofibrous filters during filter clogging. However, we believe that far better results can be achieved by designing a filter with the optimum gradation in fiber packing density.

Another property of the filter medium that is closely related to the fiber packing density is the compressibility of the filter mat. Since compressing the filter mat will increase the fiber packing density and consequently the pressure drop, we want to have filter media that has a minimum compressibility. Figure 7 shows the filter compression that occurs due to the air flow through the media. We have plotted the filter thickness as a function of the air velocity for clean and clogged AF-4 and AF-18 filters. We see that the AF-18 medium is only moderately compessed compared to the AF-4 medium. Figure 7 also shows that there is an additional compression due to the particle deposits in clogged filters. Although this additional compression is insignificant for the AF-18 medium, it is very large for the AF-4 medium. The increased compression for the AF-4 medium is due to the smaller diameter fibers that are easier to bend. The AF-4 filter has a median fiber diameter of 0.73 μm while the AF-18 filter has a median fiber diameter of 3.5 μm.

The final criterion listed in Table I for the ideal filter medium is a minimum water adsorption. It is a well established phenomenon that water adsorbed on an insulator will dramatically increase the surface conductivity. For example, the surface conductivity of soda lime glass increases from 10^{-12} to 10^{-7} mhos as the relative humidity increases from 40 to 90%[13]. This increased conductivity will lead to an increased current flow and eventually short circuiting across the high voltage electrodes.

This phenomenon is illustrated in Fig. 8 which shows the filter efficiency and the electrode current as a function of the relative humidity. The data was obtained using an AF-18 medium sandwiched between two electrode screens as shown in Fig. 1. Since sodium chloride aerosols are hygroscopic, we used DOP aerosols generated by nebulizing a solution of DOP in alcohol. Efficiencies were determined using a Sinclair-Phoenix light scattering photometer. Figure 8 shows that the filter efficiency with and without an applied voltage remains constant over the relative humidities tested. Below 70% relative humidity, the electrode current is less than 0.5 μA. However, beyond 80% relative humidity, the current rapidly increases until there is a short circuiting across the electrodes at 90% relative humidity. Since the water adsorption is much less for most plastics than for glass (e.g., polypropylene absorbs about 0.02% water compared to 0.3% for glass), we would expect that electrofibrous filters made from plastic fibers can operate at a much higher relative humidity.

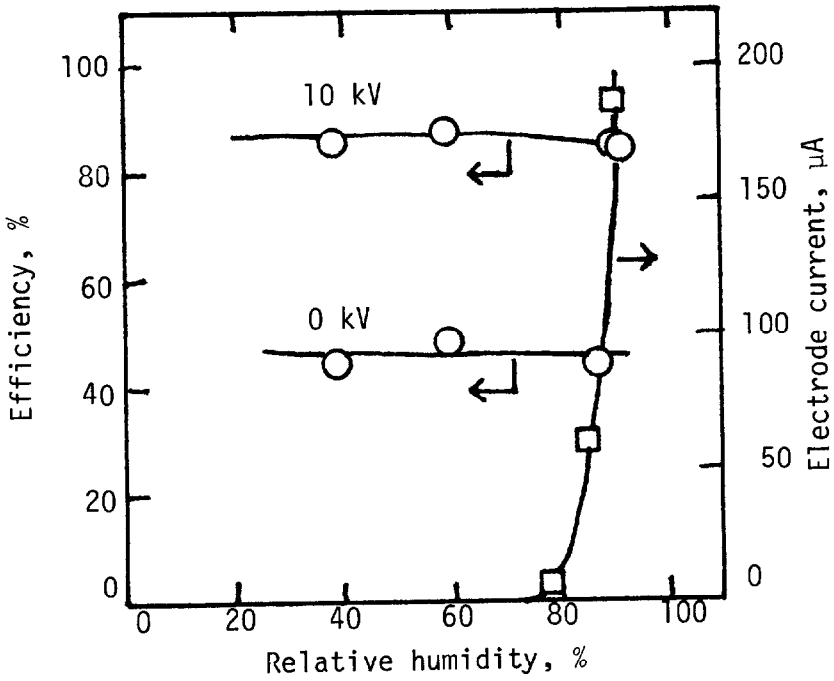

Figure 8

Filter efficiency and electrode current as a function of relative humidity for electrofibrous filter.

Although we have not yet conducted an extensive search of the available media for use in our electrofibrous filters, we have made a tentative selection based on the criteria discussed above. We chose a glass fibrous filter primarily because it is nonflammable and has reasonable values for the conductivity, fiber packing density, compressibility and water adsorption. Moreover, these filters are inexpensive and available in large quantities. The most frequently used medium in our prototype filters is the AF-18 filter obtained from Johns Manville. We have already illustrated typical performance data for the increased efficiency, the increased service life (Fig. 3), the effect of face velocity (Fig. 6), the compressibility (Fig. 7), and the effects of water adsorption (Fig. 8).

Once we have selected the proper filter medium, we must determine the optimum design for the high voltage electrodes based on the criteria in Table I. These electrodes must have a maximum open area to minimize the air resistance and to prevent blinding the filter medium. We found that the front electrode can blind off a major fraction of the filter surface and thereby accelerate the clogging process. To prevent the blinding problem on the front electrode, we selected a wire screen electrode with over 90% open area. Moreover, since the front electrode does not support the filter medium it does not have to have a rigid construction. In contrast, the major criterion for the rear electrode is to provide a good structural support for the filter medium. The rear electrode can have a relatively small open area since it can not blind the filter medium and adds very little resistance. We therefore selected a perforated metal sheet with a 40% open area for our rear electrode.

One of the most important criteria for the design of the high voltage electrodes is a good electrical contact with the filter medium. We have shown that if the filter medium does not have good electrical contact with the electrodes, the electrofibrous filter will have the same performance as a filter with no applied voltage[2,9]. This phenomenon occurs because the fiber charge migrates across the filter bed and accumulates next to the electrodes if they are not in contact with the medium. The accumulated charge creates an electric field within the filter medium that cancels the field produced by the high voltage electrodes. However, if the electrodes are in contact with the medium, the fiber

charge that migrates to the electrodes is neutralized and therefore can not reduce the electric field generated by the electrodes. One of the primary causes for losing electrode contact with the medium is the compression due to air flow as seen in Fig. 7.

The criterion for designing the high voltage electrode for the optimum electric field orientation is not well established. All of our studies have been conducted with the electric field either parallel or anti parallel to the air flow. No change in the filter efficiency was observed with either orientation. We chose to apply high voltage to the rear electrode in our prototype filters to minimize the possibility of particle deposits creating a leak path or even a short circuit between the high voltage and the grounded filter housing. Grounding the front electrode also provides an additional safety feature against accidental short circuits and electric shock hazard.

Lamb et al have performed a series of experiments on the effect of the electric field orientation on the filter efficiency[14]. They concluded that the electric field perpendicular to the air flow produced a much higher filter efficiency than the field parallel or anti parallel to the air flow. Unfortunately the electrodes were not contacting the filter medium in the experiments with the parallel and anti parallel configuration, thereby invalidating the conclusions. The optimum field orientation for the maximum filter efficiency must still be determined.

The criterion for having electrodes with a high electrical resistance was established to minimize the potential for sparking across the electrodes[15]. Sparking across the electrodes is undesirable because of the potential fire hazard and the decreased voltage across the electrodes which decreases the filter efficiency. Thompson et al[15] have shown that the use of high resistance electrodes can significantly reduce the potential for sparking across the electrodes. High resistance electrodes also reduce the probability for accidental short circuits and electric shock hazards. We should also point out that the high resistance electrodes will not reduce the electric field compared to highly conductive electrodes at the same applied voltage. However the high resistance electrodes must have a sufficient conductivity to pass the currents due to the particle charges[2,9].

In our design concept we considered the electrodes to be a permanent part of the filter unit and the filter medium as a disposable element. We should point out that the electrodes can also be fabricated as an integral part of the filter medium. In this case the electrodes and filter medium are discarded as an integral unit when the medium becomes clogged. Including the electrodes as part of the filter medium will increase the cost of the medium but will also reduce the cost and complexity of the filter housing. A variety of different mesh electrodes can be used for this purpose. For example, the glass fiber scrim that is routinely sewn over the glass fiber media in commercial filters can have a conductive coating applied and serve as an electrode[15]. We should emphasize that the criteria listed in Table I for the electrodes also apply for the case where the electrodes are an integral part of the filter medium.

The final component of the electrofibrous filter that must be specified is the high voltage power supply. Our previous studies have shown that much higher filter efficiencies can be obtained using d.c. rather than a.c. voltage[2,9]. The decreased filter efficiency with a.c. voltage is due to the elimination of the charged fiber mechanism (Fig. 2) that results from the periodic reversal of the electric field. The power supply must be capable of delivering the maximum d.c. electric field that can be applied across the filter medium without shorting. The

electric field equals the applied voltage divided by the distance between the electrodes. For the same electric field, the maximum voltage will be low for electrodes closely spaced and high for electrodes spaced far apart. A compromise must be reached between the greater insulation requirements at higher voltage and the increased tolerance required for closely spaced electrodes. We selected 10 mm as the minimum electrode separation that we could maintain at reasonable tolerances. At this separation, sparking occurs across the electrodes at 14-15 kV d.c. with the AF-18 medium.

In addition to the maximum output voltage, we also need the maximum electrode current for selecting the proper power supply. As seen in Fig. 8, the electrode current increases significantly above 80% r.h. until the electrodes short circuit at 90% r.h. Below 70% r.h. the electrode current is less than 0.5 μA. Based on these current and voltage requirements we selected a Spellman miniature d.c. power supply that was rated up to 15 kV at 75 μA. However, to provide for a sufficient safety factor against shorting, we only apply 10 kV to the high voltage electrodes in our prototype filters. We also added an automatic shut-off device to the power supply during overload conditions as an additional safety measure.

The remaining design parameters listed in Table I describe the performance and operating characterisitcs of the electrofibrous filter. The performance characteristics have been fixed by the criteria established for the physical dimensions, face velocity, filter medium, high volage electrodes and the power supply. These component parameters determine the following filter parameters for the prototype electrofibrous filter: efficiency, dust holding capacity, cost, and waste volume. The success of the electrofibrous prefilter in meeting its objective to reduce the filtration cost and volume of radioactive waste depends on these filter parameters. Although the addition of a prefilter will generally extend the life of the HEPA filter, it does not guarantee an overall reduction in the filter cost or the volume of radioactive waste. The added cost and waste due to the prefilter may offset the savings made in the HEPA filter.

The design parameters that we discussed so far have all dealt with the performance of the electrofibrous filter. Although designing the filter to meet the performance criteria in Table I is a necessary condition, it is not sufficient for a widespread use in nuclear ventilation systems. In addition to good performance, the electrofibrous filter must be easy to operate and maintain by maintenance personnel. Table I lists two if these operational and maintenance items. The filter medium must be easy to replace and the high voltage must not create a hazard to either plant operation or personnel. The filter design must be capable of maintaining the design performance in a plant environment with minimum maintenance. A more detailed evaluation of the practical operation of these electrofibrous filters must await our field evaluations.

V. Stationary Electrofibrous Prefilter

We have designed several prototype filters for use in nuclear ventilation systems based in the design criteria listed in Table I. Our first attempt at creating a pleated electrofibrous prefilter is shown in Fig. 9. This unit consists of two continous, pleated electrodes with the AF-18 medium sandwiched between. The continuous pleats are readily seen in Fig. 9 where the side panel has been removed. The front electrode is a stainless steel screen with 70% open area while the rear electrode is a perforated aluminum sheet with 40% open area. As shown in Fig. 9, three insultated spacer bars (one in the center and one at both ends) provide the necessary structural support to maintain the shape of the front electrode. Without this support, the electrode would behave like a spring and pop out of the housing. Three additional insulated spacer bars (not shown)

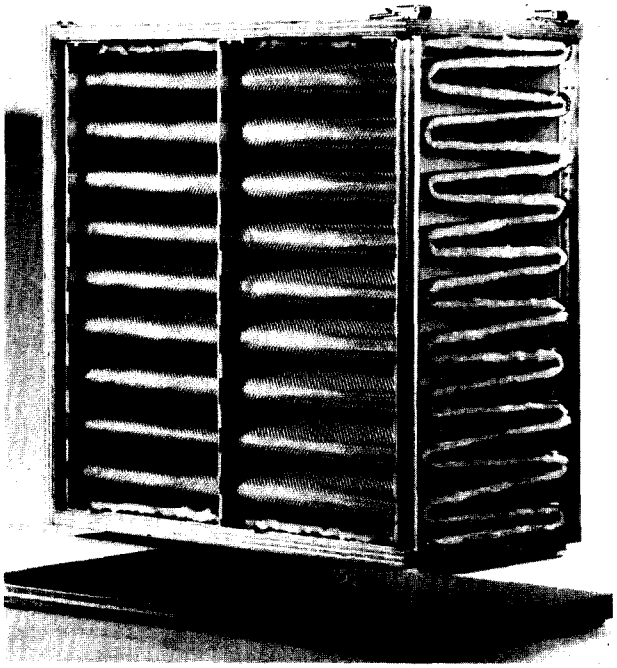

Figure 9

Stationary electrofibrous prefilter with the side panel removed to show the continuous pleated design.

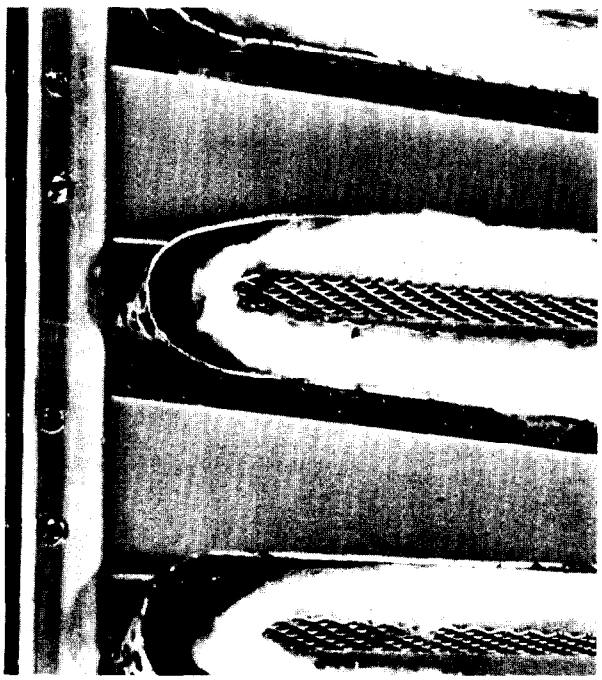

Figure 10

Enlarged view of the pleated filter element.

were used in a similar fashion to maintain the shape of the rear electrode. Pushing in the spacer bars would press the electrodes together and make a good contact with the filter medium. A 10 mm separation was maintained between the front and rear electrodes by three strips of rubber that were attached to the rear electrode.

The major difficulty in this design is maintaining the proper distance between the two electrodes to prevent sparking. This problem is illustrated in Fig. 10 which shows an enlarged view of the filter element. Both of the electrodes would distort and buckle as the unit was assembled. Although we tried a number of different schemes to maintain the proper electrode spacing, we were only able to apply 6kV before sparking occurred.

Another problem with the design is the difficulty in replacing the filter medium. To remove the filter medium, we have to first remove both side panels, take out the three spacer bars, gently pull out the front electrode and finally pull out the medium. It is very difficult to pull out the front electrode because the screen tends to expand like a spring. The rear electrode is permanently fastened to the housing. Inserting a new filter medium requires the reverse of these steps, although the process is more difficult. The filter medium first has to be carefully tucked into all of the deep pleats. Inserting the front electrode screen is especially difficult because the screen does not maintain its form and tends to behave like an accordian. The filter medium would frequently tear in this step. The entire process for replacing the filter medium takes up to four hours. After struggling with minor design improvements to reduce the sparking problem and make the media replacement easier, we finally abandoned the design.

We then designed a new stationary electrofibrous prefilter that eliminated the two major problems encountered with our first design. The problem with the medium replacement was significantly reduced by decreasing the number of pleats from nine to six. Although this increased the face velocity from 0.21 m/s to 0.32 m/s, the velocity was sufficiently low to provide a good electrical enhancement of the filter efficiency. The second change in the design was to replace the continuous sheet electrodes with individual "V" sections for both the high voltage and ground electrodes. The use of modular components for the electrodes provided the dimensional stability and close tolerances that were not achieved in our first prototype. Figure 11 shows three of these modular "V" sections. The center section is a modular unit of the high voltage electrode and the outer two sections are modular units of the ground electrode. Each modular unit is fabricated from flat sheets that are bent into "V" sections. The ground and high voltage electrodes were fabricated from stainless steel screen and perforated aluminum sheets respectively. These modular units were structurally strong at the bends. Additional strength was given to the "V" sections by welding angles on the screen edges and bending angles on the edges of the perforated metal. The proper angle of the "V" was maintained on the ground electrode by welding a triangular plate on both ends of the unit. A Plexiglas plate was used to maintain the proper angle on the high voltage electrode and to provide electrical insulation from the ground electrode and the filter housing. The Plexiglas plates also serve as spacers to maintain the desired electrode spacing and to provide a seal for the filter medium.

The electrofibrous filter was then assembled by mounting the modular high voltage units in the filter housing as shown in Fig. 12. The high voltage units were attached to the housing with bolts through the Plexiglas plates. This provides a strong support for the electrodes while maintaining a good insulation. The high voltage electrodes were fastened together at the rear to provide strength and good electrical contact between the segments. A high voltage cable connector was welded on one of the reinforcing "V" plates. The ground screen segments were then welded together in a supporting frame and two handles added to form the front ground electrode. The completed electrified filter unit is shown in Fig. 13 with the ground electrode partially removed from the housing.

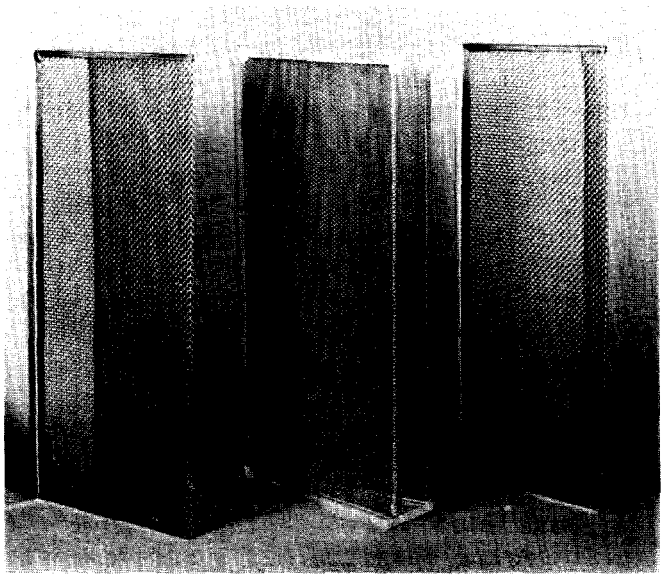

Figure 11

Modular segments of the high voltage and ground electrodes.

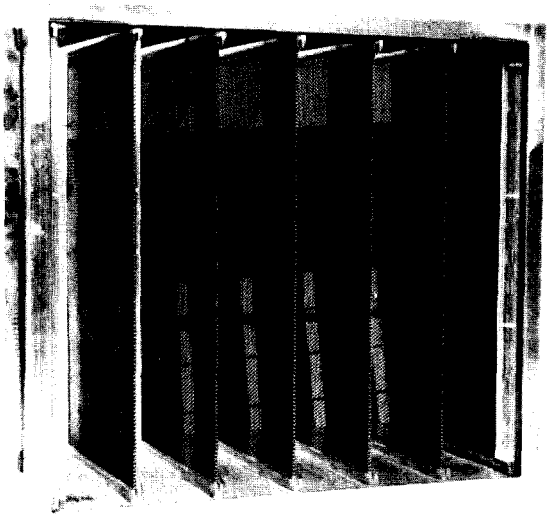

Figure 12

Stationary electrofibrous prefilter showing the modular high voltage electrode installed in the filter housing.

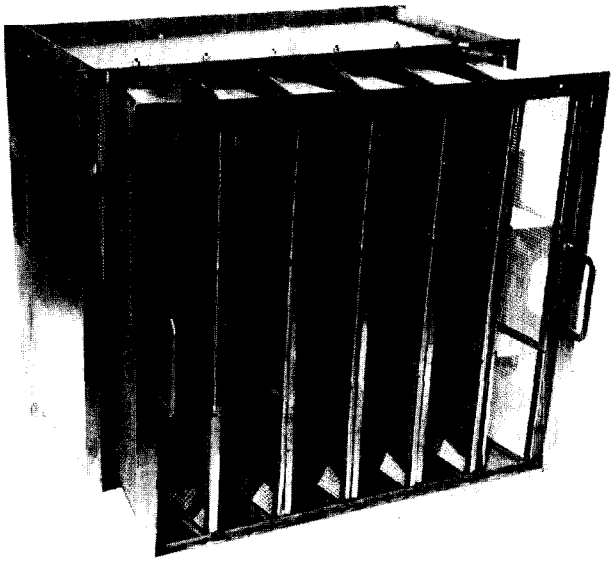

Figure 13

Stationary electrofibrous prefilter showing the modular ground electrode partially removed from the filter housing.

We then evaluated the stationary electrofibrous prefilter having the modular electrode design in our large scale filter test facility. This facility[2] houses a 610 X 610 mm ventilation test duct that was designed according to the ASHRAE Standard 52-68[16]. The facility also has various aerosol generators and instruments for measuring air flow, filter pressure drop and aerosol concentration. We planned an evaluation program to establish experimental values for the efficiency, dust holding capacity, cost and waste volume under contolled laboratory conditions. As previously discussed, these values are necessary to determine the cost benefit of the electrofibrous prefilter in reducing the cost and radioactive waste in nuclear ventilation systems. So far we have only measured the filter efficiency as a function of applied voltage at $0.47 m^3/s$ (1000 cfm) using sodium chloride aerosols (MMAD = 1.0μm and σ_g = 2.0)

Figure 14 shows the efficiency as a function of applied voltage for the stationary electrofibrous prefilter using three different grades of filter media. The filter media differ primarily in the fiber diameter which decreases in sequence for the AF-18, AF-4 and AF-3 media. It is well established that filter media with smaller fiber diameters have higher efficiencies and pressure drops than media with larger fiber diameters[6]. This accounts for the increase in pressure drop and zero voltage efficiency for the sequence AF-18, AF-4 and AF-3. As 10kV is applied to the high voltage electrode, the filter efficiency increases from 38.1 to 90.1% for the AF-18 medium, from 85.0 to 97.7% for the AF-4 medium and from 95.4 to 97.9% for the AF-3 medium. The corresponding pressure drops for the AF-18, AF-4 and AF-3 media are 60Pa, 229 Pa and 431 Pa respectively. Based on our maximum resistance criterion of 250 Pa, the AF-3 medium cannot be used in our prototype filter.

The final selection of the filter medium will depend on the results of our filter optimization and cost-benefit studies. An important parameter in both of these studies is the dust holding capacity for different filter media under various operating conditions. We plan to conduct a series of filter clogging experiments using sodium chloride aerosols and ASHRAE dust to determine this information. Once we have satisfactory laboratory results with the stationary electrofibrous prefilter, we will then install a unit in a nuclear ventilation system and conduct a field evaluation.

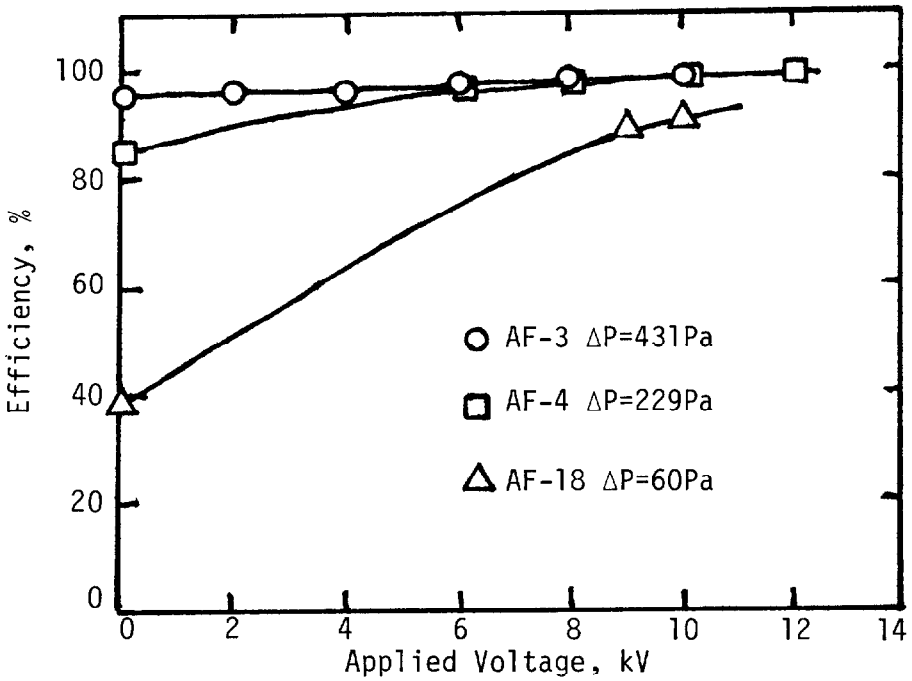

Figure 14

Filter efficiency of the stationary electrofibrous prefilter as a function of the applied voltage for AF-3, AF-4 and AF-18 media.

VI. Rolling Electrofibrous Prefilter

One of the most serious accidents that can occur in a nuclear facility is a fire. A critical factor that increases the severity of a fire is the potential loss of the ventilation system due to the plugging of HEPA filters by smoke aerosols. A recent report by Alvares et al summarizes the results of a ten year study to develop countermeasures to protect HEPA filters from heat and smoke generated by fire[7]. They identified the following three countermeasures to mitigate the problem:

1) materials management to reduce the quantity of combustible materials,
2) conventional fire detection and fire suppression techniques,
3) Smoke removal or treatment in the ventilation duct upstream of the HEPA filter.

Alvares et al concluded that facilities having a moderate quantity of combustible material and conventional fire management systems would be adequate to prevent the plugging of HEPA filters during potential fires. They also concluded that an in-duct countermeasure is necessary in facilities having a high fire risk.

We became interested in the smoke problem as an extension of our program to develop electrofibrous prefilters for prolonging the life of HEPA filters. Although we were primarily concerned with protecting the HEPA filter from the aerosols generated during normal operations, we could not ignore the problem of smoke aerosols plugging the HEPA filter. Since our program was just beginning a hardware development phase in 1978, we initiated a joint program with Alvares and his collegues to develop a prefiltration system that had the potential for effectively removing normal production aerosols as well as fire generated smoke aerosols. The difficulty of the task had been well established in various attempts to remove the smoke aerosols. Among the various methods examined were wet scrubbers, afterburners, granular beds and prefilters[17]. Although efficient prefilters appeared to stop the smoke aerosols, they were also rapidly plugged. Because of the tar like property of the smoke aerosols, cleanable prefilters, like those used in bag houses, would not offer any benefit. Once the smoke aerosol deposited on a filter, the particle deposit could not be removed.

Rolling Prefilter Design Established to Meet Fire Criterion

It became very obvious that any prefiltration technique for removing smoke aerosols would require some means for automatically replacing the prefilter once it had plugged. Two general approaches can be taken for replacing the plugged filter; replacing individual filter units in a batch process or replacing the filter medium in a continuous process. Since the filter industry had nothing available for replacing individual filter units but had an extensive selection of rolling filters, we selected the rolling prefilter (RPF) concept for further development. Two preliminary experiments were conducted to examine the feasibility of the concept. Gaskill et al had previously evaluated the RPF concept using three layers of cheese cloth that were pulled across the ventilation duct with a hand crank[18]. Although the smoke concentration was very low, the test demonstrated the cycle of increasing and decreasing pressure drop across the prefilter as the medium would be periodically advanced. Alvares et al conducted a more stringent evaluation using an automated RPF that was rented from the Andersen Corporation[19]. This evaluation confirmed that the RPF concept was capable of protecting the HEPA filter from extreme smoke concentrations. Unfortunately, using the Andersen unit as a prefilter to HEPA filters would require the installation of high pressure blowers and associated hardware, and therefore was not considered practical for use in nuclear ventilation systems.

Our objective was to establish the feasibility of a RPF that could operate in nuclear ventilation systems with a low pressure drop and still protect the HEPA filter from plugging due to smoke aerosols. Since there were no commercial RPFs that had the required high efficiency and low pressure drop, our strategy was to modify the filter housing and filter media of commercial units until the desired results were obtained. The modifications made to the filter housing consisted of removing sharp edges that could tear the filter media, sealing minor leak paths in the reservoirs holding the filter supply and take-up spools, adding an additional rear screen to support the filter medium and extending the blinders used to prevent edge leakage(17). Figure 15 shows the inlet side of the rolling filter purchased from American Air Filter after these modifications were made for our evaluation.

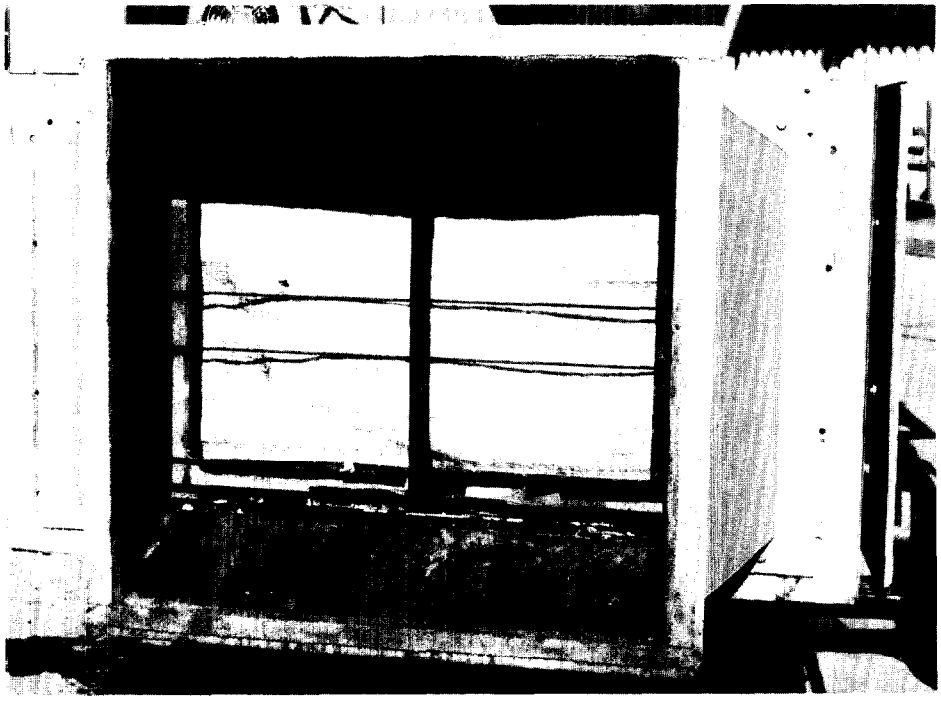

Figure 15

Commercial rolling prefilter (RPF) modified for high efficiency.

The filter medium supplied with the RPF has a very low efficiency, but can tolerate the tension stresses caused by the pulling force of the take-up reel. This medium also has a very low pressure drop due to the large diameter glass fibers and the low fiber packing density. Another important property of this medium is its low compressibility and spring-like behavior. Although the RPF medium is not flammable, the glass fibers have been coated with an oil that will burn on ignition. The modifications made to increase the efficiency of this medium were extremely simple. We added one or more layers of a more efficient filter medium on top of the RPF medium to yield a laminated system. Figure 16 shows a laminated system composed of the following media sequence from bottom to top: a 50 mm layer of the RPF medium, a 6.4 mm layer of AF-4 medium and a 6.4 mm layer of AF-18 medium. The RPF medium is a critical component of the laminated structure because it provides the necessary tensile strength for pulling the media through the filter housing and also maintains a positive seal for the more efficient media against the blinders in preventing edge leakage. We later discovered that the RPF medium also prevents the more efficient media from sticking to the rear supporting screen and tearing the media.

We then conducted a series of experiments with the RPF shown in Fig. 15 using various combinations of high efficiency media placed on top of the RPF medium. Each experiment consisted of generating a reproducible fire in the LLNL fire test cell and exhausting the smoke through a ventilation duct that contained the RPF and HEPA filter. Details of the fire test facility and experimental procedure were given in previous publications[17,19]. The primary information obtained from these experiments was the effectiveness of the RPF to prevent smoke aerosols from plugging the HEPA filter. The test results were compared on the basis of the time required for the HEPA filters to plug. Figure 17 shows the pressure drop across the HEPA filter as a function of the burn time for each of six different experiments. A comparison of tests 1-4 suggest that the RPF made little difference in protecting the HEPA filter, although the efficiency of the laminated filter media had steadily increased in the sequence of tests 2-4.

We then increased the efficiency of the laminated media another increment by replacing one of the AF-18 media with the higher efficiency AF-4 media. Test number 5 indicates that this combination of filter media is very effective in protecting the HEPA filter from smoke aerosols. The HEPA filter plugged at 1300 seconds because we had run out of prefilter media and the HEPA filter was directly exposed to smoke aerosols. We were only able to insert 9 m of media on the supply reel because of the limited space in the modified RPF. We then modified the

Figure 16

Laminated filter media used in RPF.

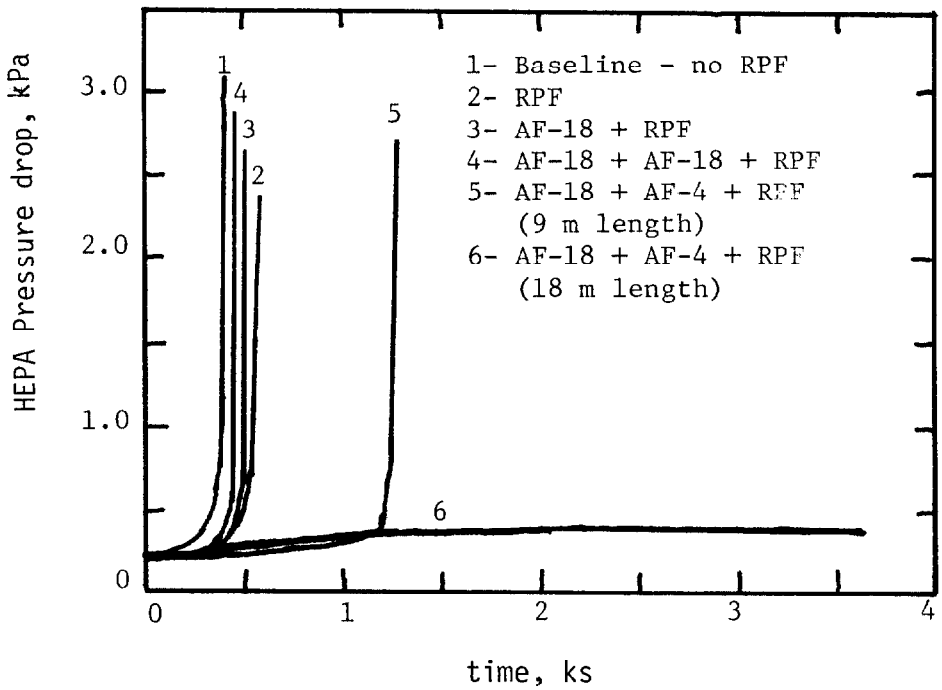

Figure 17

Effect of filter media on the RPF's ability to protect the HEPA filter from plugging by smoke aerosols.

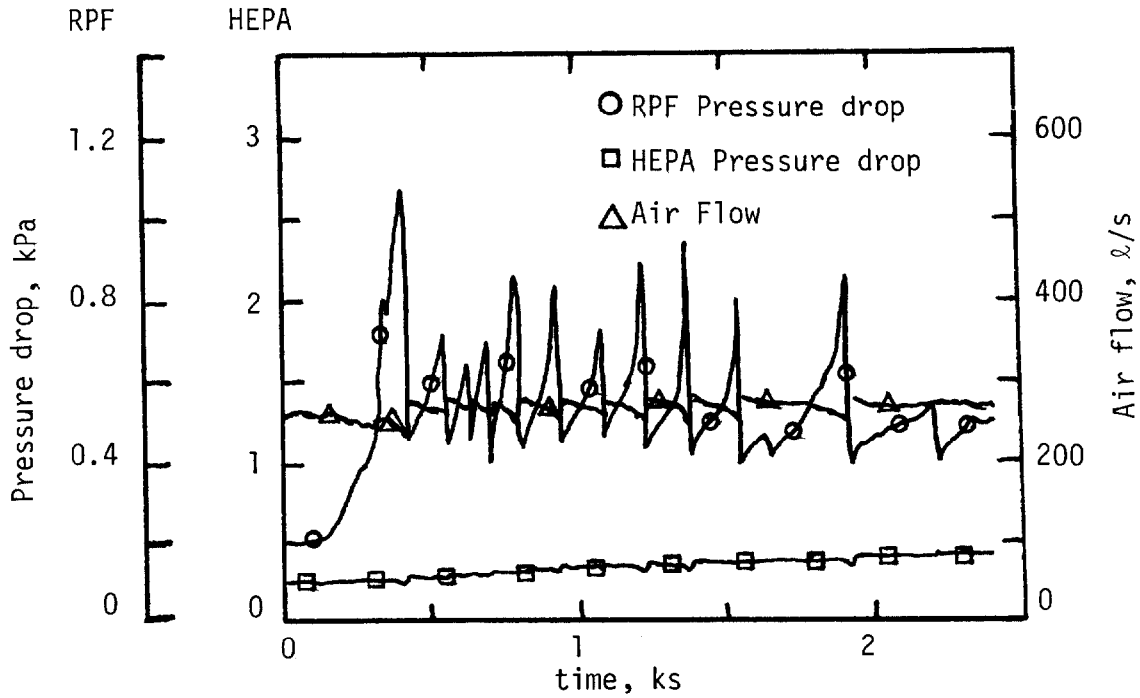

Figure 18 Operating parameters for the RPF-HEPA filter system as a function of exposure time to smoke aerosols.

supply spool so that it could accommodate 18 m of laminated media. The results, shown as test number 6, indicate that the RPF is able to protect the HEPA filter from plugging for the duration of a fire. The fire had self extinguished and was reduced to a smoldering condition at 3600 seconds, at which time we terminated the test. During this test we had used 12 m of prefilter media and the pressure drop across the HEPA filter increased from

250 Pa to 400 Pa. A more extensive analysis of experiment number 6 is shown in Fig. 18. This figure shows the pressure drop across the HEPA filter and prefilter and the total air flow rate during the first 2400 seconds of the burn. The oscillations in the pressure drop across the prefilter are due to repeated cycles of filter plugging and filter advancement. Note that the pressure fluctuations across the prefilter are also reflected in the flow rate and the pressure drop across the HEPA filter.

Although we have shown that the single pass RPF is an effective means for protecting HEPA filters from smoke aerosols, its exclusive use as an emergency fire protection device is not cost effective. However, if the RPF were designed to also function as a prefilter to extend the life of HEPA filters under normal operating conditions, then the RPF would become a cost effective device. The only difference between normal and emergency operations would be the indexing frequency of the prefilter media, which is controlled by its pressure differential.

Unfortunately, the single pass design of the RPF cannot be used for a conventional prefilter that operates under normal conditions because of the excessive pressure drop that would be encountered. For example, the initial pressure drop across the RPF that was used to generate the data in Fig. 18 is 200 Pa at 260 ℓ/s. However, since standard ventilation ducts have flow rates of 472 ℓ/s (100cfm), the corresponding pressure drop for the RPF would be 363 Pa. A prefilter with such a high pressure drop would not be acceptable in the nuclear industry. The conventional method for reducing the pressure drop is to increase the filter surface area by pleating the medium. We were therefore led to the concept of a pleated rolling prefilter. In keeping with our terminology for the single pass RPF, we shall designate this pleated filter a multi-pass RPF.

However, before proceeding with the development of the multi-pass RPF, we must establish that it can also protect HEPA filters from smoke aerosols. Although we have already established this fact for the single pass RPF, the lower face velocity in the multi-pass RPF may result in a lower efficiency. We therefore evaluated the single pass RPF at a face velocity that is comparable to that in a multi-pass RPF. Figure 19 shows the results of this evaluation that was conducted at 47 ℓ/s (100 cfm). This flow rate corresponds to a face velocity of 20 cm/s through the RPF. Figure 19 shows the pressure drop across the HEPA filter as a function of the time exposed to smoke aerosols. The baseline test with no RPF shows that the HEPA filter plugs at approximately the same time as seen in Fig. 17 for the higher flow. We then installed the RPF with the laminated media consisting of AF-18, AF-4 and the RPF medium. Figure 19 shows that the RPF was very effective in protecting the HEPA filter from plugging up to 2300 seconds into the burn. At this time, we removed the filter media from the

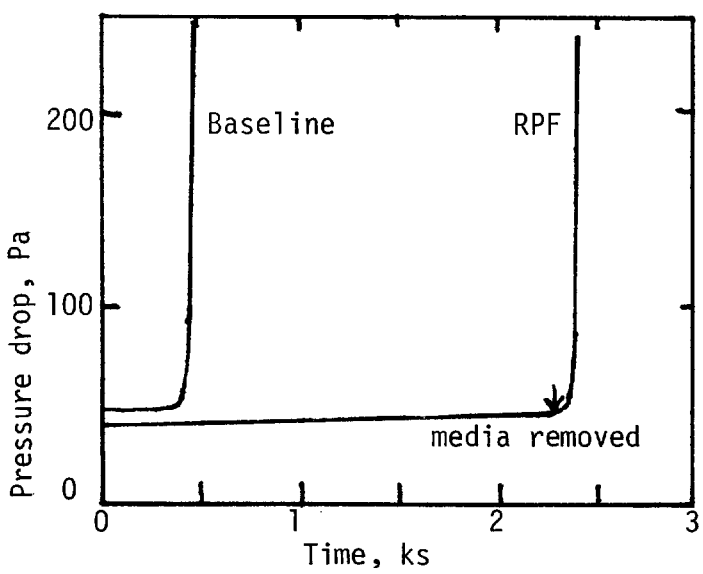

Figure 19. Pressure drop across the HEPA filter at a reduced flow as a function of exposure time to smoke aerosols with and without a RPF.

RPF, thereby exposing the HEPA filter directly to the smoke aerosols. The rapid plugging of the HEPA filter at this time confirms that the RPF is also very effective at low face velocities. These tests demonstrate that the multi-pass RPF should also be very effective in protecting HEPA filters from smoke aerosols.

Development of the Rolling Electrofibrous Prefilter

We have already stated that the development of a multi-pass RPF that operates under normal conditions as an ordinary prefilter and under fire emergency conditions as a fire protection device is cost effective. However, since the probability of having a fire is very low, the multi-pass RPF would function primarily as a stationary prefilter. From an operational point of view, the RPF would reduce maintenance costs assocated with replacing stationary prefilters, but would also have a lower performance, require more space, and cost more than our stationary electrofibrous prefilter. Converting the RPF to electrostatic operation would make the RPF performance comparable to the stationary electrofibrous prefilter without requiring a significant increase in space requirements or cost. The application of the electrofibrous RPF in a nuclear ventilation system would have to be determined on the basis of a cost-benefit study and a risk analyses of the fire hazard. For applications where the maintenance cost is very high, the RPF would be justified in a cost benefit study even if the fire risk is very low. In this case, the savings in maintenance costs will offset the capital cost of the RPF. The RPF would also be justified in ventilation systems that have high fire risks even though the maintenance costs are very low. However, if a given ventilation system has a low maintenance cost and a low fire risk, then the use of a RPF would not be justified.

Our approach for developing an electrofibrous RPF is to begin with the simplest design and increase the complexity as required. The starting point in our design was the single pass RPF that was successful in protecting HEPA filters from smoke aerosols. The key design feature of the single pass RPF that was used in our first prototype was pulling the filter medium over a fixed supporting screen. The pulling force was provided by the take up reel which was powered by an electric motor. However, four other design features of the single pass RPF were changed in building the electrofibrous RPF shown in Fig. 20. The most dramatic change was replacing the single pass design with a pleated design to reduce the face velocity. Instead of a single supporting screen across the duct opening, our prototype filter had four screen segments that were connected to form two V-shaped pleats. These screen segments would serve as the high voltage electrode. We also had to add a mating ground electrode.

We also replaced the thick, laminated filter media shown in Fig. 16 with a thinner media of equal efficiency. This change was required to provide a strong electric field without the need for excessively high voltatges. The compromise between filter thickness and high voltage requirements was previously discussed in Section IV of this report. We were able to reduce the filter thickness by eliminating the coarse RPF mdium without affecting the filter efficiency. However, in order to make up for the last tensile strength of the RPF medium, we had to sew a layer of scrim material over the two remaining filter layers. The scrim material is a very thin cloth that is commonly used in the filter industry to add strength to fibrous bag filters. Unfortunately, the strength of the reinforced media is still not comparable to the RPF media.

The final change in the electrofibrous RPF in Fig. 20 was the edge sealing mechanism. The seal is provided by the top and bottom edges of the high voltage and ground electrodes that compress the filter medium. The compressed filter

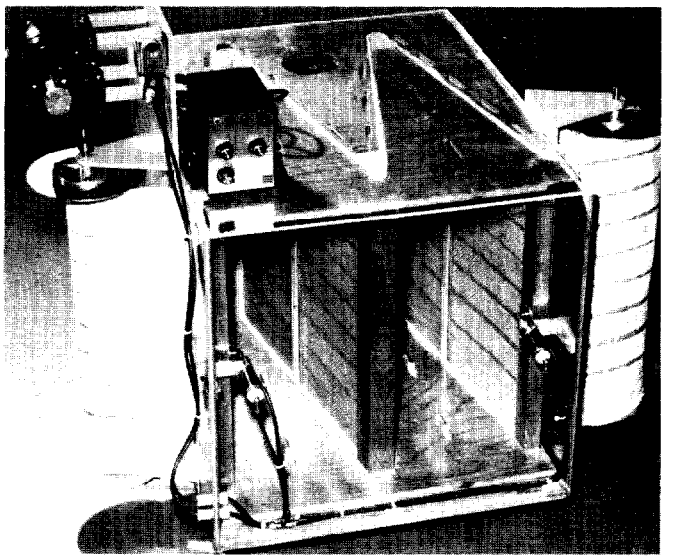

Figure 20

Rolling electrofibrous prefilter having stationary, pleated electrodes.

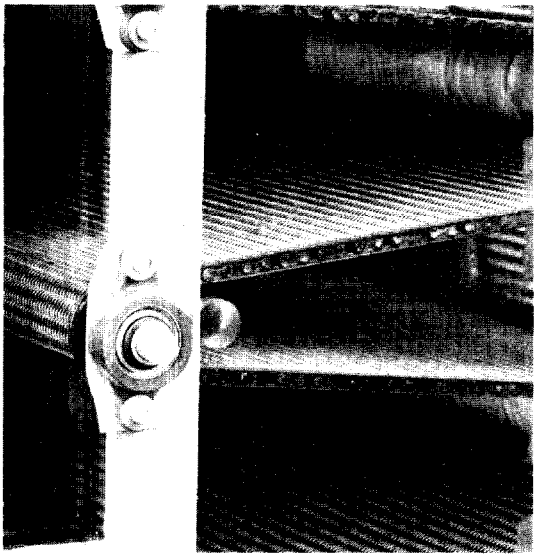

Figure 21

Prototype of the screen belting that serves as the high voltage electrode in the rolling electrofibrous prefilter.

medium can be seen through the Plexiglas top in Fig. 20. When the filter medium is advanced, hydraulic valves pull open the ground electrodes and release the filter medium.

We installed the electrofibrous RPF shown in Fig. 20 in our large-scale filter test facility and soon discovered that the design would not be practical. Although we were able to pull the medium over the pleated electrodes with no air flow, this was not possible at 472 ℓ/s (1000 cfm). The air flow had pressed the medium firmly against the rear electrode and created an excessive drag. This drag would not allow the medium to be pulled through the zig-zag path without tearing. Our attempts at reducing the drag by adding rollers at each pleat were not successful. We also considered replacing the scrim material with a stronger fabric but abandoned this idea when we realized the drag would be several times greater with a clogged media than what we encountered with a clean media. We concluded that the concept of pulling the filter medium over a stationary, pleated screen was not practical because of the excessive drag on the medium.

Our next design of the electrofibrous RPF took advantage of the high drag between the filter medium and the rear screen. The key feature in this design is a continuous screen belt that provides support for the filter medium. The filter medium would ride on the electrode belt and be advanced through the filter housing as the belt was advanced. Figure 21 illustrates the continuous belt that is used in forming the pleated rear screen. Holes were cut in the side panel of the RPF to show the continuous screen belt. The stainless steel belt consists of a wire mesh knitted over supporting rods that connect to a chain at both edges of the belt. Motor driven sprockets are connected to each chain and drive the belt around its path. Additional sprockets are used to provide pivotal points for changes in the belt direction. All of the sprockets are supported by shafts through the filter housing. The shafts penetrate the RPF housing and are supported on the outside panel by bearings.

The design of the electrofibrous RPF is complicated by applying high voltage to the screen belting. Special precautions are required to insure adequate insulation for the high voltage belt. The screen belting is insulated from the RPF housing by sheets of polyethylene or polycarbonate with specially cut grooves for supporting the belt chain. In addition to the screen insulation, all connections to the screen belting, like the sprocket shafts, are made from nonconductive material. We initially had a problem with the chain becoming jammed in the insulation plate. This occurred at the entrance of the grooved track after the chain was released from the sprocket. This problem was caused by the chain failing to pull away from the sprocket, thereby creating a kink in the chain as it entered the grooved track. The solution to this problem was to recess the groove to a sufficient distance from the sprocket to allow the chain to straighten out.

The completed electrofibrous RPF is shown in Fig. 22 with a roll of AF-18 medium threaded through the unit. The front ground electrode is not installed in this unit because we first wanted to demonstrate the RPF's ability to protect HEPA filters from smoke aerosols. Since we assumed that the high acid and water content of the smoke would short circuit the electrodes as seen in Fig. 8, all of our fire tests were conducted without the ground electrode. However, once the fire tests are completed, we will evaluate a fixed and retractable design and then select the optimum electrode design.

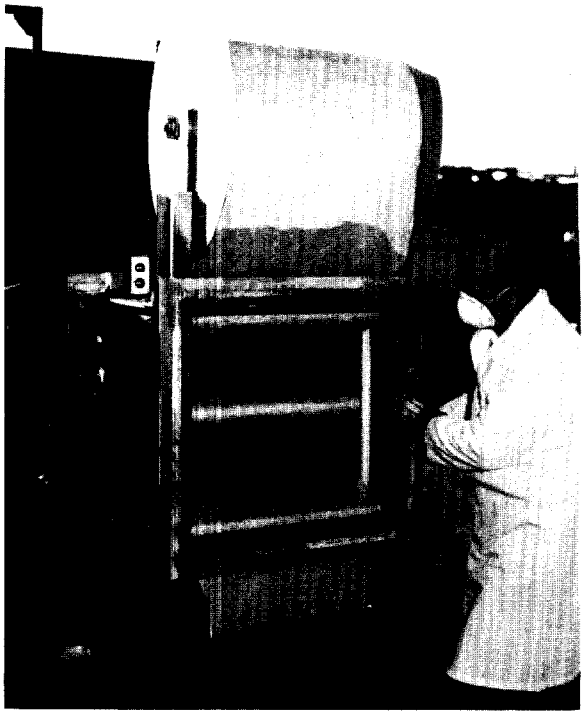

Figure 22

Rolling electrofibrous prefilter having a moving belt electrode.

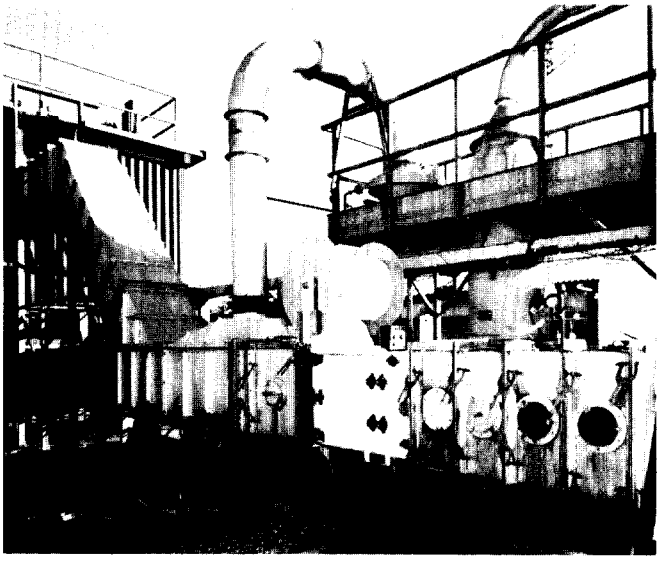

Figure 23

Rolling electrofibrous prefilter installed in the ventilation system of LLNL's fire test facility.

We then conducted a series of fire tests to evaluate the ability of the RPF to protect HEPA filters from smoke aerosols. Figure 23 shows the RPF installed in the ventilation system of LLNL's fire test facility. Reproducible fires are generated in the fire test cell which is shown on the left side of Fig. 23. The smoke from the fire test cell is exhausted through the ventilation duct and is filtered first by the RPF and then by the HEPA filter, not shown in Fig. 23. We have conducted many fire tests on the RPF that is shown in Fig. 22, but have not been able to duplicate the successful results achieved with the single pass RPF. The strategy used in our evaluation program was to identify the causes of the test failures, make the appropriate modifications to correct the problems and then evaluate the effectiveness of the modifications. This cycle would be repeated until all the problems were either eliminated or mitigated and a successful fire test was obtained. The modifications made to the RPF were generally dictated by test results obtained in our small-scale laboratory experiments using sodium chloride aerosols.

We began our evaluation with a series of fire tests using a single layer of AF-4 medium that was 13 mm thick and had reinforcing scrim or netting on both sides. Laboratory tests with sodium chloride aerosols indicated that this medium should be at least 85% efficient. The filter medium was cut extra wide so that the edges would press against the filter housing, thereby preventing excessive edge leakage. No other edge sealing mechanism was used in these initial tests. Although the RPF functioned very smoothly in these tests, the HEPA filter was plugged in nearly the same time as in the baseline tets with no RPF. We believed that the primary cause of the poor results was the inadequate efficiency of the filter media. We increased the filter efficiency by using two layers of filter media instead of one. Various combinations of AF-18, AF-4 and AF-3 filter media were used, but without success. During this phase of our evaluation, several tests were prematurely terminated because the drive mechanism could not advance the screen belting. The problem was caused by the failure of the screen belting to support the more efficient media during filter clogging. At increasing pressure drop, the screen belt was slightly deflected, and, occasionally, one of the supporting rods would pull out from the chain links. The chain link would then be free to move and would become jammed in the insulating track. This problem was corrected by welding the supporting rods to the chain links.

Another problem that developed with the use of two layers of high efficiency media was an increased tendency for the media to stick to the screen belting. The increased sticking tendency was due to the increased pressure drop pushing the filter media firmly against the screen. This is an undesirable condition since the filter media would either tear as it was pulled away from the screen or jam between the screen and the filter housing. One source of the sticking problem was due to the standard industry practice of using an adhesive when sewing the scrim material on the filter medium for added strength. When exposed to the higher temperatures encountered during a fire, the adhesive would melt and bind the filte medium to the screen. The filter medium consequently tore when it was pulled away from the screen at the exit of the RPF. We corrected this problem by specifying that no adhesives be used when sewing the scrim material on the filter media. The other source of the sticking problem was due to the smoke aerosols. At the high pressure drop, the filter medium would compress as shown in Fig. 9. The liquid smoke aerosols would then tend to saturate the filter rather than covering the filter surface. A good analogy would be pouring the same quantity of water over a compressed and an uncompressed sponge. The solution to this sticking problem is to have the high efficiency and easily compressed filter media be separated frm the screen by a filter layer that will not stick to the screen belting. The thick RPF medium (Fig. 19) provided this function for our feasibility demonstration. We also demonstrated that a cloth media would function just as well.

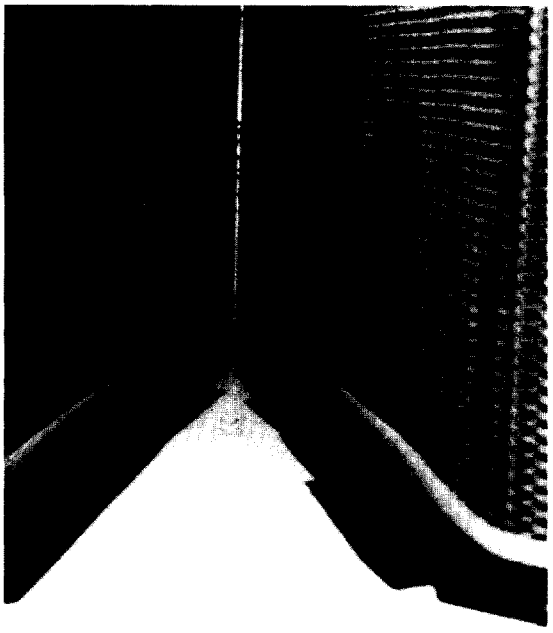

Figure 24. Experimental deflection plates used to reduce the leak paths around the filter edges.

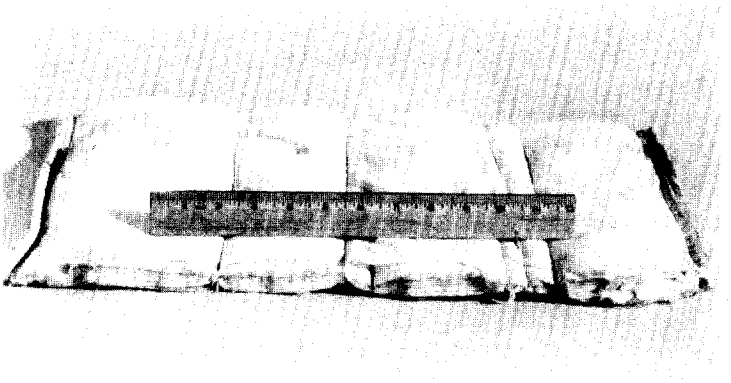

Figure 25. Filter media reinforced with a cloth envelope.

The most serious problem that we encountered during our evaluation was reducing the leak paths around the filter edges. Our initial tests with one and two layers of filter media were made with the media butted against the RPF walls. Although we recognized that we had edge leakage with this arrangement, we did not realize the extent of the leakage. We conducted a series of tests in which we visually examined these leaks using thermally generated DOP aerosols. These tests showed that nearly all of the aerosol penetration was due to edge leakage, especially around the curved portions of the filter path. Our first attempt at preventing edge leakage was to attach an angle shaped deflection plate adjacent to the screen belt. One edge of the angle would be fastened to the wall of the filter housing and the other edge would be adjacent to but not connected to the screen belting. This configuration allows the screen belting to move unobstructed behind a stationary deflection plate. Figure 24 shows the deflection plate that was quickly fabricated from polyethylene strips and tape to evaluate the leak performance. This concept has the advantage of having the air flow press the filter medium against the sealing surface. DOP tests showed that this concept made an improvement in the edge leakage but did not stop it. The deflection plate shown in Fig. 24 was not very effective because the air flow does not press the filter medium firmly against the seal at the standard flow rate. Other tests showed that better results were obtained with a sealing mechanism that slightly compresses the media.

Based on these exploratory tests, we installed deflection plates, 35 mm thick, to provide a seal around the perimeter of the filter path. These plates were positioned to maintain a 10 mm spacing between the deflection plate and the screen belting which kept the filter media under slight compression. We repeated the DOP leak tests and found that the leaks were eliminated along the straight parts but were still substantial along the curved portions. We were not able to maintain a compression seal around the curved portion of the filter path because the media

would become thinner around the outside curves due to a stretching force. We made several attempts to accommodate the changes in the filter thickness but were not successful.

The use of a compression seal along the filter edges introduced a new problem in our filer design. Since the edges of the filter media would be under a slight compression, there is a shearing force on the media when the screen belting advances the media. This shearing force would cause the filter media to tear at joints and other rough spots on the deflection plates. The solution to the tearing problem was to sew a cloth envelope around the entire medium as seen in Fig. 25. This media was run through the RPF shown in Fig. 22 several times to verify that the media would not tear nor pull out of the deflection plates. Two fire tests were then run with this media. Although the screen belting and filter media performed well in these tests, the life of the HEPA filter was not significantly extended over the baseline test. Figure 26 shows the inlet side of the RPF after it was used in the second fire test. A segment of the deflection plate on the left side was removed to provide a cutaway view of the edge sealing mechanism. An integral part of this sealing mechanism is a rubber strip that is fastened to the screen belting and presses the media against the deflector plate. We cut a portion of the filter media away in Fig. 27 to show the rubber strip. Unfortunately, because of the cut-and-fit approach used in making the deflector plates, we were unable to achieve a uniform seal around the filter edges and even had several minor gaps. Although the sealing mechanism was not yet perfected, we have demonstrated that the filter media shown in Fig. 25 functions well in the RPF with this sealing mechanism. Figure 28 shows the filter media after a fire test. We have cut out portions of the laminated media to show the relative plugging at different layers of the media. This figure shows that most of the smoke was captured on the cloth envelope and the top filter layer. There is no evidence of smoke reaching tne last layer of the media. This finding suggests that the test failure was due to edge leakage and not a poor filter efficiency.

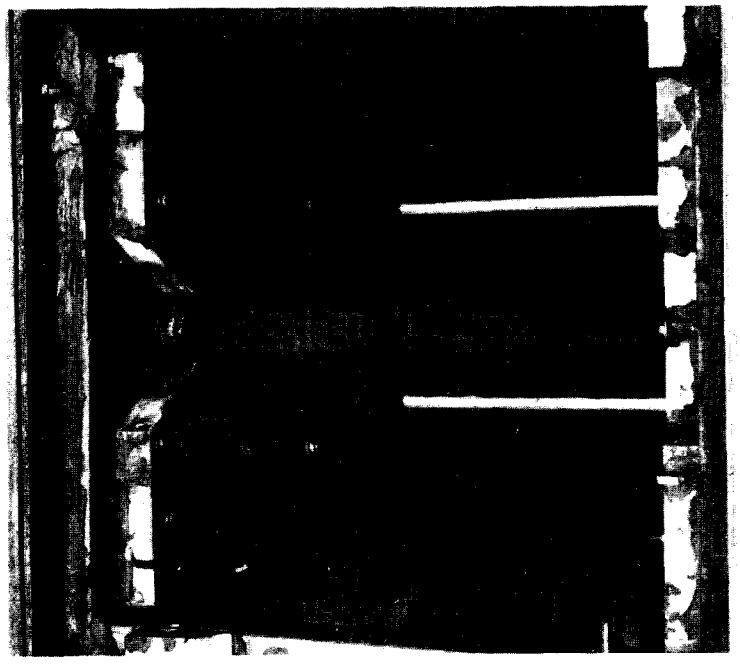

Figure 26 Cutaway view of the edge sealing mechanism used in the RPF.

Figure 27 Close up of the rubber strip that is used to compress the filter media against the deflector plate.

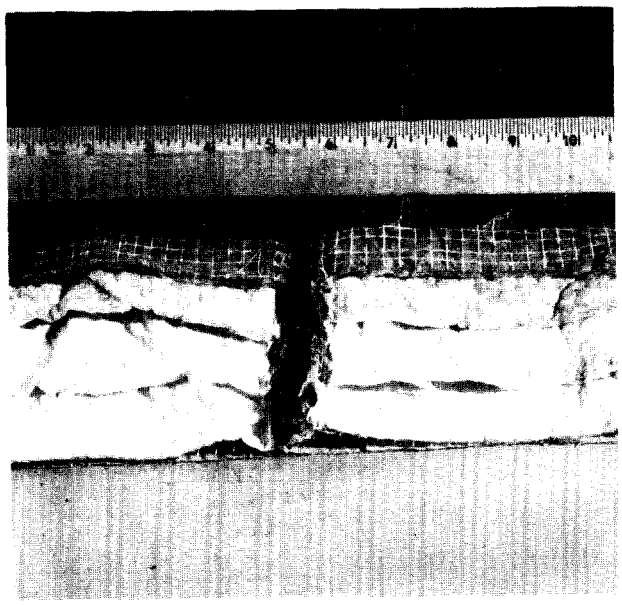

Figure 28 Laminated filter media showing the smoke deposits at different layers of the filter media.

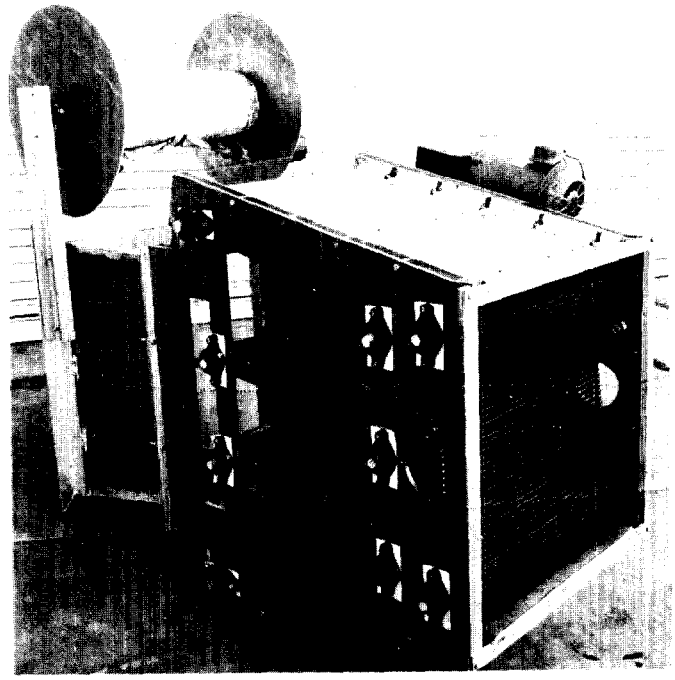

Figure 29 Second generation of the rolling electrofibrous prefilter with a moving belt electrode.

We then designed and built a new rolling electrofibrous prefilter shown in Fig. 29. Holes were cut in the side wall and a plexiglas plate inserted to allow the pleated belting to be seen. This figure shows the RPF from the side and rear angle. This new design has incorporated all of the modificatins made to our previous model. One of the major changes in the design was to increase the filter area by adding one additional pleat and increasing the length of each pleat. These changes nearly doubled the effective filtering area compared to the previous design. The screen belting also had the rods welded to the chain links to prevent the rods from pulling loose under high loads. One of the most important design changes made in our new RPF model was the deflection plate for preventing edge leakage. This deflection plate was designed to seal the filter edges by compressing the roping that was attached to the media edges. The rope, shown in Fig. 25, would be slightly compressed and ride within a grooved track that was cut in the deflection plate. DOP penetration measurements showed that this new edge sealing design was much better than our previous design although it still had a significant edge leakage. We have several plans to improve the sealing design by making changes in both the deflection plate and the filter media. We plan to make these changes before conducting fire tests on this RPF design.

VII. SUMMARY AND CONCLUSIONS

Lawrence Livermore National Laboratory (LLNL) has a comprehensive program funded by the U. S. Department of Energy to investigate the use of electrofibrous filters in the nuclear industry. The objective of this program is to develop prototype electrofibrous filters that will be used as prefilters to reduce the load on HEPA filters. Potential benefits of the combined electrofibrous prefilter, HEPA filter system include a reduction in cost and volume of

radioactive waste when compared to the present HEPA filter system alone. The electrofibrous filter being developed at LLNL is generated by applying an electric field across a conventional fibrous filter.

We have reviewed the theory and experimental results that show electrofibrous filters have a much higher efficiency and greater service life than conventional fibrous filters. Two mechanisms are responsible for the increased efficiency. One mechanism is due to a time independent attraction between polarized fibers and charged and neutral particles. The other mechanism is due to a time dependent attraction between charged fibers and charged and neutral particles. The charge on the fibers result from a dynamic process of charge accumulation due to the particle deposits and charge dissipation due to the fiber conductivity. We have also reviewed the simple model of filter clogging that explains how the electric field can extend the filter life based on the decreased formation of particle dendrites.

In this paper, we have established the design criteria for prototype electrofibrous filters for use in nuclear ventilation systems. The key design parameters that control the final performance characteristics are face velocity, filter medium, high voltage electrodes and the high voltage power supply. We have shown that the face velocity should have a minimum value. The filter medium should have minimum values for flammability, electrical conductivity, fiber packing density, compressibility and water adsorption. The high voltage electrodes should have maximum open area, good structural support for the filter medium, good electrical contact with the medium, good insulation from ground and high electrical resistance. The high voltage power supply should have a maximum d.c. voltage and an automatic shut down during overload. We have applied these design criteria in developing prototype electrofibrous prefilters for use in nuclear ventilation systems.

Two different electrofibrous filters have been developed for use in nuclear ventilation systems. One prototype is a stationary prefilter while the other is a rolling prefilter. Both prefilters use the same basic filtering technique in which a fibrous filter medium is sandwiched between a high voltage electrode and a ground electrode, both electrodes having a sufficient open area to offer minimum air resistance. The applied voltage on the electrodes generates an electric field that polarized the filter fibers, which then attract suspended particles via electrostatic forces. Since a finite time is required for this electrostatic attraction, the filter media and electrodes have been pleated to provide a sufficiently long particle residence time.

The stationary electrofibrous prefilter has the same dimensions (610 x 610 x 305 mm) as commercially available mechanical filters that are used in ventilation systems. However, the additional requirement of high voltage on the electrodes has greatly increased the complexity of the electrofibrous prefilter. Laboratory tests using DOP and NaCl aerosols in a modified ASHRAE filetr test apparatus have shown that the electrofibrous prefilter increased in efficiency from 40 to 90% as 10 kV is applied to the electrode.

The special requirement of protecting the HEPA filter from a high concentration of smoke aerosols during fire conditions led to the development of the rolling electrofibrous prefilter. We established the feasibility of this concept in a series of tests using a commercially available rolling prefilter that was modified for removing smoke aerosols. We have built two rolling electrofibrous prefilters that have a pleated electrode design. Both units use a screen belting that serves as the high voltage electrode and as the carrier for

the filter medium. We conducted a series of fire tests on the first prototype to evaluate the ability of the electrofibrous rolling prefilter to protect HEPA filters from plugging by smoke aerosols. These tests have identified problems with the screen belt jamming, the filter media tearing and edge leakage arund the filter medium. We have corrected the problems with the screen belt jamming and the filter media tearing but have not yet eliminated the edge leakage. To date, we have been unable to demonstrate that the pleated rolling prefilter can protect the HEPA filter from plugging. Excessive edge leakage was identified as the primary cause of the unsuccessful fire tests. We have built a second rolling prefilter that has incorporated design modifications to correct the problems encountered with our first unit. DOP tests have shown that the edge leakage has been significantly reduced in the second prototype, but not eliminated. We plan additional design changes to minimize the leakage problem before conducting fire tests on this unit.

VIII. Bibliography

1. Frederik, E.R., "Fibers, electrostatics, and filtration: a review of new technology," Air Pollution Control Assoc. J., Vol. 30, pp. 426-431 (1980).

2. Bergman, W., Taylor, R.D., Miller, H.H., Biermann, A.H., Hebard, H.D., daRoza, R.A. and Lum, B.Y., "Enhanced filtration program at LLL - A progress report," Proc. 15th DOE Nuclear Air Cleaning Conference, pp. 1058-1099, Boston (1978).

3. Bergman, W., Taylor, R.D., Hebard, H.D., Lum, B.Y., Kuhl, W.D., Boling, R.M. and Buttedahl, O.I., "Electrofibrous prefilters for use in the nuclear industry," Proc. Second U.S. DOE Environmental Control Symposium, Reston, Virginia, pp. 334-371 (1980).

4. Helfritch, D.J. and Ariman, T., "Electrostatic filtration and the Apitron-design and field performance," Novel Concepts, Methods and Advanced Technology in Particulate-Gas Separation, pp. 286-304, T. Ariman, ed., University of Notre Dame Press, Notre Dame (1978).

5. Reid, D.L. and Browne, L.M., "The electrostatic capture of submicron particles in fiber beds," Proc. 14th ERDA Air Cleaning Conference, Sun Valley, Idaho (1976).

6. Davies, C.N., Air Filtration, Academic Press, New York, (1973).

7. van Turnhout, J., "The use of polymers for electrets," J. of Electrostatics, Vol. 1, pp. 147-163 (1975).

8. van Turnhout, J., Albers, J.H.M., Adamse, J.W.C., Hoeneveld, W.J., and Visscher, J., "Electret filters for high efficiency air cleaning," Proc. Second World Filtration Congress, pp. 521-528, London (1979).

9. Bergman, W., Hebard, H., and Lum, B. "Electrostatic filters generated by electric fields," Proc. Second World Filtration Congress, London (1979).

10. Bergman, W., Biermann, A.H., Hebard, H.D., Lum, B.Y., and Kuhl, W.D., "Electrostatic air filters generated by electric fields," Proc. of Fine Particle Society Meeting, Maryland (1980).

11. Lamb, G.E.R. and Costanza, P.A., "A low-energy electrified filter system," Filtration and Separation, Vol. 17, pp. 319-322 (1980).

12. Payatakes, A.C., "Advances in dendritic deposition of aerosols by inertial impaction and/or interception," Proc. Second World Filtration Congress, pp. 507-519, London (1979).

13. Shand, E.B., Glass Engineering Handbook, McGraw-Hill, New York (1958).

14. Lamb, G.E.R., Costanza, P.A. and O'Meara, D.J., "Electrical stimulation of fabric filtration Part II: mechanism of particle capture and trials with a laboratory baghouse," Textile Research J., Vol. 48, pp. 566-573 (1978).

15. Thompson, J.K., Clark, R.D. and Fielding, G.H., "Improving the cost-effectiveness of HEPA filters via dielectrophoretic prefilters," Seminar on High Efficiency Aerosol Filtration, pp. 605-607, Luxembourg (1977).

16. ASHRAE Standard 52-68, "Method for testing air cleaning devices used in general ventilation for removing particulate matter," ASHRAE, Inc., New York, (1968).

17. Alvares, N., Beason, D., Bergman, W., Creighton, J., Ford, H. and Lipska, A., "Fire protection countermeasures for containment ventilation," Lawrence Livermore National Laboratory report UCID-18781, Livermore, California (1980).

18. Gaskill, J.R., Ford, H.W. and Correia, A.N., "HEPA-filter smoke plugging studies," Lawrence Livermore Laboratory report UCRL-50007-74-2, Livermore, California (1975).

19. Alvares, N.J., Beason, D.G. and Ford, H.W., "In-duct countermeasures for reducing fire-generated-smoke-aerosol exposure to HEPA filters," Proc. 15th DOE Nuclear Air Cleaning Conference, pp. 653-664, Boston (1978).

DISCUSSION

DORMAN: Dr. Bergman has followed a long line of workers in this field, and we may at last be on the verge of a practical fibrous filter on which a voltage has been imposed.